UNIVERSIDADE FEDERAL DE SÃO CARLOS

CENTRO DE CIÊNCIAS EXATAS E DE TECNOLOGIA

DEPARTAMENTO DE QUÍMICA

PROGRAMA DE PÓS-GRADUAÇÃO EM QUÍMICA

"DEEP EUTECTIC SOLVENT AND ADDITIVE MANUFACTURING: SUSTAINABLE APPROACHES FOR THE DEVELOPMENT OF ELECTROCHEMICAL SENSORS"

Karen Kenlderi de Lima Augusto*

Tese apresentada como parte dos requisitos para obtenção do título de DOUTORA EM CIÊNCIAS, área de concentração: QUÍMICA ANALÍTICA

Supervisor: Prof. Dr Orlando Fatibello-Filho

***Scholarship (CNPq and CAPES-Print)**

São Carlos – SP

2025

UNIVERSIDADE FEDERAL DE SÃO CARLOS

Centro de Ciências Exatas e de Tecnologia
Programa de Pós-Graduação em Química

Folha de Aprovação

Defesa de Tese de Doutorado da candidata Karen Kenlderi de Lima Augusto, realizada em 27/02/2025.

Comissão Julgadora:

Prof. Dr. Orlando Fatibello Filho (UFSCar)

Prof. Dr. Fernando Cruz de Moraes (UFSCar)

Prof. Dr. Rodrigo Alejandro Abarza Munoz (UFU)

Profa. Dra. Patrícia Batista Deroco (UNICAMP)

Prof. Dr. Geiser Gabriel de Oliveira (UFT-Gurupi)

O Relatório de Defesa assinado pelos membros da Comissão Julgadora encontra-se arquivado junto ao Programa de Pós-Graduação em Química.

Dedico este trabalho,

À minha mãe, Leda, por não medir esforços para me ajudar, por sempre manter a esperança e me fazer enxergar cada vez mais longe.
Às minhas irmãs, Sayo e Sam, por sempre acreditarem em mim e por todo o apoio.
À minha grande amiga de infância, Maria Caroliny, que sempre me apoiou e me acompanhou nos momentos mais importantes da minha vida.

Amo vocês com todo o meu coração!

AGRADECIMENTOS

Agradeço, primeiramente, a Deus. Nunca teria chegado até aqui sem o seu cuidado e proteção em todos os momentos. Obrigada, Deus, por sempre me guiar e sustentar.

Aos meus familiares, expresso minha imensa gratidão pelas orações, pela torcida, pela esperança e por sempre acreditarem em mim e me acompanharem nessa caminhada.

À minha amiga Maria Caroliny e à sua família, obrigada por estarem sempre presentes em minha vida, por todo apoio e por cuidarem de mim com tanto carinho.

Ao meu orientador, Prof. Dr. Orlando Fatibello-Filho, sou profundamente grata por seus ensinamentos, paciência e apoio ao longo do doutorado. Muito obrigada, professor! Todo o conhecimento adquirido neste período será levado comigo para sempre.

Ao Prof. Craig Banks, da Manchester Metropolitan University (MMU - Manchester, UK), meu agradecimento especial por me acolher em seu grupo de pesquisa durante meu doutorado sanduíche. Obrigada também aos colegas de laboratório da MMU: Jess, Muhz, Matt, Uday, Ana, e Larissa.

Também agradeço ao Dr. Robert "Bobby" e à Dr. Elena, que me orientaram com dedicação durante meu período na MMU. Serei eternamente grata por todo aprendizado, pelos trabalhos realizados e, principalmente, por me inspirarem a alçar voos mais altos. *[A special thanks to Dr Robert "Bobby" and Dr Elena, who guided me with dedication throughout my time at MMU. I will be forever grateful for all the knowledge gained, the work accomplished, and, most importantly, for inspiring me to aim higher. The best team!]*

Às amigas Ana e Larissa, pelos momentos juntas em Manchester e pela amizade que continua aqui no Brasil. Obrigada por toda ajuda, pela parceria e pela amizade sincera.

Ao David, minha gratidão pelo suporte e amizade durante o período do doutorado sanduíche. Sua presença trouxe leveza aos meus dias.

Ao Paulo, minha gratidão por sua amizade, paciência, ensinamentos e discussões. Sem dúvida, uma das melhores coisas que o doutorado me proporcionou foi te conhecer. Você é um grande amigo que levarei para a vida toda.

Ao Renan, grande amigo e excelente químico orgânico, obrigada por toda a ajuda e suporte. À Alejandra e ao Renan, vocês são fundamentais na minha vida e foram peças-chave para que eu continuasse sempre em frente. Amo vocês!

Ao Frederico, obrigada por todo apoio e por tornar meus dias mais leves. Você foi a melhor coisa que me aconteceu em Manchester. Amo você!

Ao Laboratório de Análise Térmica, Eletroquímica e Química de Soluções, agradeço o apoio com as análises térmicas. Em especial, à Dra. Ana Paula Garcia Ferreira, por suas valiosas orientações técnicas, e ao Prof. Dr. Éder Tadeu Gomes Cavalheiro, cuja disciplina de análise térmica foi essencial para compreender melhor os resultados das análises de DSC.

Ao professor Evandro, por toda assistência no laboratório e nos artigos. E também ao Gustavo por toda colaboração nos trabalhos.

Aos colegas do LABBES e da UFSCar, minha gratidão pela amizade, pela ajuda e pelos momentos de descontração que tornaram essa jornada mais leve.

Ao Programa de Pós-Graduação em Química da UFSCar e a todos os professores, obrigada pelo suporte necessário para a realização desta etapa.

Por fim, agradeço às agências de fomento CNPq (#401681/2023-8 e INCT Nano Vida #406079/2022-6), CAPES e FAPESP (#2024/04116-8), que viabilizaram a concretização deste trabalho. Em especial, ao CNPq (#140406/2021-2) e à CAPES (CAPES Print #88887.836030/2023-00) pelas bolsas concedidas.

ABBREVIATIONS AND SYMBOLS

3D	Three Dimensional
ΔE_p	Peak-to-Peak Separation Potential
5−HT	Serotonin
ACP	Acetaminophen
AFM	Atomic Force Microscopy
AgNP	Silver Nanoparticle
AM	Additive Manufacturing
AME	Additively Manufactured Electrode
BR	Britton-Robinson
CAD	Computer Aided Design
CB	Carbon Black
CNH	Carbon Nanohorns
CPE	Carbon Paste Electrode
CV	Cyclic Voltammetry
DecA	Decanoic Acid
DES	Deep Eutectic Solvent
DIU	Diuron
DPV	Differential Pulse Voltammetry

DSC	Differential Scanning Calorimetry
DTA	Differential Thermal Analysis
$E_{1/2}$	Half-Wave Potential
EDX	Energy Dispersive X-ray
EIS	Electrochemical Impedance Spectroscopy
FDM	Fused Deposition Modelling
FTIR	Fourier Transform Infrared Spectroscopy
GC	Glassy Carbon
GCE	Glassy Carbon Electrode
H_2Q	Hydroquinone
HBA	Hydrogen Bond Acceptor
HBD	Hydrogen Bond Donor
HDES	Hydrophobic Deep Eutectic Solvent
HM	Hydrophobic Mixture
I_{ap}	Anodic Peak Current
I_{cp}	Cathodic Peak Current
IL	Ionic Liquids
K	Kelvin: SI Base Unit of Thermodynamic Temperature
k^0	Heterogeneous Electron (Charge) Transfer Rate Constant

k_{app}	Apparent Heterogeneous Electron (Charge) Transfer Rate Constant
k_{cat}	Catalytic Rate Constant
LOD	Limit of Detection
LOQ	Limit of Quantification
MWCNT	Multiwalled Carbon Nanotube
NADES	Natural Deep Eutectic Solvent
NMR	Nuclear Magnetic Resonance
PB	Phosphate Buffer
pH	Logarithm of the Hydrogen Ion Concentration
ppb	Parts per Billion
rPLA	Recycled Poly(Lactic Acid)
RSD	Relative Standard Deviation
R_{ct}	Resistance of Charger Transfer
SEM	Scanning Electron Microscopy
SDG	Sustainable Development Goal
SWV	Square Wave Voltammetry
TBAB	Tetrabutylammonium Bromide
TGA	Thermogravimetric Analysis
T_m	Melting Temperature

XRD	X-ray Diffraction
XPS	X-ray Photoelectron Spectroscopy

LIST OF TABLES

TABLE 1.1 - Key principles of green chemistry[2] 4
TABLE 1.2 - The 12 criteria for a solvent to be considered green[68] 7
TABLE 1.3 - General classification of deep eutectic solvents 15
TABLE 3.1 - Molar ratio of the obtained hydrophobic mixtures based on decanoic acid and tetrabutylammonium bromide. 51
TABLE 3.2 - SWV optimization using 100 μmol L^{-1} 5–HT 54
TABLE 3.3 - Mass percentage composition of binders in the carbon paste electrode. 58
TABLE 3.4 -DPV optimization using 100 μmol L^{-1} Diuron 59
TABLE 3.5 - DPV and SWV optimization using 100 ppb (8.9×10^{-7} mol L^{-1}) of Cd(II) 68
TABLE 4.1 - Synthesis time of the HDES (DecA:TBAB) 73
TABLE 4.2 - Thermodynamic data acquired from the experiments by differential scanning calorimetry 78
TABLE 4.3 - Physicochemical properties of the hydrophobic deep eutectic solvent prepared in this work 85
TABLE 4.4 - EcoScale Score for the proposed HDES 89
TABLE 4.5 - Adherence to the Green Chemistry Principles 90
TABLE 4.6 - EIS data for 100 μmol L^{-1} 5–HT in 0.2 mol L^{-1} PB pH 7.0 96
TABLE 4.7 - Figures of merit for plots from scan rate study obtained for 100 μmol L^{-1} 5–HT 104
TABLE 4.8 - Comparison of the analytical parameters for the voltammetric determination of serotonin 108
TABLE 4.9 - Determination of serotonin in spiked synthetic urine and bovine serum using the proposed electrode DecA:TBAB(5mg)-CNH/GCE 113

TABLE 4.10 - Anodic peak current (I_{ap}), cathodic peak current (I_{cp}), ratio of the peak currents (I_{ap}/I_{cp}), and peak-to-peak potential separation (ΔE_p) obtained for 1.0 mM H_2Q 116
TABLE 4.11 - Comparison of the analytical parameters for the voltammetric determination of diuron. 122
TABLE 4.12 - Determination of diuron in tap water using the electrode HDES(8mg)/CPE 123
TABLE 4.13 - Determination of Cd (II) within spiked river water sample (n = 3) using the optimised SWASV methodology 138
TABLE 4.14 - Comparison of the analytical parameters for the voltammetric determination of cadmium in water samples 139
TABLE 4.15 - Filament composition 142
TABLE 4.16 - Comparisons of the resistance of the filaments over 10 cm 144
TABLE 4.17 - The atomic concentration of the species in each electrode 146
TABLE 4.18 - Comparisons of the electrochemical parameters for the bespoke electrodes 150
TABLE 4.19 - Results for plots from scan rate study obtained for 100 µM of acetaminophen 154
TABLE 4.20 - Results obtained for the determination of acetaminophen using the SWV method 155
TABLE 4.21 - EcoScale for HDES-based Filament Production 158
TABLE 4.22 - Green Chemistry Principles Assessment Table 160

LIST OF FIGURES

FIGURE 1.1 - Sustainable Development Goals. Adapted from The United Nations Sustainable Development Goals[1]. 1
FIGURE 1.2 - Number of publications on deep eutectic solvents according to the Web of Science database (term: deep eutectic solvent*). 10
FIGURE 1.3 - Number of publications on deep eutectic solvents in electrochemistry according to the Web of Science database (terms: deep eutectic solvent* and electrochem*). 12
FIGURE 1.4 - Main hydrogen bond donors used for the formation of Type III DES 16
FIGURE 1.5 - Representation of a 3D printing schematic, starting from the CAD (Computer-Aided Design) model of a specific object, followed by conversion using specialised software for compatibility with the 3D printer, leading to the fabrication of the desired object. 33
FIGURE 1.6 – (A) Serotonin molecule and (B) Electrochemical oxidation of serotonin. 41
FIGURE 1.7 - Diuron electrochemical behaviour involving the formation of a dimer. Adapted from Foukmeniok et al. (2022)[238]. 43
FIGURE 1.8 - Acetaminophen electrochemical oxidation. 44
FIGURE 3.1 - Illustration of a carbon paste electrode and Teflon tubes used for electrode preparation. 57
FIGURE 3.2 – Representation of a typical electrochemical cell system used consisted of a 3D-printed reference electrode in a lollipop shape, an external commercial Ag|AgCl/KCl (3.0 mol L^{-1}) reference electrode, and a nichrome wire counter electrode. 63
FIGURE 3.3 - Schematic illustration of the process for preparing AgNPs on graphite. 64

FIGURE 3.4 - Illustration of the filament production process and development of the 3D-printed electrodes. 66
FIGURE 4.1 - FTIR spectra obtained for the studied HDES (DecA:TBAB) and its precursors: TBAB and DecA. 71
FIGURE 4.2 - In situ FTIR study for monitoring the preparation of the HDES. (A) evaluation of the intensity of specific peaks for DecA:TBAB synthesis as a function of the time of synthesis. (B) Infrared spectra for DecA:TBAB synthesis. The data correspond to the preparation of DecA:TBAB in a molar ratio of 1.85:1 at the temperature of 353.15 K (80.0 °C). 72
FIGURE 4.3 - ^{1}H NMR spectrum of decanoic acid (400 MHz, DMSO-d_6). 75
FIGURE 4.4 - ^{1}H NMR spectrum of tetrabutylammonium bromide (400 MHz, DMSO-d_6) 75
FIGURE 4.5 - ^{1}H NMR spectrum of the eutectic solvent DecA:TBAB (400 MHz, DMSO-d_6) 76
FIGURE 4.6 - DSC curves with the thermal events of the pure components: TBAB and DecA, and for the mixture of DecA:TBAB at the eutectic point. T_{trans}: temperature of phase transition; T_m: melting temperature; T*: temperature of the free fraction of the precursors (DecA or TBAB). 77
FIGURE 4.7 - TG curves (solid lines) of DecA:TBAB (1.85:1), decanoic acid (DecA) and tetrabutylammonium bromide (TBAB). DTA curves (dotted lines) of the eutectic mixture and its precursors (TBAB and DecA). Conditions: N_2 at 50 ml min^{-1}, sample mass of (10.0±0.2) mg in open α-alumina sample holders. ... 82
FIGURE 4.8 - Phase diagram of the DecA:TBAB eutectic system as a function of the fatty acid molar ratio. 84
FIGURE 4.9 – CV results (A) and (B) obtained for the oxidation of 100 μmol L^{-1} 5–HT in 0.2 mol L^{-1} PB pH 7.0 using (—) GCE and electrodes with different amounts of DecA:TBAB HDES: (—) CNH/GCE (0 mg), (—) 3mg, (—) 5 mg,

(—) 8 mg, and (—) 10 mg. Scan rate: 50 mV s^{-1}. Plots of (C) I_{ap} and (D) E_{ap} versus the amount of HDES. 94
FIGURE 4.10 - Nyquist plots (65,000–0.1 Hz) (A) using 100 µmol L^{-1} 5–HT in 0.2 mol L^{-1} PB pH 7.0 at (●) GCE, (●) CNH/GCE, (●) DecA:TBAB(3mg)-CNH/GCE, (●) DecA:TBAB(5mg)-CNH/GCE, (●) DecA:TBAB(8mg)-CNH/GCE, (●) DecA:TBAB(10mg)-CNH/GCE. Inset: the proposed equivalent circuit. In (B) The Bode plot of impedance magnitude versus frequency. 96
FIGURE 4.11 - SEM images at 100,000x magnification for (A) CNH suspension and (B) CNH+HDES suspension. 3D AFM topography images for (C) CNH suspension and (D) DecA:TBAB+CNH suspension. 98
FIGURE 4.12 - Chronoamperogram produced at (A) GCE, (B) CNH/GCE, and (C) DecA:TBAB(5mg)-CNH/GCE with 100 µmol L^{-1} 5–HT in 0.2 mol L^{-1} PBS (pH 7.0) at a potential of 0.35 V. Inset plot of I_{cat}/I_L vs $t^{1/2}$. 100
FIGURE 4.13 - Potential scan rate study (15 to 100 mV s^{-1}) with 100 µmol L^{-1} 5– HT in 0.2 mol L^{-1} PBS pH 7.0 performed at (A) GCE, (B) CNH/GCE, and (C) DecA:TBAB(5mg)-CNH/GCE electrodes. Inset: Randles–Ševčík plot..... 102
FIGURE 4.14 - (A) SW voltammograms for the pH study (2.0 to 12.0) in 0.1 mol L^{-1} BR buffer for the detection of 100 µmol L^{-1} 5–HT performed at DecA:TBAB(5mg)-CNH/GCE electrodes. Inset plot of the peak potential versus the pH. In (B) the effect of pH in the current of the anodic peak. SWV parameters: a = 10 mV, f = 5 Hz, and ΔE = 8 mV..... 103
FIGURE 4.15 - SW voltammograms for 5–HT oxidation in 0.2 mol L^{-1} PB pH 7.0 in a concentration range of 0.5 to 32.71 µmol L^{-1}. SWV parameters: a: 10 mV, f: 5 Hz, and ΔE: 8 mV. Inset: the linear plot and equation: I_{ap} (µA) = –0.34+0.20 (µA L $µmol^{-1}$) [5–HT] µmol L^{-1} (R^2 = 0.993). 106
FIGURE 4.16 - (A) SW voltammograms obtained for repetitive measurements (n=5) for different concentrations of serotonin (10, 20 and 30 µmol L^{-1}) using 1 electrode. SWV parameters: a = 10 mV, f = 5 Hz, and ΔE = 8 mV. In (B) the results

obtained in the inter-day study for repetitive measurements (n=5) using three different concentrations of serotonin (10, 20 and 30 μmol L^{-1}) at three electrodes. (C) Cyclic voltammograms for 100 μmol L^{-1} 5–HT in 0.2 mol L^{-1} PBS pH 7.0 in the sensor stability study using the DecA:TBAB(5mg)-CNH/GCE electrode. Scan Rate: 50 mV s^{-1}; 100 cycles. 111
FIGURE 4.17 - Response of serotonin in the absence and presence of different interferents at a ratio of (A) 1:1 5–HT to interferent and (B) 1:10 5–HT to interferent. 112
FIGURE 4.18 – (A) and (B) CV and SW voltammograms results obtained for 1mM H_2Q in 0.1 mol L^{-1} acetate buffer pH 4.7 using CPE with different amounts of DecA:TBAB HDES. In (C) plots of I_p vs HDES content and (D) ΔE vs HDES content. Scan rate: 50 mV s^{-1}; DPV parameters: a: 70 mV, f: 30 Hz, and ΔE_s: 5 mV..... 115
FIGURE 4.19 - (A) and (B) CV and DP voltammograms obtained for 100 μmol L^{-1} Diuron in 0.01 mol L^{-1} PB pH 3.0 using CPE with different amounts of DecA:TBAB HDES. Scan rate: 10 mV s^{-1}; DPV parameters: a: 60 mV, t: 10 ms, ΔE_s: 4 mV, and Δt: 100 ms. 117
FIGURE 4.20 - (A) Nyquist plots at (●) bare CPE and (●) HDES(8mg)/CPE electrodes using 100 μmol L^{-1} diuron in 0.01 mol L^{-1} PB (pH 3.0). Inset: the proposed equivalent circuit. In (B) Chronoamperogram produced at HDES(8mg)/CPE with 100 μmol L^{-1} diuron in 0.01 mol L^{-1} PBS (pH 3.0) at a potential of 1.1 V. Inset plot of I_{cat}/I_L vs $t^{1/2}$. 118
FIGURE 4.21 - (A) DP voltammograms obtained for diuron at different pH values. (B) and (C) Plots of I_{ap} vs pH and E_{ap} vs pH. (D) DPV results for the supporting electrolyte study at pH 3.0. DPV parameters: a: 60 mV, t: 10 ms, ΔE_s: 4 mV, and Δt: 100 ms. 119

FIGURE 4.22 - DP voltammograms for diuron oxidation in 0.01 mol L^{-1} PB pH 3.0 in a concentration range of 1.0 to 47.2 µM. Inset: the calibration plot. DPV parameters: a: 60 mV, t: 10 ms, ΔE_s: 4 mV, and Δt: 100 ms. 121
FIGURE 4.23 - (A) DP voltammograms of reproducibility using three different electrodes in the presence of 100 µM. (B) .DPV parameters: a: 60 mV, t: 10 ms, ΔE_s: 4 mV, Δt: 100 ms. (B) Cyclic voltammograms for 100 µmol L^{-1} diuron in 0.01 mol L^{-1} PB pH 3.0 in the sensor stability study using the HDES(8mg)/CPE electrode. Scan Rate: 10 mV s^{-1}; 50 cycles..... 124
FIGURE 4.24 - (A) SEM image for modified graphite powder. (B to D) EDX elemental mapping analysis of graphite area, carbon map, and silver map, respectively. (E) XRD pattern of AgNP-graphite and (F) XPS data for AgNP-graphite. 129
FIGURE 4.25 - Photographs of bespoke (A) graphite and (B) AgNP-modified graphite filaments, highlighting the flexibility. 130
FIGURE 4.26 – Potential scan rate study (5–500 mV s^{-1}) with $[Ru(NH_3)_6]^{3+}$ (1 mM in 0.1 M KCl) performed in the (A) only-graphite (CB/G/PLA) and (B) AgNP-graphite (CB/Ag-G/PLA) as the WE, respectively. Inset: Randles–Ševčík plot. (C) Potential scan rate study (5–500 mV s^{-1}) with $[Fe(CN)_6]^{4-/3-}$ (1 mM in 0.1 M KCl) performed in the AgNP-graphite as the WE. Inset: the Randles–Ševčík plot. (D) Comparison of EIS Nyquist plots of $[Fe(CN)6]^{4-/3-}$ using only graphite (CB/G/PLA) and AgNP-graphite (CB/Ag-G/PLA) electrodes. Inset: the proposed equivalent circuit. 131
FIGURE 4.27 - (A) DPV and (B) SWV performed at the CB/Ag-G/PLA electrode in 0.1 mol L^{-1} BR (pH 5.0) using 100 ppb of Cd(II) at different deposition potentials (−1.2, − 1.1, − 1.0, −0.9, and −0.8 V) for 60 s. Inset: plot of the results obtained for repetitive measurements (n=3) at three different electrodes. DPV parameters: a = 25 mV, t = 0.05 s, ΔE_s = 5 mV, and $t_{deposition}$ = 60 s. SWV parameters: a = 20 mV, f = 25 Hz, ΔE_s = 5 mV, and $t_{deposition}$ = 60s. 134

FIGURE 4.28 - (A) DPV and (B) SWV performed at the CB/Ag-G/PLA electrode in 0.1 mol L^{-1} BR (pH 5.0) using 100 ppb of Cd(II) at different deposition times (0, 30, 60, 90, and 120 s). Inset: results obtained for repetitive measurements (n=3) at three different electrodes. DPV parameters: a = 25 mV, t = 0.05 s, ΔE_s = 5 mV, $E_{deposition}$ = −1.1 V. SWV parameters: a = 20 mV, f = 25 Hz, ΔE_s = 5 mV, $E_{deposition}$ = −1.1 V. 134
FIGURE 4.29 - (A) SWAS and (B) DPAS voltammograms in the presence of 100 ppb of Cd(II) performed at CB/G/PLA and CB/Ag-G/PLA electrodes in 0.1 mol L^{-1} BR (pH 5.0). SWASV parameters: a = 80 mV, f = 40 Hz, ΔE_s = 6 mV, $E_{deposition}$ = –1.1 V, and $t_{deposition}$ = 60s. DPASV parameters: a = 50 mV, t = 0.02 s, ΔE_s = 5 mV, $E_{deposition}$ = −1.0 V, and $t_{deposition}$ = 60s. 135
FIGURE 4.30 – (A) SWAS voltammograms for cadmium oxidation performed at CB/G/PLA (black line) and CB/Ag-G/PLA (blue line) in the linear range of 4.5 to 100 µg L^{-1} and 1.5 to 100 µg L^{-1} in 0.1 mol L^{-1} BR, respectively. Inset: calibration plots for CB/Ag-G/PLA. (B) SWAS voltammograms obtained for repetitive measurements (n=10) in 0.1 mol L^{-1} BR (pH 5.0) with 100 ppb of Cd(II) using CB/Ag-G/PLA electrode. SWASV parameters: a = 80 mV, f = 40 Hz, ΔE_s = 6 mV, $E_{deposition}$ = –1.1 V, and $t_{deposition}$ = 60s 136
FIGURE 4.31 – SWAS voltammograms for cadmium oxidation in (A) diluted tap water (5-fold) and (B) in diluted river water (20-fold) in 0.1 mol L^{-1} BR (pH 5.0) performed with AgNP-graphite in a concentration range of 5 to 80 ppb. Inset: calibration curve obtained by the standard addition method. SWASV parameters: a = 80 mV, f = 40 Hz, ΔE_s = 6 mV, $E_{deposition}$ = –1.1 V, and $t_{deposition}$ = 60s. 137
FIGURE 4.32 - Images of the bespoke (A) CB/Cellulose/HDES/PLA and (B) CB/HDES/PLA filaments. 143
FIGURE 4.33 - SEM surface images and XPS for the (A and C) as-printed and the (B and D) activated CB/Cellulose/HDES/PLA electrode. 145

FIGURE 4.34 - Scan rate study (5 – 500 mV s^{-1}) with 1.0×10^{-3} mol L^{-1} $[Ru(NH_3)_6]^{3+}$ in 0.1 mol L^{-1} KCl performed in (A) Commercial CB/PLA, (B) bespoke CB/PLA, (C) CB/Cellulose/PLA, (D) CB/Cellulose/HDES/PLA and (E) CB/HDES/PLA electrodes as the WE. Inset: The Randles–Ševčík plot. (F) EIS Nyquist plots using $[Fe(CN)_6]^{4-/3-}$ for the same electrodes. Inset: the proposed equivalent circuit. 148
FIGURE 4.35 – (A) SW voltammograms with 100 µM acetaminophen in PBS pH 7.55 using CB/Cellulose/PLA and CB/Cellulose/HDES/PLA electrodes as the WE. (B) SWV comparing the CB/Cellulose/HDES/PLA electrodes activated in 0.5M NaOH and non-activated. Scan rate: 50 mV s^{-1}. SWV parameters: a = 20 mV, f = 25 Hz, ΔE_s = 5 mV. 152
FIGURE 4.36 - (A) Scan rate study (5–150 mV s^{-1}) with 100 µM acetaminophen in PBS pH 7.55 performed in the CB/Cellulose/HDES/PLA as the WE. (B) Randles–Ševčík plot (I_p vs $v^{1/2}$), (C) plot of the logarithm of I_{ap} vs logarithm of v and (D) plot of I_p vs v. 153
FIGURE 4.37 - SW voltammograms for ACP determination performed at (A) CB/Cellulose/PLA and (B) at CB/Cellulose/HDES/PLA in PBS pH 7.55 in a concentration range of 5.0 to 300 µM and 2 to 300 µM, respectively. Inset: the calibration plot. SWV parameters: a = 20 mV, f = 25 Hz, ΔE = 5 mV. 155
FIGURE 4.38 - SW voltammograms for ACP detection in spiked (A) diluted river water (50-fold) and (B) diluted tap water (20-fold) in PBS pH 7.55 performed at CB/Cellulose/HDES/PLA electrode in a concentration range of 10 to 35 µM. SWV parameters: a = 20 mV, f = 25 Hz, ΔE = 5 mV. Inset: calibration curve obtained by the standard addition method. 156

Abstract

DEEP EUTECTIC SOLVENT AND ADDITIVE MANUFACTURING: SUSTAINABLE APPROACHES FOR THE DEVELOPMENT OF ELECTROCHEMICAL SENSORS. The thesis investigated the use of hydrophobic deep eutectic solvents and additive manufacturing to develop sustainable electrochemical sensors, aligning with the principles of green chemistry. To do this, an HDES composed of decanoic acid and tetrabutylammonium bromide was studied and synthesised, characterised using techniques such as differential scanning calorimetry, infrared spectroscopy, and nuclear magnetic resonance. For the first time, the synthesis of HDES was optimised using *in situ* infrared spectroscopy, reducing the preparation time to less than five minutes at 80 ºC, thereby contributing to energy savings and the environmental feasibility of the process. The application of HDES was explored in the modification of electrodes for electrochemical sensors aimed at detecting compounds of environmental and medical interest. One of the key studies involved modifying glassy carbon electrodes with HDES and carbon nanohorns for serotonin detection. The modified electrode (DecA(5mg)-CNH/GCE) exhibited significant improvements in electrochemical performance due to the synergistic effect between HDES and CNH, promoting greater coverage of carbon nanoparticles and a homogeneous surface, facilitating electron transfer in serotonin oxidation. Another study employed HDES in the modification of carbon paste electrodes for the detection of diuron, a widely used herbicide. The voltammetric method developed demonstrated good reproducibility and effective recovery of diuron in water samples, highlighting the sensor's applicability for environmental monitoring. Beyond conventional electrodes, the research explored additive manufacturing to develop sustainable conductive filaments. One of the filaments was composed of carbon black, graphite functionalised with silver nanoparticles (AgNPs), castor oil, and recycled PLA. The AgNPs were synthesised in an eco-friendly manner without reducing agents, using the graphite itself as the forming material, and characterised by SEM/EDX, XRD, and XPS. Electrodes printed from this material demonstrated high efficiency in cadmium detection in water, with a detection limit below the global regulatory threshold of 5 μg L^{-1}, making them viable for environmental analyses. Another innovative approach was the pioneering development of a filament containing HDES. In this study, the HDES was combined with carbon black, cellulose, recycled PLA, and castor oil. Electrodes printed from this filament exhibited electrochemical improvements compared to filaments developed without HDES and a commercial filament. As proof of functionality, the electrodes were applied in the detection of acetaminophen in water, demonstrating their analytical efficiency and sustainability. This work highlighted the potential of combining HDES and additive manufacturing to create environmentally friendly electrochemical sensors, driving advancements in sustainable analytical chemistry. Additionally,

it reinforces the feasibility of using simple and green materials in the development of new sensors, aligning with the principles of green chemistry and the United Nations' Sustainable Development Goals.

Keywords: sustainability, hydrophobic deep eutectic solvent, additive manufacturing, 3D-printing, green chemistry, electrochemical sensors, sustainable development.

Resumo

SOLVENTE EUTÉTICO PROFUNDO E MANUFATURA ADITIVA: ABORDAGENS SUSTENTÁVEIS PARA O DESENVOLVIMENTO DE SENSORES ELETROQUÍMICOS. A tese investigou o uso de solventes eutéticos profundos hidrofóbicos e manufatura aditiva para desenvolver sensores eletroquímicos sustentáveis, alinhando-se aos princípios da química verde. Para isso, foi estudado e sintetizado um HDES composto por ácido decanóico e brometo de tetrabutilamônio, caracterizado por técnicas como calorimetria diferencial de varredura, espectroscopia de infravermelho e ressonância magnética nuclear. Pela primeira vez, foi otimizada a síntese do HDES utilizando espectroscopia de infravermelho *in situ*, reduzindo o tempo de preparo para menos de cinco minutos a 80 ºC, o que contribuiu para a economia de energia e a viabilidade ambiental do processo. A aplicação do HDES foi explorada na modificação de eletrodos para sensores eletroquímicos voltados à detecção de compostos de interesse ambiental e médico. Um dos estudos centrais envolveu a modificação de eletrodos de carbono vítreo com HDES e nanochifres de carbono para a detecção de serotonina. O eletrodo modificado (DecA(5mg)-CNH/GCE) apresentou melhorias significativas no desempenho eletroquímico devido ao efeito sinérgico entre HDES e CNH, promovendo maior recobrimento das nanopartículas de carbono e uma superfície homogênea, facilitando a transferência de elétrons na oxidação da serotonina. Outro estudo empregou o HDES na modificação de eletrodos de pasta de carbono para a detecção de diuron, um herbicida amplamente utilizado. O método voltamétrico desenvolvido demonstrou boa reprodutibilidade e recuperação eficaz do diuron em amostras de água, destacando a aplicabilidade do sensor para monitoramento ambiental. Além dos eletrodos convencionais, a pesquisa explorou a manufatura aditiva para desenvolver filamentos condutores sustentáveis. Um dos filamentos foi composto por negro de fumo, grafite funcionalizado com nanopartículas de prata (AgNPs), óleo de rícino e PLA reciclado. As AgNPs foram sintetizadas de forma ecológica, sem agentes redutores, utilizando o próprio grafite como material formador, e caracterizadas por MEV/EDX, DRX e XPS. Os eletrodos impressos a partir desse material mostraram alta eficiência na detecção de cádmio em água, com limite de detecção inferior ao regulatório global de 5 $\mu g\ L^{-1}$, tornando-os viáveis para análises ambientais. Outra abordagem inovadora foi o desenvolvimento pioneiro de um filamento contendo HDES. Neste estudo, o HDES foi combinado com negro de fumo, celulose, PLA reciclado e óleo de rícino. Os eletrodos impressos a partir desse filamento apresentaram melhorias eletroquímicas em comparação a filamentos desenvolvidos sem HDES e a um filamento comercial. Como prova de funcionalidade, os eletrodos foram aplicados na detecção de paracetamol em água, demonstrando sua eficiência analítica e sustentabilidade. Este trabalho evidenciou o potencial da combinação entre HDES e manufatura aditiva para a criação de sensores eletroquímicos ecologicamente corretos, promovendo

avanços na química analítica sustentável. Além disso, reforça a viabilidade do uso de materiais simples e verdes no desenvolvimento de novos sensores, alinhando-se aos princípios da química verde e aos Objetivos de Desenvolvimento Sustentável da ONU.

Palavras-chave: sustentabilidade, solvente eutético profundo hidrofóbico, manufatura aditiva, impressão 3D, química verde, sensores eletroquímicos, desenvolvimento sustentável.

TABLE OF CONTENTS

Chapter 1

1 INTRODUCTION 1

1.1 Green Chemistry 3

1.2 Green Solvents 6

1.2.1 Deep Eutectic Solvents 8

1.2.1.1 Classification of Deep Eutectic Solvents 14

1.2.1.1.1 Hydrophobic Deep Eutectic Solvents 20

1.2.1.2 Synthesis of Deep Eutectic Solvents 23

1.2.1.3 Characterization of Deep Eutectic Solvents 27

1.2.1.3.1 Physicochemical Properties 28

1.2.1.3.2 Thermal Properties and Thermodynamic Characterization 29

1.3 Design of New Materials Towards Sustainability 31

1.4 Additive Manufacturing 32

1.4.1 Additive Manufacturing and the Development of Electrodes 34

1.5 Conducting Carbonaceous Materials in the Development of Electrodes 36

1.6 Analytical Applications 39

Chapter 2

2 OBJECTIVES 46

2.1 General Objectives 46

2.2 Specific Objectives 46

Chapter 3

3 EXPERIMENTAL SECTION 48

3.1 Hydrophobic Deep Eutectic Solvent Characterization 48

3.2 Development of an Electrochemical Sensor for Serotonin Detection……..... 51
3.3 Development of an Electrochemical Sensor for Diuron Detection 56
3.4 Modification of a Filament with Silver Nanoparticles for Cadmium Detection and Fabrication of a novel HDES-based filament ……... 60

Chapter 4

PART I

4 RESULTS AND DISCUSSION 70
4.1 Optimisation of Hydrophobic Deep Eutectic Solvent Preparation: *In Situ* FTIR Study and NMR Characterisation ……..... 70
4.2 Hydrophobic Mixtures: Thermal analysis ……..... 76
4.3 Phase Behaviour of Hydrophobic Mixtures ……..... 83
4.4 Physicochemical Characterization of HDES: Viscosity, Conductivity, and Water Content 85
4.5 HDES: Green Synthesis 86
4.6 Development of Electrochemical Sensors: Modified Glassy Carbon Electrode and Carbon Paste Electrode ……..…….. 92
4.6.1 Electrochemical Sensor Based on Carbon Nanohorns and HDES for the Determination of Serotonin[272] 93
4.6.2 Physical Characterization of the Electrode 98
4.6.3 Catalytic Rate Constant for Serotonin Oxidation and Electroactive Surface Area 99
4.6.4 pH and Potential Scan Rate Studies ……..... 102

4.6.5 Analytical Performance 105
4.6.6 Analysis of Serotonin in Synthetic Biologic Fluids ……..... 113
4.6.7 Carbon Paste Electrode Modified with HDES: an Electrochemical Study ……... 114
4.6.8 Influence of pH and Supporting Electrolyte 118
4.6.9 Analytical Performance and Diuron Determination in Water ……... 120
4.7 Conclusions 124

PART II

4.8 Sustainable Silver Nanoparticle-Enhanced Graphite Filament for Additive Manufacturing 127
4.8.1 Synthesis of AgNPs on Graphite and Incorporation into Filament ….. 127
4.8.2 Electrochemical Characterization of the Additive Manufactured Electrodes ……. 130
4.8.3 Electroanalytical Determination of Cadmium(II) ……..... 133
4.8.4 Detection of Cadmium within Water Samples 137
4.9 Conclusions 140

PART III

4.10 HDES-Based Filament ……..... 142
4.10.1 Electrochemical Characterization of the HDES-based Additive Manufactured Electrodes …….…….…….... 146
4.10.2 Electrochemical Determination of Acetaminophen 151
4.11 EcoScale Assessment for Filament Production 157
4.12 Conclusions ……..…….…….... 162

Chapter 5

5 CONCLUSIONS AND PERSPECTIVES 164

Chapter 6

6 REFERENCES 168

Chapter 1

1 - INTRODUCTION

Sustainable development has emerged as a global priority to address environmental, social, and economic challenges. The United Nations Sustainable Development Goals (SDGs), adopted in 2015, emphasize the need for innovative solutions to ensure a sustainable future for the planet. The SDGs are designed to balance the global challenges of sustainable development, providing a roadmap for governments, organizations, and individuals to work together toward a sustainable future (FIGURE *1.1*)[1].

FIGURE 1.1 - Sustainable Development Goals. Adapted from The United Nations Sustainable Development Goals[1].

Key goals include ensuring clean water and sanitation (Goal 6), affordable and clean energy (Goal 7), responsible consumption and production (Goal 12), and climate action (Goal 13). These goals emphasize innovation, sustainable practices, and international cooperation to tackle global challenges such as inequality, environmental degradation, and economic instability. The SDGs also highlights the role of science, technology, and innovation in achieving sustainable development[1].

In this regard, green chemistry has potential as a transformative approach that can contribute to the SDGs. By designing processes and materials that minimise hazardous substances and environmental impacts, green chemistry aligns with the principles of sustainability and paves the way for a more resilient future[2].

In the context of green chemistry, the development of analytical detection systems focused on safe and environmentally sustainable analyses has become a priority[3]. Reflecting this growing interest, different electrochemical sensors are being continuously developed, with applications ranging from clinical, food, and environmental sectors. These sensors offer sustainable characteristics that require only small volumes of reagents and samples, thereby generating less waste and using low-toxicity reagents, such as aqueous buffer solutions or diluted acids. Furthermore, the selection of suitable materials enables the development of sensors that are sensitive, selective, cost-effective, and simple to operate[4–9].

In reference to the development of electrochemical sensors, deep eutectic solvents (DES), a class of environmentally friendly solvents, have attracted significant attention for their low toxicity, biodegradability, and versatile properties that have enabled advancements in various fields, including in electrochemistry[10,11]. In parallel, additive manufacturing (AM), also known as 3D printing, has revolutionised material fabrication by 3D-printing objects layer by layer from digital models, significantly reducing waste, enhancing precision, and enabling fabrication of complex geometries[12,13].

In this sense, hydrophobic DES was integrated with various carbonaceous materials, including multiwalled carbon nanotubes, carbon black, and carbon nanohorns, to develop novel electrochemical sensors. The electrodes utilized were glassy carbon, carbon paste, and 3D-printed electrodes, highlighting the adaptability and effectiveness of DES in improving sensor performance.

Moreover, given the promising sustainable attributes of additive manufacturing, one of the objectives of this doctoral thesis was to take advantage of the unique properties of AM to create conductive filaments and, subsequently, develop electrochemical sensors for detecting specific target analytes.

1.1 - Green Chemistry

Green chemistry, often referred to as sustainable chemistry, is a field dedicated to creating chemical processes and products that minimize or completely remove the use and production of hazardous materials. Its goal is to enhance the safety, environmental sustainability, and efficiency of chemical manufacturing by considering environmental impacts from the start of the process[2]. To achieve this, green chemistry is divided into 12 principles, summarized in TABLE *1.1*.

TABLE 1.1 - Key principles of green chemistry[2]

Item	Principle	Description
1	Prevention	Avoiding waste generation is better than cleaning it up.
2	Atom Economy	Maximizing the incorporation of all materials used in the process into the final product.
3	Less Hazardous Chemical Synthesis	Designing methods that minimize toxicity to human health and the environment.
4	Designing Safer Chemicals	Creating products that are effective while minimizing toxicity.
5	Safer Solvents and Auxiliaries	Using benign or no solvents in processes whenever possible.
6	Energy Efficiency	Conducting chemical processes at ambient temperature and pressure to reduce energy use.
7	Use of Renewable Feedstocks	Preferring renewable raw materials over depleting resources.
8	Reduce Derivatives	Minimizing the use of unnecessary derivatives to avoid additional steps and waste.
9	Catalysis	Using catalytic reactions to enhance efficiency and reduce waste.
10	Design for Degradation	Ensuring that products break down into non-toxic substances after use.
11	Real-time Pollution Prevention	Monitoring processes to minimize hazardous by-products.
12	Safer Chemistry for Accident Prevention	Designing processes to minimize the risk of accidents, including explosions, fires, and toxic releases.

Several research groups are actively working to develop innovative materials and processes aligned with the principles of green chemistry. For instance, significant progress has been made in designing DES as eco-friendly alternatives to conventional organic solvents in processes including synthesis and extraction of analytes[14–22]. Other notable advancements include the creation of biodegradable plastics and sustainable polymers for applications such as functional materials in the fields of shape memory, degradable, and self-healing materials, which address the global challenge of plastic pollution[23–29]. Moreover, green chemistry has driven breakthroughs in renewable energy technologies, such as the development of efficient hydrogen production catalysts[30–32], as well as pharmaceuticals synthesized via less toxic methods[33–35]. Additionally, eco-friendly pesticides and fertilizers are being engineered to promote sustainable agricultural practices while minimizing environmental impact[36–39].

Among the green solvents, DES stand out, gaining significant attention for their ability to replace highly toxic organic solvents in processes such as extraction, synthesis, and metal processing[15,40]. DES are distinguished by their properties, which are closely aligned with the principles of green chemistry, such as low volatility, reduced toxicity, biocompatibility, biodegradability, and ease of preparation. Their synthesis process is straightforward, involving the mixing of components at a controlled temperature under constant agitation[40–42].

Regarding novel materials, this research explores the application of additive manufacturing using the fused deposition modelling (FDM) technique. FDM is a widely used AM technique that builds objects layer by layer by extruding melted thermoplastic filament through a heated nozzle. It is popular due to its affordability, material versatility, and ease of use, making it ideal for prototyping, medical devices, electronics, and aerospace applications. Moreover, it supports the use of renewable and recycled materials, reinforcing its relevance within the context of green chemistry[43–47].

Both DES[15,16,48–55] and AM[12,45,47,56–65] have been widely applied in areas such as electrochemistry and analytical chemistry in the development of electrochemical sensors, demonstrating the potential of these approaches to drive sustainable advancements across various scientific and industrial fields.

1.2 - Green Solvents

With the introduction of the green chemistry concept, concerns regarding using organic solvents—often deemed highly toxic, volatile, reactive, and flammable—have emerged. These solvents negatively impact human health and the environment, highlighting the need for sustainable alternatives[66,67]. Various research groups have focused on developing green solvents as promising substitutes for these traditional organic solvents. These green solvents are crucial for enhancing the environmental and economic performance of chemical manufacturing and other industries. The goal is not only to minimize the environmental impact of chemical processes but also to improve efficiency by allowing for lower temperatures and pressures, thus reducing energy consumption and promoting catalyst stability[67–69].

Several works have explored new materials and reagents that ensure maximum atomic efficiency, protect the environment and the analyst, and minimize waste production at the end of the process. In addition to replacing conventional organic solvents, when combined with other materials, these new solvents can exhibit significant characteristics that enhance and modify procedures and products[67,69–72]. In a 2013 study focused on the development of environmentally friendly solvents, a set of twelve criteria was proposed that a solvent must satisfy to be classified as “green”[68]. These criteria were inspired by the twelve principles of green chemistry. A summary of these principles can be found in TABLE 1.2.

TABLE 1.2 - The 12 criteria for a solvent to be considered green[68]

Item	Criteria	Description
1	Availability	Available on a large scale.
2	Price	Attractive prices to ensure the sustainability of the chemical process.
3	Recyclability	Recycled through sustainable procedures.
4	Grade	Pure solvents are recommended, thus avoiding extra purification steps and ensuring energy savings.
5	Synthesis	Easy to prepare, avoiding high energy consumption and reagents, and presenting high atomic efficiency.
6	Toxicity	Negligible toxicity.
7	Biodegradability	Biodegradable and do not produce toxic by-products.
8	Performance	Like or even better performance compared to traditional solvents.
9	Stability	Thermally and chemically stable.
10	Flammability	Not be flammable.
11	Storage	Simple to store and comply with regulations for safe transport by road, train, boat or plane.
12	Renewability	Use of renewable raw materials to produce green solvents.

Developing an ideal sustainable solvent remains a significant challenge due to the complex criteria it must fulfil. A green solvent must exceed in various aspects, including low toxicity, high efficiency, biodegradability, and minimal environmental impact. Achieving this balance requires a comprehensive evaluation of the solvent's life cycle – from synthesis and application to final

disposal. It is essential to assess the sustainability of new solvents by comparing them to traditional solvents in terms of environmental, economic, and safety metrics. This approach ensures that the proposed solvent contributes to long-term environmental goals[68,73].

Among the most studied green solvents are Ionic Liquids, Supercritical and Subcritical Fluids, deep eutectic solvents, and Bio-Based Solvents[67–69,73]. These alternatives are gaining adoption in areas such as pharmaceuticals, biotechnology, food processing, chemistry and materials science. Their benefits include reducing hazardous waste, enhancing process efficiency, and supporting the shift toward more sustainable industrial practices.

This doctoral thesis will emphasize the utilization of deep eutectic solvents as a new class of green solvents, with a particular focus on their applications in electrochemistry. The study aims to explore how deep eutectic solvents can enhance electrochemical processes, offering advantages in terms of sustainability, conductivity, and compatibility with various electrochemical systems.

1.2.1 - Deep Eutectic Solvents

Deep eutectic solvents were first introduced due to their similarity to ionic liquids. They are created by combining two or more components that interact through hydrogen bonding, resulting in a eutectic mixture with a melting point that is lower than that of any of the individual components[74]. The concept of DES emerged from a study by Abbott *et al.* (2001)[75], which aimed to overcome some of the limitations associated with traditional ionic liquids.

Abbott *et al.* focused on developing moisture-stable room-temperature ionic liquids (RTILs) by combining quaternary ammonium salts with Lewis's acids. The researchers explored how different side chain substituents in

the ammonium salts and the choice of Lewis acid influenced the properties of the resulting liquids. Their goal was to find a substitute for ILs formed with imidazolium and aluminium by introducing new solvents made from ammonium salts, which are generally less expensive than imidazolium cations, and to use metal chlorides, such as zinc chloride ($ZnCl_2$) and tin chloride ($SnCl_2$), that are more stable in humid conditions[75].

Following that, the term "eutectic mixtures" was cited by the same research group in a 2003 study[76]. In this work, the authors prepared several eutectic mixtures using a molar ratio of 1:2 of choline chloride (ChCl) and an amide. The focus of the study was to analyse the reduction in the freezing point of these mixtures compared to their individual components. They observed that the mixtures remained liquid at room temperature and exhibited remarkable solvent properties. Key findings included a significant decrease in melting points due to hydrogen bonding, particularly observed in the mixture of ChCl with urea, which had a freezing point of 12 °C. Additionally, the researchers emphasised the high solubility of salts, organic acids, and amino acids in this eutectic mixture. These solvents demonstrated high conductivity and the ability to dissolve metal oxides, making them versatile for various applications.

Although DES emerged as an alternative to ionic liquids, they possess significant properties that make them more environmentally friendly. Key characteristics highlighted in the literature include non-volatility, ease of preparation, and non-flammability. DES are often synthesised from natural components, which enhances their biodegradability. Additionally, the preparation of these solvents requires only small quantities of reagents, and nearly all the materials used are incorporated into the final product, achieving 100% atomic efficiency. This contrasts with ionic liquids, which typically involve excess reagents and require multiple steps and longer synthesis time[40].

Overall, the number of publications with the term deep eutectic solvents has increased significantly throughout the years. Bibliographic research conducted on the Web of Science in November 2024, using the term deep eutectic solvent*, revealed a remarkable increase in publications on this topic, counting over 14,000 articles and review papers between 2004 and 2025, as illustrated in FIGURE 1.2. This substantial growth can be attributed to the unique characteristics of these solvents, which render them suitable for a wide range of applications across various fields.

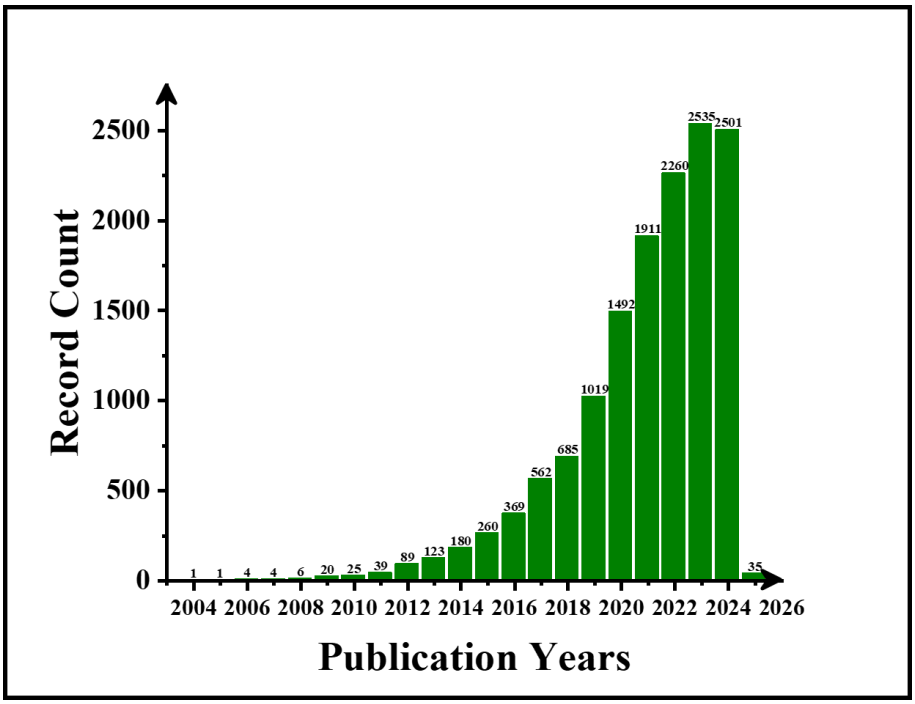

FIGURE 1.2 - Number of publications on deep eutectic solvents according to the Web of Science database (term: deep eutectic solvent*).

DES are being widely investigated and applied across various fields, as described, due to their unique characteristics[77]. In organic synthesis, these solvents are used as a green alternative to traditional solvents, while in catalysis, they facilitate diverse chemical reactions with improved yields and selectivity[18,78]. In the field of electrochemistry, the use of DES has grown significantly, as their

electrical conductive properties, wide potential range using electrodes such as glassy carbon, gold, and platinum electrodes, and ability to dissolve metal ions make them suitable for applications such as electrodeposition, electropolymerisation, supporting electrolytes, electroanalysis, and metal extraction and refining[10,11,49,50,79,80].

In pharmaceutical and biotechnological applications, DES are effective in solubilising poorly soluble drugs, making them suitable for more efficient drug delivery systems. Moreover, they are used to stabilise sensitive biomolecules, such as enzymes and proteins, preserving their activity over time. They are also valuable for the extraction of bioactive compounds, such as antioxidants, flavonoids, and other phytochemicals[81,82].

In polymer production, DES act, for example, as plasticisers, enhancing flexibility. They are also employed in processing biopolymers, such as cellulose, contributing to the creation of sustainable materials and the controlled synthesis of nanomaterials[83,84]. Furthermore, DES are effective in functionalising and/ or as a medium for creating nanomaterials, such as surface modification of carbonaceous materials and synthesis of metallic nanoparticles, which enhances their stability, dispersibility, and reactivity[51,85–87]. An example is using DES to introduce specific functional groups to carbon materials, making them more compatible with different matrices[19,86].

The use of deep eutectic solvents in electrochemistry has grown significantly over the years. A search conducted on the Web of Science using the terms deep eutectic solvent* and electrochem* revealed more than 1,600 publications on this topic, as illustrated in FIGURE 1.3. This increase can be attributed to the ability of DES to dissolve a variety of ionic and molecular compounds, as well as their acceptable ionic conductivity, thermal stability, and broad electrochemical window[10]. These properties often enable DES to outperform traditional solvents and ionic liquids in many applications.

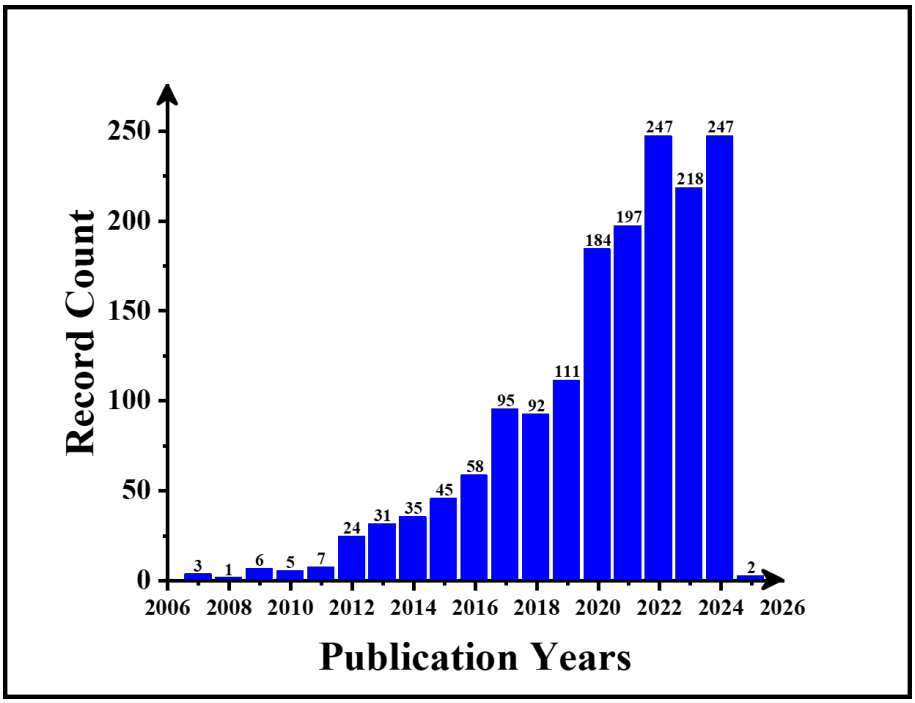

FIGURE 1.3 - Number of publications on deep eutectic solvents in electrochemistry according to the Web of Science database (terms: deep eutectic solvent* and electrochem*).

A significant application of deep eutectic solvents in electrochemistry is in the electropolymerisation and electrodeposition of conductive materials[10,11,22,88]. Researchers have found that utilizing DES improves the morphology of the resulting polymers. The controlled ionic environment that DES provides facilitates the formation of uniform, conductive, and stable polymeric films[89–92]. Additionally, in the electrodeposition of metals and alloys, DES has been shown to enhance the deposition of nanoparticles, nanowires, and thin films that have a high surface area and controlled morphology[22,54,80,93–96].

In addition to electrodeposition, DES have been explored for synthesizing nanomaterials through various approaches. These include the solvothermal method, anhydrous DES-based techniques, and the synthesis of nanoparticles in a DES medium followed by calcination in a muffle furnace[51,85,97,98]. Overall, the results in the literature indicate that DES effectively

stabilizes nanoparticles during synthesis, preventing agglomeration and ensuring uniform size distribution[22,51,96].

Our research group has successfully demonstrated the synthesis of different nanoparticles, such as platinum and cerium oxides, in a eutectic medium using the solvothermal method[51,85]. These results indicate the capability to create ultrasmall nanoparticles in DES media, which can be linked to the thermal stability offered by DES, assisting in uniform nucleation and growth throughout the synthesis process. This might account for the notable decrease in the size of the nanoparticles that were synthesized. In both studies, the synthesized nanoparticles were used to develop novel electrochemical sensors. These sensors demonstrated remarkable improvements in catalytic effect and electroanalytical response toward target analytes when utilizing nanoparticles synthesized in DES compared to conventional synthesis methods. Additionally, the performance was notably superior when compared to electrodes that did not incorporate these DES-based nanoparticles.

In the development of electrochemical sensors, several studies have explored the use of eutectic solvents as electrode modifiers. These works highlight the enhanced electrical conductivity and stability of electrodes after modification with deep eutectic solvents. Additionally, the synergistic effect between DES and other components of the electrodes, such as carbonaceous materials, nanoparticles, and polymers, has been shown to improve analytical parameters, including the limit of detection and sensitivity[49,50,79,99–104].

In previous research conducted by our group[49], we demonstrated that using a deep eutectic solvent composed of choline chloride and glycerol alongside a carbon black and a crosslinked chitosan film improved the kinetic parameters of the glassy carbon electrode when evaluated with the well-known redox probe, hexacyanoferrate(II/III) ($[Fe(CN)_6]^{4-/3-}$). However, there was no increase in surface area observed. Similar enhancements were noted when assessing the

target analytes, diclofenac and acetaminophen. The authors concluded that the increases in current were related to a kinetic factor, suggesting that the analytes accumulate on the electrode surface. This was supported by scanning electron microscopy results, which indicated that the addition of DES coat the carbon black nanoparticles, thereby facilitating the adsorption of the analytes, as confirmed by differential pulse adsorptive stripping voltammetry results.

As demonstrated, DES plays a crucial role in electrochemistry, particularly as a modifier for developing novel electrodes. The effect of DES varies depending on the type of carbonaceous material and other particles used in the electrode, as well as the specific DES composition. This variability comes from how DES interacts with these materials to enhance the electrode's properties.

1.2.1.1 - Classification of Deep Eutectic Solvents

Initially, DES were categorized based on the following general formula:

$$Cat^+ X^- zY$$

Cat^+ can be any ammonium, phosphonium, or sulfonium cation. Among these, quaternary ammonium salts are the most used (*e.g.*, choline chloride and tetrabutylammonium salts). The species X^- is typically a Lewis base, often a halide anion, while Y represents a Brønsted or Lewis acid, with *z* indicating the number of Y molecules present[77,105].

Based on the general formula provided, these solvents were categorized into four main types, as summarised in TABLE 1.3:

TABLE 1.3 - General classification of deep eutectic solvents

Type	General Formula	Example
I	$Cat^+ X^- + zY$	Y (metal salt) = $ZnCl_2$
II	$Cat^+ X^- + zY \bullet zH_2O$	Y = Cr, Co, Cu, Ni (hydrated metal salt)
III	$Cat^+ X^- + z$HBD	HBD = amide, fatty acid, alcohol
IV	Y + HBD	Y (metal salt) = $ZnCl_2$

HBD: hydrogen bond donor.

Types I, II, and IV are frequently compared to ionic liquids, especially when involving imidazolium salts combined with metal halides or chloroaluminate[77].

Type III deep eutectic solvents are the most researched in literature. They mainly consist of quaternary ammonium salts as the $Cat^+ X^-$, known as hydrogen bond acceptors (HBAs), combined with various hydrogen bond donors (HBDs). The most used HBAs include choline chloride and tetrabutylammonium salts, such as tetrabutylammonium chloride and tetrabutylammonium bromide. Among the hydrogen bond donors, fatty acids, amides, and alcohols are particularly notable. Examples include octanoic acid, decanoic acid, urea, glycerol, and ethylene glycol[77,105]. FIGURE *1.4* shows some of the main HBDs used in combination with quaternary ammonium salts for the formation of Type III DES.

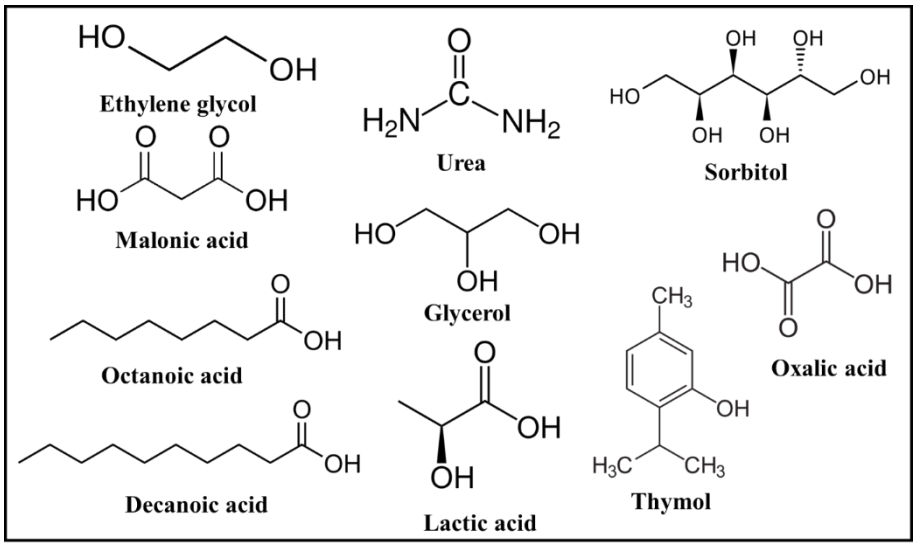

FIGURE 1.4 - Main hydrogen bond donors used for the formation of Type III DES.

Additionally, in 2019, Abranches *et al.* introduced a new category of DES known as type V[106], which consists solely of molecular substances that function as HBA and HBD. Their study explored mixtures of non-ionic compounds like the thymol-menthol system and identified a strong interaction from the contrasting acidity between phenolic and aliphatic hydroxyl groups. This interaction is key to forming stable non-ionic DES, expanding potential applications due to their favourable properties.

Following, types III, IV, and V DES are further categorized based on the origin of their components. Common classifications in the literature include[107,108]:

i. Natural Deep Eutectic Solvents (NADES)
ii. Hydrophobic Deep Eutectic Solvents (HDES)
iii. Therapeutic Deep Eutectic Solvents (THEDES)
iv. Amino Acid Deep Eutectic Solvents (AADES)
v. Magnetic Deep Eutectic Solvents (MDES)
vi. Water-based Deep Eutectic Solvents (WDES)

vii. Polymerized Deep Eutectic Solvents (PDES)

viii. Supramolecular Deep Eutectic Solvents (SUPRADES)

ix. Acidic or Basic Deep Eutectic Solvents (ADES or BDES)

Natural deep eutectic solvents are a subclass of DES derived from natural, bio-based compounds like sugars, amino acids, organic acids, and other plant-derived substances. These solvents are of particular interest due to their biocompatibility, non-toxicity, and biodegradability, making them ideal for applications in the food, pharmaceutical, and cosmetic industries. They often mimic the natural microenvironment found in living organisms, facilitating the extraction, stabilization, and delivery of bioactive compounds. NADES are also valued for their ability to dissolve a wide range of polar and non-polar substances, offering a green alternative to conventional organic solvents[42,109].

Hydrophobic deep eutectic solvents are a category of DES characterized by their water-repelling properties. HDES are formed using hydrophobic components, including long-chain fatty acids or alcohols, which result in a non-polar solvent medium. This makes them suitable for non-aqueous applications, such as extraction and separation processes and catalytic reactions in organic media. HDES are gaining attention as sustainable alternatives to conventional organic solvents, presenting features such as low volatility and adjustable solubility[21,110].

Therapeutic deep eutectic solvents are a specialised subclass of deep eutectic solvents designed for biomedical and pharmaceutical applications. Unlike traditional DES, THEDES incorporate Active Pharmaceutical Ingredients (APIs) as one of their core components, making them an integral part of drug formulation and delivery. These solvents are designed to emphasise therapeutic activity, stability, and safety, often using naturally derived compounds such as amino acids, organic acids, sugars, or other bioactive substances[108,111].

The main advantages of THEDES include improved solubility, enhanced drug stability, controlled drug release, biocompatibility, and minimal toxicity. These features make them ideal for diverse medical applications, such as advanced drug delivery systems, topical formulations, and the stabilisation and delivery of natural bioactive compounds[111,112].

Amino Acid deep eutectic solvents are a subgroup of DES that incorporate amino acids as key components. These solvents are gaining attention toward developing biocompatible and sustainable alternatives to conventional solvents, with applications comprising pharmaceuticals, biotechnology, and green chemistry. Using amino acids in AADES ensures several desirable properties, including biocompatibility, non-toxicity, versatility, and sustainability. Overall, AADES aims to offer a promising platform for creating safe, adaptable, and environmentally friendly solvents that meet the demands of pharmaceutical, biotechnological, and industrial applications[113,114].

Magnetic deep eutectic solvents are a type of deep eutectic solvent that includes magnetic components, such as metal salts, metal nanoparticles, or magnetic ionic liquids, which give magnetic properties to the solvent. This category of solvents is gaining attention for its potential applications in separation processes, catalysis, environmental remediation, and other fields that can benefit from magnetic responsiveness. MDES combine the versatility of traditional DES with the advantages of magnetic materials, offering a unique solution to various scientific and industrial challenges[115,116].

Water-based deep eutectic solvents combine water with traditional DES components to improve solubility, reduce viscosity, and enhance sustainability. Water in DES has been studied in various roles, such as a precursor, impurity, or intentionally added component to modify the solvent's physicochemical properties. These solvents benefit applications including

extraction, catalysis, and electrochemistry due to their tuneable properties, biocompatibility, and low toxicity[14,117,118].

Research has shown that the presence of water leads to the weakening of hydrogen bonds between DES components, especially at higher water concentrations. As water is added, the viscosity and density of the mixture decrease, suggesting a reduction in the interaction strength between the components. Even small amounts of water can significantly alter the molecular dynamics of DES, impacting their overall behaviour and properties[14].

Polymerized deep eutectic solvents are a subclass of DES where the solvent system is chemically polymerized to create a more stable, solid, or gel-like material. The polymerization of DES is achieved by crosslinking one or more components, which alters the original liquid state into a solid or semi-solid form. PDES combine the benefits of DES, such as biocompatibility, low toxicity, and sustainability, with enhanced mechanical properties, such as higher viscosity and stability. These properties make PDES attractive for applications as environmentally friendly polymer materials[119,120].

Supramolecular deep eutectic solvents are a class of DES that rely on supramolecular interactions, such as host-guest interactions, to stabilize their structure. Components such as cyclodextrins are essential in facilitating these interactions. SUPRADES offer additional functionalities compared to traditional DES, including the potential for dynamic reactivity and improved solubility for various substrates. They are being investigated for a wide range of applications, including catalysis, extraction, encapsulation, and the delivery of functional components, as well as food analysis and sensing. Their tunability and selective interaction with target molecules makes SUPRADES a promising area of research[108,121,122].

Acidic or Basic deep eutectic solvents are categories of deep eutectic solvents characterized by their acidic and basic components, respectively[108].

ADES consists of components like organic acids or acidic salts, resulting in a medium with a low pH. They are particularly useful for applications such as dissolution, extraction, organic reactions, and metal electrodeposition[123].

On the other hand, BDES contain basic compounds such as urea or amines, leading to a high pH environment. BDES are advantageous for base-catalysed reactions, biomass processing, and deprotonation processes. Both ADES and BDES offer the ability to adjust pH levels to optimize reaction conditions, which enhances their use in various fields, including catalysis, separation, and material synthesis[124]. The unique properties of ADES and BDES enable the targeted solubilization of specific compounds, making them valuable for a range of applications.

Overall, most of the cited classes of deep eutectic solvents fall under the categories of NADES and HDES. This is mainly because the precursors in these categories are often derived from natural sources and include hydrophobic components, making them suitable for several applications. Hence, the next section will focus on hydrophobic deep eutectic solvents, which was the focus of this doctoral research.

1.2.1.1.1 - Hydrophobic Deep Eutectic Solvents

Hydrophobic deep eutectic solvents were first studied by van Osch *et al.* (2015)[125]. In this study, the authors explored the development and application of HDES composed of decanoic acid and various quaternary ammonium salts. These solvents are designed to be immiscible with water, allowing for efficient extraction of volatile fatty acids from aqueous solutions. The research highlighted that the extraction efficiency is influenced by the alkyl chain length of the components, with longer chains enhancing hydrophobicity. HDES were shown to be a sustainable and green alternative to traditional solvents,

offering high selectivity and efficiency for separation processes, emphasizing their potential in environmentally friendly chemical applications.

In relation to the types, the HDES can be classified into two main categories based on their ionic or neutral nature: ionic HDES and neutral HDES. Both types share the fundamental characteristics of being eutectic mixtures but differ in their overall charge properties and behaviour. Ionic HDES contain at least one ionic component, typically a quaternary ammonium salt, that provides charge carriers within the solvent alongside a fatty acid such as decanoic acid. These systems have similar characteristics to ionic liquids but with the added benefit of being less expensive and more environmentally friendly. In contrast, neutral HDES are made from non-ionic components, where neither of the components is ionic. A typical example would be a combination of menthol with fatty acids, such as octanoic acid. These solvents rely on hydrogen bonding between the components for their functionality, and they are typically more hydrophobic fluids than ionic HDES[126,127].

Since their development, HDES have found widespread use, particularly in separation and extraction, for isolating non-polar and water-insoluble compounds like phenolics and fatty acids from aqueous solutions [128–131]. They are also effective in environmental remediation, removing pollutants—such as heavy metals, dyes, and oils—from water[132–137]. Additionally, HDES are employed to extract target analytes across various samples, such as bioactive compounds from plants[138–143], and nutraceuticals, dyes and fatty acids from food[48,144–147]. Apart from these primary applications, HDES are utilized in catalysis as a medium for water-sensitive organic reactions[148] and in electrochemistry for applications such as supporting electrolyte and electroanalysis[50,149–153].

In the field of electrochemistry, it is important to mention that the use of HDES has been somewhat limited. However, the studies conducted so far

demonstrate remarkable features of HDES in electrochemical properties in different applications, such as electrode modifiers and supporting electrolytes.

Ruggeri *et al.* (2019)[149] investigated the electrochemical behaviour of HDES based on tetrabutylammonium chloride and decanoic acid in a 1:2 molar ratio. The authors examined characteristics such as density, viscosity, and ionic conductivity of various HDES prepared with different water contents. These included anhydrous conditions, equilibrium with the atmosphere, equilibrium with water vapour saturated at 30 °C, and equilibrium with water vapour saturated at 60 °C. According to the authors, the HDES in equilibrium with water-vapour saturated at 60 °C exhibited higher conductivity and lower viscosity levels, effectively reducing solution resistance to acceptable values, thus enabling efficient mass transfer to and from the electrode surface. They proposed that water disrupts hydrogen bond interactions between the components in the hydrophobic eutectic solvent, which increases ionic mobility within the medium. Furthermore, the research highlights the applicability of these solvents in electrochemical processes, noting their wide electrochemical potential window and suitability for reversible redox systems. The study also evaluates the potential of HDES in liquid-liquid extraction of metal ions, illustrating their versatility in separation processes.

In a previous report by our research group (2022)[50], we investigated the use of different hydrophobic deep eutectic solvents synthesised from fatty acids in combination with tetrabutylammonium bromide or 1-octanol. Our focus was on modifying carbon paste electrodes to develop a novel electrode for detecting hydroquinone. The results indicated that incorporating HDES into the carbon paste electrode significantly enhanced its electroanalytical properties. This improvement was attributed to the improved interactions between the graphite particles, which, in turn, enhanced the kinetic parameters of the electrode. Consequently, the electrode exhibited a wide linear range for hydroquinone

detection and a low detection limit, making it effective for analysing real-world samples, such as dermatological creams.

In a study published by Chaabene *et al.* (2020)[150], the authors proposed using an HDES made from menthol, ethanolamine, and acetic acid as a supporting electrolyte. They evaluated the electrochemical behaviour of hydroxymethyl ferrocene in this eutectic medium, determining the diffusion coefficient and comparing it to the same experiment conducted in an ionic liquid medium. The results indicated that the HDES developed in this study was suitable for electrochemical experiments.

The main limitations of hydrophobic deep eutectic solvents are their low conductivity and high viscosity, which slow charge transfer and mass transport. These issues are often linked to low water content. Increasing water content can improve conductivity and reduce viscosity, enhancing mass transfer and electrode efficiency[149,154]. However, excessive water can compromise DES stability[154,155]. Despite these challenges, the examples above highlight the successful application of HDES in electrochemical procedures.

1.2.1.2 - Synthesis of Deep Eutectic Solvents

Deep eutectic solvents are prepared by mixing at least two components to form the eutectic mixture. The literature reports various synthesis methods, including microwave-assisted, mechanical mixing and grinding, ultrasonic, vacuum evaporation, freeze-drying, and heating and stirring methods[83,156].

Microwave-assisted synthesis provides several advantages over conventional heating methods, such as faster reaction times, reduced energy consumption, and potentially higher yields. In this synthesis process, precursors are irradiated in a closed system at controlled power and temperature. According to the literature, the radiation interacts with the material, causing dipole rotation

that leads to molecular collisions among the precursors. These results are in dielectric heating, which shortens the synthesis time[156–158]. For instance, a study by Gomes *et al.* (2018)[158] reported a synthesis time of just 20 seconds using a microwave. However, the authors noted that further research is necessary to evaluate the use of microwaves for preparing DES with different components. In fact, Santana *et al.* (2019)[157] observed that, when using microwaves, the energy consumption was higher compared to other methods, and the synthesis time was not as quick as indicated, for example, in the previous study. However, the authors still emphasized the speed and effectiveness of microwaves in preparing DES.

The grinding method involves mixing the compounds at room temperature and grinding them in a mortar with a pestle until a clear liquid is formed[83]. In a 2014 study[159], the authors examined two synthetic methodologies, heating and grinding, to prepare DES. Nuclear Magnetic Resonance studies indicated that the DES obtained through the grinding method was purer than those synthesized using the heating method, which showed impurities. Furthermore, to effectively use the grinding methodology, it is important to consider the compatibility between the components, as not all combinations are suitable for grinding. Some mixtures may require heating to enhance interaction. Additionally, the molar ratio must be carefully determined to achieve the desired properties, since incorrect ratios can impact the formation of the eutectic mixture.

Ultrasound-assisted synthesis is a technique that uses ultrasonic waves to improve the mixing and interaction of components in order to form a deep eutectic solvent. Like the microwave method, ultrasound-assisted synthesis offers several advantages, including shorter reaction times, lower energy consumption, and potentially enhanced yields or properties of the resulting DES[156,157]. A study has shown that ultrasound-assisted synthesis is one of the most energy-efficient methods, using approximately 130% less energy (0.006 kWh mL^{-1}) than traditional heating and stirring methods (0.014 kWh mL^{-1})[157].

However, this technique requires a semi-fluid environment for the sound waves to propagate effectively, which means that at least one of the components must be in liquid form[156].

In the evaporation method, the components of the DES are initially dissolved in an additional solvent, typically water, to ensure uniform mixing. Once a homogeneous solution is achieved, the solvent is evaporated under reduced pressure—often using a rotary evaporator—to prevent thermal degradation of the components. The remaining viscous liquid is then placed in a desiccator until it reaches a constant weight, indicating that all residual solvent has been removed.

For the freeze-drying method, a small amount of water (about 5 % by mass) is added to dissolve the components. The solution is frozen to immobilize the mixture and then subjected to freeze-drying (lyophilization) to remove the water under vacuum, resulting in a clear and homogeneous liquid DES[156,160]. Gutiérrez *et al.* (2009)[161] demonstrated the preparation of DES using lyophilization. They first prepared aqueous solutions of the DES precursors, choline chloride and urea, in the desired molar ratio. The resulting solutions were mixed, frozen, and then lyophilized, yielding a viscous liquid. According to the researchers, this technique is advantageous for incorporating additional components into the eutectic mixture, allowing for a broader range of tailored properties in the final DES.

Although the methods described above significantly present characteristics such as reduced synthesis time and energy consumption, the most used method remains the heating and stirring technique. This approach is one of the simplest and most popular ways to synthesise deep eutectic solvents. It primarily utilises a magnetic stirring plate, allowing for the preparation of large quantities of DES. In this method, a glass vessel is used to heat the components of the DES while stirring them. This facilitates the formation of a homogeneous

eutectic mixture. Typically, the temperatures employed for preparing DES are below 100 ºC, and the synthesis time usually ranges from 1 to 2 hours. These parameters can vary depending on the characteristics, such as melting point and stability of the precursors used[157,162].

Despite some studies promoting 'green synthesis' methods, such as microwave-assisted synthesis, due to their rapid preparation and low energy consumption, it's important to note that many laboratories lack this type of equipment to prepare DES using these methods. A comparative study has shown that the electricity consumption for synthesising DES was 0.014 kWh mL^{-1} when using heating and stirring (2 hours of synthesis), compared to 0.106 kWh mL^{-1} for microwave-assisted synthesis (45 minutes of synthesis). Additionally, the EcoScale scores [163] for the DES synthesized by these methods were 97 for heating and stirring and 94 for microwave. According to the authors, scores above 75 indicate an excellent green procedure according to the EcoScale criteria[157,160]. On the other hand, another study showed that using a microwave allowed a decrease in synthesis time from 60 minutes to 20 seconds and an energy consumption 650 times lower than the heating and stirring method[158].

The literature also indicates that the ultrasound method is the most effective when comparing these synthesis techniques, with most cases showing high energy consumption for microwave-assisted synthesis, while ultrasound and heating and stirring are somewhat comparable[157,160,164].

Overall, these results suggest that several factors must be considered when choosing a synthesis method, including the characteristics of the precursors used, the available laboratory equipment, the scalability of the method, and, primarily, the analysis of preparation time and temperature. It is worth noting that there is a significant lack of studies in the literature addressing and optimising these parameters, as many proposed synthesis times are unnecessarily long and may lead to wrong estimated energy consumption. In this doctoral thesis, the

heating and stirring method was applied and thoroughly investigated the temperature and synthesis time for a HDES to address this gap in the literature and provide insights into faster preparation times aimed at energy saving.

1.2.1.3 - Characterization of Deep Eutectic Solvents

Characterising deep eutectic solvents is crucial for understanding their physicochemical properties, interactions, and potential applications[40,77]. The primary characteristics examined include the physicochemical and thermal properties of DES. Techniques used to assess these properties include density, viscosity and conductivity measurement, water content analysis, as well as thermal analysis methods such as Thermogravimetric Analysis (TGA) and Differential Scanning Calorimetry (DSC)[40,41,165].

Electrochemical characterization is also important, employing methods such as cyclic voltammetry and electrochemical impedance spectroscopy to gather information on conductivity and the behaviour of interfaces with electrodes[49,50]. All these characterization methods are essential for gaining insights into molecular packing, intermolecular interactions, composition, mass transport, diffusion rates, and the suitability of DES for electrochemical and extraction applications. They also help in understanding the effect of moisture on DES performance, thermal stability, decomposition temperatures, phase behaviour, and crystallinity[41]. Furthermore, computational methods have been widely used, such as molecular dynamics simulations, which investigate hydrogen bonding networks and dynamic behaviour. These simulations also analyse the electronic structure and energy interactions within DES[166–168].

Some of the properties mentioned will be discussed in more detail below.

1.2.1.1.1 - Physicochemical Properties

Understanding the physicochemical properties of DES is crucial for optimising their applications in fields such as electrochemistry, pharmaceuticals, biotechnology, and green chemistry. These properties are determined by the nature of the components and their interactions. As previously discussed, water plays a significant role in the physicochemical properties, stability, and functionality of DES. Its impact can be either beneficial or detrimental, depending on the concentration and the specific application of the DES. Additionally, water can affect key properties such as viscosity and conductivity[41,50,165].

Density is one of the most important factors that influences the solvation ability of DES. It is affected by how molecules are organized and packed, as well as the presence of holes and vacancies within the liquid DES[41,165]. Typically, DES have densities ranging from 1.0 to 1.6 g cm^{-3} at room temperature[165], while hydrophobic deep eutectic solvents can have densities lower than that of water[48,126]. Additionally, the density of DES shows temperature-dependent behaviour, decreasing linearly as the temperature increases[165].

Most reported deep eutectic solvents to date have high viscosities at room temperature, typically greater than 100 mPa s. This is primarily due to the extensive hydrogen bonding network and the van der Waals and electrostatic forces between the components of the DES, which lead to increased viscosity and decreased ionic mobility[41,165]. A notable exception is the mixture of choline chloride and ethylene glycol in a 1:2 ratio, which has a viscosity of 37 mPa·s at 25 °C. In contrast, deep eutectic solvents based on sugars exhibit significantly higher viscosities. For instance, a 1:1 mixture of choline chloride and sorbitol has a viscosity of 12,730 mPa s at 30 °C, while a 1:1 combination of choline chloride and glucose reaches 34,400 mPa s at 50 °C. Even higher viscosities have been recorded for deep eutectic solvents that include metal salts; for example, a 1:2

combination of choline chloride and zinc chloride has a viscosity of 85,000 mPa s at 25 °C[40].

For hydrophobic deep eutectic solvents, Florindo *et al.*[126] demonstrated that the viscosity of hydrophobic DES follows this tendency: fatty acids ≈ thymol < menthol < quaternary ammonium salts, with quaternary ammonium salts being the most viscous due to strong coulombic forces. In these salts, viscosity decreases as the alkyl chain length increases, such as from tetrabutylammonium chloride to tetraheptylammonium chloride, as better charge shielding occurs on the nitrogen atom because of the bulky alkyl side chains.

In general, deep eutectic solvents exhibit low ionic conductivity at ambient temperature because of their elevated viscosities, highlighting a significant connection between viscosity and conductivity. The ionic conductivity of DES is influenced by the molar ratio of hydrogen bond donors to hydrogen bond acceptors, the length of the alkyl chain in the cation, and the temperature[41,165].

1.2.1.1.2 - Thermal Properties and Thermodynamic Characterization

The thermal behaviour of deep eutectic solvents is an essential property for understanding their stability, performance, and potential applications. It is typically characterized using thermogravimetric analysis. TGA enable the determination of the onset temperature (T_{onset}), which is the temperature at which a material begins to experience a thermal event, such as decomposition, phase transition, or evaporation. A significant weight loss in the TGA measurements indicates this onset temperature[169].

Deep eutectic solvents typically exhibit good thermal stability, although their decomposition temperatures can vary depending on their components. Generally, DES first decompose into its components, hydrogen bond donor and hydrogen bond acceptor, at elevated temperatures due to the weakening

of hydrogen bond interactions. Following this, HBDs, especially those with relatively low boiling points or poor stabilities, may undergo volatilization or further decomposition[170].

The thermodynamics of DES revolves around understanding their phase behaviour, melting point depression, and the negative deviations from thermodynamic ideality. These deviations are driven by strong hydrogen bonding or other enthalpic interactions between components. Thermodynamic analysis focuses on properties like enthalpy and entropy, and Gibbs free energy, which explain the stability of the liquid phase, low vapour pressures, and the enhanced solvation abilities of DES.

It is possible to assess the phase behaviour of DES by studying their solid-liquid equilibrium (SLE) using DSC, which can provide melting temperature data for any system composition[171]. Understanding this data is crucial for gaining a comprehensive insight into the eutectic nature of the proposed mixture and for determining the temperature at which the eutectic point occurs.

Furthermore, recent studies have shown that the classification of a solvent as a 'deep' eutectic solvent depends on how the mixture deviates from ideal behaviour when compared to an ideal system. Specifically, negative deviations characterise the system as a deep eutectic solvent, while positive deviations indicate that it is merely a eutectic solvent[172,173]. This behaviour can be quantified using the activity coefficient (γ), in which a γ value of 1 suggests an ideal system, while a γ value less than 1 indicates a deep eutectic system[172].

Overall, accessing the thermodynamic data of DES is essential for understanding their stability, phase behaviour, and component interactions. This data facilitates the prediction of temperature-dependent properties, including viscosity, conductivity, and solubility. Moreover, thermodynamic insights are crucial for determining operational temperature ranges and ensuring thermal

stability in various processes, making DES design more efficient and reliable[171,173].

1.3 - Design of New Materials Towards Sustainability

New materials are continually being developed to tackle emerging challenges in sustainability, performance, and innovation, with green chemistry principles at their core. These materials are designed to minimize environmental impact while optimizing functionality, efficiency, and economic viability. By prioritizing sustainability and resource efficiency, they aim to reduce dependence on non-renewable resources and promote energy-efficient production processes. This approach emphasises the use of renewable resources and promotes environmentally conscious manufacturing techniques to create materials that are both innovative and sustainable. In this way, the use of natural resource feedstocks such as cellulose, starch, vegetable oils, polylactic acid (PLA), and similar materials is a preferred choice for designing materials such as packaging, 3D printing components, textiles, and disposable items[44,174–176].

In relation to the design of new materials, AM is transforming the design and development of new materials by offering opportunities for customisation, resource optimisation, and innovation in material properties. This technology facilitates the creation of complex geometries, reduces waste, and allows for the integration of advanced functionalities in a wide range of applications[12]. Given that, the second part of this doctoral thesis was to apply AM to develop new electrochemical sensors using as many sustainable methods and materials as possible.

1.4 - Additive Manufacturing

Additive manufacturing is a technology that fabricates objects by building them layer upon layer using computer-aided design (CAD). This process differs fundamentally from traditional subtractive methods, which design parts from a larger block of material, FIGURE *1.5* shows a representation of the additive manufacturing process. By selectively adding material, AM minimizes waste, enhances design flexibility, and opens unprecedented possibilities in manufacturing. Furthermore, additive manufacturing offers a sustainable alternative to conventional processes. By using only the required material, it significantly reduces waste. Furthermore, its capacity for local production reduces transportation needs, contributing to lower carbon emissions[12,46,57].

AM's versatility has led to its widespread use across various sectors. In aerospace, it allows for the creation of lightweight and complex components. In healthcare, it helps produce personalised prosthetics and implants. The automotive sector takes advantage of quick prototyping and the production of specialised parts, while the consumer goods and construction sectors utilize AM for customised, on-demand products[60].

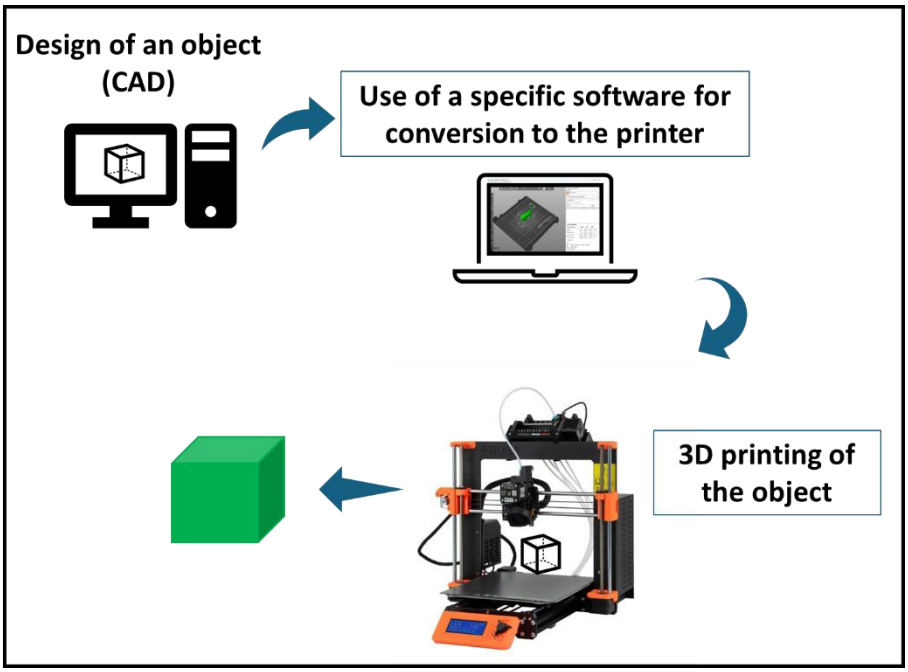

FIGURE 1.5 - Representation of a 3D printing schematic, starting from the CAD (Computer-Aided Design) model of a specific object, followed by conversion using specialised software for compatibility with the 3D printer, leading to the fabrication of the desired object.

This technology comprises various advanced techniques, including FDM (or Fused Filament Fabrication, FFF), stereolithography (SLA), selective laser sintering (SLS), and electron beam melting (EBM), each tailored to different needs. These methods utilize diverse materials such as plastics, metals, ceramics, and composites, enabling the creation of products with specific and customized properties[43].

With a focus on FDM techniques, this is one of the most widely used additive manufacturing. It involves the layer-by-layer deposition of a thermoplastic material to create 3D objects. FDM operates by feeding a thermoplastic filament through a heated nozzle, where it is melted and then deposited onto a build platform. The nozzle moves in a precise pattern, following the digital design, and lays down material in thin layers. As each layer cools, it

solidifies, and the next layer is added on top. This process is repeated until the entire object is completed[57].

FDM printers use a variety of thermoplastics, including popular materials like PLA, acrylonitrile butadiene styrene (ABS), polypropylene (PP), and polyethylene terephthalate glycol (PETG). One of the main advantages of FDM is its cost-effectiveness. The materials and equipment are relatively inexpensive compared to other 3D printing methods. FDM printers are widely accessible and used in various fields. Moreover, the process is straightforward and user-friendly, making it an ideal choice for quick prototyping[57,177].

With the advancements enabled by additive manufacturing, its application in electrochemistry has seen significant growth. AM is increasingly being explored for its potential to enhance electrochemical and electroanalytical applications, offering new possibilities for the development of customised, high-performance electrodes, sensors, and devices for various applications, such as energy storage and sensing[12].

1.4.1 - Additive Manufacturing and the Development of Electrodes

Additive manufacturing has become promising in the development of electrochemical devices. The ability to control geometry, integrate different materials, and rapidly prototype devices makes AM a powerful tool for electrochemical technologies. Researchers are increasingly turning to FDM, as it utilizes thermoplastic filaments and benefits from the availability of electrically conductive filaments as effective electrode materials. The most used filament is Protopasta®, one of the first commercially available conductive printing materials. This filament consists of PLA (over 65 wt%) as the primary component,

an unidentified polymer (less than 12.7 wt%) serving as a plasticiser, and carbon black (under 21.43 wt%) as the conductive material[12,57].

Various studies have harnessed the conductive properties of Protopasta® to develop novel electrochemical devices for a wide range of analytical applications. Silva *et al.* (2024) developed a fully 3D-printed electrochemical sensor for detecting gallic acid in complex samples. The authors used additive manufacturing to fabricate the entire sensing platform, including the electrodes, which were made of Protopasta® conductive filament. The sensor's performance was evaluated through electrochemical measurements, demonstrating high sensitivity and selectivity for gallic acid, even in complex sample matrices[178]. Also, Veloso *et al.* (2024) proposed a novel method to enhance the electrochemical performance of 3D-printed electrodes for glucose detection. The authors improved the conductivity of 3D-printed electrodes from Protopasta® conductive filament by depositing a nanostructured gold film directly onto the electrode surface using infrared laser photothermal treatment. The modified electrodes demonstrated a 44-fold increase in current response for glucose oxidation compared to a standard gold disc electrode, indicating significantly improved electrochemical performance[179].

Although conductive filament from Protopasta® has found extensive applications, the literature highlights certain limitations, particularly the high electrical resistance of this filament[46,64], which negatively affects its performance in analytical applications. To address this challenge, researchers have developed new conductive filaments incorporating various carbon-based materials, such as graphite, graphene, and multi-walled carbon nanotubes (MWCNTs)[47,64,180]. Additionally, alternative polymers like Poly(ethylene terephthalate glycol (PETg)[59] and polypropylene[63] have been explored, as well as different plasticisers[46,181] and metallic nanoparticles[182] to further enhance the properties and versatility of these conductive filaments.

In addition, Bernalte *et al.* (2025) introduced an innovative strategy to enhance the electrochemical performance of 3D-printed electrodes by integrating gold nanoparticles into conductive filaments. In their approach, graphite flakes served a dual purpose as a natural reducing agent for forming AuNPs and as a contributor to the filament's conductivity. The AuNP-graphite was combined with recycled PLA, carbon black, and castor oil, as a plasticiser, to produce a conductive filament. Electrodes fabricated from this novel filament demonstrated notable improvements in their electrochemical performance. As a proof of concept, these electrodes were effectively employed for lead(II) detection, achieving a sensitivity of 37 nA ppb^{-1} and a detection limit of 0.89 ppb. The method was successfully validated for the analysis of lead(II) in river water samples, highlighting its practical applicability[45].

1.5 - Conducting Carbonaceous Materials in the Development of Electrodes

Carbonaceous materials play an important role in the development of electrodes due to their remarkable properties. Overall, these materials are known for their high electrical conductivity, large surface area, chemical stability, and versatility in functionalization. Their application covers various technologies, such as batteries, supercapacitors, fuel cells, and electrochemical sensors[183–186]. The unique structural features of carbonaceous materials enable enhanced electron transfer, improved electrochemical performance, and tailored surface interactions with target analytes[186,187].

This thesis shows the use of carbonaceous materials in the development of electrochemical sensors, focusing on the properties they impart to electrode performance. Specifically, it highlights the application of carbon black, MWCNT, graphite, glassy carbon (GC), and carbon nanohorns (CNH). A

selection of each material was based on previously reported studies in the literature and research conducted in our laboratory, specifically focused on optimisations using DES[45–47,49–51,62,188].

Carbon black was chosen as the carbonaceous base material for filament development. According to the literature, CB is widely used for this purpose due to its properties and compatibility with PLA. As demonstrated by Hussain *et al.* (2023)[188], CB/PLA composites enabled the printing of complex shapes with high definition and reproducibility, outperforming other thermoplastic materials based on carbon materials, such as graphite, graphene, and MWCNTs. Graphite was chosen as a complementary material to CB in filament development, primarily because it is a natural material, supporting the sustainable aspect of the study, and it is considered a low-cost material[47,62]. This enables the production of a low-cost filament, as evidenced in a previous study (2024), contributing to more sustainable practices[47]. Finally, the selection of materials such as CNH, MWCNT, and the GCE, used as a base for modifications, was based on compatibility studies with DES conducted by our research group.

Additionally, these materials were chosen due to their unique properties. For example, CB is one of the most used carbon materials in electrochemical applications[189,190]. It is a fine, black powder composed primarily of elemental carbon in the form of tiny, spherical particles, characterized by its amorphous structure, high surface area, and greater thermal and chemical stability. Produced through the partial combustion or thermal decomposition of hydrocarbons, it exhibits unique properties that make it an important material in a wide range of applications[187,189,191,192]. Its small particle size (ranging from 3 to 100 nm) and ability to form aggregates provide a significant surface area, ideal for applications requiring enhanced reactivity or conductivity. Its high electrical conductivity and strong dispersibility in various media further broaden its utility in the development of electrochemical sensors[187,193,194].

Similarly, MWCNT, a type of carbon nanotube consisting of multiple concentric layers of graphene sheets composed of sp^2 carbon, are widely used in the development of electrodes due to their high surface area, excellent electrical conductivity, mechanical strength, and chemical stability. These properties enhance electron transfer, improve reaction efficiency, and increase the active surface area for electrochemical reactions. Additionally, MWCNTs can be functionalized to tailor their properties, making them versatile for a range of applications requiring improved sensitivity electrodes[195–197].

Following, graphite is a naturally occurring form of crystalline carbon known for its unique structure and diverse applications. It is a crystalline form of carbon characterized by its layered structure. Each layer consists of carbon atoms arranged in a hexagonal lattice, forming strong covalent bonds within the plane, while weaker van der Waals forces hold the layers together. This unique structure imparts graphite with excellent electrical conductivity, as the delocalized electrons within its layers facilitate efficient electron flow[198]. Additionally, its chemical stability and ease of functionalization make it a versatile material, particularly in the development of electrochemical sensors. These sensors are important in detecting a wide range of analytes in fields such as environmental monitoring, medical diagnostics, and food safety[9,199–201].

Likewise, GC is a different form of carbon that combines the properties of graphite and glass. Its structure can be described as a hybrid between the graphitic and amorphous states. Unlike graphite, GC lacks a well-defined layered structure. It consists of randomly oriented carbon planes, forming a three-dimensional network. Also, GC does not convert to graphite, even at very high temperatures, due to its structural arrangement[202,203]. In electrochemical applications, especially in the development of electrochemical sensors, GC is widely applied as GC electrodes. Glassy carbon electrodes are indispensable tools in electrochemical research and applied science. Their properties, including

chemical inertness, a wide potential window, and ease of modification, make them ideal for diverse applications. The modification of GCE enhances their performance by improving sensitivity, selectivity, and catalytic properties for specific applications[204–206].

Finally, carbon nanohorns are a class of nanomaterials that belong to the family of carbon nanotubes. They are essentially cone-shaped aggregates of graphene sheets, forming hollow, horn-like structures that simulate the shape of a horn. Also, the CNHs can form spherical aggregates known as dahlia, bud, and seed aggregates based on their appearances[207,208]. CNHs have attracted significant attention due to their properties, including high surface area, electrical conductivity, and chemical stability, which make them ideal candidates for various applications in fields such as energy applications and electrochemical sensors[209,210].

1.6 - Analytical Applications

Electroanalytical techniques are promising for monitoring target analytes due to their short analysis times and the production of results characterised by high precision and sensitivity. This prominence is attributed mainly to the ability to employ various materials in the preparation and/or modification of sensors and biosensors, which enables significant improvements in lowering detection limits and enhancing selectivity[8].

These techniques comprise the use of an electrochemical cell, which is the fundamental setup to study redox reactions, electrode processes, and material properties. The most used configuration is the three-electrode system, which consists of a working electrode (WE), which is the electrode where the electrochemical reaction of interest occurs (*e.g.,* glassy carbon, 3D-printed electrodes). Also, it comprises a reference electrode (RE), that maintains a stable

potential and serves as a reference for measuring the working electrode's potential (*e.g.,* Ag/AgCl or saturated calomel electrode), and a counter (auxiliary) electrode (CE), that completes the circuit by allowing current to flow (*e.g.,* platinum wire or graphite)[211,212].

Moreover, electroanalytical techniques include voltammetric, amperometric, and other techniques, each offering distinct advantages depending on the application. The voltammetric techniques involve sweeping or pulsing the potential of the working electrode while measuring the resulting current. They are widely used for studying redox reactions, electrode modifications, and sensor development. Examples include cyclic voltammetry (CV), differential pulse voltammetry (DPV), and square wave voltammetry (SWV). The amperometric techniques measure the current response over time at a fixed or stepped potential. They are commonly used in sensors and kinetic studies. An example includes chronoamperometry (CA), in which a potential is applied to the working electrode, and the resulting current response is recorded over time[212].

Overall, electroanalytical techniques help minimise issues related to interferents, due to the possibility of adding materials to improve selectivity, for example, the use of enzymes to construct biosensors and the use of antigen-antibody in immunosensors[213,214]. Furthermore, using techniques such as additive manufacturing facilitates the development of portable devices for *in situ* analyses[215,216]. Another advantage is cost reduction, as low-cost materials can be used to construct these devices. All these attributes make electroanalytical techniques a promising tool, particularly in the preparation and application of more accessible and efficient electrochemical devices[7,8,217].

Regarding applications for diagnosis, several researchers have been exploring different approaches to develop new electrochemical sensors that can enhance the detection of important substances, such as biomarkers and neurotransmitters, as these compounds play a crucial role in diagnostic

applications[6,85,218]. In this context, serotonin (5–HT) (FIGURE *1.6*A) plays a significant role in the human body, regulating emotions, mood, appetite, and sleep. Monitoring 5–HT levels in the body is vital, as abnormal concentrations can be linked to various diseases and disorders[219]. Therefore, it is essential to invest in sensitive methods capable of detecting 5–HT in a straightforward and rapid manner. Numerous studies in the literature have aimed to create electrochemical sensors modified with various materials, such as metallic nanoparticles, conductive polymers, and carbon materials for this purpose[220–224], especially considering the well-known electrochemical behaviour of this analyte, facilitating its analysis using electroanalytical techniques (FIGURE *1.6*B).

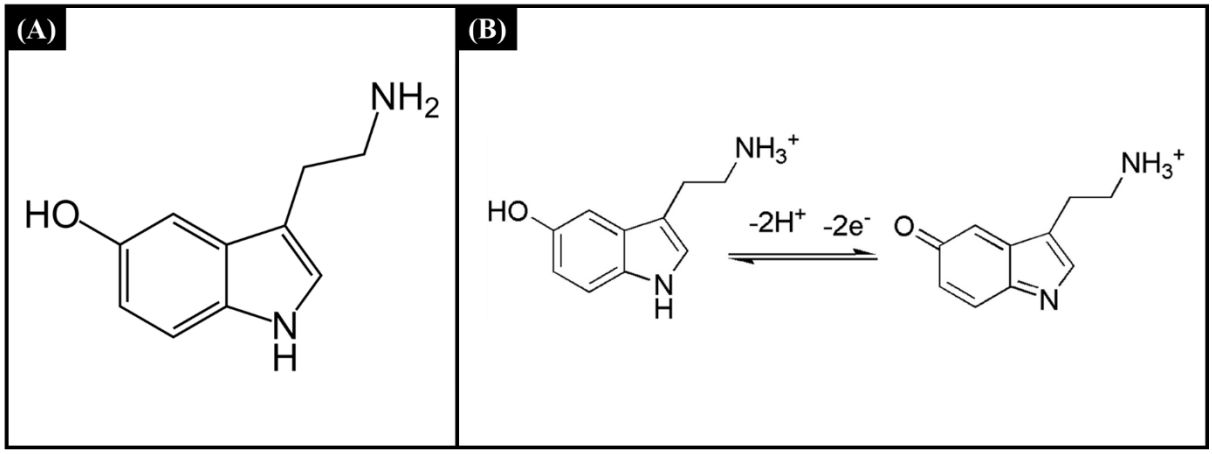

FIGURE 1.6 – (A) Serotonin molecule and (B) Electrochemical oxidation of serotonin.

Equally important are electrochemical sensors developed for environmental monitoring. The literature has shown several electrochemical sensors that offer promising solutions for enhancing environmental monitoring, allowing more effective detection of trace levels of pollutants, such as heavy metals, pesticides, and organic contaminants[5,45,47,225].

In this sense, heavy metals have been one of the major environmental pollutants due to industrial use and release. Cadmium (Cd(II)) concentrations

have increased in environmental water due to the industrial development and agriculture. Exposure to Cd(II) is concerning as it binds to protein sites, displaces essential metals, accumulates in the body, and causes harm, leading to health issues like cancer, kidney dysfunction, hypertension, and damage to the immune and nervous systems[226]. The World Health Organization (WHO) has established a maximum allowable concentration of 5 ppb for Cd (II)[227]. In this way, various methodologies using different carbonaceous materials as well as enzymes, bismuth, and ionic liquids, among other materials, aim for Cd (II) detection to meet WHO standards[228–231].

Moreover, in relation to pesticide use, the herbicide diuron (DIU) (FIGURE *1.7*) is widely used in agriculture for controlling a broad range of weeds and is also recognized as a biologically active pollutant with significant health and environmental risks[232]. Consequently, developing effective methodologies for monitoring this pesticide in the environment is extremely important. In this context, researchers have proposed novel electrochemical approaches based on polymers[233], 3D printing[234], and different composites[235–237] to enhance the detection and quantification of this pollutant, based on its electrochemical behaviour, which undergoes irreversible oxidation at the electrode surface and can involve electron transfer in the urea group. This process may generate reactive radical intermediates that can subsequently undergo coupling reactions, leading to the formation of dimers[238] (FIGURE *1.7*).

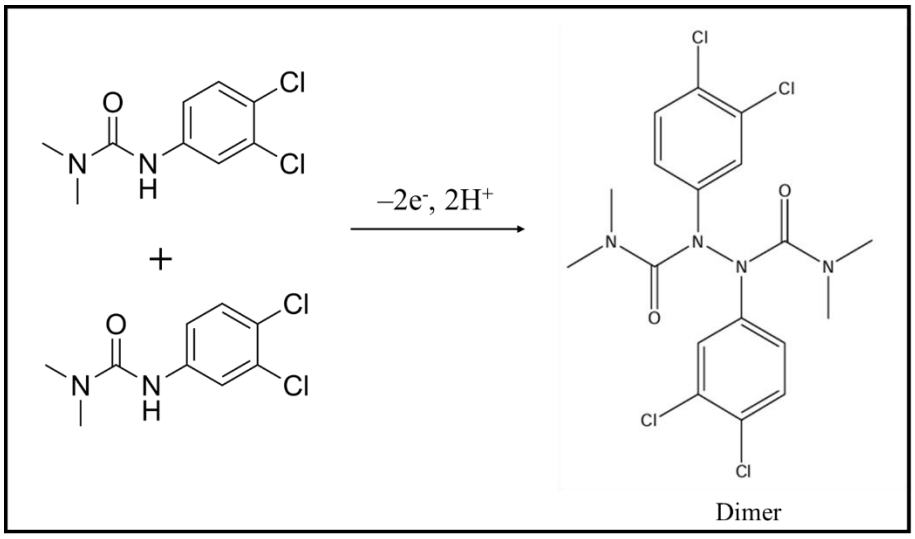

FIGURE 1.7 - Diuron electrochemical behaviour involving the formation of a dimer. Adapted from Foukmeniok *et al.* (2022)[238].

Finally, the presence of pharmaceuticals in water has emerged as a significant environmental concern due to their persistence and potential adverse effects on ecosystems and human health. Among these, acetaminophen (ACP, FIGURE *1.8*), or paracetamol, a widely used over-the-counter analgesic and antipyretic, has gained attention as a pollutant in water sources, primarily attributed to its extensive usage and improper disposal practices[239,240]. Furthermore, ACP was selected because of its widely recognised electrochemical behaviour (FIGURE *1.8*) that is extensively reported in the literature[241]. One can highlight approaches such as composites of carbonaceous materials[239,240,242], nanoparticles[243], and paper[244] to enhance the detection of ACP in water matrices.

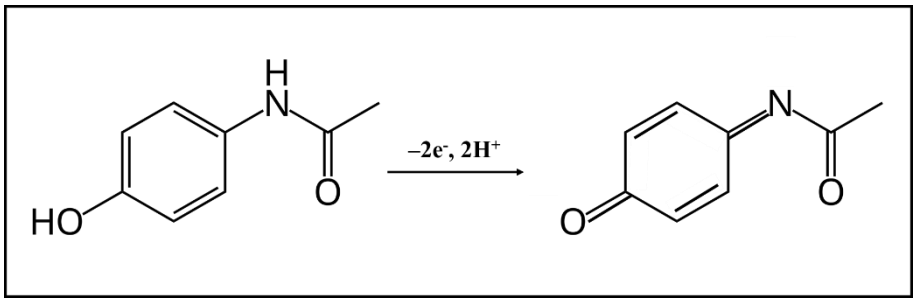

FIGURE 1.8 - Acetaminophen electrochemical oxidation.

Chapter 2

2 - OBJECTIVES

2.1 - General Objectives

This doctoral research aimed to combine hydrophobic deep eutectic solvents and 3D printing to develop novel electrochemical sensors with the goals of enhancing electrochemical conductivity, optimising analytical performance, and promoting sustainability.

2.2 - Specific Objectives

- Prepare and characterize a hydrophobic deep eutectic solvent based on decanoic acid and tetrabutylammonium bromide.
- Investigate the effect of the proposed HDES as an electrode modifier for glassy carbon electrodes and carbon paste electrodes.
- Prepare and characterize a novel sustainable silver nanoparticle-enhanced graphite filament.
- Develop an electrochemical sensor for cadmium detection in water using the modified filament.
- Utilize the proposed HDES to create a new sustainable, electrically conductive filament.
- Apply this material to develop a 3D-printed electrode for detecting acetaminophen in water.

Chapter 3

3 - EXPERIMENTAL SECTION

This chapter details the experimental procedures employed in this study. For clarity, it is structured according to the proposed work:

1) HDES characterization;
2) Development of an electrochemical sensor for serotonin detection;
3) Development of an electrochemical sensor for diuron detection;
4) Modification of a filament with silver nanoparticles for cadmium detection and Fabrication of a novel HDES-based filament.

3.1 - Hydrophobic Deep Eutectic Solvent Characterization

I. Chemicals

Tetrabutylammonium bromide (TBAB, ≥ 99.0 %) and decanoic acid (DecA, ≥ 98.0 %) were acquired from Sigma-Aldrich (St. Louis, USA) and Neon (São Paulo, Brazil), respectively. Dimethyl sulfoxide-d_6 (DMSO-d_6 ≥ 99.9 %) was purchased from Cambridge Isotope Laboratories, Inc. (Massachusetts, USA).

II. Apparatus

DSC curves were obtained in a Q10 Differential Scanning Calorimetric module, controlled by the Thermal Advantage Series® software (v.5.5.24), both from TA Instruments (New Castle, USA). Analyses were carried out using sample mass of 5.0 ± 0.1 mg, at a heating rate of 10 °C min^{-1} and under dynamic N_2 atmosphere flowing at 50 mL min^{-1}. Closed aluminium sample holders with a pin hole in the centre of the lid (ø = 0.7 mm) were utilized in all experiments. The measurements were performed in the temperature range of 223.15 to 393.15 K (–50 ºC to 120 ºC). The endothermic peak temperatures were used to characterize the melting event.

TG/DTA curves were obtained in a simultaneous TG/DTA SDT-Q600 module controlled by the Thermal Advantage software® for Q Series v.5.5.24 from TA Instruments (New Castle, USA). The measurements were performed under a dynamic nitrogen atmosphere flowing at 50 mL min^{-1} in temperatures ranging from the ambient to 873.15 K (600 ºC). After that, the atmosphere was changed to dynamic dry air (flow 50 mL min^{-1}) until 1273.15 K (1000 ºC). Sample mass of (10.0 ± 0.2) mg, heating rate of 20 °C min^{-1} and open α-alumina sample holders were used in all experiments.

The physicochemical properties of the proposed HDES were determined by viscosity, electrical conductivity, and water content assays. Viscosity measurements were performed using IKA Rotavisc viscometer model lo-vi (Staufen, Germany). Electrical conductivity was determined using a CA 150 Marconi conductivity meter (Piracicaba, São Paulo). The conductivity cell was calibrated with standard KCl aqueous solutions. The degree of uncertainty of these measurements was 2 %. The water content in the mixture was determined by the Karl-Fischer method, which was performed using an 899 KF Coulometer (Metrohm; Utrecht, Netherlands) with a generator electrode in the absence of diaphragm. A pyridine-free solvent was used in all measurements (Hydranal, Coulometer AG, Honeywell, Brazil). All measurements were carried out in triplicate at 298.15 K (25 ºC).

NMR measurements were performed on a Bruker ULTRASHIELD (Billerica, USA) operating at 400 MHz at the hydrogen frequency. The sample temperature was set at 298.15 K (25 ºC). Chemical shifts were referenced to the DMSO-d_6 solvent signal. ^{1}H NMR spectra were recorded with a spectral width of 16 ppm and with 16 scans acquired for each spectrum.

A Fourier transform infrared spectrometer model IR Prestige-21 (Shimadzu Instrument, Kyoto, Japan) was used to characterize the eutectic mixtures. The FTIR spectra were obtained in the range of 400 to 4000 cm^{-1}. An

ATR accessory was coupled to the instrument to measure HDES sample and KBr pellets were used for solids samples.

In situ mid-infrared monitoring was used to assess the formation of the HDES and estimate the optimum synthesis temperature. The experiments were performed on ReactIR™ 15 equipment (Mettler Toledo, Columbus, USA) using a DSTFP-9 AgX Fiber Conduit probe. Spectra were acquired using IC IR™ 7.0 software.

III. Hydrophobic Mixtures Preparation

Hydrophobic mixtures (HM) with different molar ratios of the fatty acid (DecA) and TBAB were prepared (TABLE 3.1), using a similar procedure as reported by Augusto *et al.* (2022)[50]. Thus, the fatty acid was melted before adding TBAB. The synthesis was conducted in closed glass vessel by controlling the temperature at 353.15 K (80 ºC) and stirring at 500 rpm until a homogeneous liquid was formed. The melting point obtained for each HM was used to plot a phase diagram aiming at finding the eutectic compositions and the eutectic point for DecA:TBAB.

The selection of the fractions described in TABLE 3.1 was based on the results obtained from DSC analysis. Initially, common ratios such as 1:1, 2:1, 3:1, and 9:1 were analysed. Based on the DSC curves, additional fractions were evaluated to confirm the eutectic point.

TABLE 3.1 - Molar ratio of the obtained hydrophobic mixtures based on decanoic acid and tetrabutylammonium bromide.

Molar Ratio (DecA:TBAB)	Components	
	DecA	TBAB
1:0	1.000	0.000
9:1	0.900	0.100
3:1	0.750	0.250
2.6:1	0.725	0.275
2.5:1	0.715	0.285
2.3:1	0.700	0.300
2:1	0.667	0.333
1.85:1	0.650	0.350
1.67:1	0.625	0.375
1.5:1	0.600	0.400
1.22:1	0.550	0.450
1.1:1	0.525	0.475
1:1	0.500	0.500
0:1	0.000	1.000

3.2 - Development of an Electrochemical Sensor for Serotonin Detection

I. Chemicals and Solutions

All chemicals were of analytical grade and used as received without any further purification. All solutions were prepared with ultrapure water (resistivity ≥ 18.0 MΩ cm) obtained from a Millipore Milli-Q system (Billerica, USA). Serotonin hydrochloride (≤ 100 %), bovine calf serum (sterile-filtered, hemoglobin ≤ 35 mg/dL), and carbon nanohorns were purchased from Sigma-Aldrich (St. Louis, USA). Potassium phosphate monobasic (≥ 99%) and

potassium phosphate dibasic (≥ 99%) were acquired from Synth (Diadema, São Paulo). A phosphate buffer solution (PB) of 0.20 mol L^{-1} pH 7.0 was used as a supporting electrolyte. A 1.0×10^{-2} mol L^{-1} 5–HT standard stock solution was prepared by dissolution in PB solution. Dilution processes were adopted to obtain different concentrations of standard solutions.

II. Apparatus

Morphological characterization of the composite films was carried out on a field-emission gun scanning electron microscopy (FEG/SEM, FEI Magellan 400 L). Also, an atomic force microscopy (Bruker Nanoscope 6 Multimode 8) was used to acquire the film topography and for roughness characterization.

Electrochemical measurements were conducted using an Autolab (Metrohm) potentiostat/galvanostat model PGSTAT101, and data was collected using NOVA 2.1.6 software. EIS measurements were performed in the frequency range from 65 kHz to 0.1 Hz, with 10 points per decade and an amplitude of 10 mV on a Sensit Smart potentiostat (PalmSens, the Netherlands) using the PStrace 5.9 software for data acquisition. The half-wave potential ($E_{1/2}$) determined via CV was used as the applied potential.

A conventional three-electrode system was used, with a platinum plate as a counter electrode (area 1.0 cm^2), the reference electrode used was Ag|AgCl/KCl (3.0 mol L^{-1}), and a glassy carbon electrode (with or without modification) as the working electrode (d = 3.0 mm). The catalytic rate constant (k_{cat}) of 5–HT oxidation in the proposed film was carried out using chronoamperometry, applying a potential of 0.35 V and an interval time of 0.01 s.

III. Preparation of Glassy Carbon Electrodes Modified with DecA:TBAB

The GCE was modified using a suspension containing DecA:TBAB and carbon nanohorns. The effect of DecA:TBAB amount (0, 3, 5, 8, and 10 mg) in the suspension was carefully studied by CV and EIS. Prior to the modification, the GCE surface was polished with 0.5 μm alumina slurry and washed with deionized water. The modifying dispersions containing DecA:TBAB and CNH were prepared as follows: 1.0 mg of CNH was suspended in 980 μL of N,N-dimethylformamide (DMF) with 20 μL of Nafion™, and DecA:TBAB. The suspensions were sonicated for 30 min in an ultrasonic bath for complete dispersion of the materials. Then, 10.0 μL of these suspensions were dropped on the GCE surface and allowed to dry in a desiccator for roughly 2 hours until the film was formed. The HDES DecA:TBAB was prepared following the procedure described in section 3.1-III.

IV. Synthetic Urine and Bovine Serum Preparation

Synthetic urine samples were prepared using the method previously described by Laube *et al.* [245], with 0.20 mmol L^{-1} KCl, 0.18 mmol L^{-1} NH_4Cl, 0.10 mmol L^{-1} NaCl, 0.10 mmol L^{-1} $CaCl_2$, 0.15 mmol L^{-1} KH_2PO_4, and 0.18 mmol L^{-1} urea in a 25 mL volumetric flask. This sample was spiked with three concentrations of 5–HT (2.0, 5.0 and 5.0 μmol L^{-1}, respectively) and recovery percentages were calculated accordingly. Similarly, the serum (bovine serum) sample was diluted 10 times with ultrapure water, spiked with three known concentrations of 5–HT (2.0, 3.0, and 5.0 μmol L^{-1}, respectively), and analysed by calculating the recovery percentage.

V. Analytical Procedure

Studies were conducted to establish the optimal conditions for determining serotonin. The optimized parameters included the pH of the supporting electrolyte as well as parameters influencing the SWV technique (TABLE 3.2) technique, namely frequency (*f*), amplitude (*a*), and potential increment (ΔE). The parameters using the DPV technique were also evaluated; however, the results for 5–HT determination were less favourable (data not shown). Therefore, SWV was selected as the optimal technique.

TABLE 3.2 - SWV optimization using 100 μmol L^{-1} 5–HT

Parameters	Studied interval
Amplitude, *a* (mV)	10 – 100
Frequency, *f* (Hz)	5 – 40
Potential increment, ΔE (mV)	1 – 10

The electrochemical characterization of the modified working electrode was performed using a 5–HT solution (100 μmol L^{-1}) in 0.2 mol L^{-1} PB solution at pH 7.0 as the supporting electrolyte, employing CV. Initially, the voltammetric profile of the analyte was evaluated using various electrodes: GCE, CNH/GCE, and electrodes modified with different HDES compositions (3, 5, 8, and 10 mg). The CV measurements were conducted in a potential window ranging from –0.1 to +0.9 V, at a scan rate of 50 mV s^{-1}.

To construct the analytical curves, successive additions of small volumes of standard solution of the analyte were performed. The limits of detection (LOD) and quantification (LOQ) were calculated using EQUATION 1 and EQUATION 2[246], respectively, where *s* is the standard deviation of 10 blank measurements (n = 10), and the slope of the analytical curve.

LOD=3×s/slope EQUATION 1

LOQ=10×s/slope EQUATION 2

The catalytic rate constant of the oxidation of 5–HT was calculated based on data obtained from a chronoamperometry study using 100 μmol L^{-1} of 5–HT at a fixed potential of 0.35 V. This study compared the influence of adding HDES to modify the electrodes. The k_{cat} values were calculated using the slope of the plot of I_{cat}/I_L *vs* $t^{1/2}$ with the EQUATION 3[247].

$$\frac{I_{cat}}{I_L} = \pi^{1/2}(k_{cat}ct)^{1/2} \qquad \text{EQUATION 3}$$

where I_{cat} and I_L are the catalytic and limited current (A) responses in the presence and absence of 5–HT, c is the concentration of 5–HT (mol L^{-1}), and t is the time (s).

The reproducibility of the voltammetric signals and the interference study in the presence of other compounds commonly found in the samples of biological fluids for 5–HT determination was studied. The inter-day and intra-day repeatability studies were performed to evaluate the sensor precision. In the intra-day repeatability, the voltammetric responses of 5–HT were measured five times in one day at three different concentrations (10, 20, and 30 μmol L^{-1}) at the same electrode. For the inter-day repeatability, SWV measurements were conducted for three days at three electrodes. In addition, the stability of the analyte's voltammetric response was assessed using CV through 100 consecutive cycles.

3.3 - Development of an Electrochemical Sensor for Diuron Detection;

I. Chemicals and Solutions

All chemicals were of analytical grade and used as received without any further purification. All solutions were prepared with ultrapure water (electric resistivity ≥18.0 MΩ cm) obtained from a Millipore Milli-Q system (Billerica, USA). Diuron (PESTANAL®, analytical standard), multiwalled carbon nanotube (O.D. × L 6-9 nm × 5 μm, > 95 % carbon), and mineral oil (≤ 100 %) were acquired from Sigma-Aldrich (St. Louis, USA). Hydroquinone (H_2Q, 99.0 %) was acquired from Vetec Ltd (Rio de Janeiro, Brazil). Boric acid (≥ 99.5 %). Potassium phosphate monobasic (≥ 99 %) and potassium phosphate dibasic (≥ 99 %) were acquired from Synth (Diadema, São Paulo).

A 1.0×10^{-2} mol L^{-1} standard stock solution of the diuron was prepared in 0.01 mol L^{-1} PB solution (pH 3.0). Dilution processes were adopted to obtain different concentrations of standard solutions. Tap water samples were obtained from the laboratory LABBES, Federal University of São Carlos, São Carlos, Brazil.

II. Apparatus

Morphological characterization of the carbon paste was carried out on a field-emission gun scanning electron microscopy (FEG/SEM, FEI Magellan 400 L).

For the analysis of diuron, electrochemical measurements were conducted using an Autolab (Metrohm) potentiostat/galvanostat model PGSTAT101, and data was collected using NOVA 2.1.6 software. Electrochemical Impedance Spectroscopy (EIS) measurements were performed in the frequency range from 65 kHz to 0.1 Hz, applying a potential of +1.1 V and 0.010 V of signal amplitude to perturb the system on a Sensit Smart potentiostat (PalmSens, the

Netherlands) using the PStrace 5.9 software for data acquisition. ZView 2 software was used to fit Nyquist plots obtained to adequate equivalent circuit.

A conventional three-electrode system was used, with a platinum plate as a counter electrode (area 1.0 cm^2), the reference electrode used was Ag|AgCl/KCl (3.0 mol L^{-1}), and a carbon paste electrode (d = 3.0 mm). The catalytic rate constant (k_{cat}) of diuron oxidation in the proposed electrode was carried out using chronoamperometry, applying a potential of +1.1 V and at an interval time of 0.01 s.

III. Preparation of Carbon Paste Electrodes Modified with Deca:TBAB

The bare carbon paste electrode was prepared by mixing 70% w/w MWCNT and 30 % w/w mineral oil. The components were blended using a mortar and pestle until a homogeneous paste was achieved, which was then placed into a Teflon tube to hold the carbon paste (FIGURE *3.1*).

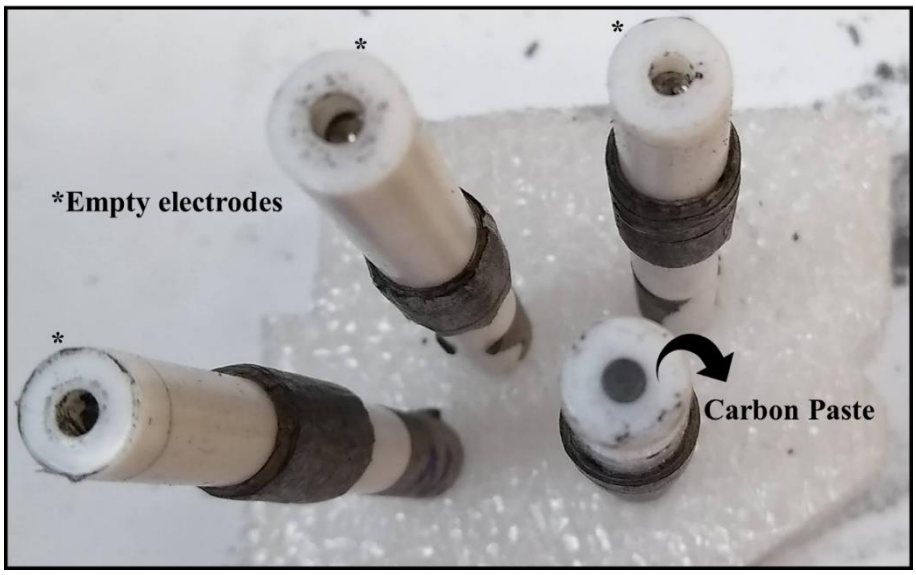

FIGURE 3.1 - Illustration of a carbon paste electrode and Teflon tubes used for electrode preparation.

The HDES-based CPEs were formulated by partially substituting mineral oil with HDES (DecA:TBAB) while maintaining fixed the MWCNT at 70% (w/w). The effect of DecA:TBAB amount (from 0 to 15 mg, TABLE 3.3) in the paste was carefully studied by CV and EIS. These studies were carried out using both hydroquinone and diuron as the redox probe. The HDES DecA:TBAB was prepared following the procedure described in section 3.1-III.

TABLE 3.3 - Mass percentage composition of binders in the carbon paste electrode.

Carbon Paste Electrode	Binder (% w/w)	
	Mineral oil	HDES
bare/CPE	30	0
HDES(3)/CPE	27	3
HDES(5)/CPE	25	5
HDES(8)/CPE	22	8
HDES(10)/CPE	20	10
HDES(15)/CPE	15	15

IV. Analytical Procedure

Studies were conducted to establish the optimal conditions for the determination of diuron. The optimized parameters included the pH of the supporting electrolyte as well as parameters influencing the DPV technique (TABLE 3.4), the optimized parameters were time modulation (t), amplitude (a), potential increment (ΔE), and interval time (Δt). The parameters using the SWV technique were also evaluated; however, the results for diuron determination were less favourable (data not shown). Therefore, DPV was selected as the optimal technique.

TABLE 3.4 -DPV optimization using 100 μmol L^{-1} Diuron

Parameters	Studied interval
Amplitude, *a* (mV)	10 – 75
Modulation time, *t* (ms)	10 – 30
Potential increment, Δ*E* (mV)	1 – 6
Interval time, Δ*t*, (ms)	100 – 300

For the diuron sensor, first, different proportions of HDES used in the construction of the CPE were studied (TABLE 3.3), as these can influence the voltammetric response. CV and SWV was performed using H_2Q (1.0×10^{-3} mol L^{-1}) in 0.1 mol L^{-1} acetate buffer at pH 4.74 as the redox probe. CV measurements were conducted within a potential range of –0.6 to +0.9 V at a scan rate of 25 mV s^{-1}. Additionally, SWV was carried out in the potential range of –0.3 to +0.9 V under the following optimized conditions: f = 30 Hz, ΔE = 5.0 mV, and a = 70 mV. This procedure was carried out as established in a previous study by our research group, where H_2Q was used as an electrochemical probe to characterise a carbon paste electrode[50].

After determining the optimal composition of materials for CPE development, the same HDES proportions were tested with diuron (100 μmol L^{-1}) in 0.01 mol L^{-1} PB pH 3.0 to validate the chosen composition. CV was applied in the potential range of +0.8 to +1.6 V at a scan rate of 10 mV s^{-1}. DPV was performed within the +0.9 to +1.4 potential range using the following conditions: modulation time (t) = 10 ms, ΔE = 4.0 mV, a = 60 mV, and interval time (Δt) = 100 s.

To construct the analytical curves, successive additions of small volumes of standard solution of the analyte were performed. The LOD and LOQ were calculated using EQUATIONS 1 and 2, respectively.

The k_{cat} for the oxidation of diuron was calculated based on data obtained from a chronoamperometry study using 100 μmol L^{-1} diuron, at a fixed potential of +1.1 V and using EQUATION 3. This study compared the influence of adding HDES to modify the electrodes.

The reproducibility and repeatability of the voltammetric signals at the proposed electrode were evaluated to assess sensor precision. Inter-electrode and intra-day studies were conducted by measuring the voltammetric response of the analyte three times at three different electrodes within a single day. Additionally, the stability of the analyte's voltammetric response was examined using cyclic voltammetry over 50 consecutive cycles.

3.4 - Modification of a Filament with Silver Nanoparticles for Cadmium Detection and Fabrication of a novel HDES-based filament

I. Chemicals and Solutions

All chemicals used throughout this work were used as received without any further purification. All aqueous solutions were prepared with deionised water of a measured electric resistivity not less than 18.2 MΩ cm, sourced from a Milli-Q Integral 3 system from Millipore UK (Watford, UK). Hexaammineruthenium (III) chloride (98 %), castor oil, potassium ferricyanide (99 %), potassium ferrocyanide (98.5 – 102 %), sodium hydroxide (> 98 %), potassium chloride (99.0 – 100.5 %), graphite powder (< 20 μm), boric acid (≥ 99.5 %), phosphoric acid (≥ 85 %), acetic acid (≥ 99 %), nitric acid (70 %), microcrystalline cellulose (20 μm, 99 %), acetaminophen (≥ 99.0 %), and cadmium standard for AAS were purchased from Merck (Gillingham, UK). Silver nitrate (> 99 %) was purchased from Alfa Aesar (Massachusetts, USA). Carbon black was purchased from PI-KEM (Tamworth, UK). Recycled poly(lactic acid) (rPLA) was purchased from Gianeco (Turin, Italy). River water samples were

obtained in accordance with EPA guidelines from the River Irwell, Greater Manchester, UK (approx. location: 53.517464, -2.302739). Tap water samples were obtained from laboratory 5.39, John Dalton Tower, Manchester, UK.

II. Apparatus

SEM micrographs were obtained using a Crossbeam 350 Focussed Ion Beam – Scanning Electron Microscope (FIB-SEM) (Carl Zeiss Ltd., Cambridge, UK) fitted with a field emission electron gun. Secondary electron imaging was completed using a Secondary Electron Secondary Ion (SESI) detector. Also, Energy Dispersive X-ray Spectroscopy (EDX) analysis was performed using an Ultim Max 170 detector (Oxford Instruments plc, Abingdon, UK.) installed on the FIB-SEM. An acceleration voltage of 20kV was used to image the samples for EDX analysis experiments. Samples were mounted on the aluminium SEM pin stubs (12 mm diameter, Agar Scientific, Essex, UK) using adhesive carbon tabs (12 mm diameter, Agar Scientific, Essex, UK) and coated with a 5 nm layer of Au/Pd metal using a Leica EM ACE200 coating system before imaging. Quantification of EDX spectra was carried out using a standardless quantification procedure developed by Oxford Instruments and integrated into the AZtec 6.1 (Oxford Instruments, Abingdon, UK).

X-ray diffraction (XRD) measurements were performed on the powder of AgNPs on graphite samples to obtain the structural information using PANalytical X'Pert Powder X-ray diffractometer with Cu (λ = 1.54 Å) as the source with 45 kV voltage and 40 mA current settings. The data were collected in a continuous mode over the 2Θ scan range of 5º – 90º, with a step size of 0.01º for 108 seconds per step at room temperature under ambient conditions. The samples were spinning at 16 rpm during the measurements for uniform data collection. PreFIX module on the incident beam side with the automatic divergence and fixed anti-scatter slit of 4º along with PreFIX module on the

diffracted side with PIXcel 1D detector in scanning line mode with programmable anti-scatter slit were used to collect the diffraction patterns from a constant irradiated length of 0.5 mm.

X-ray Photoelectron Spectroscopy (XPS) data were acquired using an AXIS Supra (Kratos, UK), equipped with a monochromatic Al X-ray source (1486.6 eV) operating at 225 W and a hemispherical sector analyser. It was operated in fixed transmission mode with a pass energy of 160 eV for survey scans and 20 eV for region scans with the collimator operating in slot mode for an analysis area of approximately 700×300 μm, the FWHM of the Ag $3d_{5/2}$ peak using a pass energy of 20 eV was 0.613 eV. The binding energy scale was calibrated by setting the graphitic sp^2 C 1s peak to 284.5 eV; this calibration is acknowledged to be flawed[248] but was nonetheless used in the absence of reasonable alternatives, and because only limited information was to be inferred from absolute peak positions.

For the analysis of ACP and cadmium, all electrochemical experiments were performed on an Autolab 100N potentiostat controlled by NOVA 2.1.7 (Utrecht, The Netherlands). Identical additive manufactured electrodes were used throughout this work for all filaments, printed in a lollipop shape (Ø 5 mm disc with 8 mm connection length and 2×1 mm thickness[249]) alongside an external commercial Ag|AgCl/KCl (3.0 mol L^{-1}) reference electrode with a nichrome wire counter electrode (FIGURE *3.2*). All solutions of $[Ru(NH_3)_6]^{3+}$ were purged of O_2 thoroughly using N_2 prior to any electrochemical experiments. Solutions of $[Fe(CN)_6]^{4-/3-}$ were prepared in the same way without the need of further degassing.

The electrochemical cells and additional glassware used in the cadmium work has been pre-treated accordingly for trace heavy metals analysis prior to use, which involved a 24 h immersion in 10 %v/v nitric acid solution, rinse with deionised water and keep in sealed bags to avoid further contamination.

EIS was recorded in the frequency range 0.1 Hz to 100 kHz applying 10 mV of signal amplitude to perturb the system under quiescent conditions. NOVA 2.1.7 software was used to fit Nyquist plots obtained to adequate equivalent circuit.

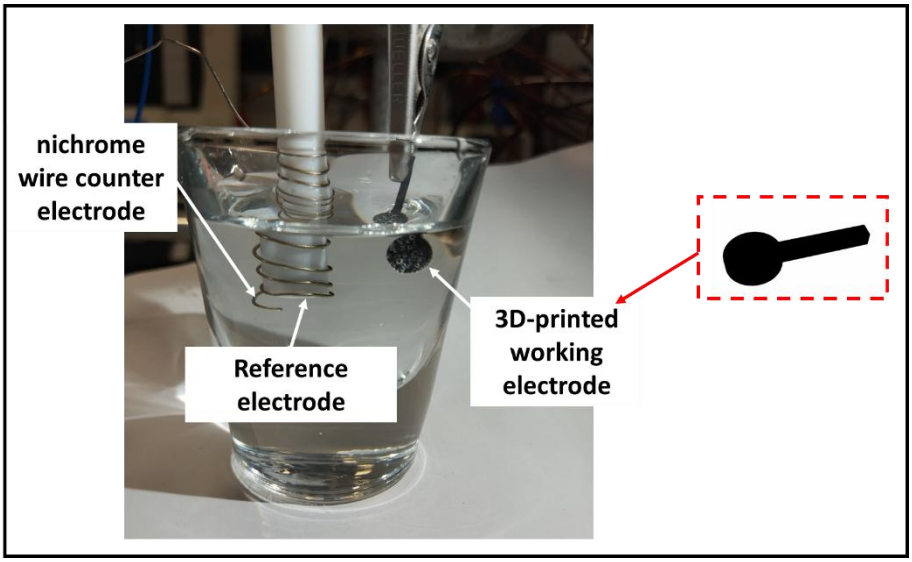

FIGURE 3.2 – Representation of a typical electrochemical cell system used consisted of a 3D-printed reference electrode in a lollipop shape, an external commercial Ag|AgCl/KCl (3.0 mol L^{-1}) reference electrode, and a nichrome wire counter electrode.

Activation of the AMEs was performed before electrochemical experiments for CB/Cellulose/HDES/PLA. This was achieved electrochemically in NaOH (0.5 M), as described in the literature[56]. Briefly, the AMEs were connected as the working electrode in conjunction with a nichrome wire coil counter and Ag|AgCl/KCl (3.0 mol L^{-1}) reference electrode and placed in a solution of 0.5 M NaOH. Chronoamperometry was used to activate the additive manufactured electrodes by applying a set voltage of +1.4 V for 200 s, followed by applying –1.0 V for 200 s. The additive manufactured electrodes were then thoroughly rinsed with deionised water and dried under compressed air before further use.

III. Silver Nanoparticles Synthesis on Graphite

The AgNPs were synthesised directly onto graphite flakes based on the procedure reported by Pandey *et al.*[250] performed on graphite sheet. Briefly, a 50 mL solution of $AgNO_3$ (20 mg mL^{-1}/ ~6.0×10^{-6} mol L^{-1}) was prepared, to which 20 g of graphite powder was added. This was placed on a stirrer plate at room temperature and left to stir overnight, after which the solution was removed through vacuum filtration on a standard filter paper and dried in the oven at 60 °C overnight. This powder was then ready for use within filament production. FIGURE *3.3* presents a schematic representation of the preparation of AgNPs on graphite (AgNP-G). This powder was then ready for use within filament production.

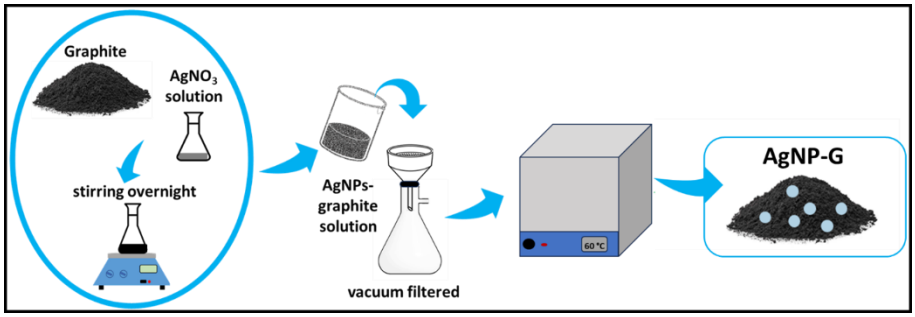

FIGURE 3.3 - Schematic illustration of the process for preparing AgNPs on graphite.

IV. Recycled filament production

All commercially acquired recycled PLA was dried in an oven at 60 °C for at least 2.5 hours to eliminate residual moisture. The polymer composition was prepared by incorporating, in a 63 cm^3 chamber, appropriate amounts of rPLA, castor oil, carbon black (CB), and functionalized graphite for developing an electrochemical sensor for cadmium detection. Additionally, a separate

composition was prepared with rPLA, castor oil, CB, cellulose, and HDES for fabricating a 3D-printed electrode used in ACP determination.

All filaments made throughout this work utilised 10 wt% castor oil as a plasticiser[46]. The PLA content was optimised at 60 wt% for the cadmium study and 55 wt% for the HDES-based filament. The CB content in the HDES filament was 20 wt%. For the cadmium study, the total carbon loading was 30 wt%, consisting of 12 wt% AgNP-G and 18 wt% CB, as previously optimised[47], The concentrations of cellulose and HDES were carefully investigated as part of a study that will soon be submitted to a relevant journal. The compounds were mixed using a Thermo Haake Polydrive dynameter fitted with a Thermo Haake Rheomix 600 (Thermo-Haake, Germany) at 190 °C with Banbury rotors at 70 rpm for 5 min. The resulting polymer composites were allowed to cool to room temperature before being granulated to create a finer particle size using a Rapid Granulator 1528 (Rapid, Sweden). The polymer composites were collected and processed through the hopper of a EX2 extrusion line (Filabot, VA, United States). The EX2 was set up with a single screw with two set heat zones of 60, and 195 °C, respectively.

The molten polymer was extruded from a 1.75 mm die head, pulled along an airpath cooling line (Filabot, VA, United States) and collected on a spool. After which the filament was then ready to use for additive manufacturing, FIGURE *3.4* presents an illustration representing the filament production process, followed by the 3D printing of electrodes.

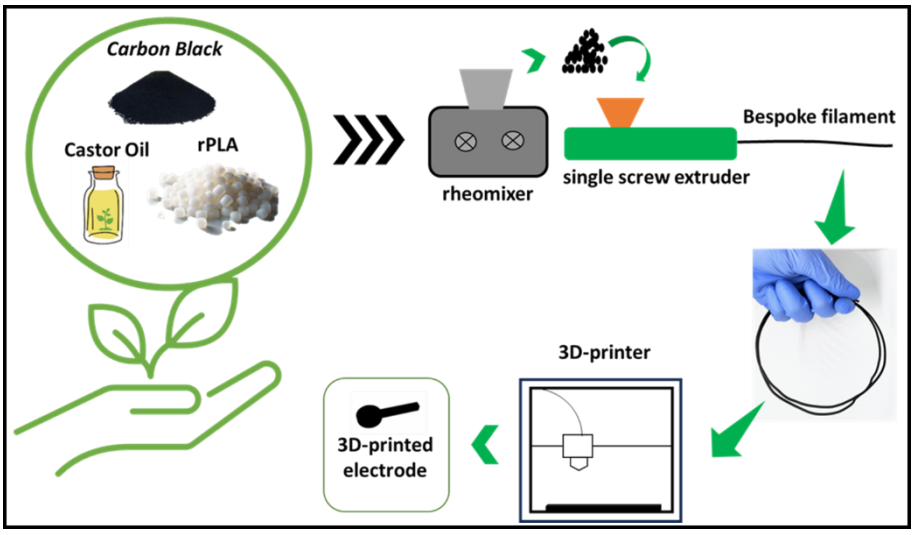

FIGURE 3.4 - Illustration of the filament production process and development of the 3D-printed electrodes.

V. Additive Manufacturing of the Electrodes

All computer designs and 3MF files were produced using Fusion 360® Software (Autodesk®, CA, United States). Then, these files were sliced and converted to GCODE files in PrusaSlicer Software (Prusa Research, Prague, Czech Republic) to prepare them for 3D printing. The AMEs were produced using fused filament fabrication technology on a 3D printer Prusa i3 MK3S+ (Prusa Research, Prague, Czech Republic). All additive manufactured electrodes were printed using identical printing parameters, namely a 0.6 mm nozzle with a nozzle temperature of 215 °C, 100 % rectilinear infill[251], 0.15 mm layer height, and print speed of 35 mm s^{-1}.

VI. Analytical Procedures

The AMEs were electrochemically characterised against both the near-ideal outer-sphere redox probe $[Ru(NH_3)_6]^{3+}$ (1.0×10^{-3} mol L^{-1} in 0.1 mol L^{-1} KCl) and the commonly used inner-sphere probe $[Fe(CN)_6]^{4-/3-}$ (1.0×10^{-3} mol L^{-1} in 0.1 mol L^{-1} KCl). Initially, scan rate studies (5 – 500 mV s^{-1}) were

performed against $[Ru(NH_3)_6]^{3+}$ as this allowed for the determination of the heterogeneous electron charge transfer rate constant (k^0) and the real electrochemical surface area (A_e)[252]. For the EIS experiments, the 3D-printed electrodes were tested using the $[Fe(CN)_6]^{4-/3-}$ probe, in the frequency range 0.1 Hz to 100 kHz applying 10 mV of signal amplitude to perturb the system under quiescent conditions.

To test the CB/Cellulose/HDES/PLA electrode, the SWV values were based on previous research[64,253,254].

To test the CB/Ag-G/PLA electrodes towards the detection of Cd (II) the Britton Robinson (BR) buffer was optimised in pH = 5.0 for the detection of 100 μg L^{-1} (100 ppb/ 8.9×10^{-7} mol L^{-1}). Following this, the deposition potentials and deposition times were optimised for both the DPV and SWV techniques (TABLE 3.5). Unlike the optimisation for 5–HT and diuron determination, where only a single technique optimisation is shown (sections 3.2 - and 3.3 -), the analysis of Cd(II) presents the optimisation of both techniques, as both produced favourable results for the determination of this analyte.

TABLE 3.5 - DPV and SWV optimization using 100 ppb (8.9×10^{-7} mol L^{-1}) of Cd(II)

Technique parameter	Studied range
DPV	
Step potential (V)	0.001 – 0.010
Amplitude (V)	0.010 – 0.100
Modulation time (s)	0.010 – 0.100
Deposition potential (V)	–0.8 – –1.2
Deposition time (s)	0 – 120
SWV	
Step potential (V)	0.001 – 0.010
Amplitude (V)	0.010 – 0.100
Frequency (Hz)	5 – 45
Deposition potential (V)	–0.8 – –1.2
Deposition time (s)	0 – 120

LOD and LOQ were calculated using EQUATIONS 1 and 2, respectively. The repeatability of 3D-printed electrodes was evaluated using SWV through ten consecutive measurements (n=10) using three electrodes (n=3).

Chapter 4

Part I

4 - RESULTS AND DISCUSSION

This section presents the results on the preparation, characterisation, and application of the HDES based on DecA and TBAB. This HDES was selected based on previous research conducted in our laboratory[50]. First, the preparation and characterization of HDES are detailed, including spectroscopic and thermal data to assess interactions leading to its formation, the eutectic point, and physicochemical properties. Subsequently, the efficacy of HDES as a modifier for developing electrochemical sensors is discussed.

Next, the focus shifts to the development of additive-manufactured conductive filaments and their application in creating 3D-printed electrodes. The results highlight the feasibility and performance of these electrodes.

Finally, this section reports on the application of the proposed HDES in developing novel conductive filaments and their subsequent use in fabricating advanced electrochemical sensors using 3D printing technology.

4.1 - Optimisation of Hydrophobic Deep Eutectic Solvent Preparation: *In Situ* FTIR Study and NMR Characterisation

The approach based on controlling the temperature and stirring is the most used to synthesise deep eutectic solvents[255]. In this way, the initial approach started with an *in situ* FTIR study to monitor the preparation of the HDES. The aim was to optimise the temperature, and the time required for the synthesis.

FIGURE *4.1* presents FTIR spectra obtained for the studied HDES (DecA:TBAB) and for the respective precursors. Clear spectral shifts in the region between 930 and 880 cm^{-1} compared to the fatty acid precursor could be observed in the HDES spectra. Bands in the 930 and 880 cm^{-1} region were attributed to the out-of-plane bending of O—H from the fatty acid carboxyl groups. It is well

known that the HDES preparation involves the non-covalent chemical interaction between carboxyl groups and the bromide ion of the TBAB[256]. Therefore, this region was first selected for the *in situ* FTIR study. It is worth to point that shifts in the stretching of C—O (1300 – 1200 cm^{-1} range) and of O—H (near 3000 cm^{-1}) are commonly used to evidence the formation of this class of HDES[257,258]. However, monitoring these regions was not possible due to spectral overlap in the C—O band region and equipment limitations for regions near 3000 cm^{-1}.

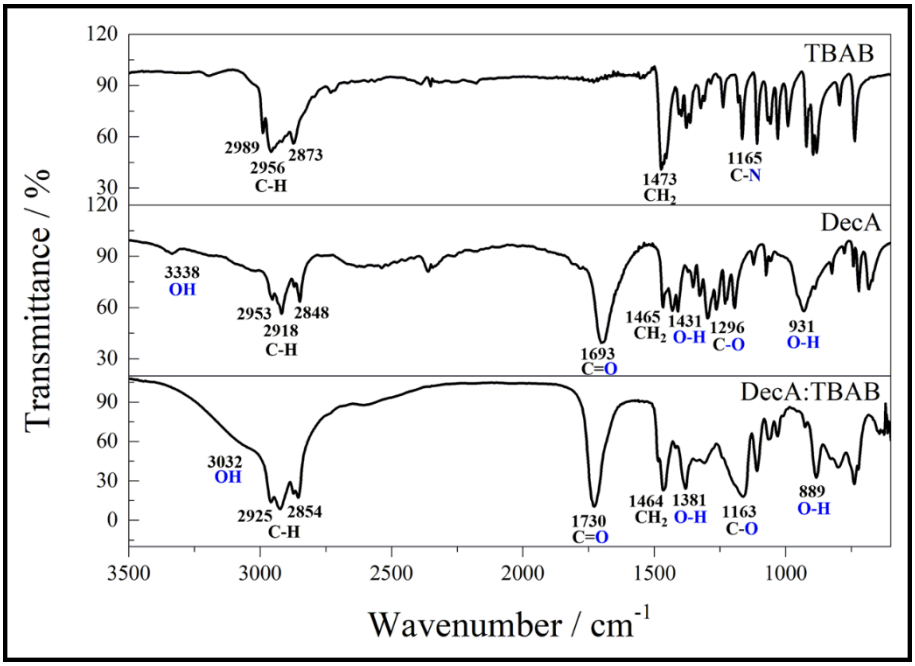

FIGURE 4.1 - FTIR spectra obtained for the studied HDES (DecA:TBAB) and its precursors: TBAB and DecA.

The *in situ* FTIR study was then performed by recording infrared spectra at every 30 seconds of reaction. The synthesis of DecA:TBAB in a molar ratio of 1.85:1 was evaluated. As it will be presented in the following sections, the molar ratio of 1.85:1 corresponds to the eutectic point of the proposed HDES. FIGURE *4.2*A present the changes in the IR bands intensities (in the 930 – 880 cm^{-1} range) as a function of the synthesis time and FIGURE *4.2*B present the

spectra recorded during the synthesis, that were carried out at a temperature of 353.15 K (80.0 °C). The results for all the temperatures analysed are provided in the Appendix *I* at the end of this thesis.

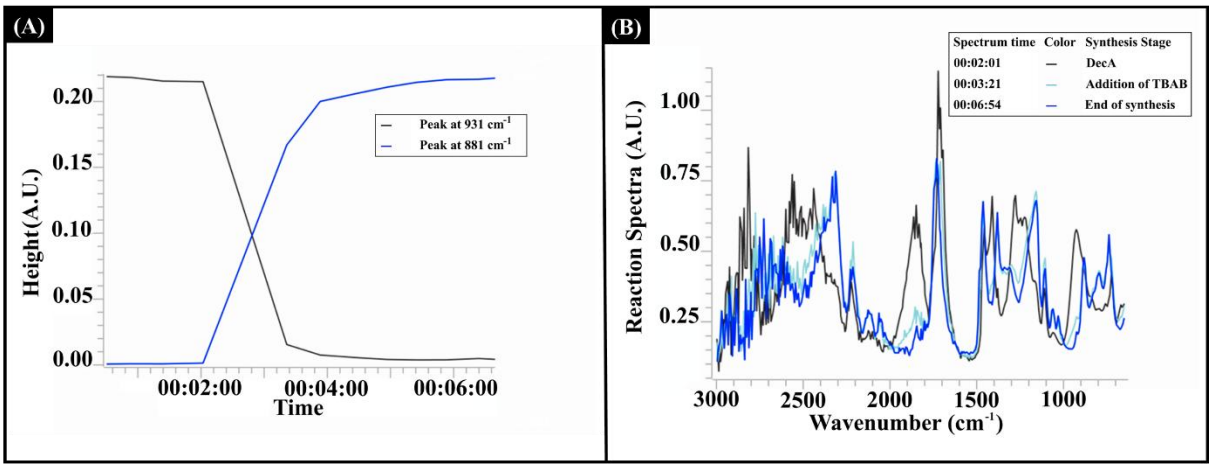

FIGURE 4.2 - *In situ* FTIR study for monitoring the preparation of the HDES. (A) evaluation of the intensity of specific peaks for DecA:TBAB synthesis as a function of the time of synthesis. (B) Infrared spectra for DecA:TBAB synthesis. The data correspond to the preparation of DecA:TBAB in a molar ratio of 1.85:1 at the temperature of 353.15 K (80.0 °C).

The temperature study for the HDES preparation was performed by primarily considering the fatty acid melting point temperature (T_m). As it will be demonstrated in the following section, this temperature was determined by thermal analysis, with the results showing T_m 305.5 K (32.3 °C) for DecA. Thus, the temperature range studied was from 323.15 to 353.15 K (50.0 to 80.0 °C) for DecA:TBAB. TABLE *4.1* shows the total time of synthesis for each studied temperature. The initial time was defined as the moment of adding the second component (TBAB), while the final time was when no further changes in the infrared spectrum were observed. The optimal reaction temperature for preparing the eutectic solvent was 353.15 K, taking 4 minutes and 50 seconds. These results

demonstrate for the first time that longer synthesis times, as adopted in some works previously presented in the literature[50,259–261], are unnecessary. Furthermore, they highlight the importance of evaluating synthesis duration, as it significantly impacts the sustainability of the process, particularly in terms of energy consumption, as discussed further in section 4.5 - .

TABLE 4.1 - Synthesis time of the HDES (DecA:TBAB)

Temperature (K)	Time (minutes)
323.15	17’40”
333.15	07’00”
343.15	07’23”
353.15	04’50”

It is worth to notice that working at temperatures higher than 353.15 K would not have a significant impact on the preparation time. Few variations were observed in the reaction time when increasing the temperature from 333.15 to 353.15 K (TABLE *4.1*). Additionally, the synthesis of eutectic solvents involves the fusion of the component with the lowest melting point before adding the component with the highest melting point[11]. As TBAB melts at around 376 K (103 °C), the synthesis temperature would be closer to the TBAB melting point. Therefore, this study only considered temperatures up to 353.15 K.

During the synthesis, it was observed that at temperature of 323.15 K, the TBAB have not fully interact with the fatty acid even after one hour of reaction. Probably, it did not provide sufficient thermal energy to form a homogeneous liquid. As a result, an 'excess' of TBAB remains in the system.

Further examination in the FTIR spectra of DecA:TBAB (FIGURE *4.1*) reveals some characteristic bands, such as stretching (ν) bands of sp^3 C—H bonds in the interval 2925 – 2854 cm^{-1}. Bands of bending (δ) of CH_2 near 1460

cm^{-1} similar to the precursor' spectra can also be observed. Moreover, characteristic bands of in-plane δO—H and *v*C—O vibrations for carboxylic acids are present in 1381 and 1163 cm^{-1}, respectively. These bands are shifted when compared to the fatty acid: δO—H: 1431 cm^{-1} and *v*C—O: 1296 cm^{-1} for DecA. The same can be observed for the out-of-plane δO—H present in 931 cm^{-1}, for DecA, shifted to 889 cm^{-1} to DecA:TBAB. These results suggest the interactions to form the HDES, in agreement with the *in situ* infrared experiments. Furthermore, the stretching of C=O of decanoic acid changed from 1693 to 1730 cm^{-1}. This shift to higher frequencies of carboxyl stretching vibrations can be attributed to the cationic complex formed between the carboxyl and the tetrabutylammonium cation[257].

The HDES and the precursors were also characterized by ^{1}H NMR (FIGURE *4.3*, FIGURE *4.4*, and FIGURE *4.5*). The ^{1}H NMR spectra obtained for DecA:TBAB, (FIGURE *4.5*) presented a broad singlet at δ = 11.98 ppm, which were attributed to carboxyl hydrogens. No variation in the chemical shifts of the carboxyl hydrogens were observed in the HDES spectrum when compared to the pure components' spectra. This is mainly due to the low strength of the hydrogen bond, indicating that the site of interaction is located mainly at the carboxyl group.

^{1}H NMR of the fatty acid revealed sharp and well-defined signal for the hydrogen of the carboxyl group. In contrast, this signal was broader and with low intensity in the HDES spectrum. This may be attributed to the high viscosity (about 723 mPa s for DecA:TBAB at 293.15 K, TABLE *4.3*) of the HDES. As a result, inter- and intra-dipolar interactions are expected to cause an effect of baseline magnification on that signal in the ^{1}H NMR spectrum[262,263]. These data indicate that hydrogen bonds are formed between the carboxyl group and the bromide ion, involving the formation of complex anions (formed between the acid and the bromide anion), which interact with the tetrabutylammonium cation[262].

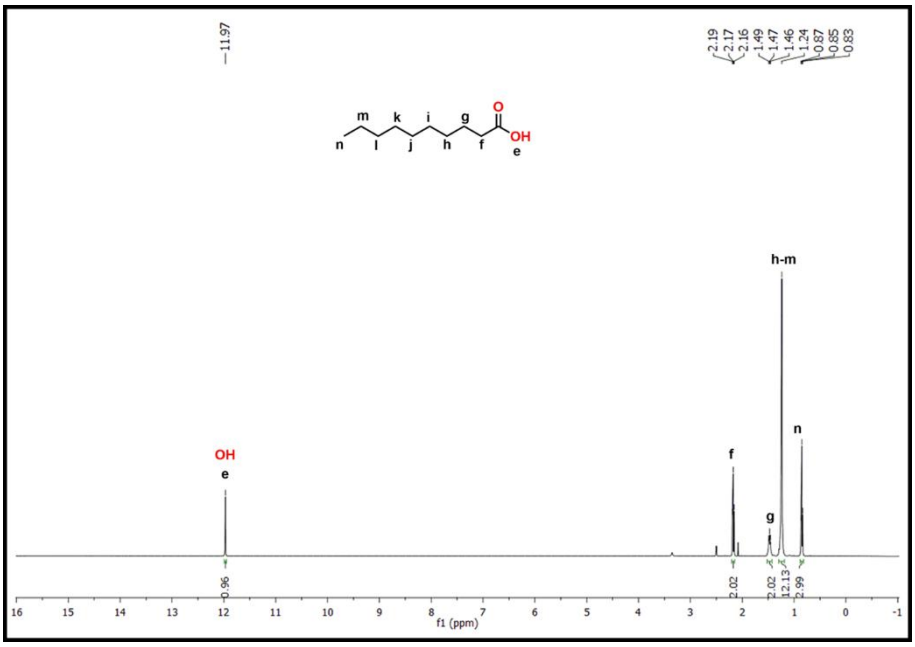

FIGURE 4.3 - ^{1}H NMR spectrum of decanoic acid (400 MHz, DMSO-d_6).

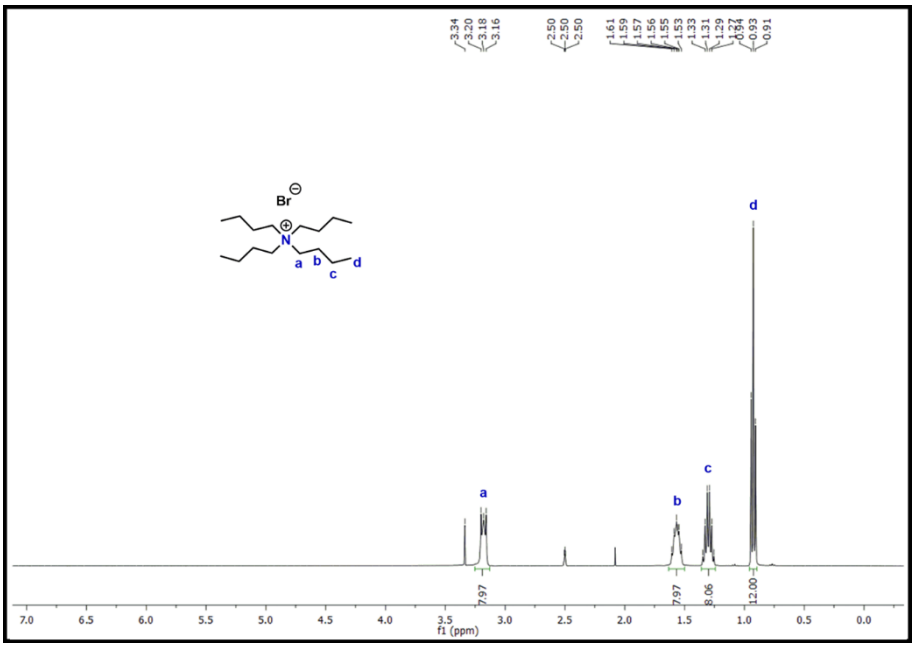

FIGURE 4.4 - ^{1}H NMR spectrum of tetrabutylammonium bromide (400 MHz, DMSO-d_6).

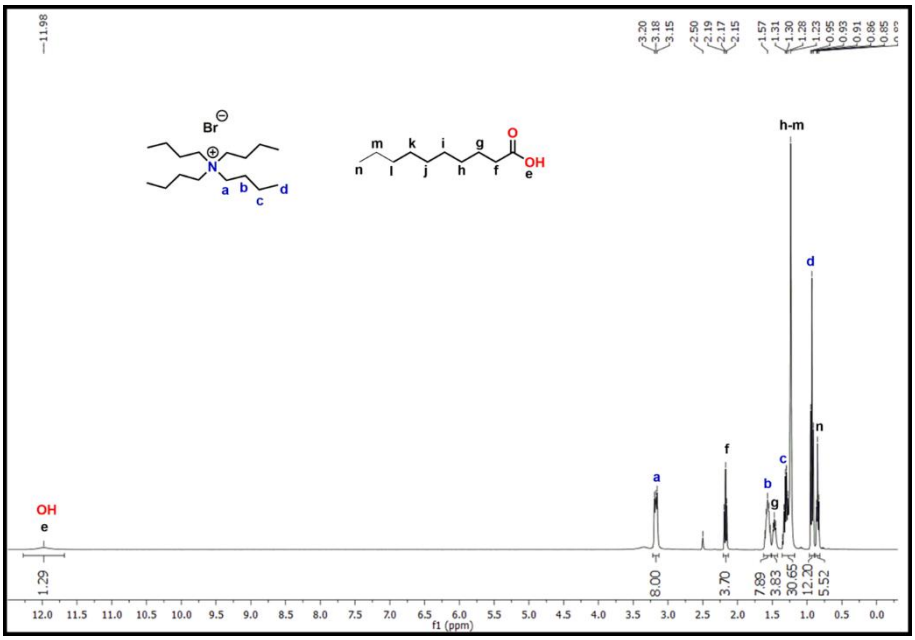

FIGURE 4.5 - ^{1}H NMR spectrum of the eutectic solvent DecA:TBAB (400 MHz, DMSO-d_6).

4.2 - Hydrophobic Mixtures: Thermal analysis

After the optimisation of the HDES synthesis, the next step was using differential scanning calorimetry to acquire the melting temperature of several DecA:TBAB-based mixtures (TABLE 3.1) to construct a phase diagram and establish the eutectic point. FIGURE 4.6 shows the DSC curves for TBAB, DecA, and 1.85:1 (mol/mol) DecA:TBAB mixture, which exhibited the lowest melting temperature among the mixtures studied. Appendix II present all DSC curves obtained and Ttrans: temperature of phase transition; Tm: melting temperature; T*: temperature of the free fraction of the precursors (DecA or TBAB).

TABLE *4.2* summarizes the temperatures of all thermic events and thermodynamic data (ΔH_m and ΔS_m) for the compositions studied in this work.

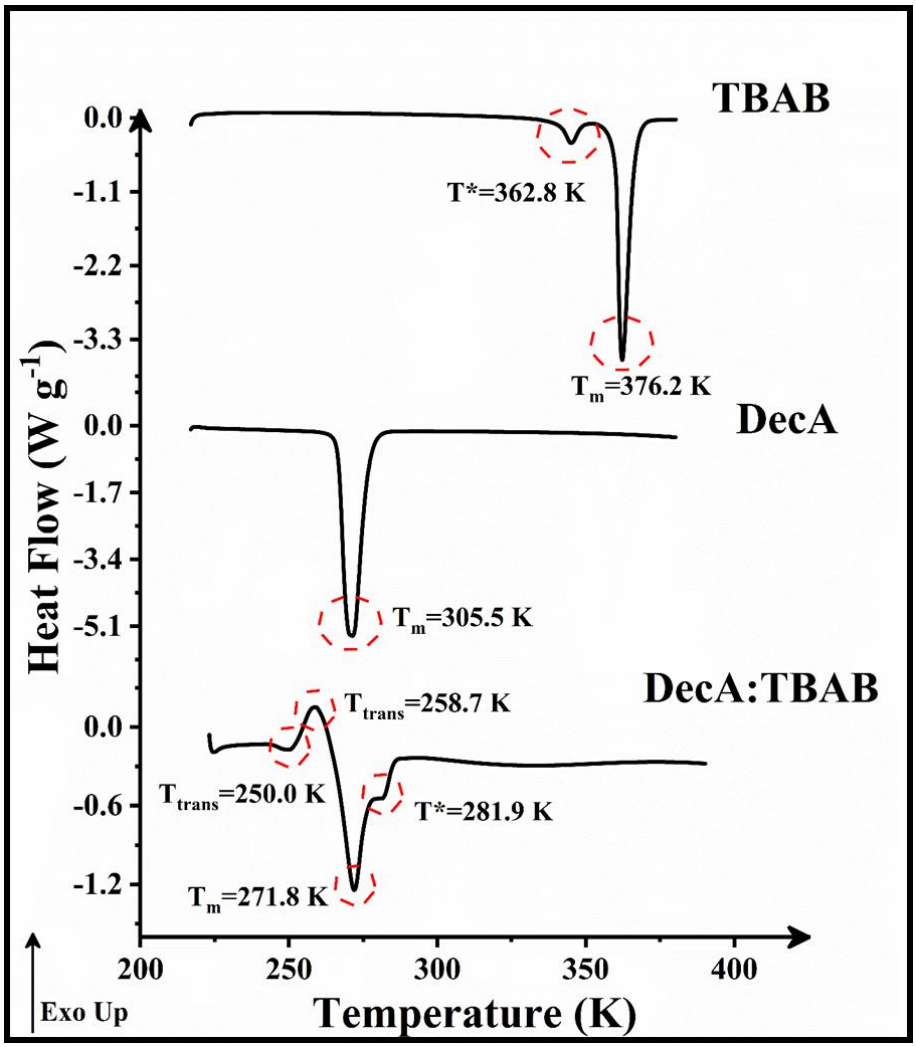

FIGURE 4.6 - DSC curves with the thermal events of the pure components: TBAB and DecA, and for the mixture of DecA:TBAB at the eutectic point. T_{trans}: temperature of phase transition; T_m: melting temperature; T*: temperature of the free fraction of the precursors (DecA or TBAB).

TABLE 4.2 - Thermodynamic data acquired from the experiments by differential scanning calorimetry

X_{DecA}	T_{trans} / K	T^* / K	T_m / K	ΔH_m (J g^{-1})	ΔS_m (J g^{-1} K^{-1})	γ_{DecA}
0.500	263.9/ 274.3	344.4	[b]	—	—	—
0.525	260.0/ 275.3	340.6	[b]	—	—	—
0.550	263.8	307.0	[b]	—	—	—
0.600	235.8/ 255.4/ 265.5[c]	—	[b]	—	—	—
0.625	253.3/ 264.0/ 270.4	—	274.9	15.53	0.056	0.26
0.650	250.0/ 258.7	281.9	271.8[a]	39.95	0.15	0.23
0.667	252.7/ 260.3	283.8	272.9	18.57	0.068	0.24
0.700	255.9/ 264.6	288.2	275.5	5.023/ 9.37	0.018/ 0.033	0.27
0.715	264.2/ 276.5	—	290.4	17.14	0.059	0.54
0.725	260.7/ 276.7	—	291.4	18.48	0.063	0.56
0.750	251.2/ 275.2	—	291.5	19.41	0.067	0.56
0.900	276.1	—	302.1	76.28	0.25	0.87

X_{DecA}	T_{trans} / K	T^* / K	T_m / K	ΔH_m (J g^{-1})	ΔS_m (J g^{-1} K^{-1})	γ_{DecA}
1.000	—	—	305.5	176.7	0.58	—
X_{TBAB}	T_{trans} / K	T^* / K	T_m / K	ΔH_m (J g^{-1})	ΔS_m (J g^{-1} K^{-1})	
1.000	362.8	—	376.2	79.5	0.21	—

[a]Eutectic point; [b]No melting event was detected; [c]Probably the beginning of melting for a free precursor (DecA). T_m: melting temperature; T_{trans}: temperature of phase transition; T^*: temperature of the free fraction of the precursors (DecA or TBAB); ΔH_m: melting enthalpy; ΔS_m: melting entropy; γ: activity coefficient of component i (DecA).

From FIGURE 4.6, one can see the curve for TBAB, where two endothermic peaks are presented. The first peak at 362.8 K (89.7 °C) could be attributed to crystal readjustment and conformational disorder[264]. In contrast, the second peak at 376.2 K (103.0 °C) is relative to its melting point, in agreement with the melting temperature of the pure compound declared by the supplier. The decanoic acid (FIGURE 4.6) showed a sharp melting peak at 305.5 K (32.3 °C), which agrees with the reported melting temperature of the pure compounds[171].

The DSC curve for HDES DecA:TBAB (FIGURE *4.6*) show that HDES had a melting temperature below 273.15 K (0 °C). The DSC curve for DecA:TBAB highlights four thermal events during the heating step. The first two events, occurring at 250.0 K (–23.15 °C) and 258.7 K (–14.45 °C), precede the melting process and can be attributed to a solid-solid phase transition[166]. This behavior has been reported in the literature for fatty acid-based eutectic systems, which generally present a transition from an amorphous solid to a crystalline solid, characterizing a phase transformation[265–267]. This transition was also observed for the other fractions of the mixtures studied (see Appendix *II* and TABLE *4.2*).

The third thermal event, at 271.8 K (–1.35 °C), can be attributed to the melting temperature of the crystalline phase, which refers to the eutectic point for the DecA:TBAB system. The fractions' experimental enthalpy values (TABLE *4.2*) were not linear with the compositions approaching the eutectic temperature, probably associated with other events that precede or follow the eutectic region.

Regarding the last thermal event, an endothermic peak close to 281.9 K (8.75 °C) was observed, and its occurrence may be related to the increase in acid or TBAB fractions that may not have been incorporated into the hydrophobic mixture. Similar results were observed by Shishov *et al.*[257] when characterizing eutectic mixtures based on nonanoic acid and tetrabutylammonium bromide, where the free acid fraction was responsible for the appearance of a peak with a temperature close to 277 K (3.85 °C).

Additionally, one can highlight that the 1.50:1 composition for DecA:TBAB (Appendix *II*D) showed a broad endothermic event at 265.5 K (–7.65 °C). Nevertheless, this event should not be interpreted as the eutectic point once in all mixtures studied based on DecA, it was observed the phase transformation phenomenon for fatty acids at temperatures close to 260 K (–13.15 °C) as previously discussed.

It is worth noting that the first peak of DSC curves for DecA:TBAB, nearly 225 K (–48.15 ºC) (FIGURE *4.6*), is related to the thermal inertia effect, which could be attributed to a gradient of temperature created between the end of the cooling process and the beginning of the heating of the sample[266], associated with the experiment process, in which an isotherm was applied for 5 minutes during the cooling process prior the heating of the sample. Also, it occurred for other mixtures studied in this work (see Appendix *II*).

Then, the thermal behaviour of the DecA:TBAB at the eutectic point (1.85:1) and its precursors were investigated by their thermogravimetric curves under a nitrogen atmosphere (FIGURE *4.7*). The changes in thermal profiles observed in the TG/DTA curves for the DecA:TBAB HDES, regarding the profiles of the precursors suggest that there is an interaction between the precursors in the composition of the eutectic point. Moreover, thermal events at 376 and 305 K (103 and 32 °C) for TBAB and DecA, respectively, confirm the melting temperature of these precursors (temperatures confirmed by DSC). However, this thermal event was not observed for the HDES because it melts below room temperature.

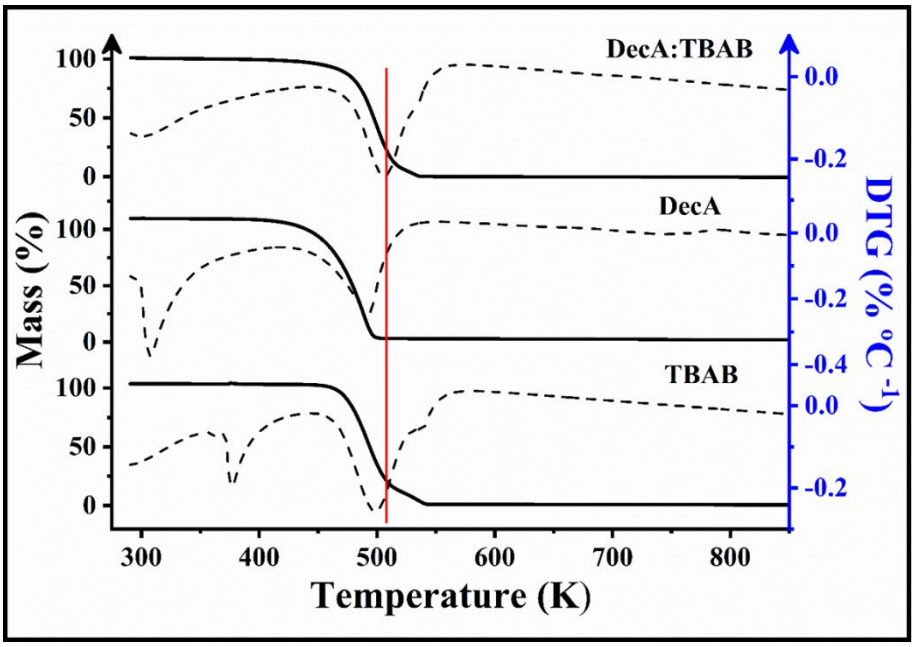

FIGURE 4.7 - TG curves (solid lines) of DecA:TBAB (1.85:1), decanoic acid (DecA) and tetrabutylammonium bromide (TBAB). DTA curves (dotted lines) of the eutectic mixture and its precursors (TBAB and DecA). Conditions: N_2 at 50 ml min^{-1}, sample mass of (10.0±0.2) mg in open α-alumina sample holders.

In short, all pure compounds exhibited similar decomposition behavior, proving to be suitable for applications at temperatures close to 450 K (177 °C). As presented in FIGURE *4.7*, the mass loss for decanoic acid was 98.6 % at 492 K (219 °C), which correspond to the decomposition of this acid. The mass loss for tetrabutylammonium bromide was at 499 K (226 °C), corresponding to 98.8 %. Furthermore, another thermal event at approximately 540 K (267 °C) was also observed, possibly due to some impurities presented by TBAB.

Regarding the mixture at the eutectic point, the decomposition of DecA:TBAB was at 506 K (233 °C), with 99.4 % mass loss. Based on this thermal behaviour, this hydrophobic solvent in the eutectic point composition showed slightly higher thermal stability than their precursors. This probably occurred due to the interaction between the two precursors to form eutectic mixtures, which was observed in NMR and FTIR studies.

4.3 - Phase Behaviour of the Hydrophobic Mixtures

Recent studies suggest that the term 'deep' in DES is defined by deviations from ideal mixing behaviour. These deviations arise from the specific interactions between the components of the eutectic system. In the case of DecA and TBAB, the "deep" nature of the system depends on the strength of DecA—TBAB interactions relative to DecA—DecA and TBAB—TBAB interactions. When DecA—TBAB interactions are favoured over self-interactions, the system exhibits deep eutectic characteristics. Conversely, if DecA—DecA and TBAB— TBAB interactions dominate, the mixture behaves as a conventional eutectic solvent[172]. This behavior can be measured in terms of activity coefficient (γ) according to EQUATION 4[173], where γ = 1 indicates an ideal system and γ < 1 a deep eutectic system.

$$\ln(x_i\gamma_i) = \frac{\Delta_m H_i}{R}\left(\frac{1}{T_{m,i}} - \frac{1}{T}\right) \qquad \text{EQUATION 4}$$

Following EQUATION 4, x_i, γ_i, $\Delta_m H_i$ (J mol^{-1}), and $T_{m,i}$ (K) are, respectively, the molar ratio, activity coefficient, melting enthalpy, and melting temperature of component *i*. R (8.314 J mol^{-1} K^{-1}) and T (K) are the ideal gas constant and the temperature of the system, respectively.

The results obtained in the thermal analysis study (section 4.2 -) and EQUATION 4 used to elaborate a phase diagram aim to evaluate the thermodynamic behaviour of the studied mixtures. FIGURE *4.8* represents the phase diagram for the mixture based on DecA:TBAB as a function of the molar ratio of DecA.

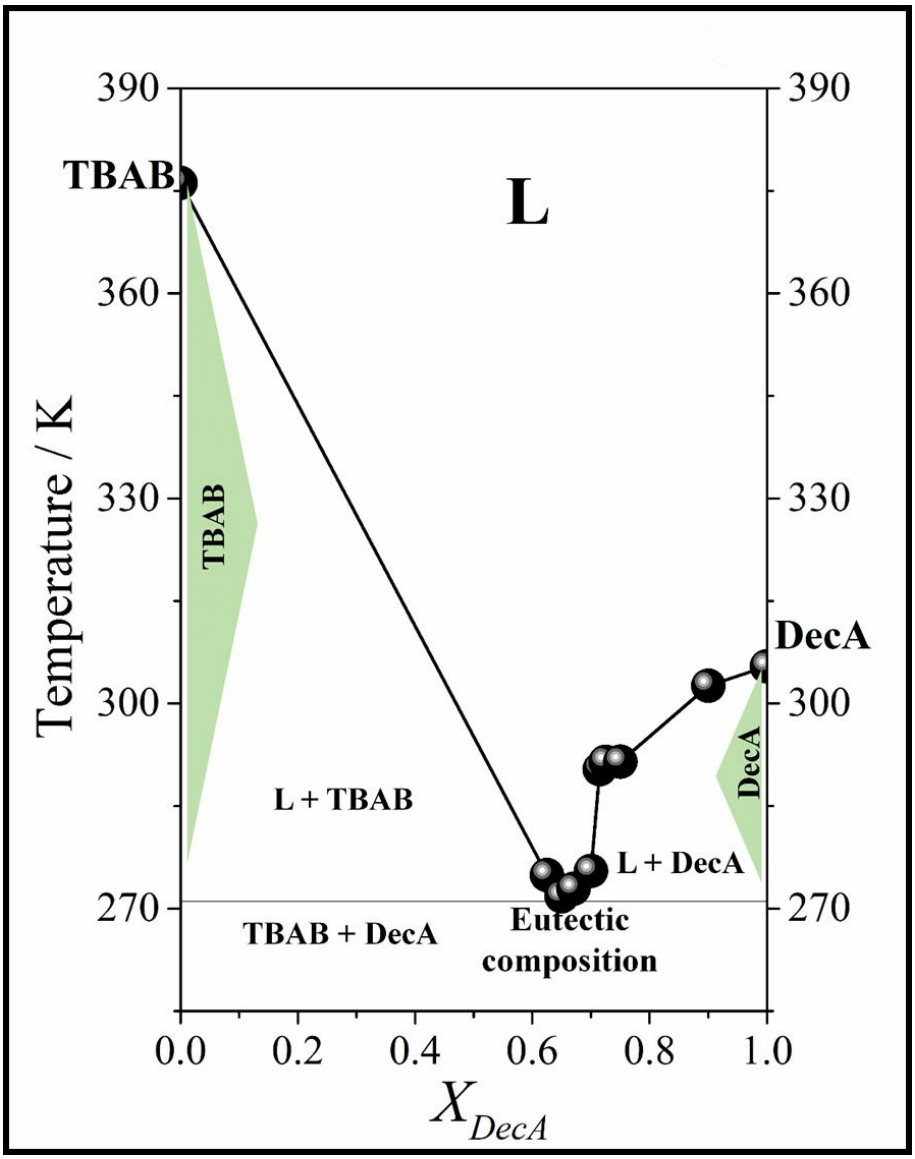

FIGURE 4.8 - Phase diagram of the DecA:TBAB eutectic system as a function of the fatty acid molar ratio.

The γ values for the DecA:TBAB mixtures were calculated based on DecA enthalpy and melting temperature data obtained experimentally applied to EQUATION 4, TABLE *4.2* shows the γ results for all studied eutectic mixtures, when applicable.

For the studied system, all compositions exhibiting a well-defined melting temperature were classified as deep eutectic mixtures. These compositions displayed melting temperatures lower than those of the precursors

(TBAB and DecA), which aligns with the γ results (see TABLE *4.2*). In addition, a linear increase in γ is observed with the increase in the decanoic acid fraction approaching the pure acid composition ($\gamma \rightarrow 1$) in the mixtures from the composition of the eutectic point. Furthermore, values of $\gamma < 1$ suggest that the DecA:TBAB system presents a negative deviation from ideality, classifying it as a deep eutectic solvent.

4.4 - Physicochemical Characterization of the HDES: Viscosity, Conductivity, and Water Content

Physical and chemical properties such as viscosity, conductivity, and water content significantly influence the HDES applications. Thus, these parameters were quantified to better characterize the studied HDES. TABLE *4.3* shows the results obtained in this study.

TABLE 4.3 - Physicochemical properties of the hydrophobic deep eutectic solvent prepared in this work

Viscosity[a] / mPa s	Conductivity[a] / μS cm^{-1}	Water content[a] / %
723±21	35±1	0.15±0.04

[a]n = 3.

The water content of eutectic solvents has a significant impact on their viscosity and conductivity. Higher water content results in lower viscosity and increased conductivity. Various studies have explored the synthesis of DES by adding water to modify these properties depending on the intended application[155,268]. For instance, Ruggeri *et al.* (2019)[149] investigated the formation of HDES using decanoic acid and tetrabutylammonium chloride with different water contents. Their primary objective was to enhance the electrical conductivity

of the proposed HDES by incorporating small amounts of water. The results showed that a small water content is advantageous, as it significantly affects the electrical conductivity and viscosity of the solvent, thereby enhancing its electrochemical properties.

It is well known that HDES based on quaternary ammonium salts commonly present high viscosities (higher than 200 mPa s)[125–127]. In fact, the HDES DecA:TBAB has a viscosity equal to 723 mPa s. This is mainly due to these salts' coulomb force and other interactions forces between the components that limit the solvent mobility[40,126]. Studies reported in the literature have found similar results for viscosity, conductivity, and water content for the same class of HDES studied[50,125,127,149].

4.5 - HDES: Green Synthesis

To better assess the environmental sustainability of the HDES synthesis, we quantified its greenness by calculating the Environmental Factor (E-factor)[269], the electrical energy consumption during the synthesis[157], and the EcoScale[163] for producing approximately 10 mL of HDES over a 5-minutes process.

The E-factor is a metric used to evaluate the environmental impact of a chemical process. It is calculated as the ratio of the total waste mass-generated to the desired product's mass[269]. For DES, the E-factor calculation is generally straightforward because these solvents are typically synthesized through simple mixing without producing significant byproducts. As a result, waste is often negligible, with the components almost entirely incorporated into the final product (100 % atomic efficiency)[40].

In this work, the HDES synthesised was based on 1 mol of DecA (172.26 g) to 0.541 mol of TBAB (174.25 g), yielding 346.51 g of HDES. The

waste was negligible since the components were fully incorporated into the product, so this resulted in an E-factor of 0, reflecting a waste-free process. The E-factor may increase slightly during synthesis in cases of minor losses, such as spillage or non-recoverable residues. Nevertheless, it remains low, highlighting DES synthesis's inherently environmentally friendly nature.

Furthermore, the electric energy consumption for the synthesis of HDES was assessed through EQUATION 5[157].

$$Consumption = \frac{Pt/_{1000}}{V} \qquad \text{EQUATION 5}$$

where consumption (kWh) represents the electrical energy used during synthesis, P is the equipment power (415 W), t (h) is the time of synthesis, and V (mL) corresponds to the volume of HDES prepared. The electric energy consumption calculated for the HDES was 0.0035 kWh mL^{-1}. This value is lower than those reported in the literature. For instance, Gomez *et al.* (2018)[158] documented an energy consumption of 0.650 kW per sample for the synthesis of NADES using the same method. It is worth noting that the authors utilised a preparation time of one hour and did not mention any optimisation of the synthesis duration. In another study, Santana *et al.* (2019)[157] demonstrated that the electric energy consumption for the synthesis of eutectic solvents using the heating and stirring method for 2 hours was 0.014 kWh mL^{-1}. Interestingly, both Gomez *et al.* (2018)[158] and Santana *et al.* (2019)[157] showed that alternative methods, such as microwave- and ultrasound-assisted synthesis, significantly reduced energy consumption. For instance, microwave-assisted synthesis required just 0.001 kW $sample^{-1}$ (20 seconds), while ultrasound-assisted synthesis consumed 0.006 kWh mL^{-1} (45 minutes). However, neither study showed optimisation of the synthesis time for the heating and stirring method, as presented in this thesis. These results

demonstrate the importance of optimising the synthesis time as it presents a great influence on energy consumption.

Moreover, the EcoScale for preparing the proposed HDES was accessed. EcoScale is a tool designed to assess the sustainability of chemical reactions by assigning a score based on various factors such as energy consumption, reaction time, waste production, use of hazardous chemicals, and the overall environmental impact. It provides a simple method to evaluate the "green" credentials of a reaction, encouraging more sustainable practices in chemistry[163].

The EcoScale score ranges from 0 to 100, where 100 represents an ideal, sustainable process. Points are subtracted for factors such as low yield, excessive energy consumption, the use of non-renewable or toxic reagents, and poor waste management[163]. Key parameters include:

i. Yield: Higher yields result in fewer subtractions.
ii. Energy efficiency: Minimal energy consumption is ideal.
iii. Safety: Safer, non-toxic reagents and solvents are preferred.
iv. Waste generation: Less waste improves the score.
v. Reagent availability: Renewable and readily available reagents score higher.

Considering that the HDES synthesis involves simple mixing of components with low energy consumption, no byproducts, and a yield of ~100 %, the EcoScale score calculated is 95.8, which is in accordance with previous works in the literature for DES synthesis and application in different processes[157,270]. TABLE *4.4* shows the results for each calculated parameter of the EcoScale score.

TABLE 4.4 - EcoScale Score for the proposed HDES

Criterion	Score
Yield (~100%)	10/10
Energy Efficiency	9.5/10[1]
Reagent Safety	8/10[2]
Waste Production	10/10
Synthesis Time	10/10
Process Optimisation	10/10
Total Score	57.5/60 → 95.8/100

[1]Minimal deduction for energy use in comparison to completely passive processes. [2]Decanoic Acid: A natural, biodegradable, and relatively safe reagent. Deduction: None. TBAB: Synthetic, limited biodegradability, and potential aquatic toxicity. Deduction: Moderate deduction for environmental and safety concerns. Score: Decanoic Acid (10/10), TBAB (6/10): Weighted average: 8/10.

Finally, considering all the results discussed above and the principles of green chemistry (TABLE *1.1*), we can identify which concepts of green chemistry are adhered to by the proposed HDES. The adherence to the green chemistry principles is summarised in TABLE *4.5*. Overall, one can see the proposed HDES synthesis adheres strongly to several green chemistry principles, particularly in the prevention of waste, atom economy, energy efficiency, and the use of renewable feedstocks (DecA). However, the use of TBAB reduces the adherence to principles such as designing safer chemicals, safer solvents and auxiliaries, and design for degradation, due to TBAB's potential toxicity and environmental impact.

TABLE 4.5 - Adherence to the Green Chemistry Principles

Green Chemistry Principle	Adherence	Description
Prevention	Full adherence	The proposed HDES synthesis generates minimal or no waste, with all reagents being fully incorporated into the final product. There is no need for waste disposal, aligning with this principle.
Atom Economy	Full adherence	The synthesis of HDES has a high atom economy, as both components (decanoic acid and TBAB) react without the formation of by-products.
Less Hazardous Chemical Syntheses	Partial adherence	**Pro:** DecA is a natural, relatively safe reagent, reducing toxicity concerns. **Con:** TBAB is a synthetic, potentially toxic quaternary ammonium salt, which could pose hazards to aquatic environments and human health[271]. This limits full adherence to the principle.
Designing Safer Chemicals	Partial adherence	**Pro:** DecA **Con:** TBAB

Green Chemistry Principle	Adherence	Description
Safer Solvents and Auxiliaries	Partial adherence	**Pro:** DecA **Con:** TBAB
Design for Energy Efficiency	Full adherence	The synthesis is highly energy-efficient, with a low energy consumption of 0.0035 kWh mL^{-1} and a rapid synthesis time of just 5 minutes.
Use of Renewable Feedstocks	Partial adherence	**Pro:** DecA **Con:** TBAB
Reduce Derivatives	Full adherence	The synthesis does not require additional steps or derivatives. The process is direct and simple, reducing unnecessary chemical modifications.
Catalysis	Not applicable	The HDES synthesis does not involve catalytic processes. Therefore, this principle is not relevant to the specific reaction.
Design for Degradation	Partial adherence	**Pro:** DecA is biodegradable. **Con:** TBAB is not readily biodegradable, limiting its environmental degradation, which reduces adherence to this principle.

Green Chemistry Principle	Adherence	Description
Pollution Prevention	Not applicable	This principle focuses on real-time monitoring of processes to minimise waste and pollution. It is not directly relevant to the synthesis of this HDES.
Inherently Safer Chemistry for Accident Prevention	Partial adherence	The process is relatively simple and uses no hazardous chemicals, but the presence of TBAB, a potentially toxic substance, lowers the level of safety compared to other processes that avoid toxic reagents entirely.

4.6 - Development of Electrochemical Sensors: Modified Glassy Carbon Electrode and Carbon Paste Electrode

This section will demonstrate the application of the proposed HDES in the development of new electrochemical sensors, focusing on their electrochemical properties. The first type of electrochemical sensor involves a film made from HDES and carbonaceous material, which is used to modify the surface of a GCE. This work is part of a paper published in the journal *Electrochimica Acta*, vol 520, 2025 by Karen Kenlderi de Lima Augusto, Paulo Cardoso Gomes-Junior, Gustavo Patelli Longatto, Evandro Piccin, Éder Tadeu Gomes Cavalheiro, Elena Bernalte, Craig E. Banks, and Orlando Fatibello-

Filho[272]. A second application of HDES as a conductive binder in combination with mineral oil will be discussed.

4.6.1 - Electrochemical Sensor Based on Carbon Nanohorns and HDES for the Determination of Serotonin[272]

In this study, we evaluated the impact of adding increasing amounts of HDES within the suspension with CNH on the GCE surface. The investigation sought to examine the effectiveness of this approach in enhancing the performance of the GCE. Different amounts of DecA:TBAB were studied: 0, 3, 5, 8, and 10 mg. The study was conducted using CV and EIS, and 100 μmol L^{-1} 5–HT in 0.2 mol L^{-1} PB pH 7.0. FIGURE *4.9* shows the CV results for all electrodes.

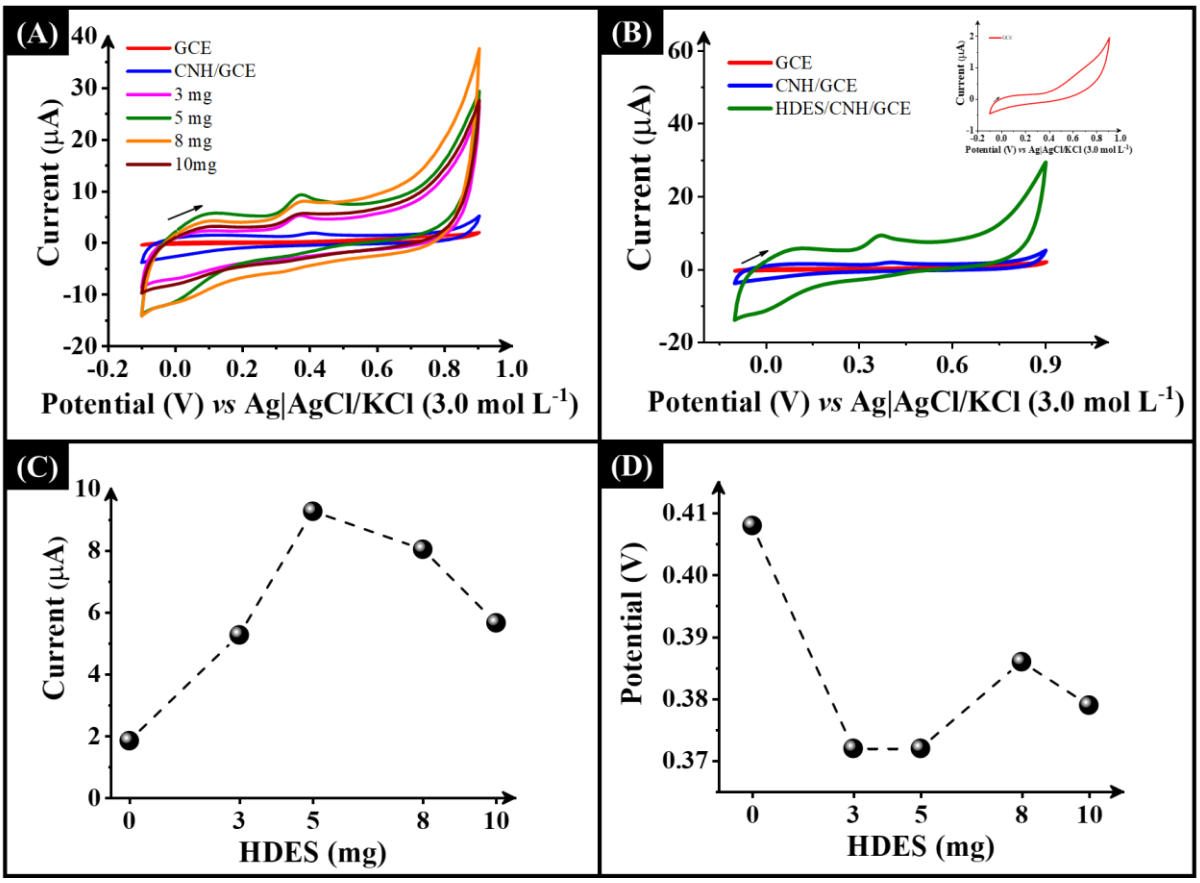

FIGURE 4.9 – CV results (A) and (B) obtained for the oxidation of 100 μmol L^{-1} 5–HT in 0.2 mol L^{-1} PB pH 7.0 using (—) GCE and electrodes with different amounts of DecA:TBAB HDES: (—) CNH/GCE (0 mg), (—) 3mg, (—) 5 mg, (—) 8 mg, and (—) 10 mg. Scan rate: 50 mV s^{-1}. Plots of (C) I_{ap} and (D) E_{ap} versus the amount of HDES.

It can be observed that the analytical signal improved as the DecA:TBAB content in the film increased up to a concentration of 5 mg. From 8 mg of DecA:TBAB, the oxidation peak for 5–HT slightly decreased. This phenomenon is more apparent when evaluating the peak currents and potentials shown in FIGURE *4.9*C and D. The GCE electrode did not exhibit a well-defined oxidation peak to 5–HT, as demonstrated in FIGURE *4.9*B (inset). Compared to the CNH/GCE electrode (which had 0 mg of DecA:TBAB), the 5 mg electrode improved the analytical current by 5-fold. Furthermore, even the electrodes with

concentrations of 3 and 10 mg enhanced the peak current by approximately 3-fold despite presenting lower peak currents among the electrodes modified with HDES.

It is important to note that all concentrations of DecA:TBAB caused a shift in the peak potential towards more negative values. This suggests that modifying the electrode with HDES may have a catalytic effect. The electrodes with 3 and 5 mg of HDES showed a decrease of 36 mV compared to CNH/GCE and an increase of current of 8 μA for the 5 mg HDES modified electrode.

Furthermore, as shown in the EIS results, FIGURE 4.10 and TABLE *4.6* the presence of 5 mg HDES decreased the resistance of charger transfer (R_{ct}) in 127 and 2-folds compared with GCE and CNH/GCE, respectively. Also, the higher value of the R_{ct} (34.75 kΩ) for GCE explains why it was not possible to observe a defined oxidation peak for the 5–HT at this electrode, indicating that the bare electrode is not suitable for 5–HT determination. By modifying the electrode with CNH, the reactions that occur in the interface between the electrode and the solution have been improved. The 5-mg electrode has shown better results compared to GCE and CNH/GCE, with a significant improvement in the apparent heterogeneous electron-transfer rate constant (k_{app}) by 255 and 1.7-folds, respectively. Furthermore, it performed better compared to all the electrodes in this study.

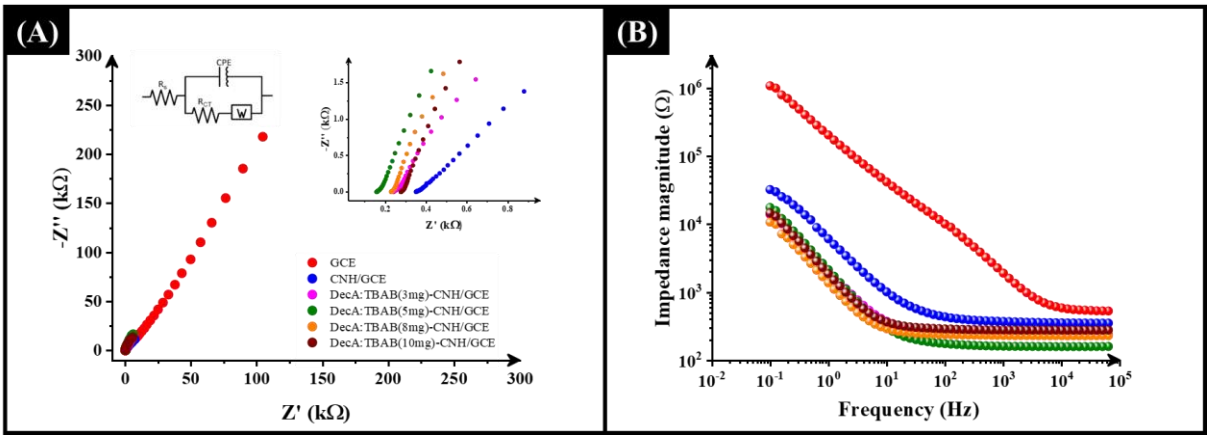

FIGURE 4.10 - Nyquist plots (65,000–0.1 Hz) (A) using 100 µmol L^{-1} 5–HT in 0.2 mol L^{-1} PB pH 7.0 at (●) GCE, (●) CNH/GCE, (●) DecA:TBAB(3mg)-CNH/GCE, (●) DecA:TBAB(5mg)-CNH/GCE, (●) DecA:TBAB(8mg)-CNH/GCE, (●) DecA:TBAB(10mg)-CNH/GCE. Inset: the proposed equivalent circuit. In (B) The Bode plot of impedance magnitude versus frequency.

TABLE 4.6 - EIS data for 100 µmol L^{-1} 5–HT in 0.2 mol L^{-1} PB pH 7.0

Electrode	R_s / Ω	R_{ct} / Ω	*CPE* / µF	α	k_{app} / *cm* s^{-1}
GCE	498.5	34753.0	0.348	0.85	$(3.8\pm1.2)\times10^{-5}$
CNH/GCE	349.6	468.5	55	0.70	$(5.7\pm0.9)\times10^{-3}$
DecA:TBAB(3mg)-CNH/GCE	238.9	502.6	233	0.71	$(5.3\pm0.4)\times10^{-3}$
DecA:TBAB(5mg)-CNH/GCE	158.0	274.1	131	0.81	$(9.7\pm0.7)\times10^{-3}$
DecA:TBAB(8mg)-CNH/GCE	228.4	761.1	279	0.72	$(3.5\pm1.7)\times10^{-3}$
DecA:TBAB(10mg)-CNH/GCE	276.5	456.5	432	0.75	$(5.8\pm1.4)\times10^{-3}$

The enhancement observed with HDES-modified electrodes may be attributed to the ability of HDES to create a more uniform suspension by coating the CNH particles, as discussed further. This could be observed by the α value, which was 0.81 for the electrode modified with 5 mg of DecA:TBAB. This value was close to the GCE value of 0.85. The α represents the roughness associated with capacitance measurements in the EIS, where α = 1 represents a smooth surface[273]. As mentioned in 4.6.2 - , it was observed that the surface of the CNH/GCE electrode is irregular. The α value obtained for this electrode is consistent with this observation. It is possible that such unevenness may have also occurred in the other electrodes that were modified with different amounts of HDES. This is evident as these electrodes exhibit a similar α value to the CNH/GCE electrode. Additionally, the decrease in the analytical signal, observed using amounts of HDES greater than 5 mg, could be attributed to the higher viscosity of the HDES (723±21 mPa s). The viscosity of the HDES influences the electrical conductivity and ionic mobility within the film, potentially reducing redox reactions at the electrode surface and increasing its resistivity, as demonstrated in our previous work[50].

Additionally, using EIS allows for the impedance magnitude to be used as a comparison parameter, which results from the resistive and capacitive behaviours of the electrode at a specific frequency[274]. The Bode plot in FIGURE 4.10B shows a graph of impedance magnitude (|Z|) versus frequency for all modified electrodes. As expected, at low frequencies (between 10^{-1} and 10^{1} Hz), the graph displays a linear decrease in the response of |Z|. However, as the frequency increases, the |Z| reaches a plateau. This pattern can be observed from around 10^{2} Hz to higher frequencies[274]. In general, all the modified electrodes demonstrated lower impedance values compared to the GCE and CNH/GCE electrodes, indicating that the resistance of the material has decreased, leading to an improved flow of electrons through the electrode film. This can be attributed

to the inclusion of HDES, which coated the CNH particles, thereby facilitating electron transfer[50,149].

4.6.2 - Physical Characterization of the Electrode

In this study, we used SEM analysis to examine the surface morphology of the carbon nanohorns in the film without and with HDES. The SEM image in FIGURE *4.11*A and B displays spherical aggregates of the carbon nanohorns for both films. This is consistent with previous literature, which has shown that carbon nanohorns can form spherical aggregates known as dahlia, bud, and seed aggregates based on their appearances[207].

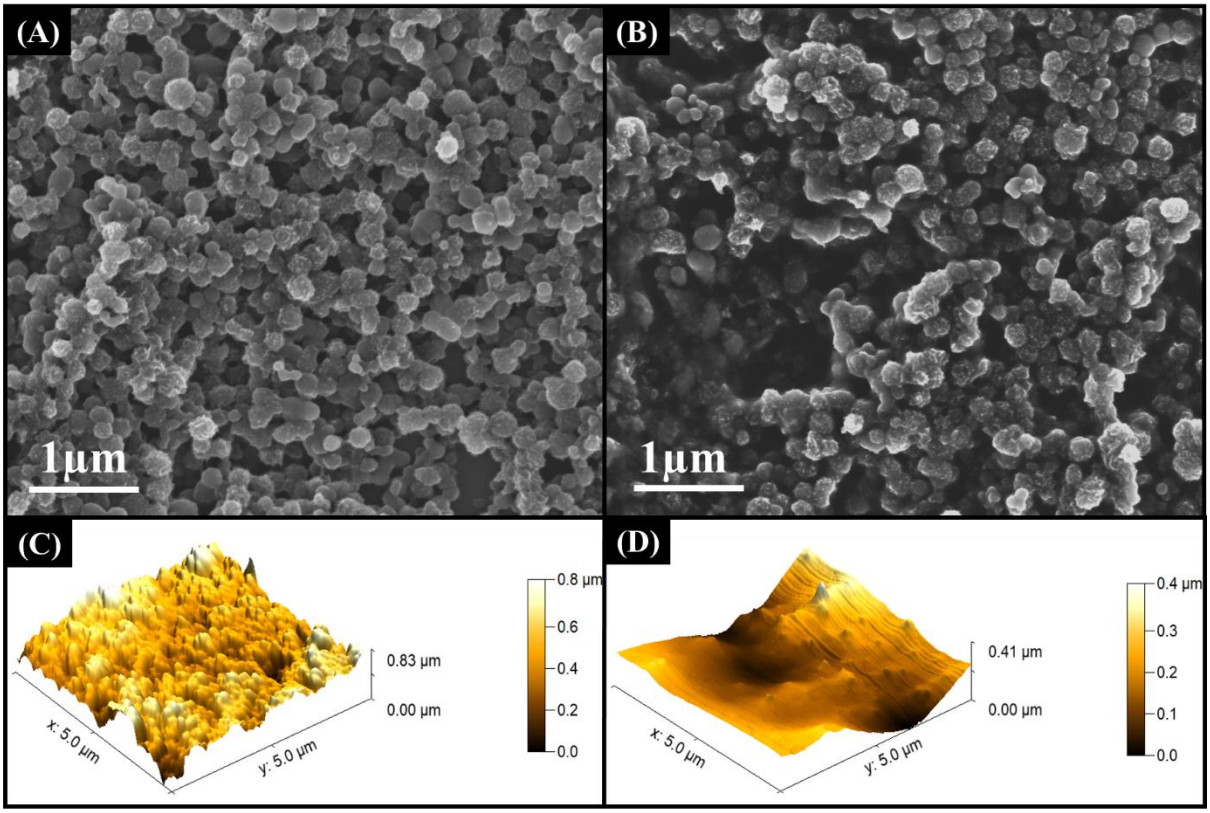

FIGURE 4.11 - SEM images at 100,000x magnification for (A) CNH suspension and (B) CNH+HDES suspension. 3D AFM topography images for (C) CNH suspension and (D) DecA:TBAB+CNH suspension.

Based on the SEM image, it seems that the presence of HDES did not alter the morphology of the carbon material. However, in the film containing HDES, the CNH particles appear more interconnected, forming agglomerates. This observation is further supported by the 3D topography images obtained via atomic force microscopy (FIGURE *4.11*C and D), which indicate that the presence of HDES coated the carbon nanomaterial, resulting in a more uniform surface compared to the rough surface without HDES. These results align with those discussed previously, where the electrode with HDES exhibited a higher α value than the electrode without HDES (CNH/GCE), indicating a smoother surface. To confirm this, we calculated the root mean square (*RMS*) roughness (R_q) for both surfaces modified with and without the HDES-containing film. The results showed an R_q value of 34.93 nm for the surface without HDES and a lower value for the film with HDES, 6.32 nm. These findings support the idea that adding HDES to the suspension generated a more uniform and thin film, which facilitates electron transfer in the electrode-solution interface.

4.6.3 - Catalytic Rate Constant for Serotonin Oxidation and Electroactive Surface Area

The catalytic rate constant of the oxidation of serotonin was calculated based on data obtained from a chronoamperometry study using 100 μmol L^{-1} serotonin (FIGURE *4.12*). This study compared the influence of adding HDES in the film to modify the electrode, and it was carried out using the GCE, CNH/GCE, and DecA:TBAB(5mg)-CNH/GCE. The k_{cat} value of 5–HT oxidation was calculated using the slope of the plot of I_{cat}/I_L *vs* $t^{1/2}$ (FIGURE *4.12* inset) with the EQUATION 3.

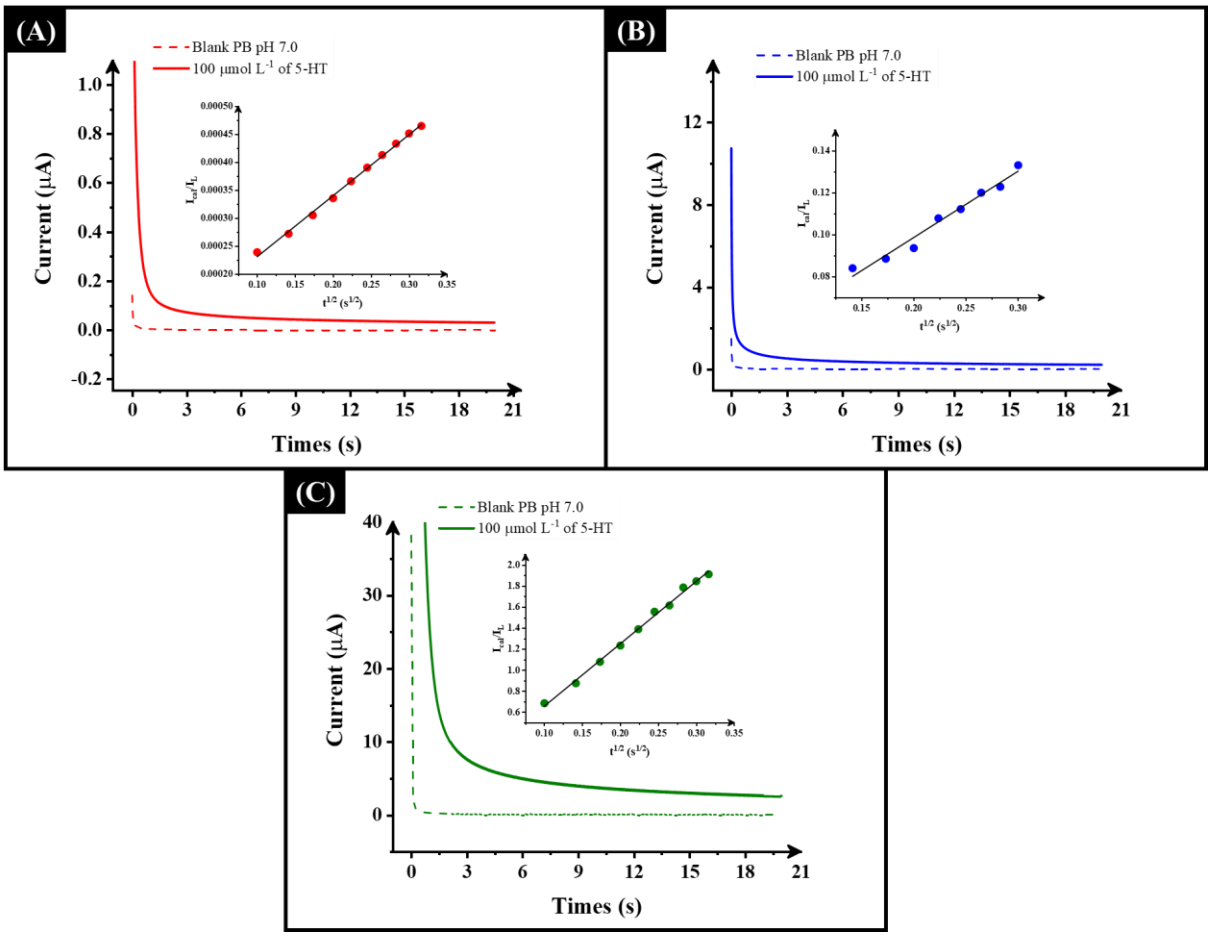

FIGURE 4.12 - Chronoamperogram produced at (A) GCE, (B) CNH/GCE, and (C) DecA:TBAB(5mg)-CNH/GCE with 100 µmol L^{-1} 5–HT in 0.2 mol L^{-1} PBS (pH 7.0) at a potential of 0.35 V. Inset plot of I_{cat}/I_L *vs* $t^{1/2}$.

The obtained k_{cat} values were 2.7×10^2, 4.1×10^3, and 9.0×10^3 L mol^{-1} s^{-1} for GCE, CNH/GCE, and DecA:TBAB(5mg)-CNH/GCE, respectively. These values showed an increase of 2.4 and 34–fold in the k_{cat} value compared to CNH/GCE and GCE, respectively. The values obtained for the k_{cat} using the CNH/GCE and DecA:TBAB(5mg)-CNH/GCE electrodes presented the same magnitude as a report in the literature for 5–HT[275]. This supports the results observed in EIS and CV regarding the catalytic performance of the proposed modified electrode towards oxidizing serotonin.

Furthermore, cyclic voltammetry experiments were conducted to assess the electroactive areas of bare GCE, CNH/GCE, and DecA:TBAB(5mg)-CNH/GCE electrodes. A 100 μmol L^{-1} 5−HT solution was prepared in a supporting electrolyte, consisting of 0.2 mol L^{-1} phosphate buffer at pH 7.0, and cycled at potential scan rates from 15 to 100 mV s^{-1} (FIGURE *4.13*). The electroactive area was calculated using the modified Randles–Ševčík equation for irreversible systems EQUATION 6[276]:

$$I_p = (2.99 \times 10^5 \alpha^{1/2} c D^{1/2} A v^{1/2}) \qquad \text{EQUATION 6}$$

Following EQUATION 6, I_p is the anodic peak current (A), D is the diffusion coefficient of 5−HT (9.0154×10^{-6} cm^2 s^{-1}[277]), A is the electroactive area (cm^2), c is the concentration of 5−HT (1.0×10^{-7} mol cm^3), v is the potential scan rate (V s^{-1}), and α is the transfer coefficient, a measure of the symmetry of the energy barrier for a single electron transfer step. For an irreversible reaction, α can be calculated from the relation $|E_p–E_{p/2}| = 47.7/\alpha$[276]. The electroactive areas for bare GCE, CNH/GCE, and DecA:TBAB(5mg)-CNH/GCE electrodes are 0.012, 0.10, and 0.75 cm^2, respectively. These results suggest that adding the HDES into the film increased the electroactive area by 62 and 7.5-fold, compared to the bare GCE and CNH/GCE. This increase in the electroactive area is likely attributed to the synergistic interaction between HDES and CNH. The results indicate that the enhanced electroactive surface area also plays a crucial role in facilitating serotonin oxidation.

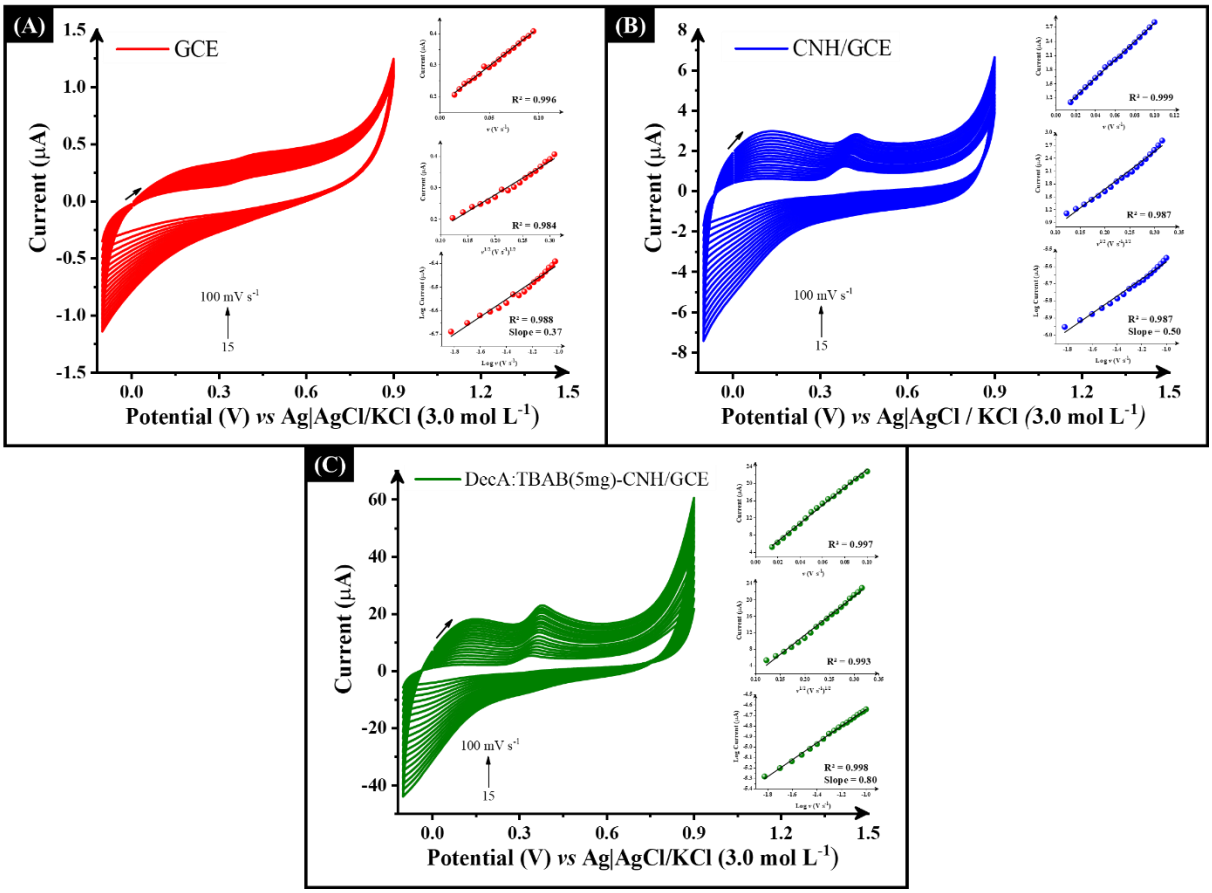

FIGURE 4.13 - Potential scan rate study (15 to 100 mV s^{-1}) with 100 µmol L^{-1} 5– HT in 0.2 mol L^{-1} PBS pH 7.0 performed at (A) GCE, (B) CNH/GCE, and (C) DecA:TBAB(5mg)-CNH/GCE electrodes. Inset: Randles–Ševčík plot.

4.6.4 - pH and Potential Scan Rate Studies

To study the dependence of serotonin oxidation on the pH, a study was carried out using SWV for 100 µmol L^{-1} 5–HT in 0.1 mol L^{-1} BR buffers in the pH range of 2.0 to 12.0 (FIGURE *4.14*).

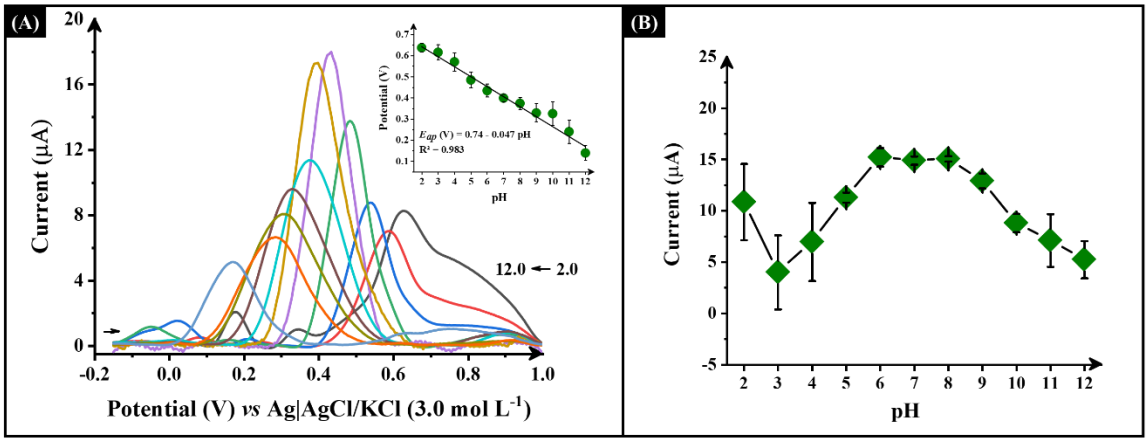

FIGURE 4.14 - (A) SW voltammograms for the pH study (2.0 to 12.0) in 0.1 mol L^{-1} BR buffer for the detection of 100 μmol L^{-1} 5–HT performed at DecA:TBAB(5mg)-CNH/GCE electrodes. Inset plot of the peak potential *versus* the pH. In (B) the effect of pH in the current of the anodic peak. SWV parameters: a = 10 mV, f = 5 Hz, and ΔE = 8 mV.

The results in the inset of FIGURE *4.14*A show a linear correlation between the peak potential and pH. As pH increased, the E_{ap} shifted towards more negative values. The slope of E_{ap} *vs* pH was 47 mV pH^{-1}, indicating that only one proton was involved in the two-electron oxidation process of 5–HT. This behaviour has also been reported in other studies[224,278]. In addition, the I_{ap} *vs* pH plot (FIGURE *4.14*B) shows that the peak current reaches its maximum at pHs 6.0 and 7.0 and decreased in more basic mediums. Considering this result and the lower standard deviation of the measurements, pH 7.0 was selected for further experiments. Moreover, in a study of supporting electrolytes, a 0.2 mol L^{-1} PB solution at pH 7.0 was compared with BR buffer (data not shown). Due to improvements in peak current, PB was chosen as the supporting electrolyte.

A potential scan rate effect on the electrode response was performed to determine which process controls the oxidation reaction of serotonin in the interface electrode solution. CV was carried out in 100 μmol L^{-1} 5–HT in 0.2 mol

L^{-1} PB pH 7.0 at potential scan rate from 15 to 100 mV s^{-1}, FIGURE *4.13* shows the voltammograms with the plots for I_{ap} *vs* $v^{1/2}$ inset. TABLE *4.7* shows the data obtained in the plots for I_{ap} *vs* $v^{1/2}$, *log* (I_{ap}) *vs log (v)*, and I_{ap} *vs v*.

TABLE 4.7 - Figures of merit for plots from scan rate study obtained for 100 µmol L^{-1} 5–HT

Parameters	Plot	Electrode		
		GCE	CNH/GCE	DecA:TBAB(5mg)-CNH/GCE
Slope		1.06	8.73	94.41
Intercept	I_{ap} *vs* $v^{1/2}$	0.065	–0.074	–7.56
R^2		0.984	0.987	0.993
Slope		0.37	0.50	0.80
Intercept	log I_{ap} *vs* log *v*	–6.04	–5.08	–3.84
R^2		0.988	0.987	0.998
Slope		2.43	19.51	210.18
Intercept	I_{ap} *vs v*	0.17	0.84	2.33
R^2		0.996	0.999	0.997

The logarithm of current *versus* the logarithm of the potential scan rate plot can help determine whether a process is diffusion-controlled or adsorption-controlled. A slope closer to 0.5 indicates a diffusion-controlled process, while a value closer to 1 indicates an adsorption-controlled process[247]. In this experiment, the logarithm of I_{ap} and *v* showed a linear relationship for all the electrodes (TABLE *4.7*). The slopes for GCE and CNH/GCE were 0.37 and 0.50, respectively. This means that the reaction for 5–HT is diffusion-controlled in both electrodes. On the other hand, the slope of the logarithmic curve for DecA:TBAB(5mg)-CNH/GCE was 0.80. This indicates that the oxidation of

serotonin may be controlled by both adsorption and diffusion. However, it can be observed from the data of I_{ap} *vs* $v^{1/2}$ plot a linear increase of the peak current with the square root of the scan rate, that may indicate a predominance of a diffusion process. These findings are consistent with other works in the literature, where the redox reaction of serotonin is also controlled by the diffusion process[221,279].

4.6.5 - Analytical Performance

To improve the determination of 5−HT, the SWV parameters were optimized as described in TABLE 3.2. The optimised values based on the oxidation response of serotonin at the proposed electrode, DecA:TBAB(5mg)-CNH/GCE were a = 10 mV, f = 5 Hz, and ΔE = 8 mV.

Under optima conditions, an analytical curve for 5–HT oxidation was constructed in the concentration ranging from 0.50 to 32.71 μmol L^{-1}, FIGURE *4.15* shows the SW voltammograms obtained using DecA:TBAB (5mg)-CNH/GCE electrode and the corresponding linear plot for this concentration range. The LOD and LOQ were calculated using the EQUATIONS 1 and 2 and are 90 nmol L^{-1} and 0.30 μmol L^{-1}, respectively.

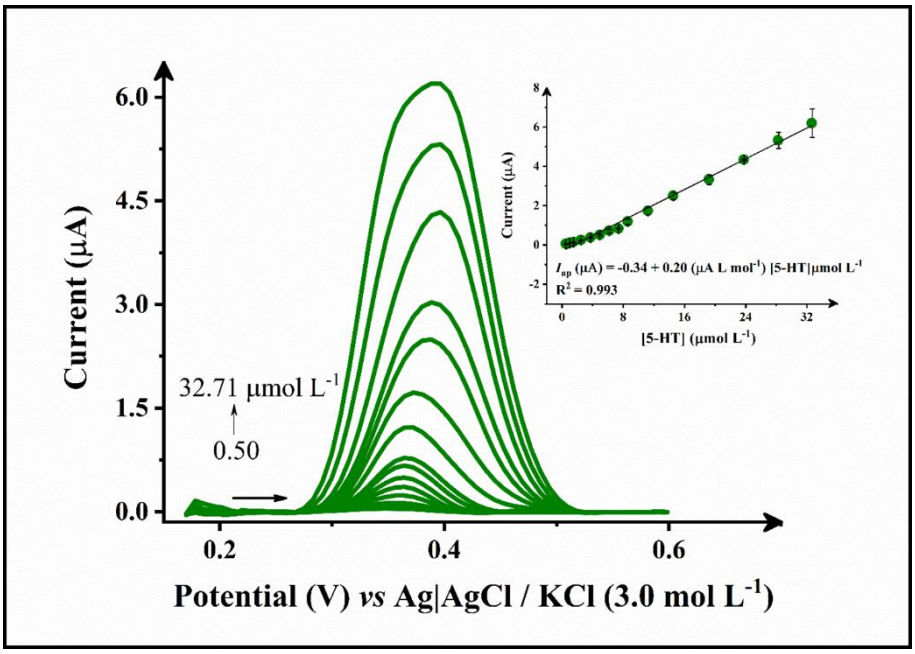

FIGURE 4.15 - SW voltammograms for 5–HT oxidation in 0.2 mol L^{-1} PB pH 7.0 in a concentration range of 0.5 to 32.71 μmol L^{-1}. SWV parameters: *a*: 10 mV, *f*: 5 Hz, and Δ*E*: 8 mV. Inset: the linear plot and equation: I_{ap} (μA) = –0.34+0.20 (μA L $μmol^{-1}$) [5–HT] μmol L^{-1} (R^2 = 0.993).

The results obtained in this study were compared to those reported in the literature for the electrochemical determination of serotonin. As observed in TABLE *4.8*, the figures of merit were satisfactory compared to other sensors reported in the literature. Additionally, the proposed electrode proved to be suitable for analysing serotonin levels commonly found in urine (300 nM to 1650 nM) and serum (270 nM to 1490 nM)[280]. It is important to highlight that a significant advantage of this approach compared to others in the literature is the simplicity and sustainability of the fabrication process, driven by the green nature of the HDES. The eutectic solvent was prepared in a straightforward manner and used directly, without any pre-treatment or additional steps, to modify the surface of the GCE. This method not only reduces the need for complex modification steps but also aligns with environmentally friendly practices, offering a more

accessible and eco-conscious alternative to other electrodes reported for serotonin detection.

TABLE 4.8 - Comparison of the analytical parameters for the voltammetric determination of serotonin

Electrode	Technique	Linear range/ µmol L^{-1}	LOD / µmol L^{-1}	Ref
Fe_3O_4–MWCNT–poly(BCG)/GCE	DPV	0.5 – 100.0	0.08	[224]
NDs-AuNPs-Gr-CSN/GCE	DPV	0.3 – 3.0	0.100	[218]
MWCNT-PANI/GCE	DPV	0.1 – 12.0	0.033	[223]
AuNPs@PPyNPs-based sensor	SWV	0.1 – 15.0	0.03322	[220]
SPCE/ZnONR/PMBDES/AuNP	DPV	0.1 – 25.0	0.00191	[281]
P-WO_3 NS/GCE	LSV	0.01 – 100	0.06	[222]
CS/GCE	DPV	40 – 750	0.7	[282]
DDF-CNT-TiO_2/IL/GC	DPV	1.0 – 650.0	0.154	[283]
Pt/MWCNT/PPy/AgNPs	DPV	0.50 – 5.0	0.15	[284]
MWCNT/Nafion/MAO-A	DPV	0.56 – 2.26	0.2	[285]
GCE/MWCNT-NiO	SWV	5.98 – 62.8	0.118	[286]
DecA:TBAB(5mg)-CNH/GCE	SWV	0.50 – 32.71	0.09	This work

MWCNT: multiwalled carbon nanotube; BCG: bromocresol green; NDs-AuNPs-Gr-CSN: a film based on incorporation of nanodiamonds, gold nanoparticles, and graphite anchored in casein; MWCNT-PANI: multiwalled carbon nanotube-poly (aniline); CUCR: C-undecylcalix[4]resorcinarene;

AuNPs@PPyNPs: polypyrrole nanoparticles decorated with gold nanoparticles; SPCE/ZnONR/PMBDES/AuNP: zinc oxide nanorod/polymethylene blue (deep eutectic solvent)/gold nanoparticles modified screen-printed carbon electrode; P-WO3 NS: phosphorous-doped tungsten trioxide nanosheet; CS: Carbon Spheres; DDF-CNT-TiO2/IL/GC: functionalized carbon nanotubes with titanium dioxide and benzofuran derivative/ionic liquid modified glassy carbon electrode; Pt/MWCNT/PPy/AgNPs: platinum electrode modified with carbon nanotubes/polypyrrole/silver nanoparticles nanohybrid; MWCNT/Nafion/MAO-A: enzyme monoamine oxidase-A (MAO-A) immobilized by covalent binding on multi-walled carbon nanotubes (MWCNT); GCE/MWCNT-NiO: glassy carbon electrodes modified with multiwalled-carbon-nanotube (MWCNT) doped with nickel oxide nanoparticles;

Finally, the reproducibility of the serotonin voltammetric signals and the interference study in the presence of other compounds of interest using the proposed modified electrode were studied. The inter-day and intra-day repeatability studies were performed to evaluate the sensor precision. In the intra-day repeatability, the 5–HT voltammetric response was measured five times in one day (n = 5 for each 5–HT concentration). For the inter-day repeatability, SWV measurements were conducted for three days. FIGURE *4.16*A shows the SW voltammograms obtained for the detection of three different concentrations of 5–HT using one electrode. The relative standard deviation (RSD) values obtained were 2.60 % for 10 μmol L^{-1}, 4.10 % for 20 μmol L^{-1}, and 3.52 % for 30 μmol L^{-1} of 5−HT. FIGURE *4.16*B summarizes the inter-day reproducibility obtained for detecting three different concentrations of 5–HT with three different electrodes showing RSD results between 1 and 5 %. In addition, the stability of the 5−HT voltammetric response was assessed using cyclic voltammetry, FIGURE *4.16*C.

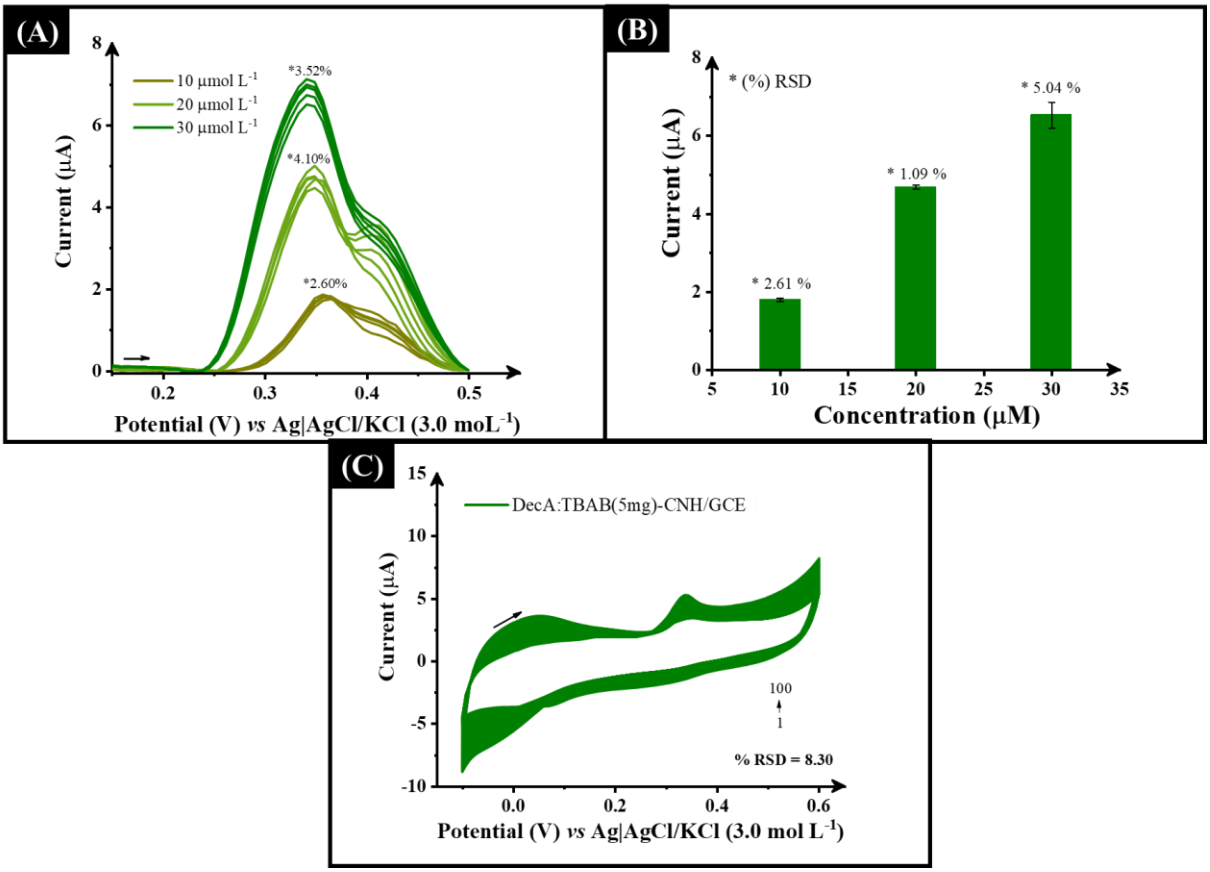

FIGURE 4.16 - (A) SW voltammograms obtained for repetitive measurements (n=5) for different concentrations of serotonin (10, 20 and 30 µmol L^{-1}) using 1 electrode. SWV parameters: a = 10 mV, f = 5 Hz, and ΔE = 8 mV. In (B) the results obtained in the inter-day study for repetitive measurements (n=5) using three different concentrations of serotonin (10, 20 and 30 µmol L^{-1}) at three electrodes. (C) Cyclic voltammograms for 100 µmol L^{-1} 5–HT in 0.2 mol L^{-1} PBS pH 7.0 in the sensor stability study using the DecA:TBAB(5mg)-CNH/GCE electrode. Scan Rate: 50 mV s^{-1}; 100 cycles.

Even after 100 consecutive cycles, the sensor maintained a stable performance, exhibiting a signal reduction of less than 9 % in the 5−HT oxidation process. This can be attributed to the excellent homogeneity obtained by adding HDES in the film suspension to modify the GCE.

The electrode DecA:TBAB(5mg)-CNH/GCE was used to assess the interference of common substances found in biological fluids. The study involved fixing the concentration of 5–HT at 5.0 µmol L^{-1} and adding interfering substances at two different concentration ratios: 1:1 and 10:1 ([interferent]: [5–HT]). The potential interferents evaluated included urea, glucose, ascorbic acid, dopamine, caffeine as well as chloride, sodium, potassium, and sulphate ions. The results of the study were analysed by comparing the analytical response of 5–HT in the presence and absence of interference. FIGURE *4.17* illustrate the comparison of peak current responses of 5–HT in the absence and presence of the potential interfering compounds. The results indicated that, overall, no interference was observed when the interferents were present in a 1:1 and 10:1 excess. This suggests that the proposed electrode demonstrated good selectivity over the set of tested species.

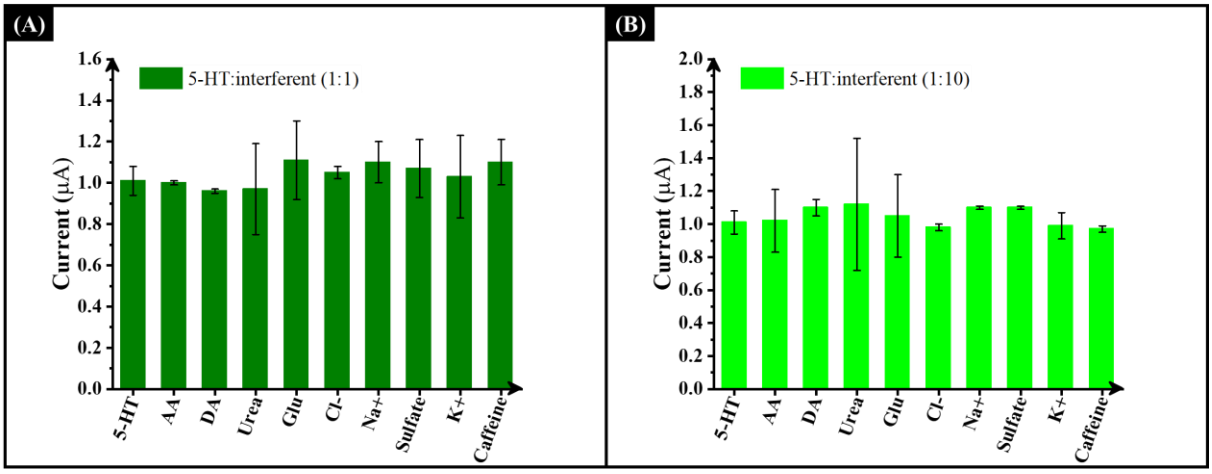

FIGURE 4.17 - Response of serotonin in the absence and presence of different interferents at a ratio of (A) 1:1 5–HT to interferent and (B) 1:10 5–HT to interferent.

4.6.6 - Analysis of Serotonin in Synthetic Biological Fluids

Finally, the DecA:TBAB(5mg)-CNH/GCE electrode was used to detect 5–HT in synthetic urine and bovine serum to assess its suitability for biological fluid analysis. For the analysis, the samples were spiked with three different concentrations of 5–HT and then analysed using SWV under optimised conditions. The recovery values obtained from this analysis, as shown in Table 3, ranged from 92.0 to 101%. These results indicate that the proposed method to modify GCE with carbon nanohorns composites in HDES has great potential for successfully detecting serotonin in biological samples.

TABLE 4.9 - Determination of serotonin in spiked synthetic urine and bovine serum using the proposed electrode DecA:TBAB(5mg)-CNH/GCE

Sample[a]	[5–HT]		
	Added / µM	Found / µM	Recovery[b] / %
Synthetic urine	2.0	1.98±0.09	99.0
	3.0	2.79±0.09	93.0
	5.0	5.07±0.03	101
Bovine serum	2.0	1.84±0.03	92.0
	3.0	2.87±0.09	95.7
	5.0	4.9±0.2	98.2

[a]n=3; [b]Recovery = ([5–HT]Found/[5–HT]Added)×100 %.

4.6.7 - Carbon Paste Electrode Modified with HDES: an Electrochemical Study

As a proof of concept for HDES application, this doctoral research also examined the development of a carbon paste using HDES as a conductive binder alongside mineral oil. A composition of 70 % (w/w) MWCNT and 30 % (w/w) binder (mineral oil and HDES) was utilised. The mineral oil content was partially replaced with varying amounts of HDES, ranging from 0 % to 15 % (w/w), as shown in TABLE 3.3. These proportions were optimised based on previous research[50], where various HDES concentrations were tested to modify a CPE using graphite as the carbonaceous material.

To determine the optimal composition for forming the carbon paste, preliminary studies were conducted using 1.0×10^{-1} mol L^{-1} (1.0 mM) H_2Q in 0.1 mol L^{-1} acetate buffer at pH 4.7, employing both SWV and CV techniques. H_2Q was selected as the redox probe, due to its well-defined and reversible redox behaviour. Its oxidation and reduction occur via a two-electron, two-proton mechanism, making it an ideal candidate for evaluating electrode properties[50].

The voltammetric results (CV and SWV FIGURE *4.18*A and B) reveal a clear correlation between the increased proportion of HDES in the CPEs and higher peak currents. This indicates that incorporating HDES into the CPE enhances the analytical response for H_2Q. Moreover, the HDES used in this study exhibits greater conductivity compared to mineral oil. Consequently, the observed increase in peak currents can be attributed to the superior conductivity of the HDES.

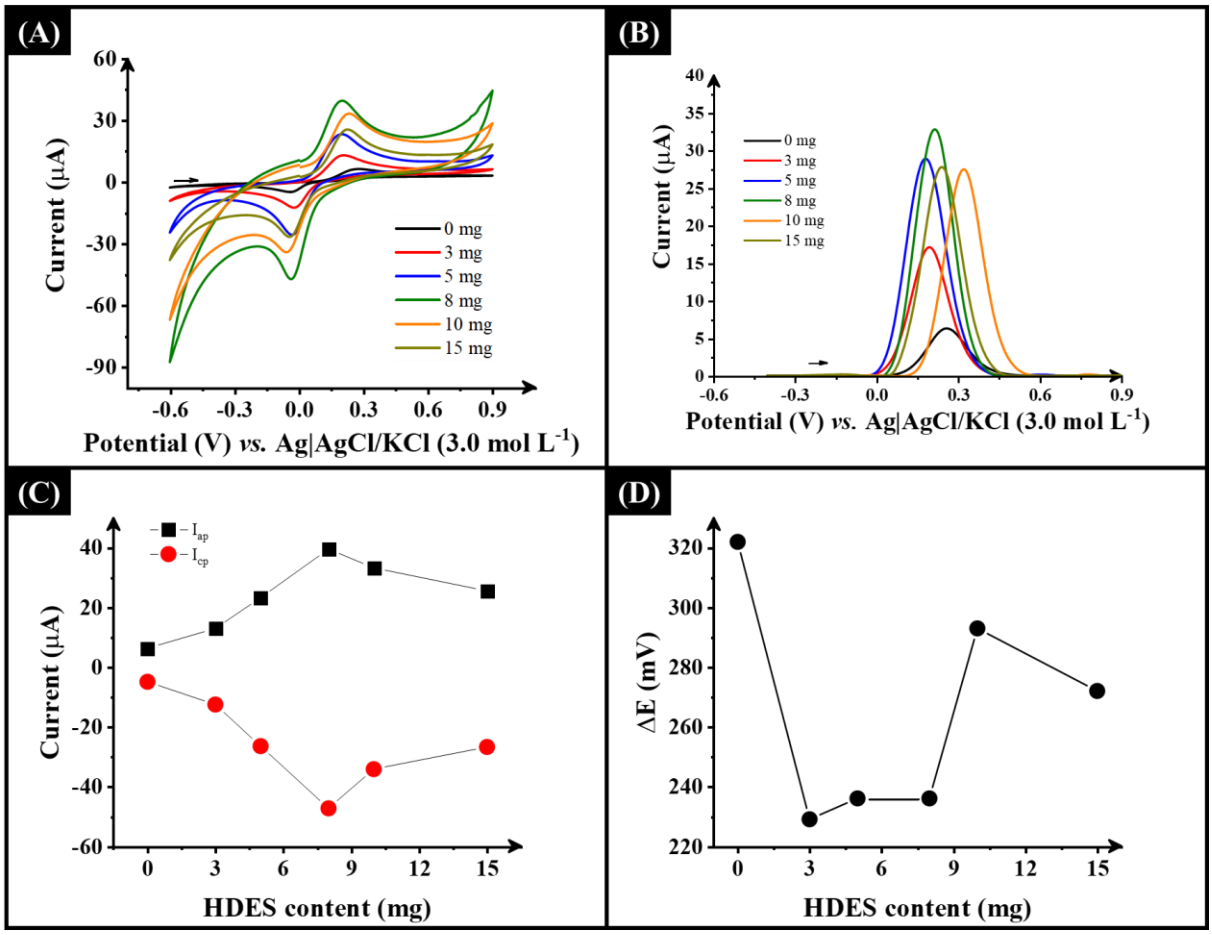

FIGURE 4.18 – (A) and (B) CV and SW voltammograms results obtained for 1mM H_2Q in 0.1 mol L^{-1} acetate buffer pH 4.7 using CPE with different amounts of DecA:TBAB HDES. In (C) plots of I_p *vs* HDES content and (D) ΔE *vs* HDES content. Scan rate: 50 mV s^{-1}; DPV parameters: *a*: 70 mV, *f*: 30 Hz, and ΔE_s: 5 mV.

Well-defined anodic and cathodic peaks were observed for all the electrodes. Also, the I_{ap}/I_{cp} values suggest a *quasi*-reversible behaviour across all electrodes. It can be observed that the analytical signal improved as the HDES content in the film increased up to a concentration of 8 mg. From 10 mg of HDES, the redox peaks for H_2Q slightly decreased. This is apparent when evaluating the peak currents shown in FIGURE *4.18*C. Compared to the bare CPE (which had 0 % of HDES), the 8 mg electrode improved the I_{ap} and I_{pc} by 6.3 and 9.7-fold,

respectively, and presented a reduction in the ΔE_p of 86 mV. Furthermore, all the electrodes modified with HDES significantly enhanced the peak current and reduced the ΔE_p compared to bare CPE. This suggests that modifying the electrode with HDES may have a catalytic effect. The same was observed in the modification of GCE with a film containing the HDES (section 4.6 -).

TABLE 4.10 - Anodic peak current (I_{ap}), cathodic peak current (I_{cp}), ratio of the peak currents (I_{ap}/I_{cp}), and peak-to-peak potential separation (ΔE_p) obtained for 1.0 mM H_2Q

HDES Content / mg	I_{pa} / µA	I_{pc} / µA	I_{pa}/I_{pc}	ΔE_p / mV
0	6.3±0.4	−4.9±0.1	1.29	322±8
3	13.0±0.2	−12.5±0.1	1.04	229±2
5	23.3±0.4	−26.5±0.2	0.88	236±7
8	39.6±0.3	−47.3±0.1	0.84	236±4
10	33.3±0.1	−34.2±0.6	0.97	293±1
15	25.5±0.2	−26.8±0.2	0.95	272±2

To validate the reliability of the results obtained with H_2Q, the proposed electrode was tested for diuron determination in water. Prior to this, the amount of HDES was optimised using CV and DPV in a similar manner to the H_2Q studies. The results (FIGURE *4.19*) confirm the consistency of the H_2Q data, with the electrode containing 8 mg of HDES demonstrating superior performance. This electrode achieved an I_{ap} increase of 2-fold and 1.3-fold in CV and DPV, respectively, compared to the bare CPE.

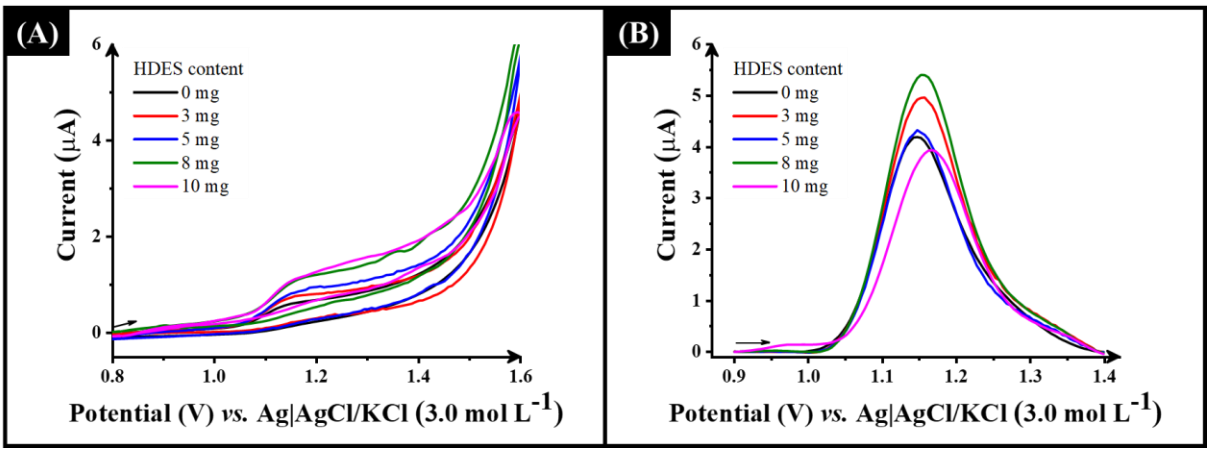

FIGURE 4.19 - (A) and (B) CV and DP voltammograms obtained for 100 µmol L^{-1} Diuron in 0.01 mol L^{-1} PB pH 3.0 using CPE with different amounts of DecA:TBAB HDES. Scan rate: 10 mV s^{-1}; DPV parameters: *a*: 60 mV, *t*: 10 ms, ΔE_s: 4 mV, and Δt: 100 ms.

To complete the electrochemical characterisation, EIS and chronoamperometry studies were conducted to evaluate the electrochemical behaviour and determine the catalytic rate constant for the oxidation of diuron using the HDES(8mg)/CPE. The experiments were conducted in 0.01 mol L^{-1} PB pH 3.0 using 100 µmol L^{-1} of diuron. FIGURE *4.20* shows the results obtained in these studies.

The semicircle diameter, corresponding to the R_{ct}, decreased approximately 5.4-fold upon modifying the CPE with HDES, as shown in FIGURE *4.20*. This significant reduction is likely attributed to the incorporation of HDES as a conductive binder, which enhanced the electrode's electrical properties by lowering the R_{ct} and increasing the apparent rate constant from 1.2×10^{-6} cm s^{-1} to 6.7×10^{-4} cm s^{-1}.

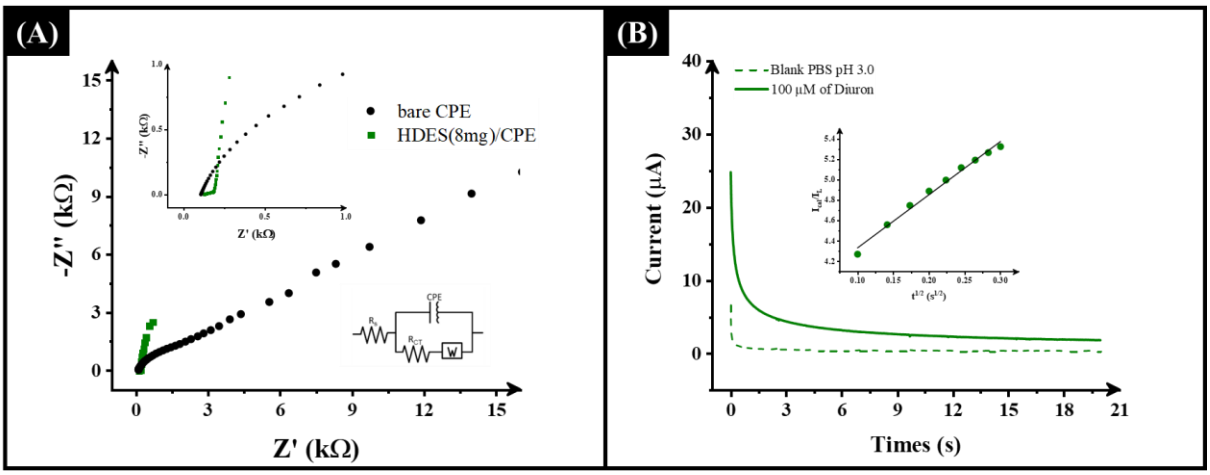

FIGURE 4.20 - (A) Nyquist plots at (●) bare CPE and (●) HDES(8mg)/CPE electrodes using 100 µmol L^{-1} diuron in 0.01 mol L^{-1} PB (pH 3.0). Inset: the proposed equivalent circuit. In (B) Chronoamperogram produced at HDES(8mg)/CPE with 100 µmol L^{-1} diuron in 0.01 mol L^{-1} PBS (pH 3.0) at a potential of 1.1 V. Inset plot of I_{cat}/I_L *vs* $t^{1/2}$.

Furthermore, the catalytic rate constant for diuron at the surface of the HDES-based CPE was determined using chronoamperometry and calculated via EQUATION 3 10^4 mol^{-1} L s^{-1}, is comparable to the value reported in the literature for diuron on a glassy carbon electrode modified with FeTAPc (iron tetraaminophthalocyanine)-single-walled carbon nanotube dendrimers (1.79×10^4 mol^{-1} L s^{-1})[287]. This finding aligns with the results from EIS and CV, confirming the enhanced sensor performance for diuron oxidation in the CPE modified with 8 mg of HDES.

4.6.8 - Influence of pH and Supporting Electrolyte

The effect of pH on the current response of diuron was investigated using DPV with the HDES(8 mg)/CPE electrode. BR buffer (0.2 mol L^{-1}) was used across a pH range of 2.0 to 7.0. As shown in FIGURE *4.21*A and B, the

anodic peak current reached its maximum at pH 3.0, which was selected as the optimal condition.

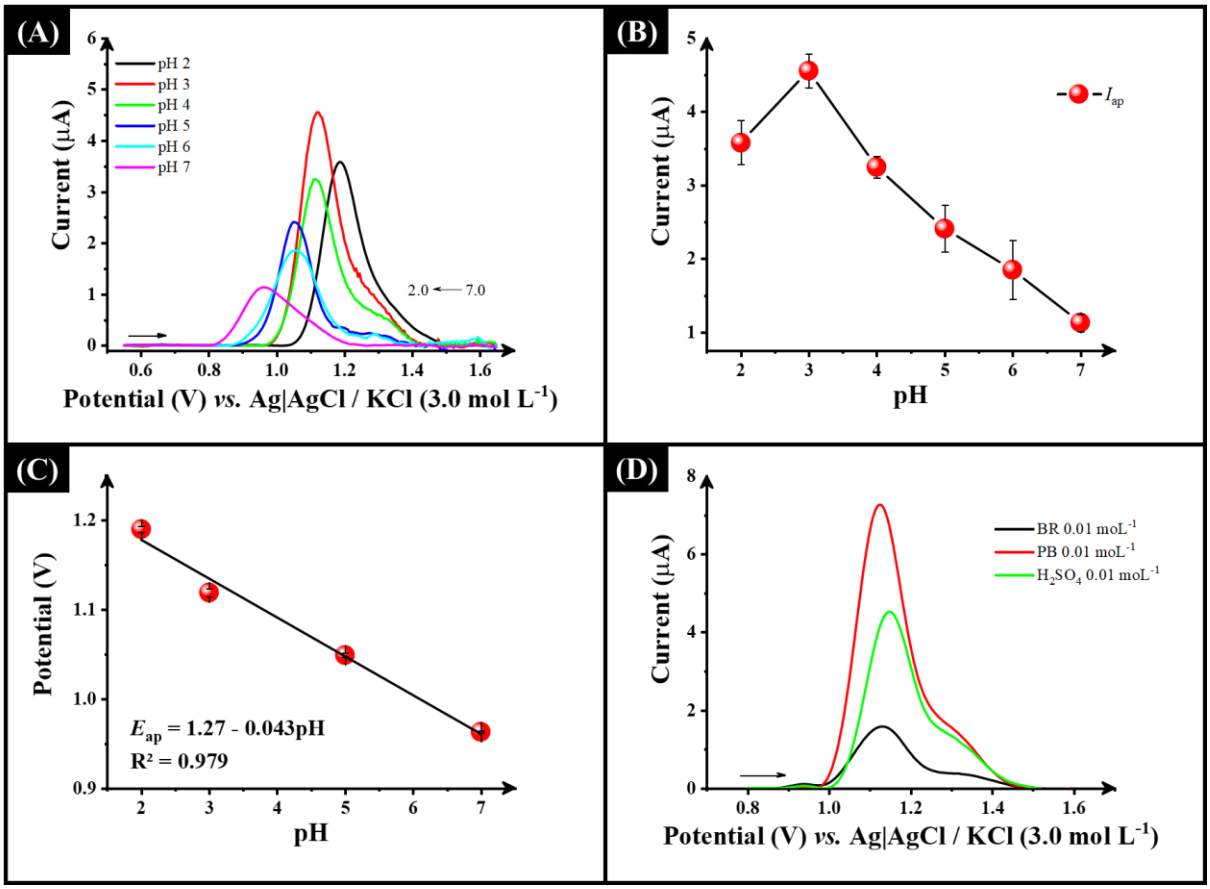

FIGURE 4.21 - (A) DP voltammograms obtained for diuron at different pH values. (B) and (C) Plots of I_{ap} *vs* pH and E_{ap} *vs* pH. (D) DPV results for the supporting electrolyte study at pH 3.0. DPV parameters: *a*: 60 mV, *t*: 10 ms, ΔE_s: 4 mV, and Δt: 100 ms.

The anodic peak potential showed a linear dependence on pH (FIGURE *4.21*C), shifting to more negative values as pH increased. This behaviour indicates the involvement of protons in the redox process of diuron. Moreover, the slope of −0.043 pH^{-1} indicates a difference in the proton-to-electron ratio. The observation suggests that although two electrons participate in the oxidation process, the role of protons might be less direct or affected by other

mechanistic factors. This result is in accordance with another report in the literature[288]. Moreover, the electrochemical behaviour of diuron at pH 3.0 was evaluated using various electrolytes, including Britton-Robinson buffer, phosphate buffer, and sulfuric acid solution, each at a concentration of 0.01 mol L^{-1}. Among these, the highest oxidation current was observed with the phosphate buffer solution (FIGURE *4.21*D). Consequently, PB solution at pH 3.0 was selected as the optimal electrolyte for subsequent experiments.

4.6.9 - Analytical Performance and Diuron Determination in Water

To enhance the determination of diuron, the DPV parameters were optimised, as summarised in TABLE 3.4. The optimised parameters were pulse amplitude (a) of 60 mV, pulse time (t) of 10 ms, step potential (ΔE_s) of 4 mV, and interval time (Δt) of 100 ms, based on the oxidation response of diuron at the proposed electrode, HDES (8 mg)/CPE.

Under these optimal conditions, an analytical curve for diuron oxidation was constructed over a concentration range of 1.0 to 47.2 μmol L^{-1}. FIGURE *4.22* shows the DP voltammograms obtained using the HDES (8 mg)/CPE electrode, along with the corresponding linear plot for this concentration range. The LOD and LOQ, calculated using the EQUATIONS 1 and 2, were determined to be 0.20 μmol L^{-1} and 0.67 μmol L^{-1}, respectively.

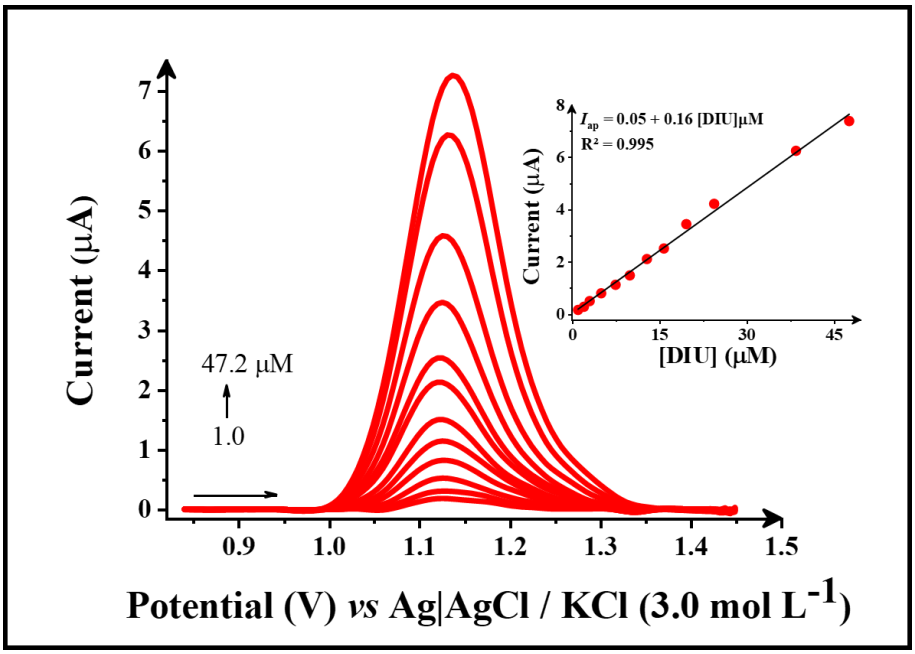

FIGURE 4.22 - DP voltammograms for diuron oxidation in 0.01 mol L^{-1} PB pH 3.0 in a concentration range of 1.0 to 47.2 μM. Inset: the calibration plot. DPV parameters: *a*: 60 mV, *t*: 10 ms, ΔE_s: 4 mV, and Δt: 100 ms.

The results of this study were compared with those reported in the literature for the electrochemical determination of diuron (TABLE *4.11*). As discussed in the section 4.6.5 - , this sensor offers significant advantages over others in the literature due to the simplicity and sustainability of its fabrication process.

TABLE 4.11 - Comparison of the analytical parameters for the voltammetric determination of diuron.

Electrode	Technique	Linear range/ μmol L^{-1}	LOD / μmol L^{-1}	Ref
MIP-PGCE	DPV	10 – 500	43.43	[289]
NiOPc/CPE	Amperomety	5.0 – 140	1.7	[290]
PPy-MWCNT/PSS	SWV	0.86 – 43	0.26	[291]
p-NiTSPc-CFME	SWV	21.46 – 150	8.030	[292]
HDES(8 mg)/CPE	DPV	1.0 – 47.2	0.20	This work

MIP-PGCE: molecularly imprinted polymer modified pencil graphite electrode. MWCNTs-CS@NGQDs/GCE: GCE modified with chitosan-encapsulated multi-walled carbon nanotubes (MWCNTs-CS) combined with nitrogen-doped graphene quantum dots (NGQDs). NiOPc/CPE: carbon paste electrode modified with hemin and nickel (II) 1,48,11,15,18,22,25-octabutoxy-29H, 31H-phthalocyanine complex. PPy-MWCNT/PSS: polypyrrole composite with functionalized multi-walled carbon nanotubes deposited onto glass substrates covered with indium tin oxide (ITO), produced with alternated layers of polystyrene sulphonated (PSS). p-NiTSPc-CFME: Nickel(II) tetrasulfonated phthalocyanine (p-NiTSPc)-modified carbon fiber microelectrode (CFME).

Finally, the HDES (8 mg)/CPE electrode was employed to determine diuron in tap water sample. Tap water was spiked with diuron at concentrations of 6 μM and 9 μM, and the results are summarized in TABLE *4.12*. The recoveries ranged from 92 % to 97 %, indicating minimal matrix effects in the tested samples. These findings highlight the sensor's potential as a promising alternative for the voltammetric determination of diuron in environmental water samples.

TABLE 4.12 - Determination of diuron in tap water using the electrode HDES(8mg)/CPE

Diuron		
Added / μmol L^{-1}	Found[a] / μmol L^{-1}	Recovery[b] / %
6.0	5.8±0.1	96.7
9.0	8.3±0.1	92.2

[a]n=3; [b]Recovery = ([DIU]Found/[DIU]Added)×100 %.

Furthermore, intra-day and inter-electrode repeatability studies were conducted to evaluate the precision of the HDES(8 mg)/CPE electrode. The diuron voltammetric response (DPV) was measured three times in a single day using three different electrodes. As shown in FIGURE *4.23*A, the relative standard deviation for this study was below 1 %, demonstrating excellent precision of the DPV method with the proposed electrode.

Additionally, the stability of the diuron voltammetric response was assessed using cyclic voltammetry. Even after 50 consecutive cycles, the sensor maintained stable performance, with a signal reduction of less than 5% for the diuron oxidation process.

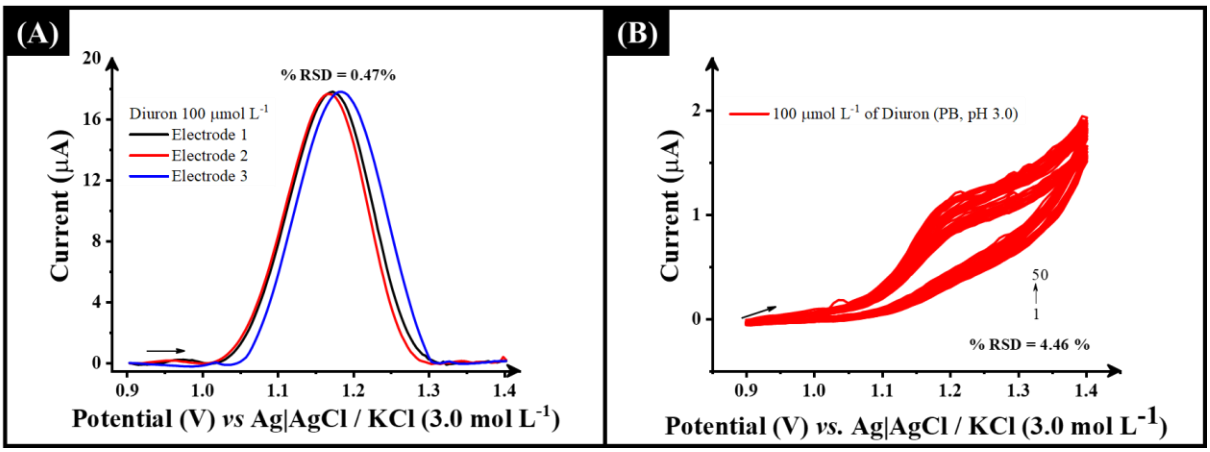

FIGURE 4.23 - (A) DP voltammograms of reproducibility using three different electrodes in the presence of 100 µM. (B) .DPV parameters: *a*: 60 mV, *t*: 10 ms, ΔE_s: 4 mV, Δt: 100 ms. (B) Cyclic voltammograms for 100 µmol L^{-1} diuron in 0.01 mol L^{-1} PB pH 3.0 in the sensor stability study using the HDES(8mg)/CPE electrode. Scan Rate: 10 mV s^{-1}; 50 cycles.

4.7 - Conclusions

The study successfully prepared and characterised a hydrophobic deep eutectic solvent based on decanoic acid and tetrabutylammonium bromide. Spectroscopic and thermal analyses confirmed its formation, eutectic point, and key physicochemical properties. For the first time, this study optimised the synthesis temperature and time, demonstrating that prolonged synthesis is unnecessary and directly impacts the process's sustainability. Furthermore, green metrics evaluation showed that the proposed HDES aligns well with green chemistry principles, making it a sustainable system.

The HDES demonstrated significant potential as an electrode modifier for developing novel electrochemical sensors. In serotonin detection, the HDES-modified electrodes exhibited enhanced sensitivity, selectivity, and stability. Optimization of parameters such as pH and potential scan rate

contributed to high-performance analytics, confirmed by the analysis of serotonin in synthetic biological fluids with minimal interference effects. For diuron detection, the HDES-modified carbon paste electrodes provided consistent performance, enabling precise and reliable measurements in environmental samples like tap water.

The outcomes emphasise the HDES's compatibility with green chemistry principles, particularly its ability to enhance electrode performance while supporting sustainable sensor fabrication. These results establish a base for the broader application of HDES in electrochemical sensing technologies.

Part II

4.8 - Sustainable Silver Nanoparticle-Enhanced Graphite Filament for Additive Manufacturing

This work focused on synthesising silver nanoparticles onto graphite using an eco-friendly methodology. Developing these high-performance filaments aims to address current challenges to the commercial viability of additive manufacturing in electrochemistry, enabling a transformative approach to achieving in situ environmental monitoring.

4.8.1 - Synthesis of AgNPs on Graphite and Incorporation into Filament

AgNPs were synthesised on the surface of graphite flakes using an eco-friendly methodology[250]. This involved submerging graphite powder in a 20 mg mL^{-1} aqueous solution of $AgNO_3$ with continuous stirring overnight. The process utilised only water as the solvent and did not require any additional reducing agents, instead relying solely on the inherent reducing properties of graphite. After filtration and drying, the modified graphite powder was characterised to confirm the presence of AgNPs. FIGURE *4.24* presents the characterisation of the AgNP-graphite powder, as analysed by SEM/EDX, XRD, and XPS.

FIGURE *4.24*A shows a micrograph obtained for the modified graphite, where the presence of small spherical moieties can be seen predominantly on the edges of the graphite flakes. To further confirm the presence of silver on the graphite surface, EDX mapping was performed on selected areas. An example region, along with its corresponding carbon and silver maps, is shown in FIGURE *4.24*B to D. These maps reveal that much of the composition consists

of carbon, corresponding to the graphite flakes, while small, dispersed silver particles appear as distinct spherical points across the sample.

XRD analysis was then performed on graphite powder modified with AgNPs, FIGURE *4.24*E. The XRD pattern of AgNP-graphite shows several reflection peaks at 2Θ values of 37.84°, 44.37°, 54.33° and 77.34°, which correspond to the (111), (200), (142) and (311) planes of the face-centred cubic (*fcc*) crystal structure of silver (JCPDS, No. 04-0783), confirming the crystalline nature of the AgNPs formed on the surface of graphite[293,294]. Furthermore, the crystallite sizes were determined from the reflection peaks for AgNPs using the Debye-Scherrer EQUATION 7[295,296]:

$$D = \frac{k\lambda}{\beta Cos\theta} \qquad \text{EQUATION 7}$$

Where D represents the average crystallite size calculated for all the reflection peaks, k is the Scherrer constant commonly taken as 0.94[297], λ is the wavelength of X-ray source, β is the corrected sample peak broadening or full width at half maximum (FWHM) and θ is the Bragg diffraction angle at peak position. Considering the four identified peaks, the average size of AgNPs deposited on graphite using the described sustainable approach was 15.05 ± 4.07 nm, confirming the nano-size nature of the likely AgNPs synthesised.

To further confirm the presence of the AgNPs on the surface of the graphite, the samples were analysed through XPS. FIGURE *4.24*F reveals two prominent peaks at 368 eV and 374 eV, corresponding to Ag $3d_{5/2}$ and Ag $3d_{3/2}$, respectively. The fitting of these peaks yields an RSD of 1.176. These results align with previous reports in the literature[298,299], confirming that the observed doublets are characteristic of Ag^0.

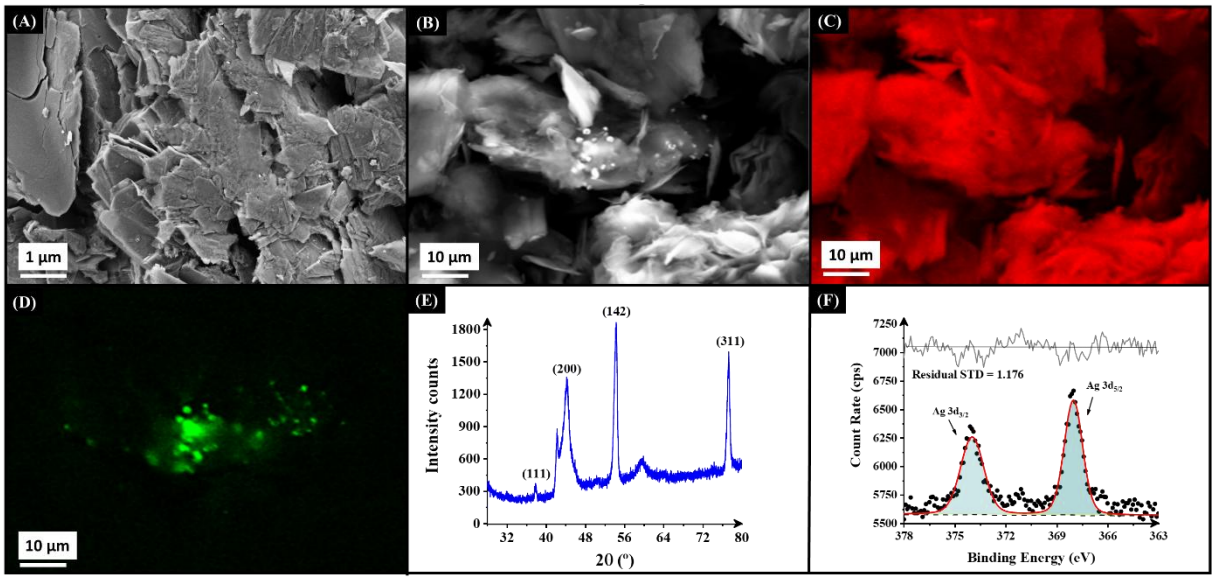

FIGURE 4.24 - (A) SEM image for modified graphite powder. (B to D) EDX elemental mapping analysis of graphite area, carbon map, and silver map, respectively. (E) XRD pattern of AgNP-graphite and (F) XPS data for AgNP-graphite.

Once the presence of AgNP on the graphite was confirmed, this was incorporated into conductive additive manufacturing filament. To produce a high-performance conductive filament with graphite, it is essential to combine carbon black and graphite. This necessity arises from the properties of the graphite content in the filament. As indicated in a previous study, higher graphite concentration in the filament can weaken the conductive network due to the size difference between small carbon black particles and large graphite flakes. A balance of both types is needed for optimal conductivity, as too many large flakes reduce connectivity[47].

Filaments were produced using a total carbon loading of 30 wt%, with an optimised ratio of carbon black (18 %) to graphite (12 %) established in a previous study[47]. These included filaments incorporating unmodified graphite (CB/G/PLA) and AgNP-modified graphite (CB/Ag-G/PLA). Both filaments demonstrated impressive low-temperature flexibility, as shown in FIGURE *4.25*, a property attributed to the castor oil plasticiser[46].

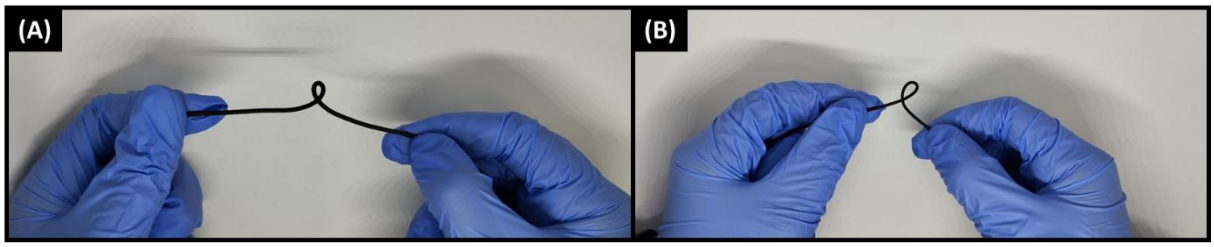

FIGURE 4.25 - Photographs of bespoke (A) graphite and (B) AgNP-modified graphite filaments, highlighting the flexibility.

In addition to flexibility, both filaments showed excellent conductivity with bulk resistances across 10 cm of filament measured to be (400 ± 37) Ω and (422 ± 33) Ω for the CB/G/PLA and CB/Ag-G/PLA respectively. This indicates that the inclusion of this loading of AgNPs doesn't statistically change the bulk resistance of the filament. Once the filament was available, additively manufactured electrodes were produced ready for electrochemical characterisation.

4.8.2 - Electrochemical Characterisation of the Additive Manufactured Electrodes

After physicochemical characterisation, the 3D-printed electrodes were evaluated for their electrochemical performance. Initial tests involved scan rate studies using the near-ideal outer-sphere redox probe $[Ru(NH3)_6]^{3+}$ (1.0×10^{-3} mol L^{-1} in 0.1 mol L^{-1} KCl). FIGURE *4.26*A and B illustrate the scan rate profiles (5–500 mV s^{-1}) for CB/G/PLA and CB/Ag-G/PLA electrodes. Both electrodes demonstrated the expected redox behaviour for $[Ru(NH_3)_6]^{3+}$, with a one-electron reduction peak at approximately –0.2 V. The CB/Ag-G/PLA electrodes exhibited a sharper and more well-defined redox profile. The insets in

FIGURE *4.26* show the corresponding Randles-Ševčík plots, confirming the diffusion-controlled nature of the electrochemical process.

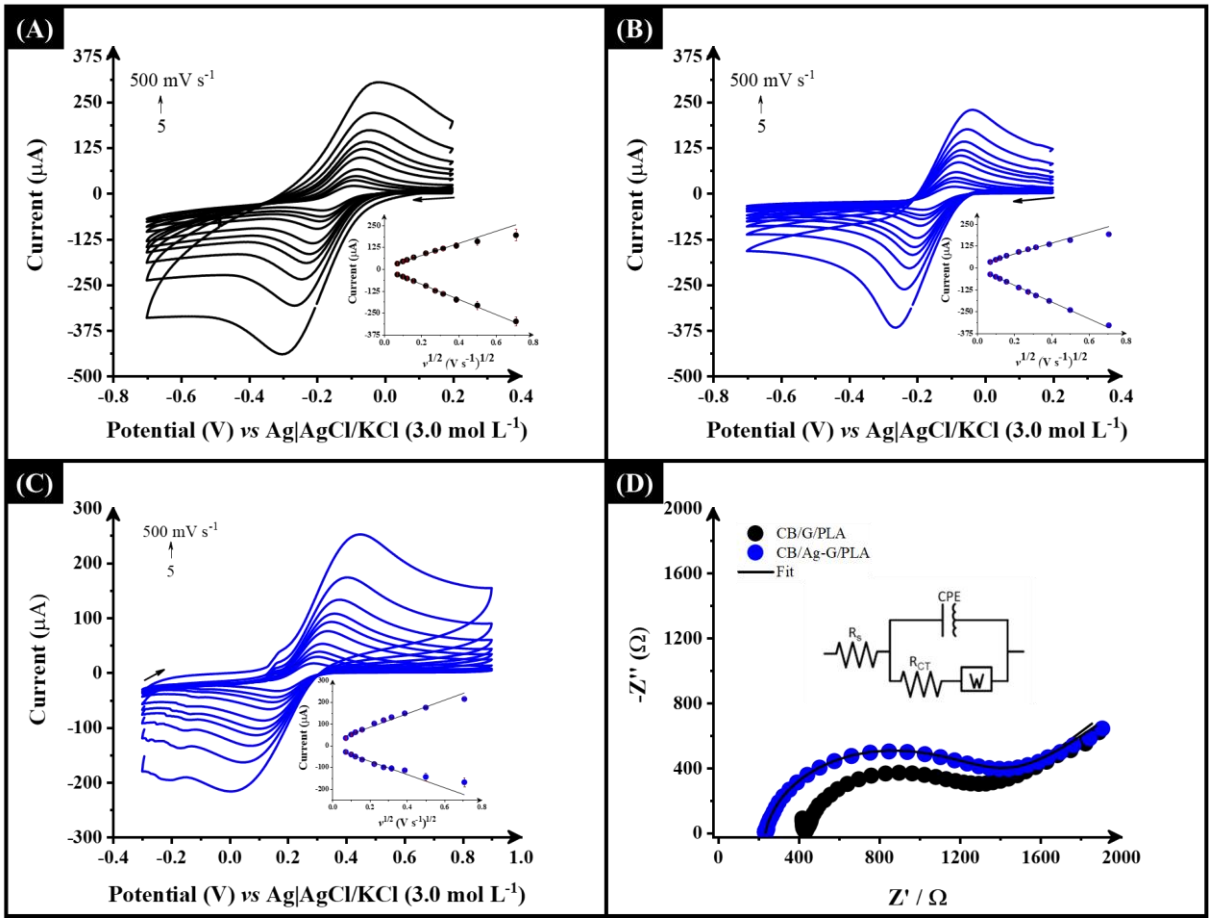

FIGURE 4.26 – Potential scan rate study (5–500 mV s^{-1}) with $[Ru(NH_3)_6]^{3+}$ (1 mM in 0.1 M KCl) performed in the (A) only-graphite (CB/G/PLA) and (B) AgNP-graphite (CB/Ag-G/PLA) as the WE, respectively. Inset: Randles–Ševčík plot. (C) Potential scan rate study (5–500 mV s^{-1}) with $[Fe(CN)_6]^{4-/3-}$ (1 mM in 0.1 M KCl) performed in the AgNP-graphite as the WE. Inset: the Randles–Ševčík plot. (D) Comparison of EIS Nyquist plots of $[Fe(CN)6]^{4-/3-}$ using only graphite (CB/G/PLA) and AgNP-graphite (CB/Ag-G/PLA) electrodes. Inset: the proposed equivalent circuit.

The results presented in FIGURE *4.26* enabled the calculation of the standard heterogeneous electron transfer rate constant (k^0), which presented an improvement from (1.75±0.06)×10^{-3} cm s^{-1} for CB/G/PLA to (1.9±0.2)×10^{-3} cm s^{-1} for the AgNP-modified electrodes. Additionally, the electrochemical surface area increased from (0.53±0.04) cm^2 for CB/G/PLA to (0.62±0.03) cm^2 for CB/Ag-G/PLA, attributed to the high surface area of the AgNPs.

The electrodes were then further tested against the commonly used inner-sphere probe $[Fe(CN)_6]^{4-/3-}$ (1 mM in 0.1 M KCl). The potential scan rate study for $[Fe(CN)_6]^{4-/3-}$ using the AgNP electrode is presented in FIGURE *4.26*C, with the Randles- Ševčík equation once again inset showing the electrochemical process is of a diffusion-controlled nature.

Finally, the CB/Ag-G/PLA electrodes were subjected to EIS using 1.0×10^{-3} mol L^{-1} $[Fe(CN)_6]^{4-/3-}$ in 0.1 mol L^{-1} KCl, with the corresponding Nyquist plot shown in FIGURE *4.26*D. By fitting the data to the equivalent circuit model (inset in FIGURE *4.26*D), the solution resistance (R_s) and charge transfer resistance were determined. The results suggest no substantial improvement in charge-transfer resistance, given the variations in standard deviation. The R_{CT} values were 0.91 (± 0.27) kΩ for CB/G/PLA and 1.08 (± 0.10) kΩ for CB/Ag-G/PLA. However, a notable improvement in solution resistance was observed for the CB/Ag-G/PLA electrode. The R_S value for CB/Ag-G/PLA was 236 (± 5) Ω, significantly lower than the 432 (± 4) Ω measured for CB/G/PLA, indicating reduced resistance introduced by the CB/Ag-G/PLA electrode. After completing the electrochemical characterisation of the AgNP electrodes, the focus shifts to evaluating their performance in the electroanalytical detection of cadmium.

4.8.3 - Electroanalytical Determination of Cadmium (II)

The detection of Cd(II) in water is crucial to achieving the United Nations Sustainable Development Goal 6: Clean Water and Sanitation. Regulatory bodies, including the EPA and EU, have set a cadmium exposure limit of 5 ppb (4.45×10^{-8} mol L^{-1})[300–302], which serves as a benchmark for developing sensors in this field. To facilitate commercial adoption, the 3D-printed electrodes utilised in this part were used without any post-print activation procedures.

To test the CB/Ag-G/PLA electrodes towards the detection of Cd(II), first, the buffer for the measurements was optimised, considering the pH as 5.0 and BR buffer, as previously established in the literature[303–307]. In this way, BR buffer and BR buffer+ 0.1 mol L^{-1} KCl, to improve the ionic strength, were tested for the detection of 100 ppb (8.9×10^{-7} mol L^{-1}), where it was found that the addition of KCl did not improve the performance of the system (data not shown).

Following this, the deposition potentials (FIGURE *4.27*) and deposition times (FIGURE *4.28*) were optimised for the DPV and SWV techniques (TABLE *3.5*). It was concluded that a deposition potential of –1.0 V and time of 60 s was optimal for DPV, and a potential of –1.1 V and time of 60 s was optimal for SWV. Finally, the parameters for both DPV and SWV were optimised, with the final value are found to be DPV: *a*: 25 mV, *t*: 0.05 s, ΔE_s: 5 mV, and $t_{\text{deposition}}$: 60 s and SWV: *a*: 20 mV, *f*: 25 Hz, ΔE_s: 5 mV, and $t_{\text{deposition}}$: 60 s.

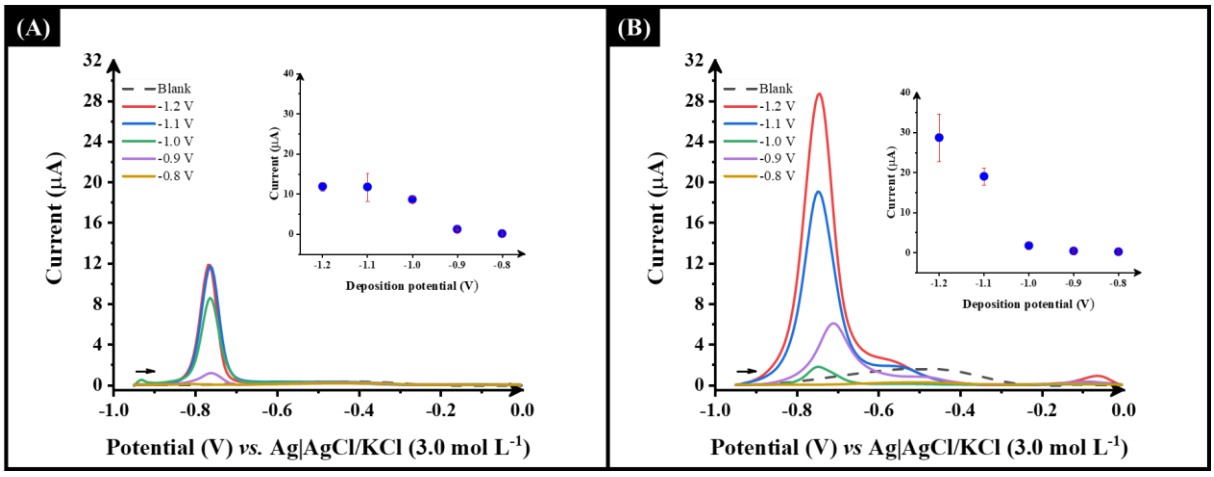

FIGURE 4.27 - (A) DPV and (B) SWV performed at the CB/Ag-G/PLA electrode in 0.1 mol L^{-1} BR (pH 5.0) using 100 ppb of Cd(II) at different deposition potentials (−1.2, − 1.1, − 1.0, −0.9, and −0.8 V) for 60 s. Inset: plot of the results obtained for repetitive measurements (n=3) at three different electrodes. DPV parameters: a = 25 mV, t = 0.05 s, ΔE_s = 5 mV, and $t_{deposition}$ = 60 s. SWV parameters: a = 20 mV, f = 25 Hz, ΔE_s = 5 mV, and $t_{deposition}$ = 60s.

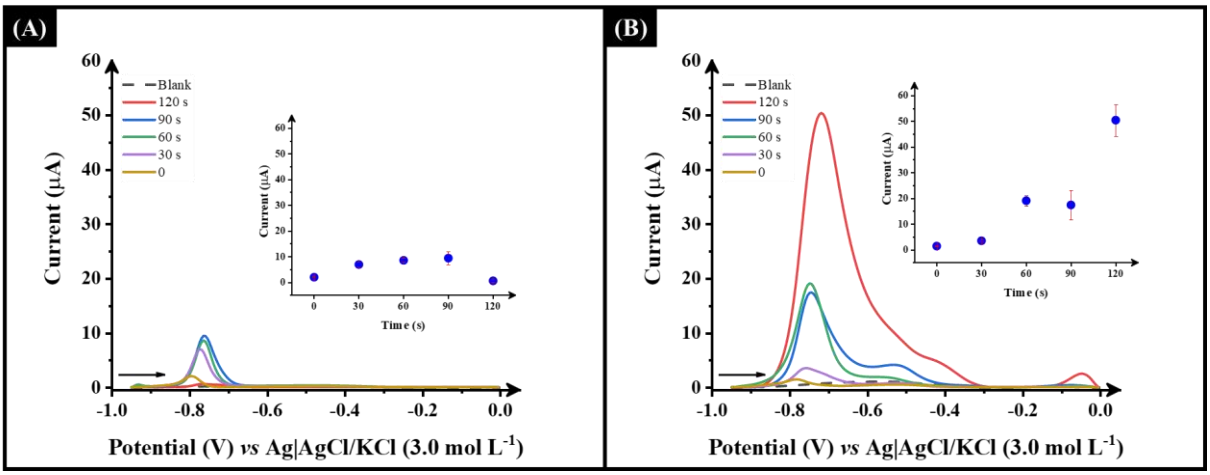

FIGURE 4.28 - (A) DPV and (B) SWV performed at the CB/Ag-G/PLA electrode in 0.1 mol L^{-1} BR (pH 5.0) using 100 ppb of Cd(II) at different deposition times (0, 30, 60, 90, and 120 s). Inset: results obtained for repetitive measurements (n=3) at three different electrodes. DPV parameters: a = 25 mV, t = 0.05 s, ΔE_s = 5 mV, $E_{deposition}$ = −1.1 V. SWV parameters: a = 20 mV, f = 25 Hz, ΔE_s = 5 mV, $E_{deposition}$ = −1.1 V.

Under the optimised conditions, CB/G/PLA and CB/Ag-G/PLA electrodes were evaluated for detecting 100 ppb Cd (II). The results from SWASV and DPASV are shown in FIGURE *4.29*A and B, respectively. In both techniques, the AgNP-modified electrodes produced significantly higher peak currents compared to the graphite-only electrodes. This enhancement is attributed to the increased surface area and superior electrochemical performance provided by the AgNPs. Additionally, the SWASV technique generated notably higher currents compared to DPASV at the same Cd (II) concentration, highlighting its greater sensitivity.

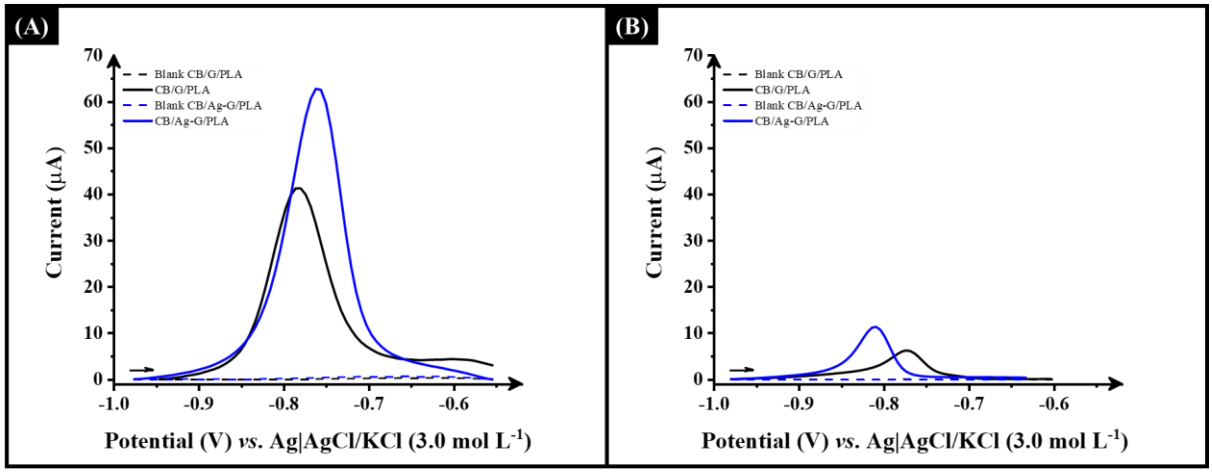

FIGURE 4.29 - (A) SWAS and (B) DPAS voltammograms in the presence of 100 ppb of Cd(II) performed at CB/G/PLA and CB/Ag-G/PLA electrodes in 0.1 mol L^{-1} BR (pH 5.0). SWASV parameters: a = 80 mV, f = 40 Hz, ΔE_s = 6 mV, $E_{deposition}$ = –1.1 V, and $t_{deposition}$ = 60s. DPASV parameters: a = 50 mV, t = 0.02 s, ΔE_s = 5 mV, $E_{deposition}$ = −1.0 V, and $t_{deposition}$ = 60s.

To further test the electrode, both the as-printed only graphite and AgNP-graphite electrodes were then used to produce an analytical curve for the detection of cadmium (II) within BR buffer (pH = 5.0) using SWASV. The SWASV results for the CB/G/PLA and CB/Ag-G/PLA electrodes are overlayed in

FIGURE *4.30*A for comparative purposes, showing the significant improvement in sensitivity with the electrode containing AgNP graphite. The detection of Cd(II) was achieved over two linear ranges, between 1.5 – 15 ppb (1.3×10^{-8} – 1.3×10^{-7} mol L^{-1}) and 30 – 100 ppb (2.7×10^{-7} – 8.9×10^{-7} mol L^{-1}). It was found that the CB/Ag-G/PLA electrode presented a LOD of 0.43 ppb (3.83×10^{-9} mol L^{-1}) and a LOQ of 1.44 ppb (1.28×10^{-8} mol L^{-1}), which are clearly well below the guidelines of 5 ppb set out by governing bodies. Importantly, this was achieved without activation of the electrode or any other post print modifications, giving enhanced viability toward commercialisation. Furthermore, the repeatability for CB/Ag-G/PLA electrode using SWV was then studied, FIGURE *4.30*B. The AgNP-electrode produced an RSD of 3.06 % after 10 repetitive SWV measurements.

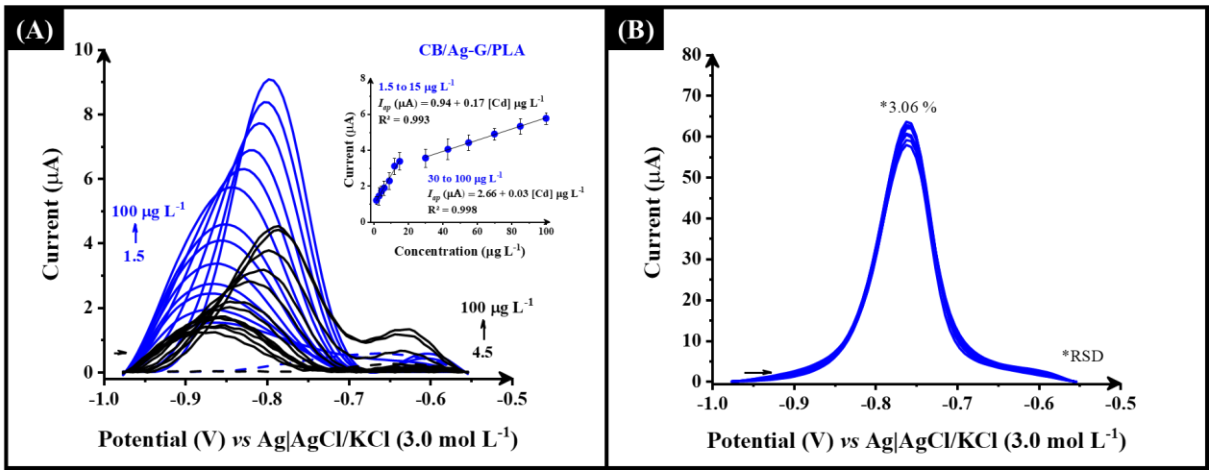

FIGURE 4.30 – (A) SWAS voltammograms for cadmium oxidation performed at CB/G/PLA (black line) and CB/Ag-G/PLA (blue line) in the linear range of 4.5 to 100 µg L^{-1} and 1.5 to 100 µg L^{-1} in 0.1 mol L^{-1} BR, respectively. Inset: calibration plots for CB/Ag-G/PLA. (B) SWAS voltammograms obtained for repetitive measurements (n=10) in 0.1 mol L^{-1} BR (pH 5.0) with 100 ppb of Cd(II) using CB/Ag-G/PLA electrode. SWASV parameters: a = 80 mV, f = 40 Hz, ΔE_s = 6 mV, $E_{deposition}$ = –1.1 V, and $t_{deposition}$ = 60s

4.8.4 - Detection of Cadmium within Water Samples

Finally, this system was applied to the detection of Cd(II) within tap and river water samples. The plot for the CB/Ag-G/PLA electrode in tap water is shown in FIGURE *4.31*A, where a linear range was found with a R^2 value of 0.98, a LOD of 0.05 ppb (4.45×10^{-10} mol L^{-1}), a LOQ of 0.15 ppb (1.34×10^{-9} mol L^{-1}), and a recovery of 98 %. Within river water, FIGURE *4.31*B, a linear relationship was found giving an R^2 value of 0.99, a LOD of 0.55 ppb (4.89×10^{-9} mol L^{-1}), a LOQ of 1.85 ppb (1.65×10^{-8} mol L^{-1}), and a recovery of 87 %. To further test the system within river water, spiked samples were tested using the AgNP-electrode, with the results summarised in TABLE *4.13*.

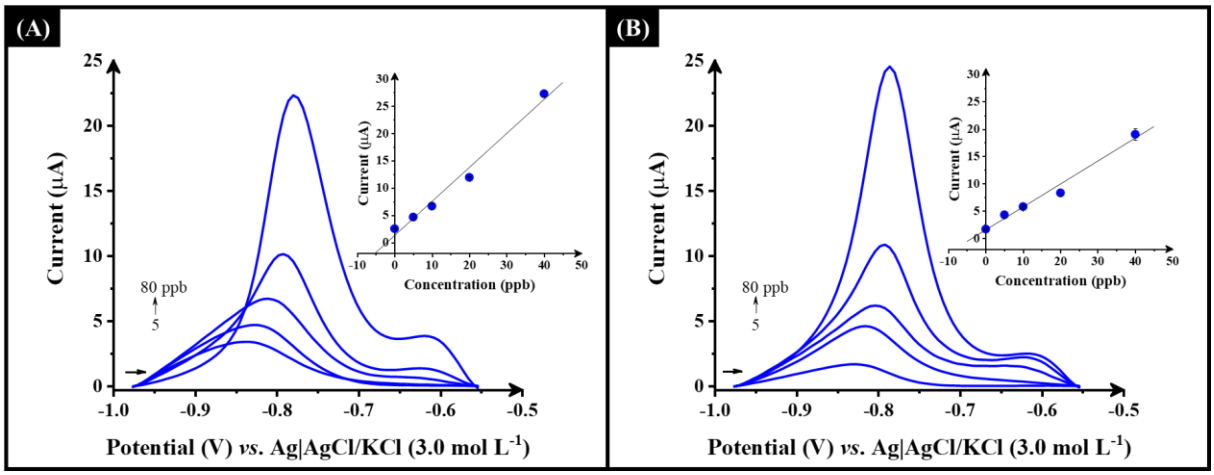

FIGURE 4.31 – SWAS voltammograms for cadmium oxidation in (A) diluted tap water (5-fold) and (B) in diluted river water (20-fold) in 0.1 mol L^{-1} BR (pH 5.0) performed with AgNP-graphite in a concentration range of 5 to 80 ppb. Inset: calibration curve obtained by the standard addition method. SWASV parameters: a = 80 mV, f = 40 Hz, ΔE_s = 6 mV, $E_{deposition}$ = –1.1 V, and $t_{deposition}$ = 60s.

TABLE 4.13 - Determination of Cd (II) within spiked river water sample (n = 3) using the optimised SWASV methodology

Cd(II) Added / ppb	Cd(II) Found / μg L^{-1}	Recovery / %
5	5.1 ± 0.5	102.0
10	9.6 ± 0.3	96.0

This shows that the electrodes printed from the CB/Ag-G/PLA filament can provide reliable sensitivity and accuracy for the detection of Cd(II) in real environmental water samples. Moreover, TABLE *4.14* shows a comparison between this system and others reported in the literature. The proposed sensor not only compares favourably with other methods in terms of LOD but also shows reliability in detecting Cd (II), effectively measuring this metal level in water within the 5-μg L^{-1} limit, as showed by the linear range of concentrations achieved and LOD.

TABLE 4.14 - Comparison of the analytical parameters for the voltammetric determination of cadmium in water samples

Electrode	Technique	Sample	Linear range / μg L^{-1}	LOD / μg L^{-1}	Ref
SPGE- Nafion /Bi	SWASV	Tap and river water	50 to 300	4	[231]
MWCNT/Bi/PGE	SWASV	Environmental water samples	5 to 80	0.43	[308]
SPE-CB-PPI	SWASV	Tap water	30 to 150	15.3	[309]
Hg-Bi/PDAAQ/GC	SWASV	Tap water	0 to 50	0.107	[310]
Nafion/IL/GO/GCE	SWASV	Tap water	2.4 to 70	0.33	[230]
indium film modified glassy carbon	SWASV	Tap water	1 to 25	0.36	[311]
3D−Bi electrode	SWASV	—	50 to 500	9.35	[312]
Bi-SPE	SWASV	Deionized and tap water	5 to 50	4.80	[229]
CB/Ag-G/PLA	SWASV	Tap and river water	1.5 to 100	0.43	This work

SPGE- Nafion /Bi: commercial screen-printed gold electrode with Nafion and bismuth film; MWCNT/Bi/PGE: Pencil graphite electrode modified with multi wall carbon nanotube and bismuth; SPE-CB-PPI: screen-printed electrode modified with a composite of poly(propylene imine) dendrimer and carbon black; Hg-Bi/PDAAQ/GC: bimetallic Hg-Bi supported on poly(1,2-diaminoanthraquinone)/glassy carbon modified electrode; Nafion/IL/GO/GCE: glassy carbon electrode modified with graphene oxide mixed ionic liquid (BMIM-PF_6) and Nafion

binder; 3D−Bi electrode: 3D-printed electrodes modified with bismuth; Bi-SPE: screen printed electrode modified by bismuth powder;

4.9 - Conclusions

This study demonstrates the environmentally friendly synthesis of silver nanoparticles onto graphite flakes, facilitating their use in the production of conductive filaments for additive manufacturing. These filaments exhibit enhanced electrochemical performance for the electroanalytical detection of Cd(II). Using an optimised SWV methodology, the AgNP electrodes achieved a LOD of 0.43 µg L^{-1} and a LOQ of 1.44 µg L^{-1}—well below the target range of 3 to 5 µg L^{-1} set by global regulatory agencies for cadmium levels in water. The electrodes were successfully applied to the determination of Cd(II) concentrations in tap and river water samples, achieving recoveries between 87 % and 102 %.

Notably, these electrodes achieved these results without requiring post-print modification or activation, a common step in additive manufacturing electrochemistry. This work highlights the successful incorporation of metallic nanoparticles into conductive additive manufacturing filaments and the substantial improvements in electrochemical performance that can be achieved as a result. With no need for specialised printers or complex electrode modifications.

Part III

4.10 - HDES-based Filament

The final part of this thesis explores the utilisation of the proposed HDES (DecA:TBAB) to design a novel, sustainable, electrically conductive filament, subsequently employing it to fabricate a 3D-printed electrode for the detection of acetaminophen in water.

To achieve this, the HDES was mixed with CB, castor oil, rPLA, and cellulose to create a new HDES-based filament, following the proportion of 20 wt% CB, 10 wt% castor oil, 5 wt% HDES, 10 wt% cellulose, and 55 wt% rPLA. This filament was then used to fabricate additively manufactured electrodes. The electrochemical properties of the proposed electrode were evaluated by comparing it with other bespoke filaments and a commercially available filament. TABLE *4.15* summarises the composition of all filaments utilised in this study.

TABLE 4.15 - Filament composition

Filament	Composition
CB/PLA	70 wt% rPLA + 10 wt% Castor Oil + 20 wt% CB
CB/Cellulose/PLA	60 wt% rPLA + 10 wt% Castor Oil + 10 wt% Cellulose + 20 wt% CB
CB/Cellulose/HDES/PLA	55 wt% rPLA + 10 wt% Castor Oil + 10 wt% Cellulose + 20 wt% CB + 5 wt% HDES
CB/HDES/PLA	65 wt% rPLA + 10 wt% Castor Oil + 20 wt% CB + 5 wt% HDES
Commercial CB/PLA	Protopasta®

For the proposed CB/Cellulose/HDES/PLA filament, the addition of cellulose played a crucial role in enhancing its structural integrity. The eutectic solvent used in the formulation is acidic, which makes the filament highly brittle due to the incompatibility of PLA with acidic environments. In an initial attempt to fabricate a filament using the HDES (DecA:TBAB) with castor oil and CB, the resulting material lacked the necessary flexibility for printability. To address this limitation, cellulose was added to the filament according to a study conducted by the MMU group (Manchester Metropolitan University, UK), in which the incorporation of cellulose into PLA-based filaments was explored as a reinforcement strategy, significantly improving their mechanical properties. It is well-established in the literature that cellulose enhances the mechanical properties of PLA, reinforcing the polymer and optimising its overall performance[313–315].

The filament composed of CB/Cellulose/HDES/PLA, shown in FIGURE *4.32*A, exhibits satisfactory low-temperature flexibility compared to the CB/HDES/PLA filament without cellulose, as depicted in FIGURE *4.32*B. This observation confirms that incorporating cellulose into the PLA-based filament enhanced its mechanical properties.

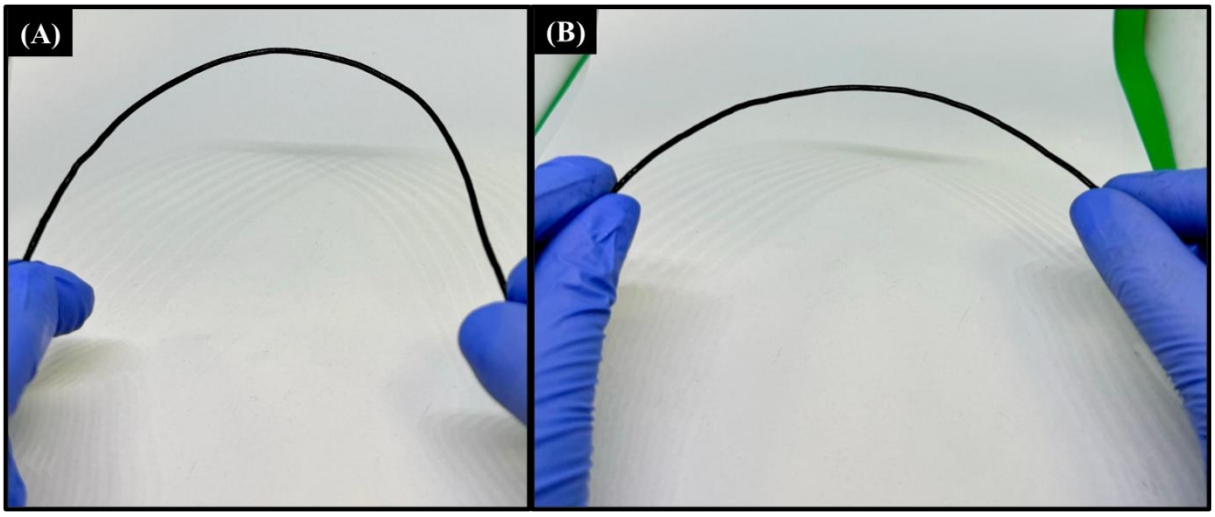

FIGURE 4.32 - Images of the bespoke (A) CB/Cellulose/HDES/PLA and (B) CB/HDES/PLA filaments.

Over a 10 cm length of the CB/Cellulose/HDES/PLA filament, a low average resistance of (0.86 ± 0.02) kΩ was measured, representing a substantial improvement compared to the commercially available conductive PLA, which exhibits a resistance of (3.9 ± 0.5) kΩ. TABLE *4.16* presents the bulk resistance values of the proposed filaments, with the CB/Cellulose/HDES/PLA filament demonstrating superior performance. This improvement highlights the contribution of HDES to enhanced conductivity, as previously demonstrated in this thesis when HDES was used to modify carbon pastes and glassy carbon electrodes.

TABLE 4.16 - Comparisons of the resistance of the filaments over 10 cm

Filament	Resistance[1,2] / kΩ
Commercial CB/PLA	3.9±0.5
CB/PLA	1.25±0.08
CB/Cellulose/PLA	1.16±0.10
CB/Cellulose/HDES/PLA	0.86±0.02
CB/HDES/PLA	1.36±0.08

[1]bulk resistance across 10 cm. [2]n=6.

After fabricating the electrodes, it is essential to characterise the surface of them to better understand their performance. When employing PLA-based materials, surface activation is a common practice. This process involves removing the outer polymer layer that coats the electrode surface, thereby exposing a greater amount of the conductive filler. Electrochemical activation in a 0.5 M sodium hydroxide solution is among the most widely used methods and will therefore be employed throughout this study[56]. Subsequently, the additively manufactured electrodes were analysed using SEM and XPS before and after electrochemical activation, FIGURE *4.33*.

As mentioned, electrochemical activation enhances the exposure and functionality of the electrode surface as a conductive material, thereby facilitating electrochemical processes. This effect is illustrated by SEM images (FIGURE *4.33*A and B), which show a smooth surface prior to activation, compared to a marked presence of conductive material observable after the activation process.

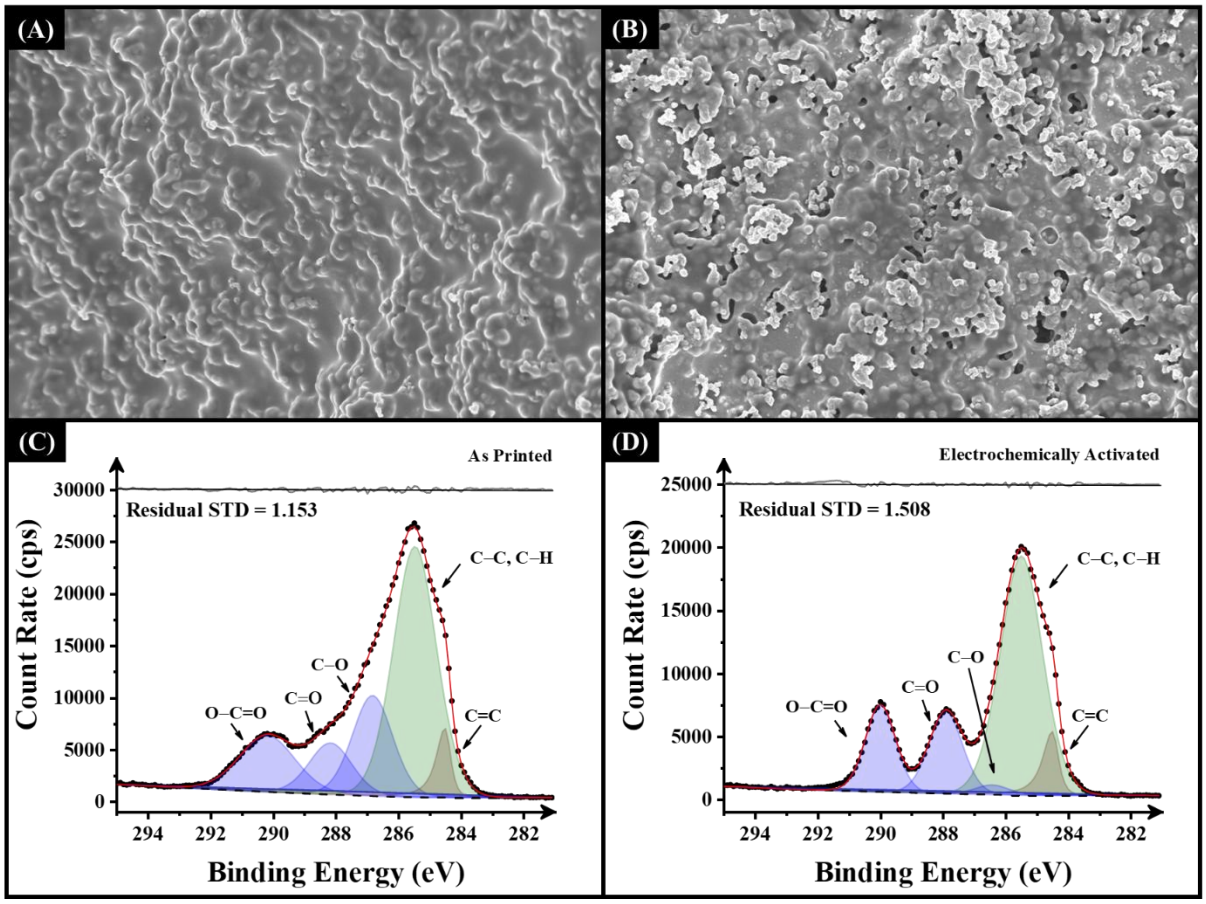

FIGURE 4.33 - SEM surface images and XPS for the (A and C) as-printed and the (B and D) activated CB/Cellulose/HDES/PLA electrode.

Furthermore, the chemical composition of the CB/Cellulose/HDES/PLA electrode was analysed using XPS. FIGURE *4.33*C and FIGURE *4.33*D display the C 1s spectra for non-activated and electrochemically activated electrodes in 0.5 M NaOH, respectively. To achieve an accurate spectral fit, five peaks were assigned. The primary asymmetric peak at 284.5 eV

corresponds to the X-ray photoemission of graphitic carbon[316,317]. Additionally, four symmetric peaks were required to fit the data, representing sp^3 C–C/C–H, C–O, C=O, and O–C=O bonding.

As shown in FIGURE *4.33*, the dominant intensity of the C–C/C–H peak is expected due to the inherent structure of rPLA and castor oil, while the C–O, C=O, and O–C=O contributions originate from the conductive materials. The C 1s spectral fitting indicates that, in the as-printed electrode, the C–C/C–H peak at 285.0 eV accounts for approximately 50 % of the atomic concentration, compared to 20 %, 9 %, and 14 % for the C–O, C=O, and O–C=O peaks, respectively (TABLE *4.17*). Upon electrochemical activation (FIGURE *4.33*D), the XPS C 1s spectrum exhibited an increased intensity of the graphitic C=C peak, suggesting greater exposure of conductive materials. Additionally, the intensities of the C=O and O–C=O bonds were enhanced (TABLE *4.17*), further supporting the improved accessibility of electroactive sites.

TABLE 4.17 - The atomic concentration of the species in each electrode

CB/Cellulose/HDES/PLA	%				
	C=C	C—C/C—H	C—O	C=O	O—C=O
Non-activated	5.7	49.8	20.6	9.12	14.8
Activated	7.3	59.4	1.9	16.1	15.4

4.10.1 - Electrochemical Characterisation of the HDES-based Additive Manufactured Electrodes

The electrochemical performance of the electrodes fabricated using the filaments from TABLE *4.15* was evaluated with 3D-printed electrodes with a simple lollipop-shaped design (FIGURE *3.2*). This design ensures a short

electrode connection length, contributing to a consistent electrochemical response[249]. All electrodes used in this work were electrochemically activated prior to the experiments. FIGURE *4.34* shows the electrochemical performance of the electrodes using $[Ru(NH_3)_6]^{3+}$ as a probe. The results for bespoke CB/PLA and CB/Cellulose/PLA were extracted from previous research conducted by the MMU group (UK). The finds indicated that incorporating HDES and cellulose into the filament resulted in a sharper and more well-defined redox profile compared to the others 3D-printed electrodes. Also, the Nyquist plots obtained using $[Fe(CN)_6]^{4-/3-}$ show that the CB/Cellulose/HDES/PLA electrode exhibited the lowest charge-transfer resistance among all the electrodes tested.

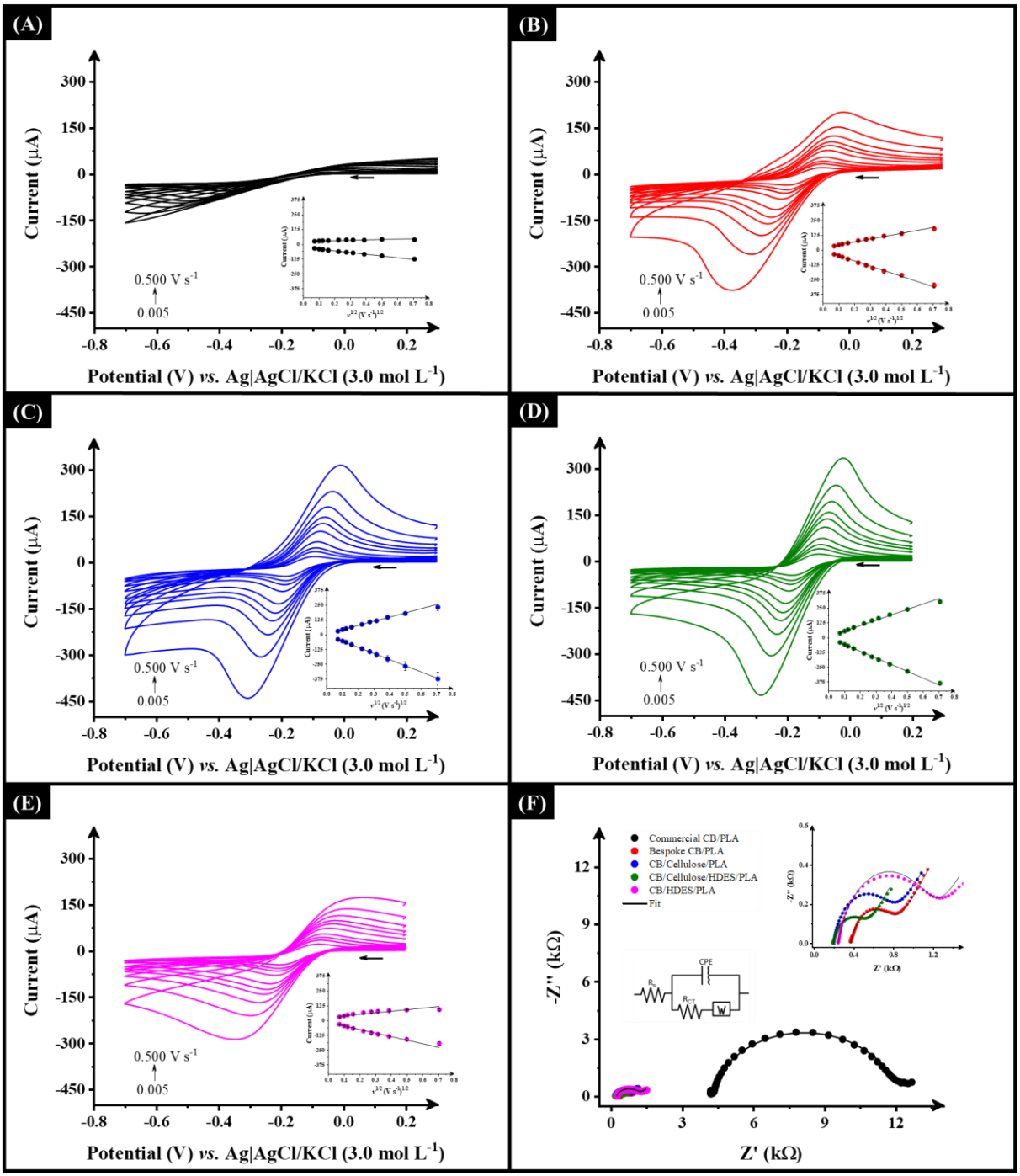

FIGURE 4.34 - Scan rate study (5 – 500 mV s^{-1}) with 1.0×10^{-3} mol L^{-1} $[Ru(NH_3)_6]^{3+}$ in 0.1 mol L^{-1} KCl performed in (A) Commercial CB/PLA, (B) bespoke CB/PLA, (C) CB/Cellulose/PLA, (D) CB/Cellulose/HDES/PLA and (E) CB/HDES/PLA electrodes as the WE. Inset: The Randles–Ševčík plot. (F) EIS Nyquist plots using $[Fe(CN)_6]^{4-/3-}$ for the same electrodes. Inset: the proposed equivalent circuit.

TABLE *4.18* highlights key parameters, including the electroactive area, heterogeneous electron charge transfer rate constant, peak-to-peak separation, cathodic peak current and the peak-to-peak measured using $[Ru(NH_3)_6]^{3+}$ at a scan rate of 100 mV s^{-1}. Additionally, the table reports the results of solution resistance and charge-transfer resistance derived from electrochemical impedance spectroscopy. Compared to all other electrodes, the proposed electrode, CB/Cellulose/HDES/PLA, demonstrated significant improvements across all electrochemical parameters. This highlights the contribution of the HDES in enhancing the filament's conductivity by working synergistically with cellulose and CB to improve electrochemical reactions at the electrode surface, as demonstrated in the previous works (section 4.6 -).

It is worth noting that, although the performance of the electrode CB/HDES/PLA was inferior to the electrodes developed in the laboratory, it still outperformed the commercial filament. These findings open avenues for further studies exploring different types of eutectic solvents for potential applications in the development of 3D-printed electrodes.

TABLE 4.18 - Comparisons of the electrochemical parameters for the bespoke electrodes

Parameters	Commercial CB/PLA	CB/PLA	CB/Cellulose/PLA	CB/Cellulose/HDES/PLA	CB/HDES/PLA
A / cm^2	0.36±0.02	0.59±0.03	0.65±0.09	0.72±0.03	0.48±0.03
k^0 / cm s^{-1}	(0.19±0.02)×10^{-3}	(1.3±0.1)×10^{-3}	(1.55±0.05)×10^{-3}	(1.62±0.09)× 10^{-3}	(1.02±0.08)×10^{-3}
ΔE_p / V	0.39±0.01	0.18±0.01	0.16±0.01	0.155±0.005	0.21±0.01
$-I_{cp}$ / μA	73±4	154±12	166±23	187±8	116±8
R_s / kΩ	3±2	0.33±0.05	0.19±0.02	0.20±0.02	0.24±0.01
R_{ct} / kΩ	7.4±0.5	0.58±0.02	0.61±0.10	0.41±0.08	0.92±0.02

To further test the performance of the proposed electrode, it was used to determine acetaminophen (ACP, paracetamol) in water. This analyte was selected due to its well-known electrochemical behaviour.

4.10.2 - Electrochemical Determination of Acetaminophen

Once electrochemically characterised, the CB/Cellulose/HDES/PLA was applied for the electroanalytical determination of ACP. The results obtained using this electrode were also compared to those from CB/Cellulose/PLA to better illustrate the improvements due to the presence of the HDES.

Prior to the electrochemical experiments, the electrodes were activated electrochemically in 0.5 M NaOH, following a procedure described in the literature[56]. The electrochemical behaviour of ACP on the CB/Cellulose/HDES/PLA and CB/Cellulose/PLA electrodes was evaluated using SWV. FIGURE *4.35*A presents the voltammetric profile of ACP on these electrodes. Notably, the CB/Cellulose/HDES/PLA electrode exhibited a significant enhancement in peak current value, with an 8.7-fold increase in peak current compared to the electrode without HDES.

Furthermore, FIGURE *4.35*B highlights the effect of NaOH activation on the electrochemical response of the electrode. Post-activation, the oxidation peak potential for ACP shifted from +0.50 V to +0.42 V. This improvement is likely attributed to the activation process exposing the conductive material within the electrode, as evidenced by XPS data, resulting in enhanced electrochemical performance.

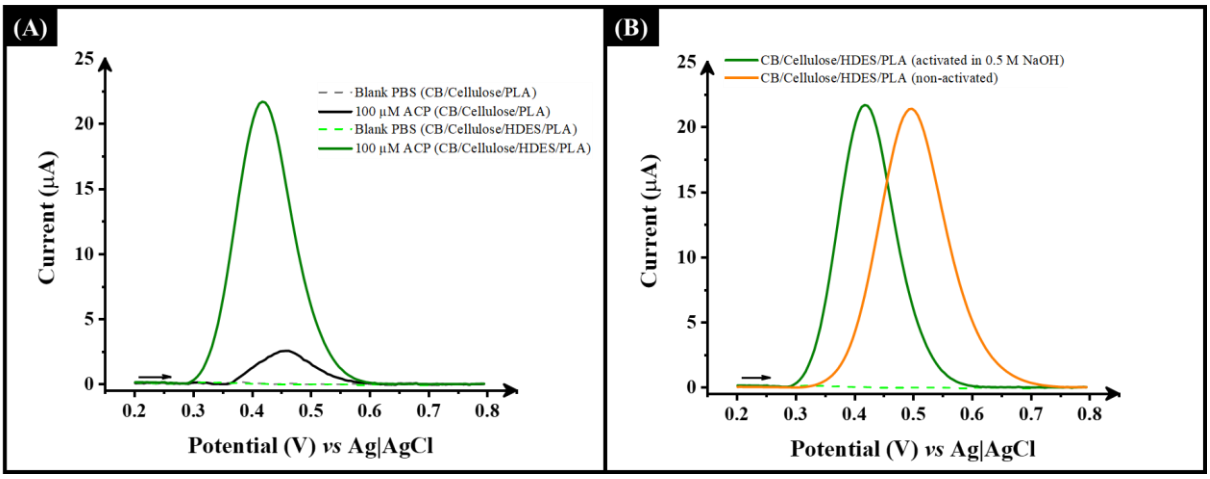

FIGURE 4.35 – (A) SW voltammograms with 100 µM acetaminophen in PBS pH 7.55 using CB/Cellulose/PLA and CB/Cellulose/HDES/PLA electrodes as the WE. (B) SWV comparing the CB/Cellulose/HDES/PLA electrodes activated in 0.5M NaOH and non-activated. Scan rate: 50 mV s^{-1}. SWV parameters: a = 20 mV, f = 25 Hz, ΔE_s = 5 mV.

To investigate the effect of potential scan rates on electrode response, a study was conducted to identify the process controlling the oxidation reaction of ACP in the electrode solution interface. Cyclic voltammetry was performed with 100 µmol L^{-1} ACP in PBS at pH 7.55, with scan rates ranging from 5 to 150 mV s^{-1}. FIGURE *4.36* presents the voltammograms alongside the plots of I_{ap} versus $v^{1/2}$, log (I_{ap}) versus log (v), and I_{ap} versus v. TABLE *4.19* summarizes the data derived from these plots.

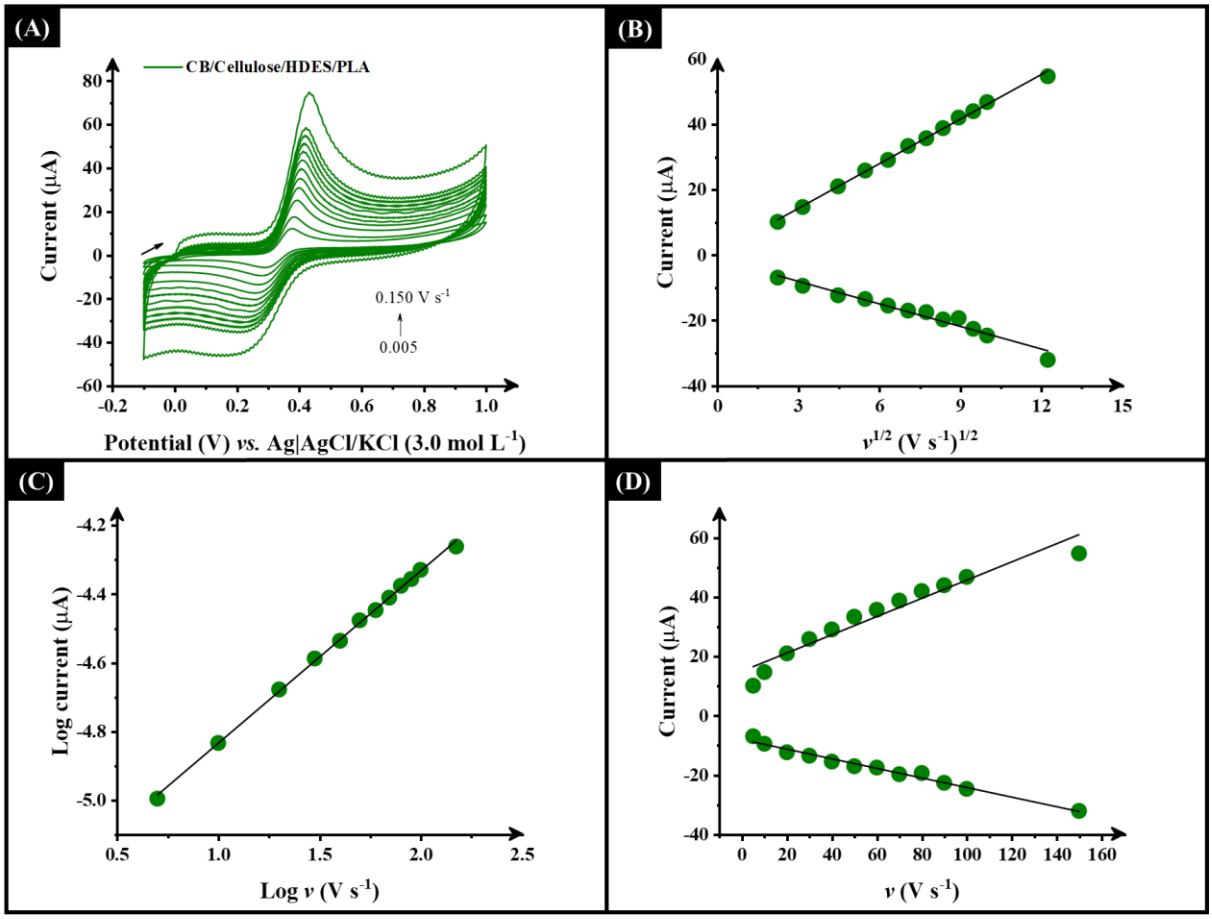

FIGURE 4.36 - (A) Scan rate study (5–150 mV s^{-1}) with 100 µM acetaminophen in PBS pH 7.55 performed in the CB/Cellulose/HDES/PLA as the WE. (B) Randles–Ševčík plot (I_p *vs* $v^{1/2}$), (C) plot of the logarithm of I_{ap} *vs* logarithm of *v* and (D) plot of I_p *vs v*.

The plots obtained in this study (TABLE *4.19*), exhibited a linear relationship, indicating that the oxidation reaction of ACP is diffusion-controlled, aligning with findings reported in the literature[318,319].

TABLE 4.19 - Results for plots from scan rate study obtained for 100 μM of acetaminophen

Parameters	Plot	Electrode CB/Cellulose/HDES/PLA
Slope		I_{ap}: 4.56; I_{cp}: −2.30
Intercept	I_p *vs* $v^{1/2}$	I_{ap}:−0.52; I_{cp}: –1.3
R^2		I_{ap}: 0.998; I_{cp}: 0.964
Slope		I_{ap}: 0.31; I_{cp}: −0.16
Intercept	I_p *vs* v	I_{ap}: 14.9; I_{cp}: −8.2
R^2		I_{ap}: 0.935; I_{cp}: 0.980
Slope		0.50
Intercept	Log I_{ap} *vs* Log v	−5.34
R^2		0.999

To evaluate the electroanalytical capabilities of the CB/Cellulose/HDES/PLA electrode, acetaminophen detection was conducted and compared to the CB/Cellulose/PLA electrode. The SW voltammograms for acetaminophen detection over the concentration range of 5.0–300 μM and 2.0–300 μM to CB/Cellulose/PLA and CB/Cellulose/HDES/PLA are shown in FIGURE *4.37*, with the corresponding calibration plot displayed as an inset. A linear relationship was observed between the peak current and concentration, yielding a LOD 0.12 and 0.63 and a LOQ of 0.39 and 2.11 nM for CB/Cellulose/HDES/PLA and CB/Cellulose/PLA, respectively. TABLE *4.20* shows de analytical parameters obtained in this study. These results demonstrate the electrode's exceptional performance.

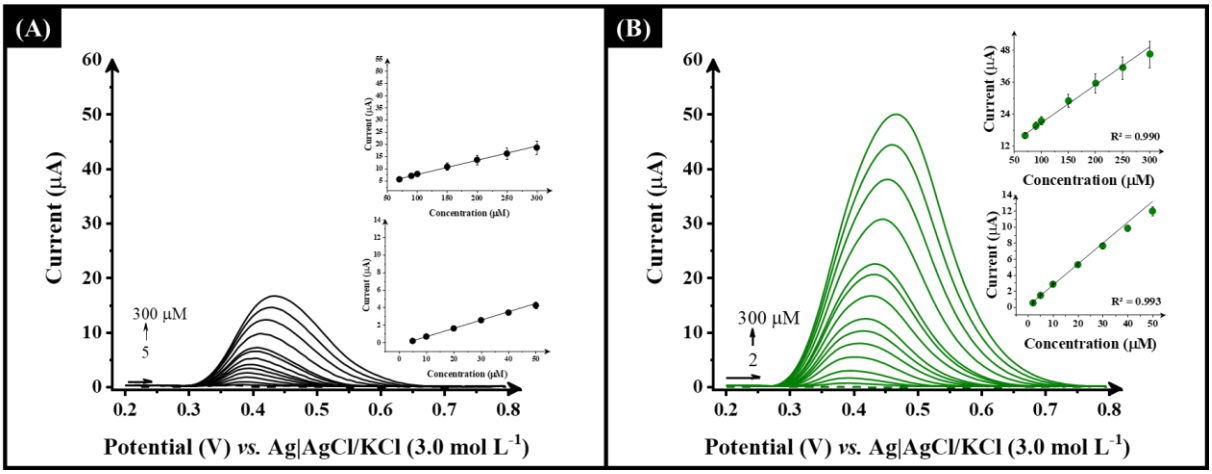

FIGURE 4.37 - SW voltammograms for ACP determination performed at (A) CB/Cellulose/PLA and (B) at CB/Cellulose/HDES/PLA in PBS pH 7.55 in a concentration range of 5.0 to 300 μM and 2 to 300 μM, respectively. Inset: the calibration plot. SWV parameters: a = 20 mV, f = 25 Hz, ΔE = 5 mV.

TABLE 4.20 - Results obtained for the determination of acetaminophen using the SWV method

Parameters	CB/Cellulose/PLA	CB/Cellulose/HDES/PLA
Linear range	5 – 50 and 70 – 300	2 – 50 and 70 – 300
Slope / μA L μmol^{-1}	0.095±0.001	0.26±0.01
	0.058±0.002	0.14±0.01
Intercept / μA	−0.26±0.01	6.5±0.7
	1.8±0.2	0.16±0.06
R^2	0.999	0.993
	0.996	0.990
LOD / μmol L^{-1}	0.63	0.12
LOQ / μmol L^{-1}	2.11	0.39

To finish, the electroanalytical performance of the CB/Cellulose/HDES/PLA electrode was tested in real water samples to assess its practical applicability. FIGURE *4.38* shows the SWV recorded for the determination of ACP in two different water samples: tap water collected from the laboratory and river water from local sources. The quantification of ACP in these samples was carried out using the standard addition method. This involved the successive addition of a standard ACP solution at concentrations of 10, 15, 20, 25, 30, and 35 µM to the electrochemical cell. The results confirm the successful detection of ACP in both water samples, with recovery rates of 80 % for tap water and 87 % for river water.

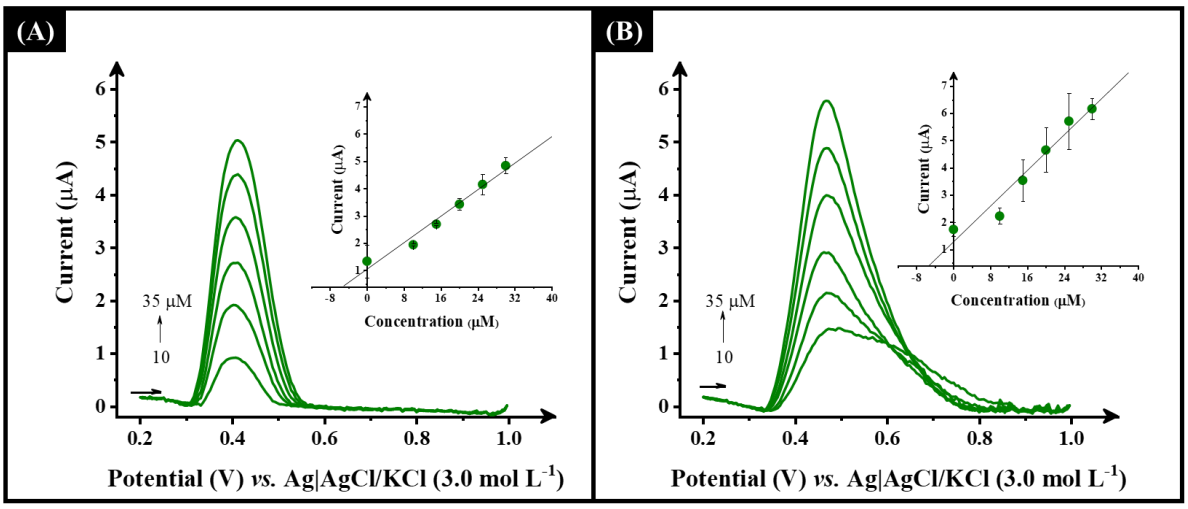

FIGURE 4.38 - SW voltammograms for ACP detection in spiked (A) diluted river water (50-fold) and (B) diluted tap water (20-fold) in PBS pH 7.55 performed at CB/Cellulose/HDES/PLA electrode in a concentration range of 10 to 35 µM. SWV parameters: a = 20 mV, f = 25 Hz, ΔE = 5 mV. Inset: calibration curve obtained by the standard addition method.

4.11 - EcoScale Assessment for Filament Production

The production of a filament composed of cellulose, carbon black, HDES (DecA:TBAB), castor oil, and recycled PLA via the thermal method at 190°C was evaluated using the EcoScale. The assessment considered key factors such as yield, energy consumption, reagents, equipment cost, and waste generation. The results are summarised in TABLE *4.21*.

TABLE 4.21 - EcoScale for HDES-based Filament Production

Criterion	Score
Yield	The process achieves a high yield (>95 %), resulting in no deductions.
Energy Consumption	Sustained heating at 190 °C contributes to moderate energy consumption. This results in a deduction of 10 points.
Reagents	Cellulose, HDES, Castor Oil, and Recycled PLA are sustainable and environmentally friendly, resulting in no deductions. Carbon Black: Due to its industrial origin[187], a deduction of 5 points was applied.
Waste Production	The process is efficient, with low waste generation. No deductions were made.
Equipment Cost	The use of high-cost equipment (*e.g.,* Thermo Haake Rheomix) impacts the affordability and scalability of the process, leading to a deduction of 5 points.
Total Score	80

The EcoScale score of 80 indicates that the process is relatively green and efficient[157]. Deductions were primarily due to energy consumption, the use of carbon black, and high equipment cost.

In relation to the green chemistry principles, TABLE *4.22* highlights the process's adherence to these guidelines. Overall, it demonstrates strong alignment with key principles, particularly Prevention, Atom Economy, and Use of Renewable Feedstocks. However, areas for improvement include energy efficiency and reducing reliance on high-cost equipment. Recent studies have explored alternative approaches to address these challenges. For instance, Silva *et al.*[181] proposed a novel method for producing lab-made composite filaments for additive manufacturing of electrochemical sensors, using a coffee grinder to mix carbon black nanoparticles with PLA pellets. Similarly, another research group developed filaments through thermal mixing on a heating plate[320], where the plasticiser Babassu oil played a crucial role in the process. These recent advancements highlight promising opportunities for the development of conductive filaments using sustainable materials and low-cost equipment.

TABLE 4.22 - Green Chemistry Principles Assessment Table

Green Chemistry Principle	Assessment	Alignment
Prevention	Minimal waste generation with efficient use of raw materials.	Strong
Atom Economy	High incorporation of input materials into the final product (>95 % yield).	Strong
Less Hazardous Chemical Syntheses	Use of non-toxic materials like HDES, castor oil, cellulose, and recycled PLA, though carbon black has minor environmental concerns.	Moderate
Designing Safer Chemicals	Components are safer and environmentally friendly compared to traditional plastics.	Strong
Safer Solvents and Auxiliaries	Likely no harmful solvents used, especially if HDES synthesis avoids organic solvents.	Strong
Design for Energy Efficiency	Operating at 190°C for 10 minutes reduces energy demands but still	Moderate

Green Chemistry Principle	Assessment	Alignment
	requires moderate thermal energy.	
Use of Renewable Feedstocks	Components like cellulose, castor oil, and recycled PLA are renewable or recycled materials.	Strong
Reduce Derivatives	No unnecessary derivatization steps involved in the process.	Strong
Catalysis	Not applicable	–
Design for Degradation	Biodegradability or recyclability is supported by materials like cellulose, castor oil, and recycled PLA.	Strong
Analysis for Pollution Prevention	Not applicable	–
Inherently Safer Chemistry for Accident Prevention	Safer, less toxic materials are used, though reliance on high-cost equipment requires careful handling	Moderate

4.12 - Conclusions

This work, for the first time, demonstrated the integration of a HDES in the development of a conductive filament. The results showed that the proposed CB/Cellulose/HDES/PLA electrode presented superior electrochemical performance compared to both commercial filaments and other bespoke filaments without HDES. And was applied successfully in the determination of ACP in water samples.

The findings of this study pave the way for the development of highly conductive filaments that align with environmentally friendly practices. By prioritising “green” materials—such as deep eutectic solvents, bio-based castor oil, recycled PLA, and cellulose—this approach enables the fabrication of 3D-printed electrodes with significantly enhanced electrochemical performance.

Chapter 5

5 - CONCLUSIONS AND PERSPECTIVES

The findings of this thesis demonstrate the successful use of hydrophobic deep eutectic solvents and additive manufacturing as a sustainable and innovative approach to develop electrochemical sensors. This work aligns closely with the principles of green chemistry, which guided the design and execution of the synthesis and fabrication processes. By prioritising renewable feedstocks, minimising waste, and enhancing energy efficiency, this thesis highlights the potential of combining eco-friendly materials and advanced manufacturing technologies.

Furthermore, in alignment with the United Nations Sustainable Development Goals, this work contributes to key objectives, including Good Health and Well-being (Goal 3), Clean Water and Sanitation (Goal 6), and Responsible Consumption and Production (Goal 12). The proposed materials were developed using eco-conscious components and sustainable approaches to minimise environmental and human health risks. Additionally, the intended application of each sensor—focusing on the detection of analytes for diagnostic and environmental (water quality) monitoring—further reinforces its relevance to these SDGs.

The HDES, composed of decanoic acid and tetrabutylammonium bromide, was synthesised using a simple, rapid, and efficient process. The synthesis demonstrated a high EcoScale score due to the use of safe reagents, minimal energy input, and a reaction time of only 5 minutes at 80 °C. The thermal stability of the HDES up to 202 °C further confirmed its suitability for various electrochemical applications. In addition, the low E-factor of the process reflects its minimal waste generation, with nearly all starting materials contributing to the final product. These attributes strongly support the sustainability of the proposed methodology.

The application of HDES in modifying electrochemical sensors significantly enhanced their performance. The HDES-modified glassy carbon electrodes exhibited reliable sensitivity and selectivity for serotonin detection. Similarly, the use of HDES in carbon paste electrodes improved the detection capabilities for diuron, achieving consistent results with minimal environmental impact. These sensors demonstrated accurate analytical performance, including high reproducibility and stability, while aligning with green chemistry principles by utilising renewable and biodegradable components.

A conductive filament was designed using carbon black, silver nanoparticle (AgNP)-functionalised graphite, recycled PLA, and castor oil, requiring no post-print modification. The 3D-printed electrodes achieved superior electrochemical performance, as demonstrated in the detection of cadmium in real water samples, with limit of detection well below regulatory thresholds.

A major advancement was the development of sustainable conductive filaments combining HDES, carbon black, castor oil, recycled PLA, and cellulose. These filaments enabled the production of 3D-printed electrodes with significantly enhanced electrochemical performance in the determination of acetaminophen in water samples compared to other bespoke and commercial filaments.

Looking forward, this work opens several avenues for future research and development. A key area for future research is the exploration of entirely green DES. The main limitation of the proposed HDES lies in the use of TBAB as a precursor, as it is considered toxic. However, among the available components that met the necessary criteria for HDES formation in this work, TBAB proved to be the most suitable option. Future studies should investigate alternative precursors, especially given the vast range of DES compositions reported in the literature.

Another important aspect for improvement is the compatibility of DES with the selected thermoplastic material. As demonstrated in this study, the acidic nature of the chosen HDES posed challenges to the stability of PLA. Therefore, further research is needed to identify DES formulations that are more compatible with the polymer, or alternatively, to explore different types of thermoplastics to optimise the DES-material combination.

Additionally, a promising research direction is to explore more natural alternatives for conductive materials, aiming to eliminate the need for toxic or high-cost components. Furthermore, investing in miniaturised electrochemical platforms can help reduce reagent consumption during analysis, ensuring a more sustainable and environmentally friendly approach.

Improving the energy efficiency of synthesis processes is also crucial, highlighting the importance of optimising the entire methodology, including synthesis time. This thesis pioneered a time-efficient approach, directly contributing to sustainability.

Furthermore, attention should be given to the disposal of electrodes, particularly 3D-printed materials. Efforts should focus on their potential reuse or transformation into value-added products, promoting more sustainable processes and circular economy principles.

Finally, the integration of sustainability metrics should always be considered to assess the potential environmental and human health risks associated with any material or process.

Chapter 6

6 - REFERENCES

1. United Nations. THE 17 GOALS. https://sdgs.un.org/goals.
2. Anastas P, Eghbali N. Green Chemistry: Principles and Practice. Chem Soc Rev [Internet]. 2009 Dec 14 [cited 2024 Nov 11];39(1):301–12. Available from: https://pubs.rsc.org/en/content/articlehtml/2010/cs/b918763b
3. Laura Soriano M, Zougagh M, Valcárcel M, Ríos Á. Analytical Nanoscience and Nanotechnology: Where we are and where we are heading. Talanta. 2018 Jan;177:104–21.
4. Stradiotto NR, Yamanaka H, Zanoni MVB. Electrochemical sensors: a powerful tool in analytical chemistry. J Braz Chem Soc. 2003 Apr;14(2):159–73.
5. Hayat A, Marty J. Disposable Screen Printed Electrochemical Sensors: Tools for Environmental Monitoring. Sensors. 2014 Jun 13;14(6):10432–53.
6. Bollella P, Fusco G, Tortolini C, Sanzò G, Favero G, Gorton L, et al. Beyond graphene: Electrochemical sensors and biosensors for biomarkers detection. Biosens Bioelectron. 2017 Mar;89:152–66.
7. Costa-Rama E, Fernández-Abedul MT. Paper-Based Screen-Printed Electrodes: A New Generation of Low-Cost Electroanalytical Platforms. Biosensors (Basel). 2021 Feb 16;11(2):51.
8. Uslu B, Ozkan SA. Electroanalytical Methods for the Determination of Pharmaceuticals: A Review of Recent Trends and Developments. Anal Lett. 2011 Nov;44(16):2644–702.
9. Stozhko NYu, Khamzina EI, Bukharinova MA, Tarasov A V. An Electrochemical Sensor Based on Carbon Paper Modified with Graphite Powder for Sensitive Determination of Sunset Yellow and Tartrazine in Drinks. Sensors. 2022 May 27;22(11):4092.
10. Abbott AP. Deep eutectic solvents and their application in electrochemistry. Curr Opin Green Sustain Chem. 2022 Aug 1;36:100649.
11. Brett CMA. Deep eutectic solvents and applications in electrochemical sensing. Curr Opin Electrochem. 2018 Aug 1;10:143–8.
12. Cardoso RM, Kalinke C, Rocha RG, dos Santos PL, Rocha DP, Oliveira PR, et al. Additive-manufactured (3D-printed) electrochemical sensors: A critical review. Anal Chim Acta. 2020 Jun 29;1118:73–91.
13. Kalinke C, Crapnell RD, de Oliveira PR, Janegitz BC, Bonacin JA, Banks CE. How to Improve Sustainability in Fused Filament Fabrication (3D Printing) Research? Global Challenges [Internet]. 2024 Jul 1 [cited 2024 Sep 30];8(7):2300408. Available from: https://onlinelibrary.wiley.com/doi/full/10.1002/gch2.202300408
14. Vilková M, Płotka-Wasylka J, Andruch V. The role of water in deep eutectic solvent-base extraction. J Mol Liq. 2020 Apr 15;304:112747.
15. Santana-Mayor Á, Rodríguez-Ramos R, Herrera-Herrera A V., Socas-Rodríguez B, Rodríguez-Delgado MÁ. Deep eutectic solvents. The new generation of green solvents in analytical chemistry. TrAC Trends in Analytical Chemistry. 2021 Jan 1;134:116108.
16. Fernández M de los Á, Boiteux J, Espino M, Gomez FJV, Silva MF. Natural deep eutectic solvents-mediated extractions: The way forward for sustainable analytical developments. Anal Chim Acta. 2018 Dec 14;1038:1–10.

17. Saravana PS, Ho TC, Chae SJ, Cho YJ, Park JS, Lee HJ, et al. Deep eutectic solvent-based extraction and fabrication of chitin films from crustacean waste. Carbohydr Polym. 2018 Sep 1;195:622–30.
18. Khandelwal S, Tailor YK, Kumar M. Deep eutectic solvents (DESs) as eco-friendly and sustainable solvent/catalyst systems in organic transformations. J Mol Liq. 2016 Mar;215:345–86.
19. Lai P, Zhou H, Niu Z, Li L, Zhu W, Dai L. Deep eutectic solvent-mediated preparation of solvothermal carbon with rich carboxyl and phenol groups from crop straw for high-efficient uranium adsorption. Chemical Engineering Journal. 2023 Feb 1;457:141255.
20. Ma S, Jin X, Wei H, Liu Y, Guo M. Hydrophobic deep eutectic solvent-based ultrasonic-assisted liquid-liquid micro-extraction combined with HPLC-FLD for diphenylamine determination in fruit. https://doi.org/101080/1944004920201852320 [Internet]. 2020 [cited 2021 Aug 27];38(2):339–49. Available from: https://www.tandfonline.com/doi/abs/10.1080/19440049.2020.1852320
21. Cao J, Su E. Hydrophobic deep eutectic solvents: the new generation of green solvents for diversified and colorful applications in green chemistry. J Clean Prod. 2021 Sep 10;314:127965.
22. Wagle D V., Zhao H, Baker GA. Deep Eutectic Solvents: Sustainable Media for Nanoscale and Functional Materials. Acc Chem Res. 2014 Aug 19;47(8):2299–308.
23. Ganewatta MS, Wang Z, Tang C. Chemical syntheses of bioinspired and biomimetic polymers toward biobased materials. Nat Rev Chem. 2021 Oct 5;5(11):753–72.
24. Balla E, Daniilidis V, Karlioti G, Kalamas T, Stefanidou M, Bikiaris ND, et al. Poly(lactic Acid): A Versatile Biobased Polymer for the Future with Multifunctional Properties—From Monomer Synthesis, Polymerization Techniques and Molecular Weight Increase to PLA Applications. Polymers (Basel). 2021 May 31;13(11):1822.
25. Zhang C, Xue J, Yang X, Ke Y, Ou R, Wang Y, et al. From plant phenols to novel bio-based polymers. Prog Polym Sci. 2022 Feb;125:101473.
26. Yan K, Wang J, Wang Z, Yuan L. Bio-based monomers for amide-containing sustainable polymers. Chemical Communications. 2023;59(4):382–400.
27. Satti SM, Shah AA. Polyester-based biodegradable plastics: an approach towards sustainable development. Lett Appl Microbiol. 2020 Jun 18;70(6):413–30.
28. Rai P, Mehrotra S, Priya S, Gnansounou E, Sharma SK. Recent advances in the sustainable design and applications of biodegradable polymers. Bioresour Technol. 2021 Apr;325:124739.
29. Moshood TD, Nawanir G, Mahmud F. Sustainability of biodegradable plastics: a review on social, economic, and environmental factors. Crit Rev Biotechnol. 2022 Aug 18;42(6):892–912.
30. Yang C, Zhong W, Shen K, Zhang Q, Zhao R, Xiang H, et al. Electrochemically Reconstructed Cu-FeOOH/Fe $_3$ O $_4$ Catalyst for Efficient Hydrogen Evolution in Alkaline Media. Adv Energy Mater. 2022 Apr 13;12(16).
31. Alamiery A. Advancements in materials for hydrogen production: A review of cutting-edge technologies. ChemPhysMater. 2023 Oct;
32. Wang S, Lu A, Zhong CJ. Hydrogen production from water electrolysis: role of catalysts. Nano Converg. 2021 Dec 11;8(1):4.
33. Simić S, Zukić E, Schmermund L, Faber K, Winkler CK, Kroutil W. Shortening Synthetic Routes to Small Molecule Active Pharmaceutical Ingredients Employing Biocatalytic Methods. Chem Rev. 2022 Jan 12;122(1):1052–126.
34. Ying P, Yu J, Su W. Liquid-Assisted Grinding Mechanochemistry in the Synthesis of Pharmaceuticals. Adv Synth Catal. 2021 Mar 2;363(5):1246–71.

35. Kar S, Sanderson H, Roy K, Benfenati E, Leszczynski J. Green Chemistry in the Synthesis of Pharmaceuticals. Chem Rev. 2022 Feb 9;122(3):3637–710.
36. Wang C, Yang J, Qin J, Yang Y. Eco-Friendly Nanoplatforms for Crop Quality Control, Protection, and Nutrition. Advanced Science. 2021 May 3;8(9).
37. Wang R, Liu S, Ma Z. Recent Development of Versatile Polyphenol Platforms in Fertilizers and Pesticides. J Agric Food Chem. 2023 Jun 28;71(25):9599–608.
38. Kapinder, Dangi K, Verma AK. Efficient & eco-friendly smart nano-pesticides: Emerging prospects for agriculture. Mater Today Proc. 2021;45:3819–24.
39. Fincheira P, Hoffmann N, Tortella G, Ruiz A, Cornejo P, Diez MC, et al. Eco-Efficient Systems Based on Nanocarriers for the Controlled Release of Fertilizers and Pesticides: Toward Smart Agriculture. Nanomaterials. 2023 Jun 29;13(13):1978.
40. Zhang Q, De Oliveira Vigier K, Royer S, Jérôme F. Deep eutectic solvents: syntheses, properties and applications. Chem Soc Rev [Internet]. 2012 Oct 8 [cited 2024 Nov 17];41(21):7108–46. Available from: https://pubs.rsc.org/en/content/articlehtml/2012/cs/c2cs35178a
41. Omar KA, Sadeghi R. Physicochemical properties of deep eutectic solvents: A review. J Mol Liq. 2022 Aug;360:119524.
42. Liu Y, Friesen JB, McAlpine JB, Lankin DC, Chen SN, Pauli GF. Natural Deep Eutectic Solvents: Properties, Applications, and Perspectives. J Nat Prod [Internet]. 2018 Mar 23 [cited 2024 Nov 19];81(3):679–90. Available from: https://pubs.acs.org/doi/full/10.1021/acs.jnatprod.7b00945
43. Prakash KS, Nancharaih T, Rao VVS. Additive Manufacturing Techniques in Manufacturing -An Overview. Mater Today Proc. 2018;5(2):3873–82.
44. Javaid M, Haleem A, Singh RP, Suman R, Rab S. Role of additive manufacturing applications towards environmental sustainability. Advanced Industrial and Engineering Polymer Research. 2021 Oct;4(4):312–22.
45. Bernalte E, Augusto KKL, Crapnell RD, Andrews HG, Fatibello-Filho O, Banks CE. Eco-friendly integration of gold nanoparticles into additive manufacturing filaments: advancing conductivity and electrochemical performance. RSC Applied Interfaces. 2025;
46. Crapnell RD, Arantes IVS, Whittingham MJ, Sigley E, Kalinke C, Janegitz BC, et al. Utilising bio-based plasticiser castor oil and recycled PLA for the production of conductive additive manufacturing feedstock and detection of bisphenol A. Green Chemistry [Internet]. 2023 Jul 17 [cited 2024 Jun 3];25(14):5591–600. Available from: https://pubs.rsc.org/en/content/articlehtml/2023/gc/d3gc01700a
47. Augusto KKL, Crapnell RD, Bernalte E, Zighed S, Ehamparanathan A, Pimlott JL, et al. Optimised graphite/carbon black loading of recycled PLA for the production of low-cost conductive filament and its application to the detection of β-estradiol in environmental samples. Microchimica Acta [Internet]. 2024 Jul 1 [cited 2024 Nov 12];191(7):1–14. Available from: https://link.springer.com/article/10.1007/s00604-024-06445-7
48. Piton GR, Augusto KKL, Santos DA, Fatibello-Filho O. Spectrophotometric Determination of Allura Red AC and Tartrazine in Food Products Using Hydrophobic Deep Eutectic Solvents as an Environmentally Sustainable Micro-Extractor. J Braz Chem Soc [Internet]. 2021 Mar 1 [cited 2024 Nov 24];32(3):564–71. Available from: https://www.scielo.br/j/jbchs/a/qjVb7mBxh8mhqVzsRFNHCpM/
49. Piton GR, Augusto KKL, Wong A, Moraes FC, Fatibello-Filho O. A Novel Electrochemical Glassy Carbon Electrode Modified with Carbon Black and Glyceline Deep Eutectic Solvent within a Crosslinked Chitosan Film for Simultaneous

Determination of Acetaminophen and Diclofenac. Electroanalysis [Internet]. 2021 Aug 21 [cited 2021 Aug 26];33:1–11. Available from: https://analyticalsciencejournals-onlinelibrary-wiley.ez1.periodicos.capes.gov.br/doi/full/10.1002/elan.202100325
50. Augusto KK de L, Piton GR, Gomes-Júnior PC, Longatto GP, de Moraes FC, Fatibello-Filho O. Enhancing the electrochemical sensitivity of hydroquinone using a hydrophobic deep eutectic solvent-based carbon paste electrode. Analytical Methods. 2022 May 27;14(20):2003–13.
51. Gomes-Junior PC, de Lima Augusto KK, Longatto GP, de Oliveira Gonçalves R, Silva TA, Cavalheiro ÉTG, et al. Ultrasmall platinum nanoparticles synthesized in reline deep eutectic solvent explored towards the voltammetric sensing of riboflavin in beverages and biological fluids. Sens Actuators B Chem. 2023 Nov 15;395:134489.
52. Cariati LSS, Buoro RM. Evaluation of ionic natural deep eutectic solvents (NADES) modified binders towards the chemical properties of carbon paste electrodes. Electrochem commun. 2019 Dec 1;109:106605.
53. Jhong HR, Wong DSH, Wan CC, Wang YY, Wei TC. A novel deep eutectic solvent-based ionic liquid used as electrolyte for dye-sensitized solar cells. Electrochem commun. 2009 Jan 1;11(1):209–11.
54. Wang S, Zou X, Lu Y, Rao S, Xie X, Pang Z, et al. Electrodeposition of nano-nickel in deep eutectic solvents for hydrogen evolution reaction in alkaline solution. Int J Hydrogen Energy. 2018 Aug;43(33):15673–86.
55. Chaabene N, Ngo K, Turmine M, Vivier V. New hydrophobic deep eutectic solvent for electrochemical applications. J Mol Liq. 2020 Dec 1;319:1–7.
56. Richter EM, Rocha DP, Cardoso RM, Keefe EM, Foster CW, Munoz RAA, et al. Complete Additively Manufactured (3D-Printed) Electrochemical Sensing Platform. Anal Chem [Internet]. 2019 Oct 15 [cited 2024 Mar 26];91(20):12844–51. Available from: https://pubs.acs.org/doi/abs/10.1021/acs.analchem.9b02573
57. Crapnell RD, Kalinke C, Silva LRG, Stefano JS, Williams RJ, Abarza Munoz RA, et al. Additive manufacturing electrochemistry: An overview of producing bespoke conductive additive manufacturing filaments. Materials Today. 2023 Dec 1;71:73–90.
58. Kalinke C, de Oliveira PR, Neumsteir NV, Henriques BF, de Oliveira Aparecido G, Loureiro HC, et al. Influence of filament aging and conductive additive in 3D printed sensors. Anal Chim Acta. 2022 Jan 25;1191:339228.
59. Camargo JR, Crapnell RD, Bernalte E, Cunliffe AJ, Redfern J, Janegitz BC, et al. Conductive recycled PETg additive manufacturing filament for sterilisable electroanalytical healthcare sensors. Appl Mater Today. 2024 Aug;39:102285.
60. Hüner B, Kıstı M, Uysal S, Uzgören İN, Özdoğan E, Süzen YO, et al. An Overview of Various Additive Manufacturing Technologies and Materials for Electrochemical Energy Conversion Applications. ACS Omega. 2022 Nov 15;7(45):40638–58.
61. Hughes JP, Dos Santos PL, Down MP, Foster CW, Bonacin JA, Keefe EM, et al. Single step additive manufacturing (3D printing) of electrocatalytic anodes and cathodes for efficient water splitting. Sustain Energy Fuels [Internet]. 2019 Dec 18 [cited 2024 Nov 23];4(1):302–11. Available from: https://pubs.rsc.org/en/content/articlehtml/2020/se/c9se00679f
62. Arantes IVS, Crapnell RD, Bernalte E, Whittingham MJ, Paixão TRLC, Banks CE. Mixed Graphite/Carbon Black Recycled PLA Conductive Additive Manufacturing Filament for the Electrochemical Detection of Oxalate. Anal Chem [Internet]. 2023 Oct 10 [cited 2024 Jun 2];95(40):15086–93. Available from: https://pubs.acs.org/doi/full/10.1021/acs.analchem.3c03193

63. Ramos DLO, Crapnell RD, Asra R, Bernalte E, Oliveira ACM, Muñoz RAA, et al. Conductive Polypropylene Additive Manufacturing Feedstock: Application to Aqueous Electroanalysis and Unlocking Nonaqueous Electrochemistry and Electrosynthesis. ACS Appl Mater Interfaces. 2024 Oct 2;
64. Crapnell RD, Arantes IVS, Camargo JR, Bernalte E, Whittingham MJ, Janegitz BC, et al. Multi-walled carbon nanotubes/carbon black/rPLA for high-performance conductive additive manufacturing filament and the simultaneous detection of acetaminophen and phenylephrine. Microchimica Acta [Internet]. 2024 Feb 1 [cited 2024 Jun 3];191(2):1–12. Available from: https://link.springer.com/article/10.1007/s00604-023-06175-2
65. Crapnell RD, Arantes IVS, Whittingham MJ, Sigley E, Kalinke C, Janegitz BC, et al. Utilising bio-based plasticiser castor oil and recycled PLA for the production of conductive additive manufacturing feedstock and detection of bisphenol A. Green Chemistry [Internet]. 2023 Jul 17 [cited 2024 Mar 25];25(14):5591–600. Available from: https://pubs.rsc.org/en/content/articlehtml/2023/gc/d3gc01700a
66. Häckl K, Kunz W. Some aspects of green solvents. Comptes Rendus Chimie. 2018 Jun 1;21(6):572–80.
67. Pacheco-Fernández I, Pino V. Green solvents in analytical chemistry. Curr Opin Green Sustain Chem. 2019 Aug;18:42–50.
68. Gu Y, Jérôme F. Bio-based solvents: An emerging generation of fluids for the design of eco-efficient processes in catalysis and organic chemistry. Chem Soc Rev. 2013 Dec 21;42(24):9550–70.
69. Cvjetko Bubalo M, Vidović S, Radojčić Redovniković I, Jokić S. Green solvents for green technologies. Journal of Chemical Technology & Biotechnology. 2015 Sep;90(9):1631–9.
70. Cao J, Su E. Hydrophobic deep eutectic solvents: the new generation of green solvents for diversified and colorful applications in green chemistry. J Clean Prod. 2021 Sep;314:127965.
71. Peng L, Hu Z, Lu Q, Tang Z, Jiao Y, Xu X. DESs: Green solvents for transition metal catalyzed organic reactions. Chinese Chemical Letters. 2019 Dec;30(12):2151–6.
72. Fan Y, Picchioni F. Modification of starch: A review on the application of “green” solvents and controlled functionalization. Carbohydr Polym. 2020 Aug;241:116350.
73. Hessel V, Tran NN, Asrami MR, Tran QD, Van Duc Long N, Escribà-Gelonch M, et al. Sustainability of green solvents – review and perspective. Green Chemistry. 2022;24(2):410–37.
74. Płotka-Wasylka J, de la Guardia M, Andruch V, Vilková M. Deep eutectic solvents vs ionic liquids: Similarities and differences. Microchemical Journal. 2020 Dec 1;159:105539.
75. Abbott AP, Capper G, Davies DL, Munro HL, Rasheed RK, Tambyrajah V. Preparation of novel, moisture-stable, Lewis-acidic ionic liquids containing quaternary ammonium salts with functional side chains. Chemical Communications [Internet]. 2001 Oct 15 [cited 2024 Nov 12];0(19):2010–1. Available from: https://pubs.rsc.org/en/content/articlehtml/2001/cc/b106357j
76. Abbott AP, Capper G, Davies DL, Rasheed RK, Tambyrajah V. Novel solvent properties of choline chloride/urea mixtures. Chemical Communications [Internet]. 2003 Dec 19 [cited 2024 Nov 12];0(1):70–1. Available from: https://pubs.rsc.org/en/content/articlehtml/2003/cc/b210714g
77. Smith EL, Abbott AP, Ryder KS. Deep Eutectic Solvents (DESs) and Their Applications. Chem Rev [Internet]. 2014 Nov 12 [cited 2024 Nov 17];114(21):11060–82. Available from: https://pubs.acs.org/doi/full/10.1021/cr300162p

78. Alonso DA, Baeza A, Chinchilla R, Guillena G, Pastor IM, Ramón DJ. Deep Eutectic Solvents: The Organic Reaction Medium of the Century. European J Org Chem [Internet]. 2016 Feb 1 [cited 2024 Nov 22];2016(4):612–32. Available from: https://onlinelibrary.wiley.com/doi/full/10.1002/ejoc.201501197
79. Cariati LSS, Buoro RM. Evaluation of ionic natural deep eutectic solvents (NADES) modified binders towards the chemical properties of carbon paste electrodes. Electrochem commun. 2019 Dec 1;109:106605.
80. Abbott AP, Ballantyne A, Harris RC, Juma JA, Ryder KS, Forrest G. A Comparative Study of Nickel Electrodeposition Using Deep Eutectic Solvents and Aqueous Solutions. Electrochim Acta. 2015 Sep;176:718–26.
81. Morozova O V., Vasil'eva IS, Shumakovich GP, Zaitseva EA, Yaropolov AI. Deep Eutectic Solvents for Biotechnology Applications. Biochemistry (Moscow) 2023 88:1 [Internet]. 2023 Feb 20 [cited 2024 Nov 22];88(1):S150–75. Available from: https://link.springer.com/article/10.1134/S0006297923140092
82. Pedro SN, Freire CSR, Silvestre AJD, Freire MG. Deep Eutectic Solvents and Pharmaceuticals. Encyclopedia 2021, Vol 1, Pages 942-963 [Internet]. 2021 Sep 9 [cited 2024 Nov 22];1(3):942–63. Available from: https://www.mdpi.com/2673-8392/1/3/72/htm
83. Jablonský M, Škulcová A, Šima J. Use of Deep Eutectic Solvents in Polymer Chemistry–A Review. Molecules. 2019 Nov 3;24(21):3978.
84. Roda A, Matias AA, Paiva A, Duarte ARC. Polymer Science and Engineering Using Deep Eutectic Solvents. Polymers 2019, Vol 11, Page 912 [Internet]. 2019 May 21 [cited 2024 Nov 22];11(5):912. Available from: https://www.mdpi.com/2073-4360/11/5/912/htm
85. Gomes-Junior PC, Longatto GP, de Lima Augusto KK, da Silveira Rocha J, Piccin E, Fatibello-Filho O. Synthesis of ultrasmall cerium oxide nanoparticles in deep eutectic solvent and their application in an electrochemical sensor to detect dopamine in biological fluid. Microchimica Acta [Internet]. 2024 Jul 1 [cited 2024 Jul 24];191(7):1–12. Available from: https://link.springer.com/article/10.1007/s00604-024-06480-4
86. Hayyan M, Abo-Hamad A, AlSaadi MAH, Hashim MA. Functionalization of graphene using deep eutectic solvents. Nanoscale Res Lett [Internet]. 2015 Dec 13 [cited 2024 Nov 22];10(1):1–26. Available from: https://link.springer.com/article/10.1186/s11671-015-1004-2
87. Ortizo RGG, Sharma V, Tsai ML, Nargotra P, Wang JX, Sun PP, et al. Exploring the potential of magnetic deep eutectic solvents and DES-functionalized nanomaterials for food analysis: Advancements and current trends. Food Biosci. 2024 Oct 1;61:104764.
88. Fernandes PM V., Campiña JM, Pereira NM, Pereira CM, Silva F. Biodegradable deep-eutectic mixtures as electrolytes for the electrochemical synthesis of conducting polymers. J Appl Electrochem. 2012 Dec 1;42(12):997–1003.
89. Ding M, Hou T, Niu H, Zhang N, Guan P, Hu X. Electrocatalytic oxidation of NADH at graphene-modified electrodes based on electropolymerized poly(thionine-methylene blue) films from nature deep eutectic solvents. Journal of Electroanalytical Chemistry. 2022 Sep;920:116602.
90. Chang YH, Woi PM, Alias YB. Electrochemical Characterization of Melamine Electropolymerized in Deep Eutectic Solvents for Selective Detection of Dopamine. Electrocatalysis. 2021 May 12;12(3):238–50.
91. Liang X, Zhou Y, Almeida JMS, Brett CMA. A novel electrochemical acetaminophen sensor based on multiwalled carbon nanotube and poly(neutral red) modified electrodes

with electropolymerization in ternary deep eutectic solvents. Journal of Electroanalytical Chemistry. 2023 May;936:117366.
92. Buoro RM, Almeida JMS, Brett CMA. Cresyl violet electropolymerization on functionalized multiwalled carbon nanotubes in carboxylic acid based ternary deep eutectic solvents for hydroquinone sensing. Electrochim Acta. 2024 Jun 20;490:144305.
93. Abbott AP, El Ttaib K, Frisch G, McKenzie KJ, Ryder KS. Electrodeposition of copper composites from deep eutectic solvents based on choline chloride. Physical Chemistry Chemical Physics. 2009;11(21):4269.
94. Abbott AP, Capper G, McKenzie KJ, Ryder KS. Electrodeposition of zinc–tin alloys from deep eutectic solvents based on choline chloride. Journal of Electroanalytical Chemistry. 2007 Jan;599(2):288–94.
95. Liu A, Shi Z, Reddy RG. Mechanism study of Cu-Zn alloys electrodeposition in deep eutectic solvents. Ionics (Kiel). 2020 Jun 3;26(6):3161–72.
96. Liao H, Jiang Y, Zhou Z, Chen S, Sun S. Shape-Controlled Synthesis of Gold Nanoparticles in Deep Eutectic Solvents for Studies of Structure–Functionality Relationships in Electrocatalysis. Angewandte Chemie International Edition. 2008 Nov 10;47(47):9100–3.
97. Baby JN, Sriram B, Wang SF, George M. Effect of Various Deep Eutectic Solvents on the Sustainable Synthesis of $MgFe_2O_4$ Nanoparticles for Simultaneous Electrochemical Determination of Nitrofurantoin and 4-Nitrophenol. ACS Sustain Chem Eng. 2020 Jan 27;8(3):1479–86.
98. Długosz O, Matyjasik W, Matysik J, Banach M. Anhydrous metal nanoparticle suspensions using deep eutectic solvents (DES) – Green approach to metal nanoparticles production. J Mol Liq. 2024 Feb;396:123966.
99. Bavandpour R, Rajabi M, Karimi-Maleh H, Asghari A. Application of deep eutectic solvent and SWCNT-ZrO2 nanocomposite as conductive mediators for the fabrication of simple and rapid electrochemical sensor for determination of trace anti-migration drugs. Microchemical Journal. 2021 Jun;165:106141.
100. Arab N, Fotouhi L, Salis A, Dorraji PS. An amplified electrochemical sensor employing a polymeric film and graphene quantum dots/multiwall carbon nanotubes in a deep eutectic solvent for sensitive analysis of paracetamol and 4-aminophenol. New Journal of Chemistry. 2020;44(36):15742–51.
101. Hamtak M, Fotouhi L, Hosseini M, Seyed Dorraji P. Improved Performance for Acyclovir Sensing in the Presence of Deep Eutectic Solvent and Nanostructures and Polymer. IEEE Sens J. 2020 Jan 15;20(2):623–30.
102. Mostafiz B, Fotouhi L, Dorraji PS. An electrochemical sensor based on an Eriochrome Black T polymer and deep eutectic solvent for the simultaneous determination of omeprazole and lansoprazole. Analytical Methods. 2020;12(32):4072–9.
103. Zarei E, Vafadar M, Asghari A. Acetaminophen and Thiosalicylic Acid Sensor Based on Carbon Paste Electrode Modified with Multi-Walled Carbon Nanotubes and Natural Deep Eutectic Solvent. Pharm Chem J. 2024 Mar 16;57(12):1862–71.
104. Bavandpour R, Rajabi M, Asghari A. Electrochemical determination of epirubicin in the presence of topotecan as essential anti-cancer compounds using paste electrode amplified with Pt/SWCNT nanocomposite and a deep eutectic solvent. Chemosphere. 2022 Feb;289:133060.
105. El Achkar T, Greige-Gerges H, Fourmentin S. Basics and properties of deep eutectic solvents: a review. Environ Chem Lett [Internet]. 2021 Aug 1 [cited 2024 Nov

17];19(4):3397–408. Available from: https://link.springer.com/article/10.1007/s10311-021-01225-8
106. Abranches DO, Martins MAR, Silva LP, Schaeffer N, Pinho SP, Coutinho JAP. Phenolic hydrogen bond donors in the formation of non-ionic deep eutectic solvents: the quest for type V DES. Chemical Communications [Internet]. 2019 Aug 22 [cited 2024 Nov 17];55(69):10253–6. Available from: https://pubs.rsc.org/en/content/articlehtml/2019/cc/c9cc04846d
107. Guimarães TGS, Andrade DF, Santana APR, Moser P, Ferreira SS, Menezes IMNR, et al. Mixture design and physicochemical characterization of amino acid-based DEEP eutectic solvents (AADES) for sample preparation prior to elemental analysis. J Mol Liq. 2022 Jan 1;345:117887.
108. Shah PA, Chavda V, Hirpara D, Sharma VS, Shrivastav PS, Kumar S. Exploring the potential of deep eutectic solvents in pharmaceuticals: Challenges and opportunities. J Mol Liq. 2023 Nov 15;390:123171.
109. Choi YH, van Spronsen J, Dai Y, Verberne M, Hollmann F, Arends IWCE, et al. Are Natural Deep Eutectic Solvents the Missing Link in Understanding Cellular Metabolism and Physiology? Plant Physiol [Internet]. 2011 Aug 5 [cited 2024 Nov 19];156(4):1701–5. Available from: https://dx.doi.org/10.1104/pp.111.178426
110. Zainal-Abidin MH, Hayyan M, Wong WF. Hydrophobic deep eutectic solvents: Current progress and future directions. Journal of Industrial and Engineering Chemistry. 2021 May 25;97:142–62.
111. Kalantri S, Vora A. Eutectic solutions for healing: a comprehensive review on therapeutic deep eutectic solvents (TheDES). Drug Dev Ind Pharm [Internet]. 2024 [cited 2024 Nov 20];50(5):387–400. Available from: https://www.tandfonline.com/doi/abs/10.1080/03639045.2024.2345131
112. Duarte ARC, Ferreira ASD, Barreiros S, Cabrita E, Reis RL, Paiva A. A comparison between pure active pharmaceutical ingredients and therapeutic deep eutectic solvents: Solubility and permeability studies. European Journal of Pharmaceutics and Biopharmaceutics. 2017 May 1;114:296–304.
113. Rahman MS, Roy R, Jadhav B, Hossain MN, Halim MA, Raynie DE. Formulation, structure, and applications of therapeutic and amino acid-based deep eutectic solvents: An overview. J Mol Liq. 2021 Jan 1;321:114745.
114. Guimarães TGS, Andrade DF, Santana APR, Moser P, Ferreira SS, Menezes IMNR, et al. Mixture design and physicochemical characterization of amino acid-based DEEP eutectic solvents (AADES) for sample preparation prior to elemental analysis. J Mol Liq. 2022 Jan 1;345:117887.
115. Khezeli T, Daneshfar A. Synthesis and application of magnetic deep eutectic solvents: Novel solvents for ultrasound assisted liquid-liquid microextraction of thiophene. Ultrason Sonochem. 2017 Sep 1;38:590–7.
116. Makoś-Chełstowska P, Kaykhaii M, Płotka-Wasylka J, de la Guardia M. Magnetic deep eutectic solvents – Fundamentals and applications. J Mol Liq. 2022 Nov 1;365:120158.
117. Rahman MS, Raynie DE. Thermal behavior, solvatochromic parameters, and metal halide solvation of the novel water-based deep eutectic solvents. J Mol Liq. 2021 Feb 15;324:114779.
118. Picciolini E, Pastore G, Del Giacco T, Ciancaleoni G, Tiecco M, Germani R. aquo-DESs: Water-based binary natural deep eutectic solvents. J Mol Liq. 2023 Aug 1;383:122057.

119. Yang K, Ge Z, Zhang M, Wang C, Peng K, Yang H, et al. Deep eutectic solvent based adhesive with dynamic adhesion, water-resistant and NIR-responsive retrieval properties. Chemical Engineering Journal. 2022 Jul 1;439:135646.
120. Ren'Ai L, Zhang K, Chen G, Su B, Tian J, He M, et al. Green polymerizable deep eutectic solvent (PDES) type conductive paper for origami 3D circuits. Chemical Communications [Internet]. 2018 Feb 27 [cited 2024 Nov 20];54(18):2304–7. Available from: https://pubs.rsc.org/en/content/articlehtml/2018/cc/c7cc09209a
121. Zhou P, Liu G, Fang H, Zhao Z, Zhang Y, Tang X, et al. Supramolecular deep eutectic solvents: Current advances and critical evaluation of cyclodextrins from solute to solvent in emerging functional food. Compr Rev Food Sci Food Saf [Internet]. 2024 Nov 1 [cited 2024 Nov 20];23(6):e70026. Available from: https://onlinelibrary.wiley.com/doi/full/10.1111/1541-4337.70026
122. Janicka P, Kaykhaii M, Płotka-Wasylka J, Gębicki J. Supramolecular deep eutectic solvents and their applications. Green Chemistry [Internet]. 2022 Jul 4 [cited 2024 Nov 20];24(13):5035–45. Available from: https://pubs.rsc.org/en/content/articlehtml/2022/gc/d2gc00906d
123. Qin H, Hu X, Wang J, Cheng H, Chen L, Qi Z. Overview of acidic deep eutectic solvents on synthesis, properties and applications. Green Energy & Environment. 2020 Jan 1;5(1):8–21.
124. Yang J, Wang Y, Zhang W, Li M, Peng F, Bian J. Alkaline deep eutectic solvents as novel and effective pretreatment media for hemicellulose dissociation and enzymatic hydrolysis enhancement. Int J Biol Macromol. 2021 Dec 15;193:1610–6.
125. Van Osch DJGP, Zubeir LF, Van Den Bruinhorst A, Rocha MAA, Kroon MC. Hydrophobic deep eutectic solvents as water-immiscible extractants. Green Chemistry [Internet]. 2015 Sep 1 [cited 2024 Nov 24];17(9):4518–21. Available from: https://pubs.rsc.org/en/content/articlehtml/2015/gc/c5gc01451d
126. Florindo C, Branco LC, Marrucho IM. Quest for Green-Solvent Design: From Hydrophilic to Hydrophobic (Deep) Eutectic Solvents. ChemSusChem [Internet]. 2019 Apr 23 [cited 2021 Jun 12];12(8):1549–59. Available from: https://doi.org/10.1002/cssc.201900147.
127. Makoś P, Słupek E, Gębicki J. Hydrophobic deep eutectic solvents in microextraction techniques–A review. Microchemical Journal. 2020 Jan 1;152:104384.
128. Maletta A, Gutiérrez A, Jian Tan P, Springstead J, Aparicio S, Atilhan M. Separation of phenolic compounds from water by using monoterpenoid and fatty acid based hydrophobic deep eutectic solvents. J Mol Liq. 2023 Jul 1;381:121806.
129. Zhang X, Wang J, Zhang Y, Qing W, Lansing S, Shi J, et al. Anhydrous volatile fatty acid extraction through omniphobic membranes by hydrophobic deep eutectic solvents: Mechanistic understanding and future perspective. Water Res. 2024 Jun 15;257:121654.
130. Darwish AS, Warrag SEE, Lemaoui T, Alseiari MK, Hatab FA, Rafay R, et al. Green extraction of volatile fatty acids from fermented wastewater using hydrophobic deep eutectic solvents. Fermentation [Internet]. 2021 Dec 1 [cited 2024 Nov 24];7(4):226. Available from: https://www.mdpi.com/2311-5637/7/4/226/htm
131. Cablé PA, Le Brech Y, Mutelet F. Liquid-liquid extraction of phenolic compounds from aqueous solution using hydrophobic deep eutectic solvents. J Mol Liq. 2022 Nov 15;366:120266.
132. Shi Y, Xiong D, Zhao Y, Li T, Zhang K, Fan J. Highly efficient extraction/separation of Cr (VI) by a new family of hydrophobic deep eutectic solvents. Chemosphere. 2020 Feb 1;241:125082.

133. Florindo C, Branco LC, Marrucho IM. Development of hydrophobic deep eutectic solvents for extraction of pesticides from aqueous environments. Fluid Phase Equilib. 2017 Sep 25;448:135–42.
134. Li J, Jiao Y, Luo Q, Hu W, Fang S, Tang C, et al. Treatment of oil-based drill cuttings by hydrophobic deep eutectic solvents. Can J Chem Eng [Internet]. 2022 Aug 1 [cited 2024 Nov 24];100(8):1747–54. Available from: https://onlinelibrary.wiley.com/doi/full/10.1002/cjce.24263
135. Makoś P, Przyjazny A, Boczkaj G. Hydrophobic deep eutectic solvents as "green" extraction media for polycyclic aromatic hydrocarbons in aqueous samples. J Chromatogr A. 2018 Oct 5;1570:28–37.
136. Sas OG, Villar L, Domínguez Á, González B, Macedo EA. Hydrophobic deep eutectic solvents as extraction agents of nitrophenolic pollutants from aqueous systems. Environ Technol Innov. 2022 Feb 1;25:102170.
137. Arcon DP, Franco FC. All-fatty acid hydrophobic deep eutectic solvents towards a simple and efficient microextraction method of toxic industrial dyes. J Mol Liq. 2020 Nov 15;318:114220.
138. Křížek T, Bursová M, Horsley R, Kuchař M, Tůma P, Čabala R, et al. Menthol-based hydrophobic deep eutectic solvents: Towards greener and efficient extraction of phytocannabinoids. J Clean Prod. 2018 Aug 20;193:391–6.
139. Kongpol K, Sermkaew N, Makkliang F, Khongphan S, Chuaboon L, Sakdamas A, et al. Extraction of curcuminoids and ar-turmerone from turmeric (Curcuma longa L.) using hydrophobic deep eutectic solvents (HDESs) and application as HDES-based microemulsions. Food Chem. 2022 Dec 1;396:133728.
140. Xu Z, Cai Y, Ma Q, Zhao Z, Yang D, Xu X. Optimization of Extraction of Bioactive Compounds from Baphicacanthus cusia Leaves by Hydrophobic Deep Eutectic Solvents. Molecules. 2021 Mar 19;26(6):1729.
141. Mastellone G, Abbasi NM, Cagliero C, Anderson JL. New Class of Tunable Choline Bromide-Based Hydrophobic Deep Eutectic Solvents for the Extraction of Bioactive Compounds of Varying Polarity from a Plant Matrix. ACS Sustain Chem Eng. 2023 May 1;11(17):6665–75.
142. Cao J, Yang M, Cao F, Wang J, Su E. Well-Designed Hydrophobic Deep Eutectic Solvents As Green and Efficient Media for the Extraction of Artemisinin from *Artemisia annua* Leaves. ACS Sustain Chem Eng. 2017 Apr 3;5(4):3270–8.
143. Kalyniukova A, Holuša J, Musiolek D, Sedlakova-Kadukova J, Płotka-Wasylka J, Andruch V. Application of deep eutectic solvents for separation and determination of bioactive compounds in medicinal plants. Ind Crops Prod. 2021 Nov;172:114047.
144. Viñas-Ospino A, Panić M, Radojčić- Redovniković I, Blesa J, Esteve MJ. Using novel hydrophobic deep eutectic solvents to improve a sustainable carotenoid extraction from orange peels. Food Biosci. 2023 Jun 1;53:102570.
145. Kyriakoudi A, Tsiouras A, Mourtzinos I. Extraction of Lycopene from Tomato Using Hydrophobic Natural Deep Eutectic Solvents Based on Terpenes and Fatty Acids. Foods. 2022 Aug 31;11(17):2645.
146. Faraji M, Mahmoodi-Maymand M, Dastmalchi F. Green, fast and simple dispersive liquid-liquid microextraction method by using hydrophobic deep eutectic solvent for analysis of folic acid in fortified flour samples before liquid chromatography determination. Food Chem. 2020 Aug;320:126486.
147. Dal Bosco C, Di Lisio V, D'Angelo P, Gentili A. Hydrophobic Eutectic Solvent with Antioxidant Properties: Application for the Dispersive Liquid–Liquid Microextraction

of Fat-Soluble Micronutrients from Fruit Juices. ACS Sustain Chem Eng. 2021 Jun 21;9(24):8170–8.
148. Wang KH, Yang C, Liang GB, Meng YF, Zou Y, Li S, et al. Hydrophobic deep eutectic solvents as emerging green reaction media for biocatalytic processes: impacts of solvent properties and compositions. Green Chemistry. 2024;26(17):9388–97.
149. Ruggeri S, Poletti F, Zanardi C, Pigani L, Zanfrognini B, Corsi E, et al. Chemical and electrochemical properties of a hydrophobic deep eutectic solvent. Electrochim Acta. 2019 Feb 1;295:124–9.
150. Chaabene N, Ngo K, Turmine M, Vivier V. New hydrophobic deep eutectic solvent for electrochemical applications. J Mol Liq. 2020 Dec;319:114198.
151. Wannasri N, Uppachai P, Seehamart K, Jantrasee S, Butwong N, Mukdasai K, et al. Novel and Highly Sensitive Electrochemical Sensor for the Determination of Oxytetracycline Based on Fluorine-Doped Activated Carbon and Hydrophobic Deep Eutectic Solvents. ACS Omega. 2022 Dec 13;7(49):45654–64.
152. Boldrini CL, Manfredi N, Perna FM, Capriati V, Abbotto A. Designing Eco-Sustainable Dye-Sensitized Solar Cells by the Use of a Menthol-Based Hydrophobic Eutectic Solvent as an Effective Electrolyte Medium. Chemistry – A European Journal. 2018 Dec 3;24(67):17656–9.
153. Patil SM, Jayachandran K, Sahu M, Gupta R. Efficient Plutonium Extraction and Electrochemical Insights in a Hydrophobic Deep Eutectic Solvent for Radioactive Waste Management. J Electrochem Soc. 2023 Nov 1;170(11):113503.
154. Kivelä H, Salomäki M, Vainikka P, Mäkilä E, Poletti F, Ruggeri S, et al. Effect of Water on a Hydrophobic Deep Eutectic Solvent. J Phys Chem B. 2022 Jan 20;126(2):513–27.
155. Dai Y, Witkamp GJ, Verpoorte R, Choi YH. Tailoring properties of natural deep eutectic solvents with water to facilitate their applications. Food Chem. 2015 Nov 15;187:14–9.
156. Długosz O. Natural Deep Eutectic Solvents in the Synthesis of Inorganic Nanoparticles. Materials. 2023 Jan 9;16(2):627.
157. Santana APR, Mora-Vargas JA, Guimarães TGS, Amaral CDB, Oliveira A, Gonzalez MH. Sustainable synthesis of natural deep eutectic solvents (NADES) by different methods. J Mol Liq. 2019 Nov;293:111452.
158. Gomez FJ V., Espino M, Fernández MA, Silva MF. A Greener Approach to Prepare Natural Deep Eutectic Solvents. ChemistrySelect. 2018 Jun 15;3(22):6122–5.
159. Florindo C, Oliveira FS, Rebelo LPN, Fernandes AM, Marrucho IM. Insights into the Synthesis and Properties of Deep Eutectic Solvents Based on Cholinium Chloride and Carboxylic Acids. ACS Sustain Chem Eng [Internet]. 2014 Oct 6 [cited 2021 Sep 3];2(10):2416–25. Available from: https://pubs.acs.org/doi/abs/10.1021/sc500439w
160. Długosz O, Banach M. Green methods for obtaining deep eutectic solvents (DES). J Clean Prod. 2024 Jan;434:139914.
161. Gutiérrez MC, Ferrer ML, Mateo CR, del Monte F. Freeze-Drying of Aqueous Solutions of Deep Eutectic Solvents: A Suitable Approach to Deep Eutectic Suspensions of Self-Assembled Structures. Langmuir. 2009 May 19;25(10):5509–15.
162. Shaibuna M, Theresa L V., Sreekumar K. Neoteric deep eutectic solvents: history, recent developments, and catalytic applications. Soft Matter. 2022;18(14):2695–721.
163. Van Aken K, Strekowski L, Patiny L. EcoScale, a semi-quantitative tool to select an organic preparation based on economical and ecological parameters. Beilstein Journal of Organic Chemistry. 2006 Mar 3;2.

164. Martín MI, García-Díaz I, Rodríguez ML, Gutiérrez MC, del Monte F, López FA. Synthesis and Properties of Hydrophilic and Hydrophobic Deep Eutectic Solvents via Heating-Stirring and Ultrasound. Molecules. 2024 Jun 28;29(13):3089.
165. El Achkar T, Greige-Gerges H, Fourmentin S. Basics and properties of deep eutectic solvents: a review. Environ Chem Lett. 2021 Aug 20;19(4):3397–408.
166. Pontes PVA, Crespo EA, Martins MAR, Silva LP, Neves CMSS, Maximo GJ, et al. Measurement and PC-SAFT modeling of solid-liquid equilibrium of deep eutectic solvents of quaternary ammonium chlorides and carboxylic acids. Fluid Phase Equilib. 2017 Sep 25;448:69–80.
167. Shakourian-Fard M, Reza Ghenaatian H, Alizadeh V, Kamath G, Khalili B. Density functional theory investigation into the interaction of deep eutectic solvents with amino acids. J Mol Liq. 2021 Dec;343:117624.
168. Li H, Chang Y, Zhu W, Wang C, Wang C, Yin S, et al. Theoretical evidence of charge transfer interaction between SO_2 and deep eutectic solvents formed by choline chloride and glycerol. Physical Chemistry Chemical Physics. 2015;17(43):28729–42.
169. Delgado-Mellado N, Larriba M, Navarro P, Rigual V, Ayuso M, García J, et al. Thermal stability of choline chloride deep eutectic solvents by TGA/FTIR-ATR analysis. J Mol Liq. 2018 Jun;260:37–43.
170. CHEN W, XUE Z, WANG J, JIANG J, ZHAO X, MU T. Investigation on the Thermal Stability of Deep Eutectic Solvents. Acta Physico-Chimica Sinica. 2018;34(8):904–11.
171. Alhadid A, Mokrushina L, Minceva M. Design of Deep Eutectic Systems: A Simple Approach for Preselecting Eutectic Mixture Constituents. Molecules. 2020 Feb 28;25(5):1077.
172. Abranches DO, Coutinho JAP. Everything You Wanted to Know about Deep Eutectic Solvents but Were Afraid to Be Told. Annu Rev Chem Biomol Eng. 2023 Jun 7;14(1):141–63.
173. Martins MAR, Pinho SP, Coutinho JAP. Insights into the Nature of Eutectic and Deep Eutectic Mixtures. J Solution Chem. 2019 Jul 4;48(7):962–82.
174. Anastas P, Eghbali N. Green Chemistry: Principles and Practice. Chem Soc Rev. 2010;39(1):301–12.
175. García-Serna J, Pérez-Barrigón L, Cocero MJ. New trends for design towards sustainability in chemical engineering: Green engineering. Chemical Engineering Journal. 2007 Sep;133(1–3):7–30.
176. Dhali K, Ghasemlou M, Daver F, Cass P, Adhikari B. A review of nanocellulose as a new material towards environmental sustainability. Science of The Total Environment. 2021 Jun;775:145871.
177. Whittingham MJ, Crapnell RD, Rothwell EJ, Hurst NJ, Banks CE. Additive manufacturing for electrochemical labs: An overview and tutorial note on the production of cells, electrodes and accessories. Talanta Open. 2021 Dec 1;4:100051.
178. R. G. Silva L, Stefano JS, de Oliveira DH, Carvalho MS, A. A. Muñoz R, Handa CL, et al. Electrochemical detection of gallic acid in complex matrices samples employing a completely 3D printed device. Microchemical Journal. 2024 Apr;199:110210.
179. Veloso WB, Meloni GN, Arantes IVS, Pradela-Filho LA, Muñoz RAA, Paixão TRLC. Gold film deposition by infrared laser photothermal treatment on 3D-printed electrodes: electrochemical performance enhancement and application. Analyst. 2024;149(15):3900–9.
180. Silva MVCO, Carvalho MS, Silva LRG, Rocha RG, Cambraia L V., Janegitz BC, et al. Tailoring 3D-printed sensor properties with reduced-graphene oxide: improved conductive filaments. Microchimica Acta. 2024 Oct 29;191(10):633.

181. Silva LRG, Bertolim LV, Stefano JS, Bonacin JA, Richter EM, Munoz RAA, et al. New route for the production of lab-made composite filaments based on soybean oil, polylactic acid and carbon black nanoparticles, and its application in the additive manufacturing of electrochemical sensors. Electrochim Acta. 2024 Dec;145566.
182. Bernalte E, Crapnell RD, El Azizi R, Augusto KKL, Banks CE. Gold nanoparticle infused castor oil for the production of high performance conductive additive manufacturing filament. Appl Mater Today. 2025 Feb;42:102578.
183. You PY, Kamarudin SK. Recent progress of carbonaceous materials in fuel cell applications: An overview. Chemical Engineering Journal. 2017 Feb;309:489–502.
184. Yang S, Li Y, Wang S, Wang M, Chu M, Xia B. Advances in the use of carbonaceous materials for the electrochemical determination of persistent organic pollutants. A review. Microchimica Acta. 2018 Feb 12;185(2):112.
185. Abdul Karim MR, Shehzad W. Transition metal compounds and their hybrids with carbonaceous materials for electrochemical energy storage applications. J Energy Storage. 2023 Nov;72:108288.
186. Sanati A, Jalali M, Raeissi K, Karimzadeh F, Kharaziha M, Mahshid SS, et al. A review on recent advancements in electrochemical biosensing using carbonaceous nanomaterials. Microchimica Acta. 2019 Dec 13;186(12):773.
187. Ferreira LMC, Silva PS, Augusto KKL, Gomes-Júnior PC, Farra SOD, Silva TA, et al. Using nanostructured carbon black-based electrochemical (bio)sensors for pharmaceutical and biomedical analyses: A comprehensive review. J Pharm Biomed Anal. 2022 Nov 30;221:115032.
188. Hussain KK, Shergill RS, Hamzah HH, Yeoman MS, Patel BA. Exploring Different Carbon Allotrope Thermoplastic Composites for Electrochemical Sensing. ACS Appl Polym Mater. 2023 Jun 9;5(6):4136–45.
189. Arduini F, Cinti S, Mazzaracchio V, Scognamiglio V, Amine A, Moscone D. Carbon black as an outstanding and affordable nanomaterial for electrochemical (bio)sensor design. Biosens Bioelectron. 2020 May 15;156:112033.
190. Vicentini FC, Ravanini AE, Figueiredo-Filho LCS, Iniesta J, Banks CE, Fatibello-Filho O. Imparting improvements in electrochemical sensors: evaluation of different carbon blacks that give rise to significant improvement in the performance of electroanalytical sensing platforms. Electrochim Acta. 2015 Mar;157:125–33.
191. Silva TA, Moraes FC, Janegitz BC, Fatibello-Filho O. Electrochemical Biosensors Based on Nanostructured Carbon Black: A Review. J Nanomater. 2017;2017:1–14.
192. Lounasvuori MM, Kelly D, Foord JS. Carbon black as low-cost alternative for electrochemical sensing of phenolic compounds. Carbon N Y. 2018 Apr;129:252–7.
193. Deroco PB, Fatibello-Filho O, Arduini F, Moscone D. Effect of Different Carbon Blacks on the Simultaneous Electroanalysis of Drugs as Water Contaminants Based on Screen-printed Sensors. Electroanalysis. 2019 Nov;31(11):2145–54.
194. Arduini F, Amine A, Majorani C, Di Giorgio F, De Felicis D, Cataldo F, et al. High performance electrochemical sensor based on modified screen-printed electrodes with cost-effective dispersion of nanostructured carbon black. Electrochem commun. 2010 Mar;12(3):346–50.
195. Trojanowicz M. Analytical applications of carbon nanotubes: a review. TrAC Trends in Analytical Chemistry. 2006 May;25(5):480–9.
196. Oliveira TMBF, Morais S. New Generation of Electrochemical Sensors Based on Multi-Walled Carbon Nanotubes. Applied Sciences. 2018 Oct 15;8(10):1925.
197. Ahammad AJS, Lee JJ, Rahman MdA. Electrochemical Sensors Based on Carbon Nanotubes. Sensors. 2009 Mar 30;9(4):2289–319.

198. Chung DDL. Review Graphite. J Mater Sci. 2002;37(8):1475–89.
199. Bellido-Milla D, Cubillana-Aguilera LM, El Kaoutit M, Hernández-Artiga MP, Hidalgo-Hidalgo de Cisneros JL, Naranjo-Rodríguez I, et al. Recent advances in graphite powder-based electrodes. Anal Bioanal Chem. 2013 Apr 28;405(11):3525–39.
200. Mafa JP, Mabuba N, Arotiba OA. An Exfoliated Graphite Based Electrochemical Sensor for As(III) in Water. Electroanalysis. 2016 Jul 12;28(7):1462–9.
201. Murugan P, Nagarajan RD, Shetty BH, Govindasamy M, Sundramoorthy AK. Recent trends in the applications of thermally expanded graphite for energy storage and sensors – a review. Nanoscale Adv. 2021;3(22):6294–309.
202. JENKINS GM, KAWAMURA K. Structure of Glassy Carbon. Nature. 1971 May;231(5299):175–6.
203. Tanzi MC, Farè S, Candiani G. Organization, Structure, and Properties of Materials. In: Foundations of Biomaterials Engineering. Elsevier; 2019. p. 3–103.
204. Vieira L de S. A review on the use of glassy carbon in advanced technological applications. Carbon N Y. 2022 Jan;186:282–302.
205. Uskoković V. A historical review of glassy carbon: Synthesis, structure, properties and applications. Carbon Trends. 2021 Oct;5:100116.
206. Desimoni E, Brunetti B. Glassy Carbon Electrodes Film-Modified with Acidic Functionalities. A Review. Electroanalysis. 2012 Jul 15;24(7):1481–500.
207. Azami T, Kasuya D, Yuge R, Yudasaka M, Iijima S, Yoshitake T, et al. Large-Scale Production of Single-Wall Carbon Nanohorns with High Purity. Journal of Physical Chemistry C [Internet]. 2008 Feb 7 [cited 2024 Jul 1];112(5):1330–4. Available from: https://pubs.acs.org/doi/abs/10.1021/jp076365o
208. Karousis N, Suarez-Martinez I, Ewels CP, Tagmatarchis N. Structure, Properties, Functionalization, and Applications of Carbon Nanohorns. Chem Rev. 2016 Apr 27;116(8):4850–83.
209. Zhang Z, Han S, Wang C, Li J, Xu G. Single-Walled Carbon Nanohorns for Energy Applications. Nanomaterials. 2015 Oct 21;5(4):1732–55.
210. Liu X, Li H, Wang F, Zhu S, Wang Y, Xu G. Functionalized single-walled carbon nanohorns for electrochemical biosensing. Biosens Bioelectron. 2010 Jun;25(10):2194–9.
211. Periasamy V, Elumalai PNN, Talebi S, Subramaniam RT, Kasi R, Iwamoto M, et al. Novel same-metal three electrode system for cyclic voltammetry studies. RSC Adv. 2023;13(9):5744–52.
212. Farghaly OA, Hameed RSA, Abu-Nawwas AAH. Analytical Application Using Modern Electrochemical Techniques. Int J Electrochem Sci. 2014 Jun;9(6):3287–318.
213. Xie Y, Liu T, Chu Z, Jin W. Recent advances in electrochemical enzymatic biosensors based on regular nanostructured materials. Journal of Electroanalytical Chemistry. 2021 Jul;893:115328.
214. Felix FS, Angnes L. Electrochemical immunosensors – A powerful tool for analytical applications. Biosens Bioelectron. 2018 Apr;102:470–8.
215. Fabri J, Silva LRG, Stefano JS, Pereira JFS, Cocco DR, Muñoz RAA, et al. In situ electrochemical determination of resorcinol using a fully 3D printed apparatus. Microchemical Journal. 2023 Aug;191:108810.
216. Arantes IVS, Crapnell RD, Whittingham MJ, Sigley E, Paixão TRLC, Banks CE. Additive Manufacturing of a Portable Electrochemical Sensor with a Recycled Conductive Filament for the Detection of Atropine in Spiked Drink Samples. ACS Applied Engineering Materials. 2023 Sep 22;1(9):2397–406.

217. Campbell FW, Compton RG. The use of nanoparticles in electroanalysis: an updated review. Anal Bioanal Chem. 2010 Jan 3;396(1):241–59.
218. Ramos MMV, Carvalho JHS, de Oliveira PR, Janegitz BC. Determination of serotonin by using a thin film containing graphite, nanodiamonds and gold nanoparticles anchored in casein. Measurement. 2020 Jan 1;149:106979.
219. Sharma S, Singh N, Tomar V, Chandra R. A review on electrochemical detection of serotonin based on surface modified electrodes. Biosens Bioelectron. 2018 Jun 1;107:76–93.
220. Tertiș M, Cernat A, Lacatiș D, Florea A, Bogdan D, Suciu M, et al. Highly selective electrochemical detection of serotonin on polypyrrole and gold nanoparticles-based 3D architecture. Electrochem commun. 2017 Feb 1;75:43–7.
221. Ran G, Xia Y, Liang L, Fu C. Enhanced response of sensor on serotonin using nickel-reduced graphene oxide by atomic layer deposition. Bioelectrochemistry. 2021 Aug 1;140:107820.
222. Musuvadhi Babulal S, Wu HF, Chien Wu C. Two-Dimensional Phosphorus-Doped Tungsten Trioxide Nanosheets for Electrochemical Detection of Serotonin in Biological Fluids. ACS Appl Nano Mater [Internet]. 2023 Aug 11 [cited 2024 Feb 21];6(15):14552–62. Available from: https://pubs.acs.org/doi/full/10.1021/acsanm.3c02724
223. Koluaçık E, Karabiberoğlu ŞU, Dursun Z. Electrochemical Determination of Serotonin Using Pre-treated Multi-walled Carbon Nanotube-polyaniline Composite Electrode. Electroanalysis [Internet]. 2018 Dec 1 [cited 2024 Feb 21];30(12):2977–87. Available from: https://onlinelibrary.wiley.com/doi/full/10.1002/elan.201800588
224. Ran G, Chen X, Xia Y. Electrochemical detection of serotonin based on a poly(bromocresol green) film and Fe 3 O 4 nanoparticles in a chitosan matrix. RSC Adv [Internet]. 2017 Jan 12 [cited 2024 Feb 20];7(4):1847–51. Available from: https://pubs.rsc.org/en/content/articlehtml/2017/ra/c6ra25639b
225. Dube A, Malode SJ, Ali Alshehri M, Shetti NP. Recent advances in the development of electrochemical sensors for detecting pesticides. Journal of Industrial and Engineering Chemistry. 2024 Sep;
226. Yi Y, Zhao Y, Zhang Z, Wu Y, Zhu G. Recent developments in electrochemical detection of cadmium. Trends in Environmental Analytical Chemistry. 2022 Mar;33:e00152.
227. Attaallah R, Amine A. Highly selective and sensitive detection of cadmium ions by horseradish peroxidase enzyme inhibition using a colorimetric microplate reader and smartphone paper-based analytical device. Microchemical Journal. 2022 Jan;172:106940.
228. Moyo M, Okonkwo JO. Horseradish peroxidase biosensor based on maize tassel–MWCNTs composite for cadmium detection. Sens Actuators B Chem. 2014 Mar;193:515–21.
229. Zhang C, Li C, Han X. Screen printed electrode containing bismuth for the detection of cadmium ion. Journal of Electroanalytical Chemistry. 2023 Mar 15;933:117291.
230. Pandey SK, Sachan S, Singh SK. Ultra-trace sensing of cadmium and lead by square wave anodic stripping voltammetry using ionic liquid modified graphene oxide. Mater Sci Energy Technol. 2019 Dec 1;2(3):667–75.
231. Albalawi I, Hogan A, Alatawi H, Moore E. A sensitive electrochemical analysis for cadmium and lead based on Nafion-Bismuth film in a water sample. Sens Biosensing Res. 2021 Dec 1;34:100454.

232. Giacomazzi S, Cochet N. Environmental impact of diuron transformation: a review. Chemosphere. 2004 Sep;56(11):1021–32.
233. He Y, Luo L, Li L, You T, Chen X. Synergistic signal−amplification effect of silver nanowires and bifunctional monomers on molecularly imprinted electrochemical sensor for diuron analysis. Biosens Bioelectron. 2024 Oct;262:116570.
234. Santos Oliveira R, Batista da Silva H, Cunha de Souza C, Burger Veríssimo W, Auxiliadora Costa Matos M, Pedrosa Lisboa T, et al. Development of an electrochemical sensor utilizing recycled ABS filaments for 3D printing in the determination of diuron. Microchemical Journal. 2024 Jun;201:110454.
235. Munusamy N, Don Disouza FP, Chen SM, Krishnan K, Jothinathan MKD, Prakash B. Facile fabrication of bismuth oxide anchored graphene oxide for the effective electrochemical sensing of diuron. J Taiwan Inst Chem Eng. 2024 Dec;165:105708.
236. Zhu J, He Y, Luo L, Li L, You T. Electrochemical Determination of Hazardous Herbicide Diuron Using MWCNTs-CS@NGQDs Composite-Modified Glassy Carbon Electrodes. Biosensors (Basel). 2023 Aug 11;13(8):808.
237. Manasa G, Bhakta AK, Mascarenhas RJ, Shetti NP. BaO-MWCNT composite material-based electrocatalytic amperometric sensor for the detection of environmentally hazardous Diuron. Microchemical Journal. 2023 Aug;191:108778.
238. Mbokou Foukmeniok S, Bako RFY, Ilboudo O, Karanga Y, Njanja E, Pontie M, et al. Sensitive Carbon Fiber Microelectrode for the Quantification of Diuron in Quality Control of a Commercialized Formulation. Int J Anal Chem. 2022 Mar 11;2022:1–9.
239. Yi W, Han C, Li Z, Guo Y, Liu M, Dong C. A strategy of electrochemical simultaneous detection of acetaminophen and levofloxacin in water based on g-C $_3$ N $_4$ nanosheet-doped graphene oxide. Environ Sci Nano. 2021;8(1):258–68.
240. Alam AU, Qin Y, Howlader MMR, Hu NX, Deen MJ. Electrochemical sensing of acetaminophen using multi-walled carbon nanotube and β-cyclodextrin. Sens Actuators B Chem. 2018 Jan;254:896–909.
241. Charithra MM, Manjunatha JG. Electroanalytical Determination of Acetaminophen Using a Polymerised Carbon Nanotube Based Sensor. J Electron Mater. 2021 Dec 28;50(12):6929–40.
242. Kavai MS, de Lima LF, de Araujo WR. A disposable and low-cost laser-scribed graphene electrochemical sensor for simultaneous detection of hydroquinone, paracetamol and methylparaben. Mater Lett. 2023 Jan;330:133211.
243. Wang K, Wu C, Wang F, Jing N, Jiang G. Co/Co $_3$ O $_4$ Nanoparticles Coupled with Hollow Nanoporous Carbon Polyhedrons for the Enhanced Electrochemical Sensing of Acetaminophen. ACS Sustain Chem Eng. 2019 Nov 18;7(22):18582–92.
244. Miglione A, Raucci A, Cristiano F, Mancini M, Gioia V, Frugis A, et al. Paper-based 2D configuration for the electrochemical and facile detection of paracetamol in wastewaters. Electrochim Acta. 2024 Jun;488:144255.
245. Laube N, Mohr B, Hesse A. Laser-probe-based investigation of the evolution of particle size distributions of calcium oxalate particles formed in artificial urines. J Cryst Growth. 2001 Nov 1;233(1–2):367–74.
246. BRUNS RE, SCARMINIO IS, DE BARROS NETO B. Statistical design-chemometrics. Vol. 25. Elsevier; 2006.
247. Bard A, Faulkner L. Electrochemical Methods: Fundamentals and Applications. Vol. 2nd. New York: Wiley; 2001.
248. Greczynski G, Hultman L. The same chemical state of carbon gives rise to two peaks in X-ray photoelectron spectroscopy. Scientific Reports 2021 11:1 [Internet]. 2021 May

27 [cited 2024 Mar 25];11(1):1–5. Available from: https://www.nature.com/articles/s41598-021-90780-9
249. Crapnell RD, Garcia-Miranda Ferrari A, Whittingham MJ, Sigley E, Hurst NJ, Keefe EM, et al. Adjusting the Connection Length of Additively Manufactured Electrodes Changes the Electrochemical and Electroanalytical Performance. Sensors. 2022 Dec 6;22(23):9521.
250. Pandey RK, Chen L, Teraji S, Nakanishi H, Soh S. Eco-Friendly, Direct Deposition of Metal Nanoparticles on Graphite for Electrochemical Energy Conversion and Storage. ACS Appl Mater Interfaces [Internet]. 2019 Oct 9 [cited 2024 Mar 25];11(40):36525–34. Available from: https://pubs.acs.org/doi/abs/10.1021/acsami.9b09273
251. Bernalte E, Crapnell RD, Messai OMA, Banks CE. The Effect of Slicer Infill Pattern on the Electrochemical Performance of Additively Manufactured Electrodes. ChemElectroChem. 2024 Feb 16;11(4).
252. Crapnell RD, Banks CE. Perspective: What constitutes a quality paper in electroanalysis? Talanta Open. 2021 Dec;4:100065.
253. Aktürk M, Dursun Z. A novel composite electrode based on graphene oxide/MnO_2:h-MoO_3 particles for square wave voltammetric determination of acetaminophen. Electroanalysis. 2024 Oct 18;36(10).
254. Qian L, Elmahdy R, Raj Thiruppathi A, Chen A. An ultrasensitive electrochemical sensor for the detection of acetaminophen *via* a three-dimensional hierarchical nanoporous gold wire electrode. Analyst. 2021;146(14):4525–34.
255. Tomé LIN, Baião V, da Silva W, Brett CMA. Deep eutectic solvents for the production and application of new materials. Appl Mater Today. 2018 Mar 1;10:30–50.
256. Hansen BB, Spittle S, Chen B, Poe D, Zhang Y, Klein JM, et al. Deep Eutectic Solvents: A Review of Fundamentals and Applications. Chem Rev [Internet]. 2021 Feb 10 [cited 2023 Oct 15];121(3):1232–85. Available from: https://pubs.acs.org/doi/epdf/10.1021/acs.chemrev.0c00385
257. Shishov A, Makoś-Chełstowska P, Bulatov A, Andruch V. Deep Eutectic Solvents or Eutectic Mixtures? Characterization of Tetrabutylammonium Bromide and Nonanoic Acid Mixtures. Journal of Physical Chemistry B [Internet]. 2022 Jun 2 [cited 2023 Apr 27];126(21):3889–96. Available from: https://pubs.acs.org/doi/full/10.1021/acs.jpcb.2c00858
258. Yuvali D, Seyhaneyildizi M, Soylak M, Narin İ, Yilmaz E. An environment-friendly and rapid liquid-liquid microextraction based on new synthesized hydrophobic deep eutectic solvent for separation and preconcentration of erythrosine (E127) in biological and pharmaceutical samples. Spectrochim Acta A Mol Biomol Spectrosc. 2021 Jan 5;244:118842.
259. Tang N, Liu L, Yin C, Zhu G, Huang Q, Dong J, et al. Environmentally benign hydrophobic deep eutectic solvents for palladium(II) extraction from hydrochloric acid solution. J Taiwan Inst Chem Eng. 2021 Apr 1;121:92–100.
260. Ji Y, Meng Z, Zhao J, Zhao H, Zhao L. Eco-friendly ultrasonic assisted liquid–liquid microextraction method based on hydrophobic deep eutectic solvent for the determination of sulfonamides in fruit juices. J Chromatogr A. 2020 Jan 4;1609:460520.
261. Tang W, Dai Y, Row KH. Evaluation of fatty acid/alcohol-based hydrophobic deep eutectic solvents as media for extracting antibiotics from environmental water. Anal Bioanal Chem [Internet]. 2018 Nov 1 [cited 2023 Jul 17];410(28):7325–36. Available from: https://link.springer.com/article/10.1007/s00216-018-1346-6

262. D'Agostino C, Harris RC, Abbott AP, Gladden LF, Mantle MD. Molecular motion and ion diffusion in choline chloride based deep eutectic solvents studied by 1H pulsed field gradient NMR spectroscopy. Physical Chemistry Chemical Physics [Internet]. 2011 Nov 29 [cited 2023 Jul 17];13(48):21383–91. Available from: https://pubs.rsc.org/en/content/articlehtml/2011/cp/c1cp22554e
263. Han OH, Kim C. Magic Angle Spinning NMR Techniques for the Study of Surfactants. Bull Korean Chem Soc [Internet]. 1997 [cited 2023 Sep 20];18(3):271–3. Available from: https://pure.korea.ac.kr/en/publications/magic-angle-spinning-nmr-techniques-for-the-study-of-surfactants
264. Sutjahja IM, Wonorahardjo S, Wonorahardjo S. Study on Physicochemical and Thermal Properties of Tetrabutylammonium-Based Cation Ionic Salts Induced by Al2O3 Additive for Thermal Energy Storage Application. Inorganics 2020, Vol 8, Page 51 [Internet]. 2020 Sep 18 [cited 2023 Apr 23];8(9):51. Available from: https://www.mdpi.com/2304-6740/8/9/51/htm
265. Hayler HJ, Perkin S. The eutectic point in choline chloride and ethylene glycol mixtures. Chemical Communications [Internet]. 2022 Nov 15 [cited 2023 Apr 25];58(91):12728–31. Available from: https://pubs.rsc.org/en/content/articlehtml/2022/cc/d2cc04008e
266. Maximo GJ, Carareto NDD, Costa MC, dos Santos AO, Cardoso LP, Krähenbühl MA, et al. On the solid–liquid equilibrium of binary mixtures of fatty alcohols and fatty acids. Fluid Phase Equilib. 2014 Mar 25;366:88–98.
267. Costa MC, Sardo M, Rolemberg MP, Ribeiro-Claro P, Meirelles AJA, Coutinho JAP, et al. The solid–liquid phase diagrams of binary mixtures of consecutive, even saturated fatty acids: differing by four carbon atoms. Chem Phys Lipids. 2009 Jan 1;157(1):40–50.
268. Rozas S, Benito C, Alcalde R, Atilhan M, Aparicio S. Insights on the water effect on deep eutectic solvents properties and structuring: The archetypical case of choline chloride + ethylene glycol. J Mol Liq. 2021 Dec 15;344:117717.
269. Sheldon RA. The E Factor: fifteen years on. Green Chemistry. 2007;9(12):1273.
270. Simone M, Pulpito M, Perna FM, Capriati V, Vitale P. Switchable Deep Eutectic Solvents for Sustainable Sulfonamide Synthesis. Chemistry – A European Journal. 2024 Sep 17;
271. Iyer S, Dhiman N, Zade SP, Mukherjee S, Singla N, Kumar M. Exposure to Tetrabutylammonium Bromide Impairs Cranial Neural Crest Specification, Neurogenic Program, and Brain Morphogenesis. ACS Chem Neurosci. 2023 May 17;14(10):1785–98.
272. Augusto KK de L, Gomes-Junior PC, Longatto GP, Piccin E, Cavalheiro ÉTG, Bernalte E, et al. Electrochemical sensor based on carbon nanohorns and hydrophobic deep eutectic solvent for the determination of serotonin in biological samples. Electrochim Acta. 2025 Apr;520:145836.
273. Pajkossy T. Impedance spectroscopy at interfaces of metals and aqueous solutions — Surface roughness, CPE and related issues. Solid State Ion. 2005 Aug 15;176(25–28):1997–2003.
274. Laschuk NO, Easton EB, Zenkina O V. Reducing the resistance for the use of electrochemical impedance spectroscopy analysis in materials chemistry. RSC Adv [Internet]. 2021 Aug 18 [cited 2024 Feb 16];11(45):27925–36. Available from: https://pubs.rsc.org/en/content/articlehtml/2021/ra/d1ra03785d
275. Sadanandhan NK, Cheriyathuchenaaramvalli M, Devaki SJ, Ravindranatha Menon AR. PEDOT-reduced graphene oxide-silver hybrid nanocomposite modified transducer for

the detection of serotonin. Journal of Electroanalytical Chemistry. 2017 Jun 1;794:244–53.
276. Trachioti MG, Lazanas ACh, Prodromidis MI. Shedding light on the calculation of electrode electroactive area and heterogeneous electron transfer rate constants at graphite screen-printed electrodes. Microchimica Acta. 2023 Jul 7;190(7):251.
277. Kathiresan V, Rajarathinam T, Lee S, Kim S, Lee J, Thirumalai D, et al. Cost-Effective Electrochemical Activation of Graphitic Carbon Nitride on the Glassy Carbon Electrode Surface for Selective Determination of Serotonin. Sensors. 2020 Oct 26;20(21):6083.
278. Jiang X, Lin X. Overoxidized polypyrrole film directed DNA immobilization for construction of electrochemical micro-biosensors and simultaneous determination of serotonin and dopamine. Anal Chim Acta. 2005 Apr 29;537(1–2):145–51.
279. Ran G, Li Y, Xia Y. Graphene oxide and electropolymerized p-aminobenzenesulfonic acid mixed film used as dopamine and serotonin electrochemical sensor. Monatsh Chem [Internet]. 2020 Mar 1 [cited 2024 Jul 17];151(3):293–9. Available from: https://link.springer.com/article/10.1007/s00706-020-02559-9
280. Khoshnevisan K, Honarvarfard E, Torabi F, Maleki H, Baharifar H, Faridbod F, et al. Electrochemical detection of serotonin: A new approach. Clinica Chimica Acta. 2020 Feb;501:112–9.
281. Atici T, Bilgi Kamaç M, Yilmaz M, Yilmaz Kabaca A. Zinc oxide nanorod/polymethylene blue (deep eutectic solvent)/gold nanoparticles modified electrode for electrochemical determination of serotonin (5-HT). Electrochim Acta. 2023 Aug 1;458:142484.
282. Zhou J, Sheng M, Jiang X, Wu G, Gao F. Simultaneous Determination of Dopamine, Serotonin and Ascorbic Acid at a Glassy Carbon Electrode Modified with Carbon-Spheres. Sensors. 2013 Oct 16;13(10):14029–40.
283. Mazloum-Ardakani M, Khoshroo A. Electrocatalytic properties of functionalized carbon nanotubes with titanium dioxide and benzofuran derivative/ionic liquid for simultaneous determination of isoproterenol and serotonin. Electrochim Acta. 2014 Jun;130:634–41.
284. Cesarino I, Galesco H V., Machado SAS. Determination of serotonin on platinum electrode modified with carbon nanotubes/polypyrrole/silver nanoparticles nanohybrid. Materials Science and Engineering: C. 2014 Jul;40:49–54.
285. Becerra-Hernández A, Galindo-de-la-Rosa J, Martínez-Pimentel Y, Ledesma-García J, Álvarez-Contreras L, Guerra-Balcázar M, et al. Novel biomaterial based on monoamine oxidase-A and multi-walled carbon nanotubes for serotonin detection. Biochem Eng J. 2019 Sep;149:107240.
286. Fayemi OE, Adekunle AS, Ebenso EE. Electrochemical determination of serotonin in urine samples based on metal oxide nanoparticles/MWCNT on modified glassy carbon electrode. Sens Biosensing Res. 2017 Apr;13:17–27.
287. Mugadza T, Nyokong T. Electrocatalytic oxidation of amitrole and diuron on iron(II) tetraaminophthalocyanine-single walled carbon nanotube dendrimer. Electrochim Acta. 2010 Mar;55(8):2606–13.
288. Morawski F de M, Winiarski JP, de Campos CEM, Parize AL, Jost CL. Sensitive simultaneous voltammetric determination of the herbicides diuron and isoproturon at a platinum/chitosan bio-based sensing platform. Ecotoxicol Environ Saf. 2020 Dec;206:111181.

289. Öndeş B, Soysal M. Determination of Diuron by Using Electrochemical Sensor Based on Molecularly Imprinted Polymer Film. J Electrochem Soc. 2019 Apr 1;166(6):B395–401.
290. Wong A, Sotomayor MDPT. Determination of carbofuran and diuron in FIA system using electrochemical sensor modified with organometallic complexes and graphene oxide. Journal of Electroanalytical Chemistry. 2014 Oct;731:163–71.
291. de Araújo GM, Simões FR. Self-assembled films based on polypyrrole and carbon nanotubes composites for the determination of Diuron pesticide. Journal of Solid State Electrochemistry. 2018 May 18;22(5):1439–48.
292. Mbokou Foukmeniok S, Bako RFY, Ilboudo O, Karanga Y, Njanja E, Pontie M, et al. Sensitive Carbon Fiber Microelectrode for the Quantification of Diuron in Quality Control of a Commercialized Formulation. Int J Anal Chem. 2022 Mar 11;2022:1–9.
293. Meng Y. A Sustainable Approach to Fabricating Ag Nanoparticles/PVA Hybrid Nanofiber and Its Catalytic Activity. Nanomaterials. 2015 Jun 23;5(2):1124–35.
294. Garibo D, Borbón-Nuñez HA, de León JND, García Mendoza E, Estrada I, Toledano-Magaña Y, et al. Green synthesis of silver nanoparticles using Lysiloma acapulcensis exhibit high-antimicrobial activity. Sci Rep. 2020 Jul 30;10(1):12805.
295. Lopes IS, Oliveira de Moraes BN, de Souza Barreto S, Le Joncour L, Couteau C, Franzolin MR, et al. Green synthesis of antimicrobial silver–copper nanoparticles using Banana and pineapple peel extracts: A sustainable approach for biomaterial sterilization. Mater Chem Phys. 2025 Mar;333:130364.
296. Afolayan JS, Varney AM, Thomas JC, McLean S, Perry CC. A rapid microwave approach for 'one-pot' synthesis of antibiotic conjugated silver nanoparticles with antimicrobial activity against multi-drug resistant bacterial pathogens. Colloids Surf B Biointerfaces. 2025 Jan;245:114280.
297. Langford JI, Wilson AJC. Scherrer after sixty years: A survey and some new results in the determination of crystallite size. J Appl Crystallogr. 1978 Apr 1;11(2):102–13.
298. Thompson AK, Hackett C, Grady TL, Enyinnia S, Moore QC, Nave FM. Development and Characterization of Membranes with PVA Containing Silver Particles: A Study of the Addition and Stability. Polymers (Basel). 2020 Aug 27;12(9):1937.
299. Bishoyi AK, Sahoo CR, Samal P, Mishra NP, Jali BR, Khan MS, et al. Unveiling the antibacterial and antifungal potential of biosynthesized silver nanoparticles from Chromolaena odorata leaves. Sci Rep. 2024 Mar 29;14(1):7513.
300. https://eur-lex.europa.eu/legal-content/EN/TXT/?uri=legissum:4499769. Drinking water — essential quality standards.
301. https://archive.epa.gov/water/archive/web/pdf/archived-consumer-factsheet-on-cadmium.pdf. Consumer Factsheet on: CADMIUM | EPA Archive.
302. Kubier A, Wilkin RT, Pichler T. Cadmium in soils and groundwater: A review. Applied Geochemistry. 2019 Sep;108:104388.
303. Ghanei-Motlagh M, Taher MA. Novel imprinted polymeric nanoparticles prepared by sol–gel technique for electrochemical detection of toxic cadmium(II) ions. Chemical Engineering Journal. 2017 Nov;327:135–41.
304. Rehman AU, Ikram M, Kan K, Zhao Y, Zhang WJ, Zhang J, et al. 3D interlayer nanohybrids composed of reduced graphenescheme oxide/SnO2/PPy grown from expanded graphite for the detection of ultra-trace Cd2+, Cu2+, Hg2+ and Pb2+ ions. Sens Actuators B Chem. 2018 Nov;274:285–95.
305. Wang Y, Wang L, Huang W, Zhang T, Hu X, Perman JA, et al. A metal–organic framework and conducting polymer based electrochemical sensor for high performance cadmium ion detection. J Mater Chem A Mater. 2017;5(18):8385–93.

306. Hormozi Jangi S, Khoobi A. Detection of cadmium heavy metal ions using a nanostructured green sensor in food, biological and environmental samples. Food Chem. 2024 Nov;458:140307.
307. Lu D, Sullivan C, Brack EM, Drew CP, Kurup P. Simultaneous voltammetric detection of cadmium(II), arsenic(III), and selenium(IV) using gold nanostar–modified screen-printed carbon electrodes and modified Britton-Robinson buffer. Anal Bioanal Chem. 2020 Jul 16;412(17):4113–25.
308. Ustabasi GS, Yilmaz I, Ozcan M, Cetinkaya E. Simultaneous, Selective and Highly Sensitive Voltammetric Determination of Lead, Cadmium, and Zinc via Modified Pencil Graphite Electrodes. Electroanalysis [Internet]. 2022 Aug 1 [cited 2024 Aug 12];34(8):1237–44. Available from: https://onlinelibrary.wiley.com/doi/full/10.1002/elan.202100512
309. Mazzaracchio V, Tshwenya L, Moscone D, Arduini F, Arotiba OA. A Poly(Propylene Imine) Dendrimer and Carbon Black Modified Flexible Screen Printed Electrochemical Sensor for Lead and Cadmium Co-detection. Electroanalysis [Internet]. 2020 Dec 1 [cited 2024 Aug 12];32(12):3009–16. Available from: https://onlinelibrary.wiley.com/doi/full/10.1002/elan.202060284
310. Hassan KM, Gaber SE, Altahan MF, Azzem MA. Single and simultaneous voltammetric sensing of lead(II), cadmium(II) and zinc(II) using a bimetallic Hg-Bi supported on poly(1,2-diaminoanthraquinone)/glassy carbon modified electrode. Sens Biosensing Res. 2020 Aug 1;29:100369.
311. Anandhakumar S, Mathiyarasu J, Narasimha Phani KL. Anodic stripping voltammetric determination of cadmium using a “mercury free” indium film electrode. Analyst [Internet]. 2013 Aug 28 [cited 2024 Aug 12];138(19):5674–8. Available from: https://pubs.rsc.org/en/content/articlehtml/2013/an/c3an01070h
312. Lee KY, Ambrosi A, Pumera M. 3D-printed Metal Electrodes for Heavy Metals Detection by Anodic Stripping Voltammetry. Electroanalysis [Internet]. 2017 Nov 1 [cited 2024 Aug 12];29(11):2444–53. Available from: https://onlinelibrary.wiley.com/doi/full/10.1002/elan.201700388
313. Mokhena TC, Sefadi JS, Sadiku ER, John MJ, Mochane MJ, Mtibe A. Thermoplastic Processing of PLA/Cellulose Nanomaterials Composites. Polymers (Basel). 2018 Dec 9;10(12):1363.
314. Suryanegara L, Nakagaito AN, Yano H. The effect of crystallization of PLA on the thermal and mechanical properties of microfibrillated cellulose-reinforced PLA composites. Compos Sci Technol. 2009 Jun;69(7–8):1187–92.
315. Elsawy MA, Kim KH, Park JW, Deep A. Hydrolytic degradation of polylactic acid (PLA) and its composites. Renewable and Sustainable Energy Reviews. 2017 Nov;79:1346–52.
316. Blume R, Rosenthal D, Tessonnier JP, Li H, Knop-Gericke A, Schlögl R. Characterizing Graphitic Carbon with X-ray Photoelectron Spectroscopy: A Step-by-Step Approach. ChemCatChem [Internet]. 2015 Sep 14 [cited 2024 Jun 3];7(18):2871–81. Available from: https://onlinelibrary.wiley.com/doi/full/10.1002/cctc.201500344
317. Gengenbach TR, Major GH, Linford MR, Easton CD. Practical guides for x-ray photoelectron spectroscopy (XPS): Interpreting the carbon 1s spectrum. Journal of Vacuum Science & Technology A: Vacuum, Surfaces, and Films. 2021 Jan 1;39(1).
318. Wang S, Chen F, Li Z, Tao H, Qu L, Li J, et al. A graphene oxide/Zn-metal organic framework electrochemical sensor for acetaminophen detection. Surfaces and Interfaces. 2023 Jul;39:102910.

319. Annadurai K, Sudha V, Murugadoss G, Thangamuthu R. Electrochemical sensor based on hydrothermally prepared nickel oxide for the determination of 4-acetaminophen in paracetamol tablets and human blood serum samples. J Alloys Compd. 2021 Jan;852:156911.
320. Silva JPC, Rocha RG, Siqueira GP, Nascimento CF, Santana MHP, Nossol E, et al. Bio-based plasticizer Babassu oil for custom-made conductive additive-manufacturing filaments: towards 3D-printed electrodes applied to cocaine detection. Microchimica Acta. 2025 Jan 31;192(1):47.

CURRICULAR SUMMARY

Published Articles

Bernalte, Elena†; **Augusto, Karen K. L.**†; Crapnell, Robert D.; Andrews, Hayley G.; Fatibello-Filho, Orlando; Banks, Craig E. *Eco-friendly integration of gold nanoparticles into additive manufacturing filaments: advancing conductivity and electrochemical performance*. RSC Applied Interfaces, v. 2, 439-450, 2025. (†Indicates joint first authorship)

Augusto, Karen K. L.; Gomes-Junior, Paulo C.; Longatto, Gustavo P.; Piccin, Evandro; Cavalheiro, Éder T. G.; Bernalte, Elena; Banks, Craig E.; Fatibello-Filho, Orlando. *Electrochemical sensor based on carbon nanohorns and hydrophobic deep eutectic solvent for the determination of serotonin in biological samples*. Electrochimica Acta, v. 520, 145836, 2025.

Bernalte, Elena; Crapnell, Robert D.; El Azizi, Rania; **Augusto, Karen K. L.**; Banks, Craig E. *Gold nanoparticle infused castor oil for the production of high performance conductive additive manufacturing filament*. Applied Materials Today, v. 42, 102578, 2025.

Augusto, Karen K. L.; Crapnell, Robert D.; Bernalte, Elena; Zighed, Sabri; Ehamparanathan, Anbuchselvan; Pimlott, Jessica L.; Andrews, Hayley G.; Whittingham, Matthew J.; Rowley-Neale, Samuel J.; Fatibello-Filho, Orlando; Banks, Craig E. *Optimised graphite/carbon black loading of recycled PLA for the production of low-cost conductive filament and its application to the detection of β-estradiol in environmental samples*. Microchimica Acta, v. 191, 1-14, 2024.

Gomes-Junior, Paulo C.; Longatto, Gustavo P.; **Augusto, Karen K. L.**; Rocha, Josias S.; Piccin, Evandro; Fatibello-Filho, Orlando. *Synthesis of ultrasmall cerium oxide nanoparticles in deep eutectic solvent and their application in an*

electrochemical sensor to detect dopamine in biological fluid. Microchimica Acta, v. 191, 1-12, 2024.

Gomes-Junior, Paulo C.; Nascimento, Evair D.; **Augusto, Karen K. L.**; Longatto, Gustavo P.; Faria, Ronaldo C.; Piccin, Evandro; Fatibello-Filho, Orlando. *Voltammetric determination of uric acid using a miniaturized platform based on screen-printed electrodes modified with platinum nanoparticles*. Microchemical Journal, v. 207, 111931, 2024.

Gomes-Junior, Paulo C.; **Augusto, Karen K. L.**; Longatto, Gustavo P.; Gonçalves, Renan O.; Silva, Tiago A.; Cavalheiro, Éder T. G.; Fatibello-Filho, Orlando. *Ultrasmall platinum nanoparticles synthesized in reline deep eutectic solvent explored towards the voltammetric sensing of riboflavin in beverages and biological fluids*. Sensors and Actuators B-Chemical, v. 395, 134489, 2023.

Augusto, Karen K. L.; Piton, Gabriela R.; Gomes-Júnior, Paulo C.; Longatto, Gustavo P.; De Moraes, Fernando C.; Fatibello-Filho, Orlando. *Enhancing the electrochemical sensitivity of hydroquinone using a hydrophobic deep eutectic solvent-based carbon paste electrode*. Analytical Methods, v. 14, 2003-2013, 2022.

Ferreira, Luís M.C.; Silva, Patrícia S.; **Augusto, Karen K. L.**; Gomes-Júnior, Paulo C.; Farra, Sinara O. D.; Silva, Tiago A.; Fatibello-Filho, Orlando; Vicentini, Fernando C. *Using nanostructured carbon black-based electrochemical (bio)sensors for pharmaceutical and biomedical analyses: A comprehensive review*. Journal of Pharmaceutical and Biomedical Analysis, v. 221, 115032, 2022.

Piton, Gabriela R.; **Augusto, Karen K. L.**; Santos, Daniel; Fatibello-filho, Orlando. *Spectrophotometric Determination of Allura Red AC and Tartrazine in Food Products Using Hydrophobic Deep Eutectic Solvents as an Environmentally*

Sustainable Micro-Extractor. Journal of The Brazilian Chemical Society, v. 00, 1-8, 2021.

Piton, Gabriela R.; **Augusto, Karen K. L.**; Wong, Ademar; Moraes, Fernando C.; Fatibello-Filho, Orlando. *A Novel Electrochemical Glassy Carbon Electrode Modified with Carbon Black and Glyceline Deep Eutectic Solvent within a Crosslinked Chitosan Film for Simultaneous Determination of Acetaminophen and Diclofenac*. Electroanalysis, v. 33, 2351-2360, 2021.

International Conferences

XXVI SIBAE: Sociedade Iberoamericana de Eletroquímica, Lisbon, Portugal. "Eletrodo de carbono vítreo modificado com solvente eutético profundo hidrofóbico para a determinação de serotonina", 2024. ***Oral presentation***. Authors: **Karen K. L. Augusto**, Paulo C. Gomes-Júnior, Gustavo P. Longatto, Elena Bernalte, Craig Banks, Orlando Fatibello-Filho.

XXVI SIBAE: Sociedade Iberoamericana de Eletroquímica, Lisbon, Portugal. "Produção sustentável de filamentos modificados com nanopartículas metálicas para impressão", 2024. ***Poster presentation***. Authors: **Karen K. L. Augusto**, Elena Bernalte, Robert Crapnell, Orlando Fatibello-Filho, Craig Banks.

74th – ISE: Annual Meeting of the International Society of Electrochemistry, Lyon, France. "Platinum nanoparticles synthesized in hydrophilic deep eutectic solvent for application in electrochemical sensor", 2023. ***Poster presentation***. Authors: Orlando Fatibello-Filho, Paulo Gomes-Júnior, **Karen K. L. Augusto**, Renan Gonçalves, Júlio Almeida, Gustavo Longatto, Eder Cavalheiro.

74th – ISE: Annual Meeting of the International Society of Electrochemistry, Lyon, France. "Hydrophobic Deep Eutectic Solvent Based on Decanoic Acid and

Tetrabutylammonium Bromide: Characterization and Evaluation Towards Electrode Modification", 2023. ***Poster presentation***. Authors: Orlando Fatibello-Filho, **Karen K. L. Augusto**, Paulo Gomes-Júnior, Renan Gonçalves, Júlio Almeida, Gustavo Longatto, Eder Cavalheiro.

Nacional Conferences

1º Encontro do INCT Nanovida, Curitiba/PR, Brasil. "Elaboração de sensor eletroquímico com nanopartículas de ouro sintetizadas em solvente eutético profundo", 2024. ***Poster presentation***. Authors: Gustavo Patelli Longatto; Paulo Cardoso Gomes Júnior; **Karen Kenlderi de Lima Augusto**; Charbel Nagib Mouchrek; Evandro Piccin; Orlando Fatibello-Filho.

1º Encontro do INCT Nanovida, Curitiba/PR, Brasil. "Solvente eutético profundo hidrofóbico: caracterização do ponto eutético e modificação de eletrodo de pasta de carbono para determinação de diuron", 2024. ***Poster presentation***. Authors: **Karen Kenlderi de Lima Augusto**; Paulo Cardoso Gomes-Júnior, Gustavo Patelli Longatto e Orlando Fatibello-Filho.

21º ENQA (Encontro Nacional de Química Analítica) | 9º CIAQA (Congresso Ibero-Americano de Química Ananlítica), Belém/PA, Brasil. "Low-Cost Conductive Filament Based on Carbon Black/Graphite Loading to Detect β-Estradiol in Water Samples", 2024. ***Poster presentation***. Authors: **Augusto, Karen K. L.**; Crapnell, Robert D.; Bernalte, Elena; Zighed, Sabri; Ehamparanathan, Anbuchselvan; Pimlott, Jessica L.; Andrews, Hayley G.; Whittingham, Matthew J.; Rowley-Neale, Samuel J.; Fatibello-Filho, Orlando; Banks, Craig E.

21º ENQA (Encontro Nacional de Química Analítica) | 9º CIAQA (Congresso Ibero-Americano de Química Ananlítica), Belém/PA, Brasil. “Electrochemical sensor based on gold nanosheets (AuNSs) synthesised in a green ternary mixture for simultaneous determination of acetaminophen and dopamine”, 2024. ***Poster presentation***. Authors: Paulo Cardoso Gomes Junior; **Karen Kenlderi de Lima Augusto**; Gustavo Patelli Longatto; Evandro Piccin; Éder Tadeu Gomes Cavalheiro; Orlando Fatibello Filho.

46ª Reunião Anual da Sociedade Brasileira de Química (46ª RASBQ), Águas de Lindóia/SP, Brasil. “Synthesis of platinum nanoparticles in deep eutectic solvent for application in electrochemical sensors”, 2023. ***Poster presentation***. Authors: Paulo Cardoso Gomes Junior, **Karen Kenlderi de Lima Augusto**, Renan de Oliveira Gonçalves, Gustavo Patelli Longatto, Julio César de Oliveira Almeida, Éder Tadeu Gomes Cavalheiro e Orlando-Fatibello.

46ª Reunião Anual da Sociedade Brasileira de Química (46ª RASBQ), Águas de Lindóia/SP, Brasil. “Hydrophobic deep eutectic solvent based on decanoic acid and tetrabutylammonium bromide: characterization and evaluation towards electrode modification”, 2023. ***Poster presentation***. Authors: **Karen Kenlderi de Lima Augusto**, Paulo Cardoso Gomes Junior, Renan de Oliveira Gonçalves, Julio César de Oliveira Almeida, Gustavo Patelli Longatto, Éder Tadeu Gomes Cavalheiro e Orlando Fatibello-Filho.

46ª Reunião Anual da Sociedade Brasileira de Química (46ª RASBQ), Águas de Lindóia/SP, Brasil. “A novel electrochemical sensor based on hydrophobic deep eutectic solvent for 17β-estradiol detection”, 2023. ***Poster presentation***. Authors: Julio César de Oliveira Almeida, **Karen Kenlderi de Lima Augusto**, Paulo Cardoso Gomes Junior, Renan de Oliveira Gonçalves, Gustavo Patelli Longatto, Éder Tadeu Gomes Cavalheiro e Orlando Fatibello-Filho.

46ª Reunião Anual da Sociedade Brasileira de Química (46ª RASBQ), Águas de Lindóia/SP, Brasil. “Development of electrochemical sensors with metallic nanoparticles synthesized in deep eutectic solvents”, 2023. ***Poster presentation***. Authors: Gustavo Patelli Longatto, Paulo Cardoso Gomes Junior, **Karen Kenlderi de Lima Augusto**, Julio César de Oliveira Almeida, Renan de Oliveira Gonçalves, Orlando Fatibello Filho e Éder Tadeu Gomes Cavalheiro.

XXIII Simpósio Brasileiro de Eletroquímica e Eletroanalítica, Mato Grosso do Sul, Brasil (online). “Eletrodo de pasta de carbono modificado com solvente eutético profundo para a determinação de hidroquinona”, 2021. ***Oral presentation***. Authors: **Karen K. L. Augusto**, Gabriela R. Piton, Fernando C. Moraes, Orlando Fatibello-Filho.

Awards

Award received in the **panel session of the 46th RASBQ**, Division of Electrochemistry and Electroanalytical, as one of the authors of the work entitled *Synthesis of platinum nanoparticles in deep eutectic solvent for application in electrochemical sensors*. (May 2023). Authors: Paulo Cardoso Gomes Junior, **Karen Kenlderi de Lima Augusto**, Renan de Oliveira Gonçalves, Gustavo Patelli Longatto, Julio César de Oliveira Almeida, Éder Tadeu Gomes Cavalheiro and Orlando-Fatibello.

Appendix

Appendix I - *In situ* Infrared

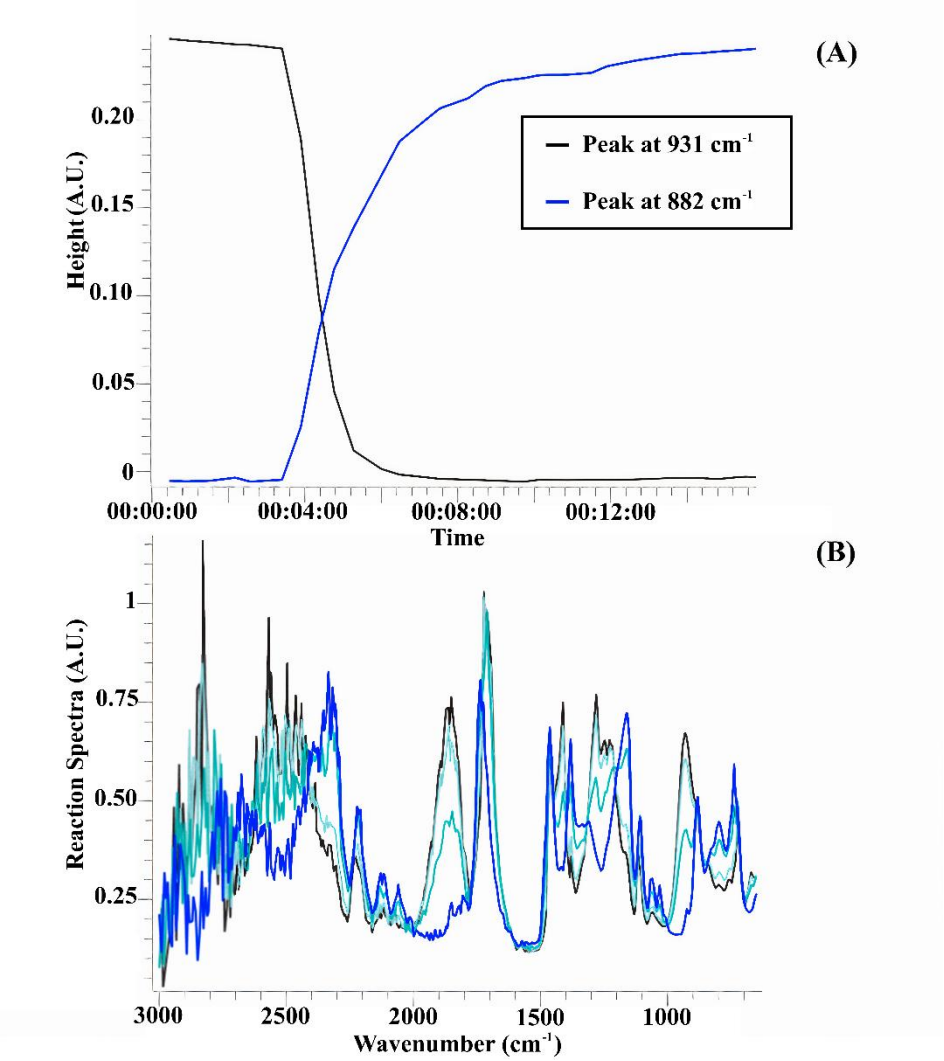

Figure A1. Synthesis of hydrophobic eutectic mixture monitored at 50 ºC (323.15 K), in (A) intensity monitoring of specific peaks in function of the time of synthesis and (B) infrared spectra.

Table A1. Time of acquisition of the spectra depicted in Figure A1

Spectrum Name	Color	Synthesis stage
00:03:24		DecA
00:03:53		Addition of TBAB

00:04:45		Middle of the synthesis
00:20:24		End of synthesis

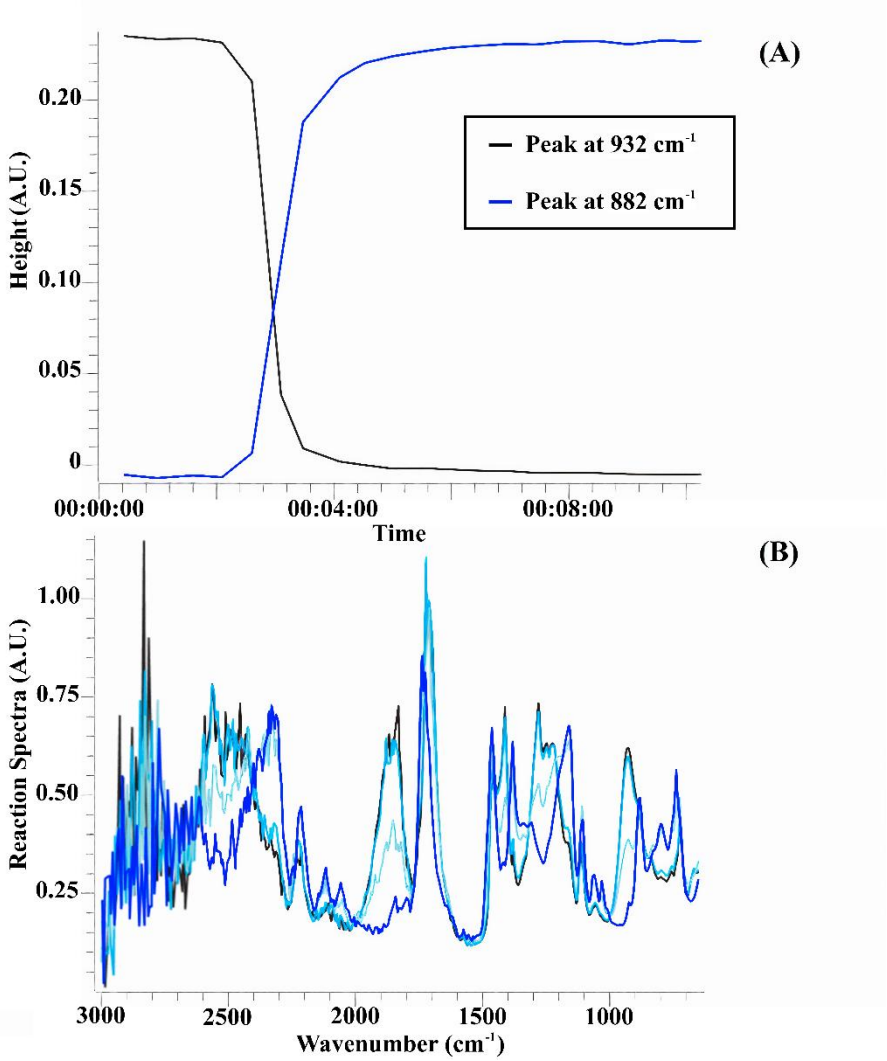

Figure A2. Synthesis of hydrophobic eutectic mixture monitored at 60 ºC (333.15 K), in (A) intensity monitoring of specific peaks in function of the time of synthesis and (B) infrared spectra.

Table A2. Time of acquisition of the spectra depicted in Figure A2

Spectrum Name	**Color**	**Synthesis stage**

00:02:05		DecA
00:02:36		Addition of TBAB
00:03:05		Middle of the synthesis
00:09:01		End of synthesis

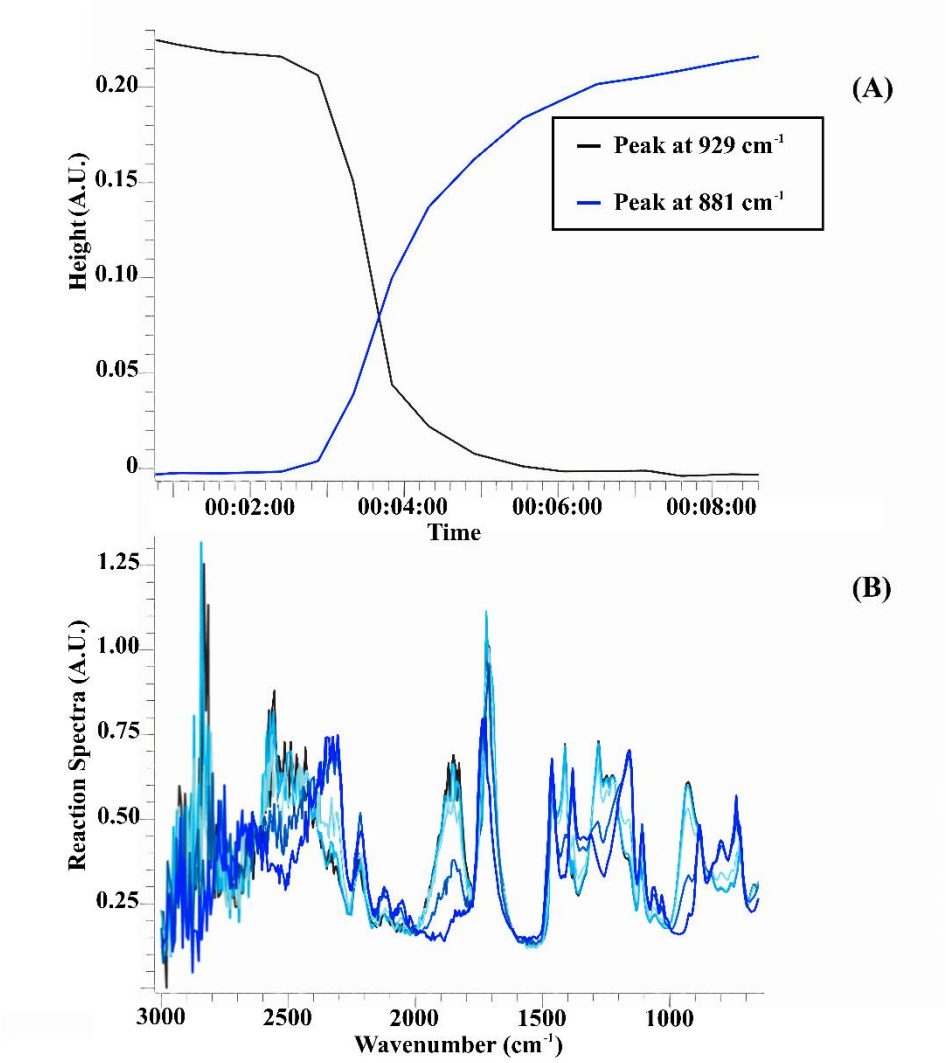

Figure A3. Synthesis of hydrophobic eutectic mixture monitored at 70 ºC (343.15 K), in (A) intensity monitoring of specific peaks in function of the time of synthesis and (B) infrared spectra.

Table A3. Time of acquisition of the spectra depicted in Figure A3

Spectrum Name	Color	Synthesis stage
00:02:24		DecA
00:02:52		Addition of TBAB
00:03:20		Middle of the synthesis
00:04:19		Middle of the synthesis
00:09:18		End of synthesis

Appendix II - DSC curves for different mixtures of DecA and TBAB.

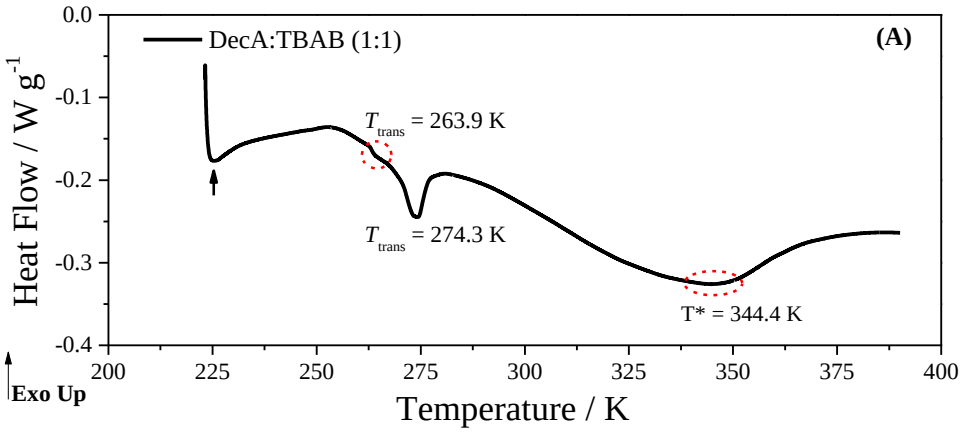

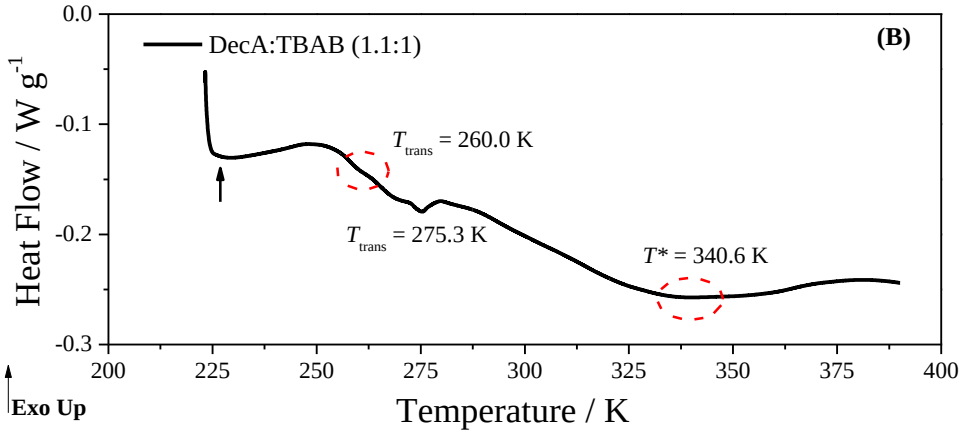

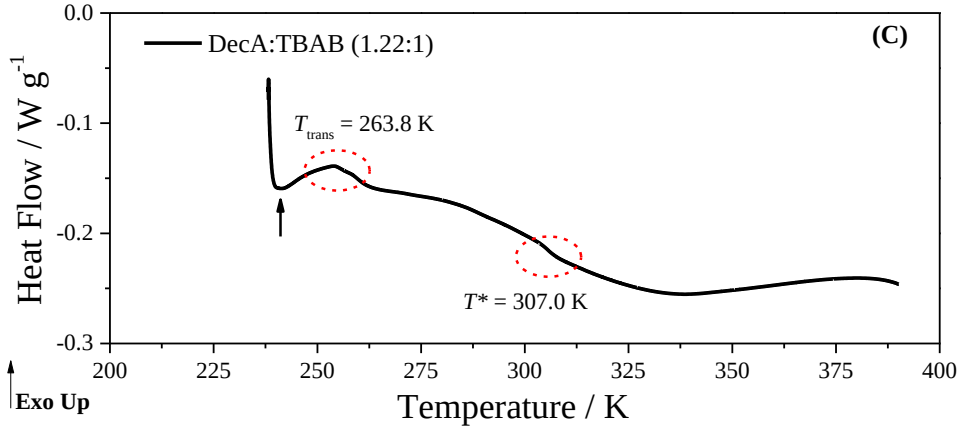

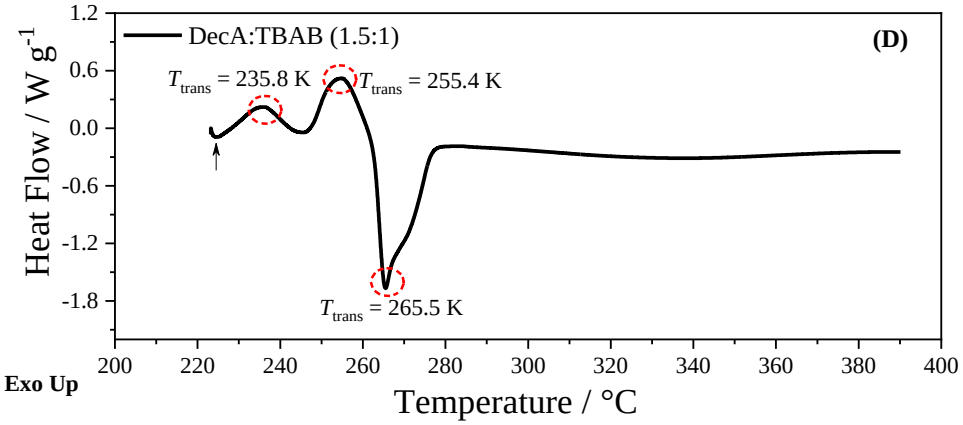
DecA:TBAB (1.5:1)
(D)
T_{trans} = 235.8 K
T_{trans} = 255.4 K
T_{trans} = 265.5 K
Heat Flow / W g^{-1}
Temperature / °C
Exo Up

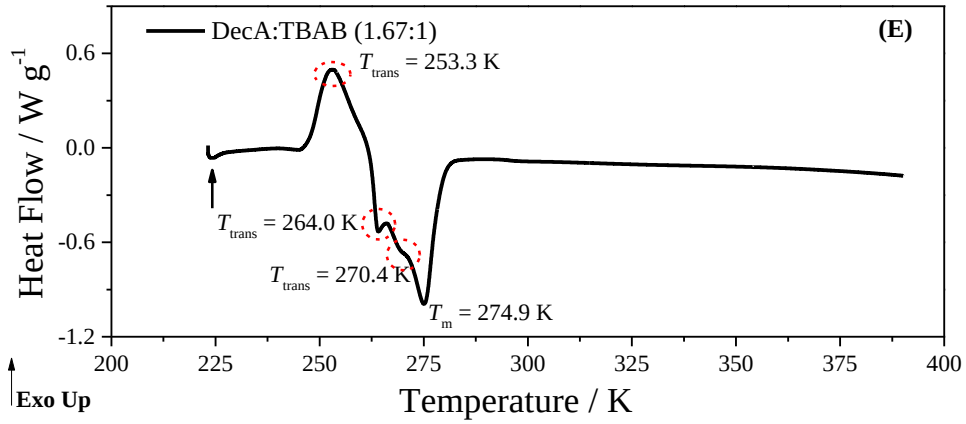
DecA:TBAB (1.67:1)
(E)
T_{trans} = 253.3 K
T_{trans} = 264.0 K
T_{trans} = 270.4 K
T_m = 274.9 K
Heat Flow / W g^{-1}
Temperature / K
Exo Up

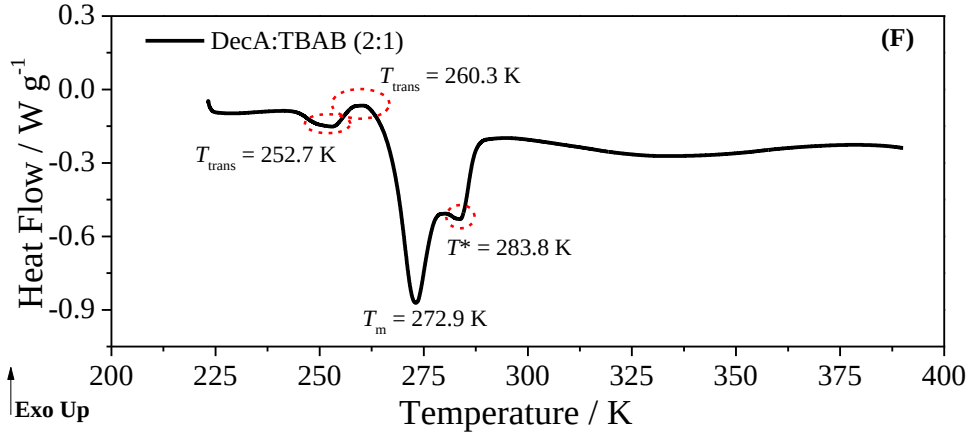
DecA:TBAB (2:1)
(F)
T_{trans} = 260.3 K
T_{trans} = 252.7 K
T^* = 283.8 K
T_m = 272.9 K
Heat Flow / W g^{-1}
Temperature / K
Exo Up

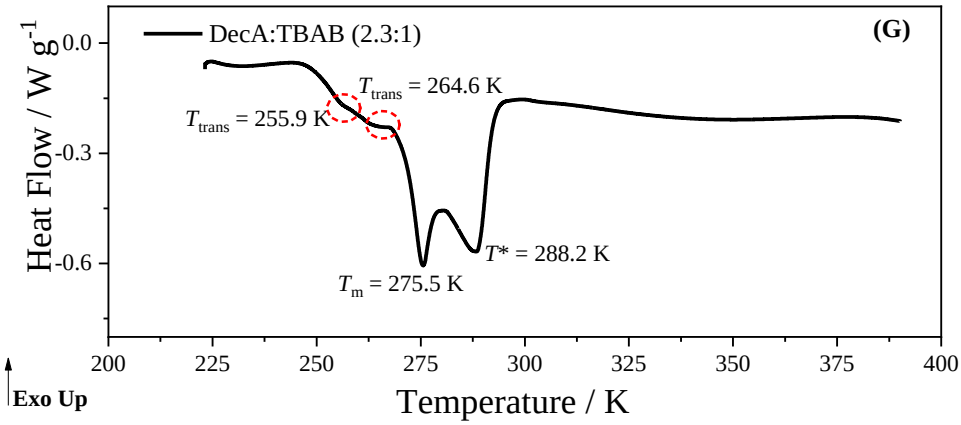
DecA:TBAB (2.3:1)
(G)
T_{trans} = 264.6 K
T_{trans} = 255.9 K
T* = 288.2 K
T_m = 275.5 K
Heat Flow / W g^{-1}
0.0
-0.3
-0.6
200
225
250
275
300
325
350
375
400
Exo Up
Temperature / K

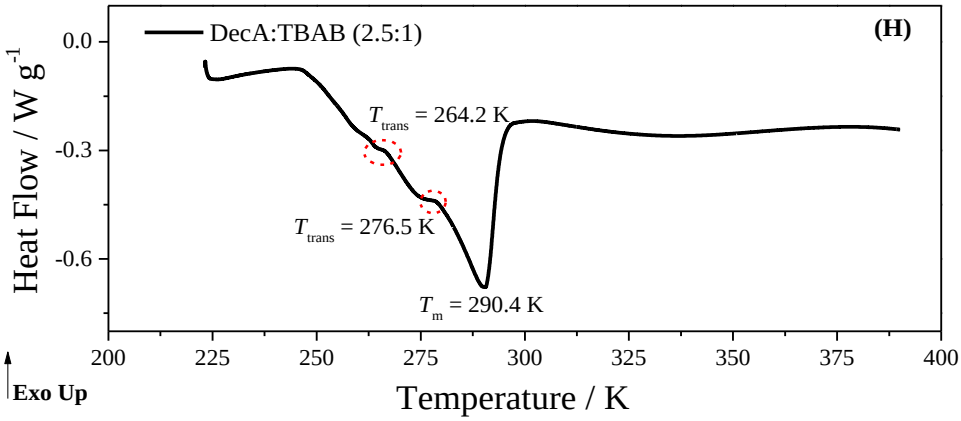
DecA:TBAB (2.5:1)
(H)
T_{trans} = 264.2 K
T_{trans} = 276.5 K
T_m = 290.4 K
Heat Flow / W g^{-1}
0.0
-0.3
-0.6
200
225
250
275
300
325
350
375
400
Exo Up
Temperature / K

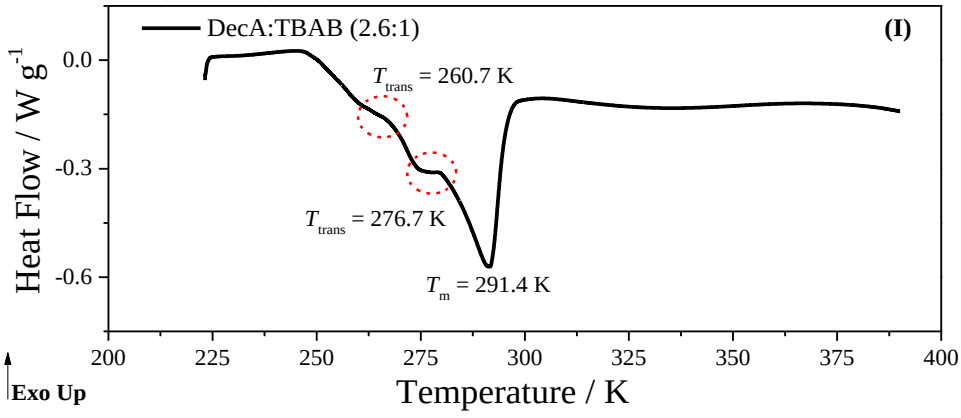
DecA:TBAB (2.6:1)
(I)
T_{trans} = 260.7 K
T_{trans} = 276.7 K
T_m = 291.4 K
Heat Flow / W g^{-1}
0.0
-0.3
-0.6
200
225
250
275
300
325
350
375
400
Exo Up
Temperature / K

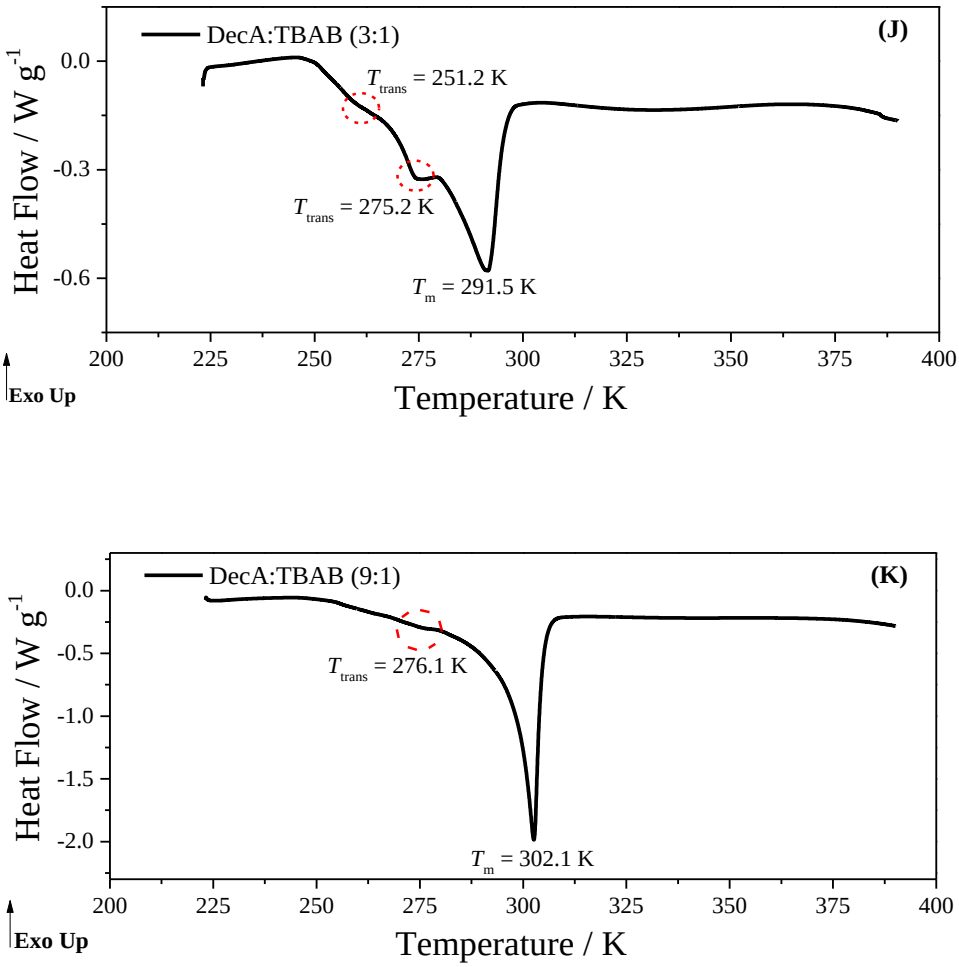

Figure A4. (A to K) DSC curves for different mixtures of DecA and TBAB according to TABLE 3.1.